

Sheffield Hallam University

Investigation of ADAM17 and ADAMTS-1, -4 and -5 in liver carcinoma.

TURNER, Sharon Louise.

Available from the Sheffield Hallam University Research Archive (SHURA) at:

<http://shura.shu.ac.uk/20827/>

A Sheffield Hallam University thesis

This thesis is protected by copyright which belongs to the author.

The content must not be changed in any way or sold commercially in any format or medium without the formal permission of the author.

When referring to this work, full bibliographic details including the author, title, awarding institution and date of the thesis must be given.

Please visit <http://shura.shu.ac.uk/20827/> and <http://shura.shu.ac.uk/information.html> for further details about copyright and re-use permissions.

LEARNING CENTRE
COLLEGIATE CRESCENT
SHEFFIELD S10 2BP

101 963 660 2



REFERENCE

ProQuest Number: 10702936

All rights reserved

INFORMATION TO ALL USERS

The quality of this reproduction is dependent upon the quality of the copy submitted.

In the unlikely event that the author did not send a complete manuscript and there are missing pages, these will be noted. Also, if material had to be removed, a note will indicate the deletion.



ProQuest 10702936

Published by ProQuest LLC (2017). Copyright of the Dissertation is held by the Author.

All rights reserved.

This work is protected against unauthorized copying under Title 17, United States Code
Microform Edition © ProQuest LLC.

ProQuest LLC.
789 East Eisenhower Parkway
P.O. Box 1346
Ann Arbor, MI 48106 – 1346

**Investigation of ADAM17 and ADAMTS-1, -4 and -5 in
Liver Carcinoma**

Sharon Louise Turner

A thesis submitted in partial fulfilment of the requirements of

Sheffield Hallam University

for the degree of Doctor of Philosophy

Collaborating Organisation: The Liver Group, University of Sheffield

September 2009

Abstract

Background

Proteolytic enzymes are important mediators of cellular proliferation, angiogenesis and remodelling of the extracellular matrix (ECM); all processes required for tumour growth and metastasis. However, the studies of proteolytic enzymes in hepatic tumours, both primary and metastatic, have largely been limited to specific matrix metalloproteinases e.g. MMP-2, -7 and -9, and urokinase-type plasminogen activator.

ADAM17 (a disintegrin and metalloproteinase 17), a membrane-bound sheddase, releases membrane-bound proteins including growth factors, which could contribute to liver tumour growth. Fractalkine is also shed by ADAM17, and can act as an angiogenic mediator, potentially aiding the development of tumour neovasculature. ADAMTS (a disintegrin and metalloproteinase with thrombospondin motifs) -1, -4 and -5 are secreted enzymes, which primarily degrade ECM components, and may participate in the remodelling of liver ECM during invasive processes. TIMP3 (tissue inhibitor of metalloproteinases) is the major, endogenous inhibitor of ADAM17, ADAMTS-1, -4 and -5, and its dysregulation in cancer could aid tumour progression.

Methods

Three liver derived cell lines were utilised throughout this investigation, namely HepG2, HuH-7 (well-differentiated hepatocellular carcinoma cell lines), and LX-2 (an activated hepatic stellate cell line). ADAM17, ADAMTS-1, -4, -5 and TIMP3 mRNA expression was investigated by quantitative real-time RT-PCR using the SYBR green method, their protein expression by western blotting using the SDS-PAGE Laemmli system, and their cellular distribution by immunocytochemistry with confocal laser scanning microscopy. The modulation of each of these characteristics by cytokines (IL-1 β , IL-6 and TNF- α) was also investigated, and MTT assays performed to determine the proliferative effect of these treatments. ADAM17 activity was studied using a fractalkine ELISA, as was the effect of ADAM17 down-regulation by siRNA. Furthermore, cell surface and intracellular ADAM17 protein levels were quantified using flow cytometry and related to shed fractalkine levels following cytokine treatments.

Results

This investigation established the presence of ADAM17, ADAMTS-1, -4, -5 and TIMP3 at the mRNA level in foetal and adult human liver, and confirmed the presence of ADAM17, ADAMTS-1 and TIMP3 at the mRNA and protein level in liver derived cells (HepG2, HuH-7 & LX-2 cell lines). Furthermore, the expression of ADAMTS-4 and -5 at the mRNA and protein level was demonstrated for the first time in liver cell lines. Their

expression in these cells was differentially modulated at the mRNA and protein level by pro-inflammatory cytokines elevated during liver tumour development (IL-1 β , IL-6 and TNF- α). The same cytokines also increased the cellular proliferation of hepatoma cells (HepG2 & HuH-7), but not activated hepatic stellate cells (LX-2). Fractalkine shedding was significantly increased following IL-1 β and TNF- α treatments of HepG2 cells, although this did not correlate with the relatively weak up-regulation of ADAM17 protein following the same treatments, and was not reduced by the down-regulation of ADAM17 with specific siRNA, indicating the involvement of other proteinases in this process.

Conclusions

The modulation of these enzymes and their endogenous inhibitor in normal or transformed hepatic cells may provide a microenvironment that facilitates ECM remodelling to allow cancer cell invasion, and subsequent growth and development of tumours into the liver parenchyma.

For my Mum and Dad

Acknowledgements

This research project would not have been possible without the support of many people.

I wish to express my gratitude to Dr. Rowena Bunning, Dr. Maria Blair, Dr. Nigel Bird and Dr. Dave Mangnall for their supervision, support and guidance throughout the course of this project.

Thanks to Dr. Gail Haddock, Dr. Alkistis Frentzou and Dr. Louise Hurst for imparting their knowledge of immuno techniques, Dr. Roger Jackson for his advice on statistical analyses, and Dr. Sarah Haywood-Small and Dr. Christine Le Maitre for their invaluable help with flow cytometry. This project would have been infinitely more difficult without these supportive colleagues.

I gratefully acknowledge the funding of this work by the Biomedical Research Centre at Sheffield Hallam University.

Lots of love and thanks must go to my fantastic parents and boyfriend Chris, for their endless patience and understanding. I must also express my thanks to Gemma and Mary who have been a constant source of support and distraction!

Table of Contents

Abstract	i
Acknowledgements	iv
Table of Contents	v
List of Figures	x
List of Tables	xiv
List of Abbreviations	xv
1. Introduction	1
1.1 Overview	2
1.2 The Microscopic Structure of the Liver	2
1.2.1 Liver Lobules	2
1.2.2 Hepatocytes	4
1.2.3 Endothelial Cells	4
1.2.4 Hepatic Stellate Cells	5
1.2.5 Kupffer Cells	6
1.2.6 Pit Cells	6
1.2.7 Intrahepatic Portal Tracts	7
1.2.8 Liver Extracellular Matrix	7
1.3 Tumour Invasion & Metastasis	8
1.4 Liver Cancer	9
1.4.1 HCC Incidence & Epidemiology	9
1.4.2 CRC Liver Metastases Incidence & Epidemiology	11
1.4.3 CRC Progression to the Liver	11
1.4.4 Liver Tumour Pathology	12
1.5 Cytokines	16
1.5.1 IL-1 β , IL-6 & TNF- α in Cancer	19
1.6 Metalloproteinases	23
1.6.1 ADAM Proteins	25
1.6.2 ADAM domain structure	26
1.6.3 ADAM17 Functions	30
1.6.4 ADAM17 in Cancer	33
1.6.5 ADAMTS Proteins	38
1.6.6 ADAMTS Domain Structure	39
1.6.7 ADAMTS-1, -4 & -5 Protein Functions	41
1.6.8 ADAMTS-1, -4 & -5 & Cancer	42
1.6.9 TIMPs	46
1.7 Conclusions	47

1.8 Aims & Objectives of the Study	48
2. Materials & Methods	49
2.1 Materials	50
2.1.1 Manufacturers of Reagents	50
2.1.2 Manufacturers of Consumables.....	53
2.1.3 Manufacturers of Equipment	54
2.2 Cell Culture	56
2.2.1 Recovery of Cryofrozen Cells.....	57
2.2.2 Cell Harvesting & Serial Passage of Cells	57
2.2.3 Cell Counting.....	59
2.2.4 Cytokine Treatment of Cells	59
2.2.5 Short Interfering RNA (siRNA) Transfection	60
2.2.6 Cellular Proliferation Assay	61
2.3 Quantitative Real-Time-Polymerase Chain Reaction (qRT-PCR).....	63
2.3.1 Total RNA Extraction.....	63
2.3.2 Deoxyribonuclease I Treatment of RNA	63
2.3.3 Agarose Gel Electrophoresis of Total RNA.....	64
2.3.4 RNA Quantification.....	64
2.3.5 cDNA Synthesis	65
2.3.6 qRT-PCR	65
2.3.7 Selection of Housekeeping Genes for qRT-PCR.....	68
2.3.8 Standard Curve Method	69
2.4 Western Blotting.....	69
2.4.1 Protein Extraction.....	73
2.4.2 Bicinchoninic Acid Assay for Protein Determination	73
2.4.3 Trichloroacetic Acid Precipitation of Protein	74
2.4.4 SDS-PAGE	74
2.4.5 Coomassie Blue Staining of Protein	74
2.4.6 Protein Electroblothing	74
2.4.7 Immunoprobng	75
2.4.8 Chemiluminescent Immunodetection.....	75
2.4.9 Stripping of Western Blot Membrane.....	78
2.5 Immunocytochemistry	78
2.6 Enzyme-Linked Immunosorbant Assay	83
2.7 Flow Cytometry.....	85
2.8 Statistical Analyses	86
3. Proliferative Responses & Modulation of ADAM17, ADAMTS-1, -4, -5 & TIMP3 mRNA in Liver Cell Lines by IL-1β, IL-6 & TNF-α	88

3.1 Introduction	89
3.1.1 Cell Culture	89
3.1.2 Cell Viability & Proliferation	89
3.1.3 The Principle of qRT-PCR	89
3.1.4 Specific Objectives	91
3.2 Results	91
3.2.1 Cell Line Characterisation	91
3.2.2 Establishing Appropriate Controls for Cytokine Treatments	93
3.2.3 Proliferative Responses of HepG2, HuH-7 & LX-2 Cell Lines to IL-1 β , IL-6 & TNF- α	93
3.2.4 qRT-PCR optimisation	98
3.2.5 Selection of housekeeping gene transcripts	100
3.2.6 Primer Efficiencies	106
3.2.7 qRT-PCR Products	106
3.2.8 Gene expression in adult & foetal liver samples	110
3.2.9 Modulation of Gene Expression by IL-1 β , IL-6 & TNF- α	115
3.2.10 Summary of Results	123
3.3 Discussion	125
3.3.1 Characterisation of the Cell Lines HepG2, HuH-7 & LX-2	125
3.3.2 IL-1 β , IL-6 & TNF- α Differentially Increase Cellular Proliferation of HepG2 & HuH-7 Cells, but Not LX-2 Cells	125
3.3.3 IL-1 β , IL-6 & TNF- α Differentially Modulate the Gene Expression of ADAM17, ADAMTS-1, -4, -5 & TIMP3 in Liver Cell Lines	126
3.4 Summary	128
4. Modulation of ADAM17, ADAMTS-1, -4, -5 & TIMP3 Protein in Liver Cell Lines by IL-1β, IL-6 & TNF-α	129
4.1 Introduction	130
4.1.1 Immunodetection of Proteins	130
4.1.2 Specific Objectives	131
4.2 Results	131
4.2.1 Western Blotting Optimisation	131
4.2.2 Modulation of Protein Expression by IL-1 β , IL-6 & TNF- α	132
4.2.3 Summary of Results	152
4.3 Discussion	159
4.3.1 IL-1 β , IL-6 & TNF- α Differentially Modulate the Protein Expression of ADAM17, ADAMTS-1, -4, -5 & TIMP3 in Liver Cell Lines	159
4.4 Summary	161

5. Cellular Localisation ADAM17, ADAMTS-1, -4, -5 & TIMP3 in Liver Cell Lines & the effect of IL-1β, IL-6 & TNF-α on this	162
5.1 Introduction	163
5.1.1 Confocal Laser Scanning Microscopy.....	163
5.1.2 Specific Objectives	165
5.2 Results.....	165
5.2.1 ICC Optimisation	165
5.2.2 Redistribution of Proteins following IL-1 β , IL-6 & TNF- α Treatment	166
5.2.3 Summary of Results	182
5.3 Discussion	188
5.3.1 IL-1 β , IL-6 & TNF- α Differentially Modulate the Cellular Location of ADAM17, ADAMTS-1, -4, -5 & TIMP3 Proteins in Liver Cell Lines	188
5.4 Summary	191
6. Assessment of ADAM17 Activity in HepG2 Cells	192
6.1 Introduction	193
6.1.1 Fractalkine	193
6.1.2 Flow Cytometry	194
6.1.3 RNA interference.....	196
6.1.4 Specific Objectives	197
6.2 Results.....	200
6.2.1 Fractalkine Shedding from HepG2 Cells.....	200
6.2.2 Flow Cytometry Optimisation.....	202
6.2.3 Modulation of ADAM17 Cellular Location by IL-1 β , IL-6 & TNF- α	206
6.2.4 siRNA Optimisation	209
6.2.5 Down-Regulation of ADAM17 expression.....	211
6.2.6 Proliferative Responses after ADAM17 Down-Regulation	217
6.2.7 Fractalkine Shedding after ADAM17 Down-Regulation	217
6.2.7 Summary of Results	220
6.3 Discussion	222
6.3.1 Fractalkine Shedding as an Indicator of ADAM17 Activity	222
6.4 Summary	224
7. General Discussion	225
7.1 <i>In Vitro</i> Model of Liver Cancer.....	226
7.2 ADAM17, ADAMTS-1, -4, -5 & TIMP3 Expression in Liver Cell Lines	227
7.2.1 ADAM17.....	227
7.2.2 ADAMTS-1, -4 & -5	229
7.2.3 TIMP3	231
7.3 Conclusions	232

7.4 Future Work	233
8. References	234
Appendix A – Publications & Presentations	259

List of Figures

- Figure 1.1 Microscopic structure of a hepatic lobule
- Figure 1.2 The metastatic cascade
- Figure 1.3 Gordon-Sweet's reticulin staining of CRC liver metastases with differing growth patterns
- Figure 1.4 Domain structures of ADAM and ADAMTS proteinases
- Figure 2.1 Colorimetric MTT based cellular proliferation assay method
- Figure 2.2 Western blotting method
- Figure 2.3 The sandwich ELISA method
- Figure 2.4 Immunocytochemistry method
- Figure 3.1 Cultured HepG2, HuH-7 and LX-2 cells imaged by phase contrast microscopy, and following ICC for the cell markers HSA and GFAP
- Figure 3.2 Viable HepG2 cell numbers following cytokine treatment
- Figure 3.3 Viable HuH-7 cell numbers following cytokine treatment
- Figure 3.4 Viable LX-2 cell numbers following cytokine treatment
- Figure 3.5 Comparison of untreated total RNA to DNase I treated total RNA by agarose gel electrophoresis
- Figure 3.6 Standard curve plots for β -actin, HPRT1, YWHAZ, ADAM17, ADAMTS-1, -4, -5 and TIMP3
- Figure 3.7 Amplification and melt curves for β -actin, HPRT1, YWHAZ, ADAM17, ADAMTS-1, -4, -5 and TIMP3
- Figure 3.8 Agarose gel electrophoresis of the qRT-PCR products for β -actin, HPRT1, YWHAZ, ADAM17, ADAMTS-1, -4, -5 and TIMP3
- Figure 3.9 ADAM17, ADAMTS-1, ADAMTS-4, ADAMTS-5 and TIMP3 mRNA expression in normal foetal liver samples compared to normal adult liver samples
- Figure 3.10 Agarose gel electrophoresis of DNase I treated RNA samples extracted from HepG2, HuH-7 and LX-2 cells following cytokine treatment
- Figure 3.11 ADAM17, ADAMTS-1, ADAMTS-4, ADAMTS-5 and TIMP3 mRNA expression in HepG2, HuH-7 and LX-2 cells
- Figure 3.12 ADAM17, ADAMTS-1, -4, -5 and TIMP3 gene expression in HepG2 cells following cytokine treatment
- Figure 3.13 ADAM17, ADAMTS-1, -4, -5 and TIMP3 gene expression in HuH-7 cells following cytokine treatment
- Figure 3.14 ADAM17, ADAMTS-1, -4, -5 and TIMP3 gene expression in LX-2 cells following cytokine treatment

- Figure 4.1 ADAM17 immunoprobed western blot of HepG2 and hCMEC/D3 protein samples following extraction with Tri Reagent or CelLytic
- Figure 4.2 Coomassie stain of HepG2, HuH-7 and LX-2 protein lysates following cytokine treatment
- Figure 4.3 ADAM17 immunoprobed western blot of HepG2 protein lysates following cytokine treatment and relative quantification of total ADAM17 protein
- Figure 4.4 ADAMTS-1 immunoprobed western blot of HepG2 protein lysates following cytokine treatment and its relative quantification
- Figure 4.5 ADAMTS-4 immunoprobed western blot of HepG2 protein lysates following cytokine treatment and its relative quantification
- Figure 4.6 ADAMTS-5 immunoprobed western blot of HepG2 protein lysates following cytokine treatment and its relative quantification
- Figure 4.7 TIMP3 immunoprobed western blot of HepG2 protein lysates following cytokine treatment and its relative quantification
- Figure 4.8 ADAM17 immunoprobed western blot of HuH-7 protein lysates following cytokine treatment and its relative quantification
- Figure 4.9 ADAMTS-1 immunoprobed western blot of HuH-7 protein lysates following cytokine treatment and its relative quantification
- Figure 4.10 ADAMTS-4 immunoprobed western blot of HuH-7 protein lysates following cytokine treatment and its relative quantification
- Figure 4.11 ADAMTS-5 immunoprobed western blot of HuH-7 protein lysates following cytokine treatment and its relative quantification
- Figure 4.12 TIMP3 immunoprobed western blot of HuH-7 protein lysates following cytokine treatment and its relative quantification
- Figure 4.13 ADAM17 immunoprobed western blot of LX-2 protein lysates following cytokine treatment and its relative quantification
- Figure 4.14 ADAMTS-1 immunoprobed western blot of LX-2 protein lysates following cytokine treatment and its relative quantification
- Figure 4.15 ADAMTS-4 immunoprobed western blot of LX-2 protein lysates following cytokine treatment and its relative quantification
- Figure 4.16 ADAMTS-5 immunoprobed western blot of LX-2 protein lysates following cytokine treatment and its relative quantification
- Figure 4.17 TIMP3 immunoprobed western blot of LX-2 protein lysates following cytokine treatment and its relative quantification
- Figure 5.1 Principle of confocal microscopy
- Figure 5.2 Negative controls for the ICC examination of cell surface and intracellular ADAM17, ADAMTS-1, -4, -5 and TIMP3 proteins in HepG2, HuH-7 and LX-2 cells.

- Figure 5.3 ICC examination of cell surface and intracellular ADAM17 under control and cytokine treatments in HepG2 cells
- Figure 5.4 ICC examination of cell surface and intracellular ADAMTS-1 under control and cytokine treatments in HepG2 cells
- Figure 5.5 ICC examination of cell surface and intracellular ADAMTS-4 under control and cytokine treatments in HepG2 cells
- Figure 5.6 ICC examination of cell surface and intracellular ADAMTS-5 under control and cytokine treatments in HepG2 cells
- Figure 5.7 ICC examination of cell surface and intracellular TIMP3 under control and cytokine treatments in HepG2 cells
- Figure 5.8 ICC examination of cell surface and intracellular ADAM17 under control and cytokine treatments in HuH-7 cells
- Figure 5.9 ICC examination of cell surface and intracellular ADAMTS-1 under control and cytokine treatments in HuH-7 cells
- Figure 5.10 ICC examination of cell surface and intracellular ADAMTS-4 under control and cytokine treatments in HuH-7 cells
- Figure 5.11 ICC examination of cell surface and intracellular ADAMTS-5 under control and cytokine treatments in HuH-7 cells
- Figure 5.12 ICC examination of cell surface and intracellular TIMP3 under control and cytokine treatments in HuH-7 cells
- Figure 5.13 ICC examination of cell surface and intracellular ADAM17 under control and cytokine treatments in LX-2 cells
- Figure 5.14 ICC examination of cell surface and intracellular ADAMTS-1 under control and cytokine treatments in LX-2 cells
- Figure 5.15 ICC examination of cell surface and intracellular ADAMTS-4 under control and cytokine treatments in LX-2 cells
- Figure 5.16 ICC examination of cell surface and intracellular ADAMTS-5 under control and cytokine treatments in LX-2 cells
- Figure 5.17 ICC examination of cell surface and intracellular TIMP3 under control and cytokine treatments in LX-2 cells
- Figure 6.1 Principle of flow cytometry
- Figure 6.2 The RNAi pathway
- Figure 6.3 Amount of fractalkine shed from HepG2 cells following cytokine treatment
- Figure 6.4 ICC examination of cell surface and intracellular fractalkine under control and cytokine treatments in HepG2 cells and its negative control.
- Figure 6.5 Optimisation of dissociation method for the detection of cell surface ADAM17 by flow cytometry in HepG2 cells - representative plots

- Figure 6.6 Optimisation of dissociation method for the detection of intracellular ADAM17 by flow cytometry in HepG2 cells - representative plots
- Figure 6.7 Quantification of cell surface and intracellular ADAM17 by flow cytometry in HepG2 cells
- Figure 6.8 ICC examination of siGLO transfected HepG2 cells and its negative control.
- Figure 6.9 Standard, amplification and melt curves for GAPDH and agarose gel electrophoresis of the qRT-PCR products for GAPDH
- Figure 6.10 GAPDH and ADAM17 mRNA expression in HepG2 cells following siRNA transfection
- Figure 6.11 ADAM17 and GAPDH immunoprobed western blots of HepG2 protein lysates following siRNA transfection and their relative
- Figure 6.12 ICC examination of cell surface and intracellular ADAM17 following siRNA transfection in HepG2 cells
- Figure 6.13 Viable HepG2 cell numbers following siRNA transfection
- Figure 6.14 Amount of fractalkine shed from HepG2 cells following siRNA transfection

List of Tables

Table 1.1	Cytokine categorisation, cell source and major functions
Table 1.2	Protease families involved in tumour invasion and metastases
Table 1.3	ADAM17 substrates
Table 1.4	Aberrant ADAM protein expression in human cancers and their functions
Table 1.5	Aberrant ADAMTS protein expression in human cancers and their functions
Table 2.1	Cell lines utilised in this study, and their appropriate complete culture medium composition
Table 2.2	qRT-PCR target gene information, including primer sequences
Table 2.3	qRT-PCR housekeeping gene information, including primer sequences
Table 2.4	Summary of primary and secondary antibodies used for western blotting
Table 2.5	Summary of primary and secondary antibodies used for ICC
Table 3.1	pH measurements of untreated and acetic acid-containing serum-free cell culture media
Table 3.2	qRT-PCR data comparing different reaction mix volumes
Table 3.3	Suitability of reference genes for the normalisation of qRT-PCR experiments
Table 3.4	geNorm analysis from the HepG2, HuH-7 and LX-2 experimental systems, indicating M-values for each independent experiment
Table 3.5	qRT-PCR primer efficiencies for each primer pair, including correlation coefficient, slope of line and cDNA source
Table 3.6	Summary of the results presented in Chapter 3
Table 4.1	Summary of the results presented in Chapter 4
Table 5.1	Summary of the results presented in Chapter 5
Table 6.1	siRNA transfection efficiencies for HepG2 cells
Table 6.2	Summary of the results presented in Chapter 6

List of Abbreviations

ADAM	A disintegrin and metalloproteinase
ADAMTS	A disintegrin and metalloproteinase with thrombospondin motifs
Ang II	Angiotensin II
ANOVA	Analysis of variance
APP	Amyloid precursor protein
β_2m	β_2 microglobulin
BCA	Bicinchoninic acid
BSA	Bovine serum albumin
CAMs	Cell adhesion molecules
CAM assay	Chick chorioallantoic membrane assay
cDNA	Complementary deoxyribonucleic acid
CHO	Chinese hamster ovary cells
CLSM	Confocal laser scanning microscopy
COX	Cyclooxygenase
CRH	Corticotropin-releasing hormone
CRC	Colorectal carcinoma
CSPGs	Chondroitin sulphate proteoglycans
CT	Cycle threshold
CX₃CL1	Fractalkine
DAPI	4', 6-diamidino-2-phenylindole
DD	Death domain
dH₂O	Distilled water
DMEM	Dulbecco's modified Eagle's medium
DNA	Deoxyribonucleic acid
DNase	Deoxyribonuclease
DPBS	Dulbecco's phosphate buffered saline
DR	Death receptor
ECs	Endothelial cells
ECM	Extracellular matrix
E^{ACT}	Efficiency to the power of delta cycle threshold
EDTA	Ethylenediaminetetraacetic acid
EGF	Epidermal growth factor
EGFR	Epidermal growth factor receptor
ELISA	Enzyme-linked immunosorbant assay
fasL	Fas ligand
fasR	Fas receptor

FCS	Foetal calf serum
FI	Fluorescence index
FSC	Forward scatter channel
g	Unit of force equal to the force exerted by gravity
GAGs	Glycosaminoglycans
GAPDH	Glyceraldehyde-3-phosphate dehydrogenase
GFAP	Glial fibrillary protein
gp130	Glycoprotein 130
HB-EGF	Heparin-binding epidermal growth factor-like growth factor
HCC	Hepatocellular carcinoma
HepG2	Well differentiated hepatocellular carcinoma cell line, human
HIF-α	Hypoxia-inducible factor alpha
HPRT1	Hypoxanthine phosphoribosyl-transferase 1
HRP	Horseradish peroxidase
HSCs	Hepatic stellate cells
HSPGs	Heparan sulphate proteoglycans
HuH-7	Well differentiated hepatocellular carcinoma cell line, human
ICC	Immunocytochemistry
IFNs	Interferons
Ig	Immunoglobulin
IL-1β	Interleukin-1 β
IL-6	Interleukin-6
IOD	Integrated optical density
JAK/STAT	Janus kinases/signal transducer and activators of transcription
kDa	Kilo Daltons
kPa	Kilo Pascals
LX-2	Activated hepatic stellate cell line, human
M	Molar
MEME	Minimal essential medium Eagle
MgCl₂	Magnesium chloride
MHC	Major histocompatibility complex
miRNA	Micro ribonucleic acid
mL	Millilitre
μL	Microlitre
MMP	Matrix metalloproteinase
mRNA	Messenger ribonucleic acid
MTT	3-(4,5-Dimethylthiazol-2-yl)-2,5-diphenyltetrazolium bromide
M-value	Measure of stability

N-CAM	Neural-cell adhesion molecule
NCM	Nitrocellulose membrane
NFκB	Nuclear factor- κ B
ng	Nanogram
NK	Natural killer
NPY	Neuropeptide Y
NTC	No template control
PCR	Polymerase chain reaction
PDAC	Pancreatic ductal adenocarcinoma
P-EGFR	Phosphorylated epidermal growth factor receptor
PFA	Paraformaldehyde
PGs	Proteoglycans
PI3-K	Phosphoinositide 3-kinase
qRT-PCR	Quantitative reverse transcriptase polymerase chain reaction
RISC	Ribonucleic acid-induced silencing complex
RNA	Ribonucleic acid
RNAi	Ribonucleic acid interference
RNase	Ribonuclease
RPL_{13A}	Ribosomal protein L13a
rRNA	Ribosomal ribonucleic acid
RT	Reverse transcription
sAPP	Soluble amyloid precursor protein
SDHA	Succinate dehydrogenase complex, subunit A
SDS	Sodium dodecyl sulphate
SDS-PAGE	Sodium dodecyl sulphate polyacrylamide gel electrophoresis
SH	Src homology domain-containing proteins
siRNA	Short interfering ribonucleic acid
sIL-6R	Soluble receptor of IL-6
SPSS	Statistical Package for Social Sciences
SSC	Side scattered channel
SVMP	Snake venom metalloproteinase
TACE	TNF alpha converting enzyme
TBS	Tris-buffered saline
TBS-T	Tris-buffered saline with Tween 20
TCA	Trichloroacetic acid
T_H2	T-helper 2 cells
TILs	Tumour infiltrating lymphocytes
TIMP	Tissue inhibitor of metalloproteinase

T_m	Melting temperature
TNF	Tumour necrosis factor
TNF-α	Tumour necrosis factor alpha
TNF-R	Tumour necrosis factor receptor
TSR	Thrombospondin repeats
Tween-20	Polyoxyethylene sorbitan monolaurate
UBC	Ubiquitin C
V	Volts
VEGF	Vascular endothelial growth factor
VEGFR	Vascular endothelial growth factor receptor
YWHAZ	Tyrosine 3-monooxygenase / tryptophan 5-monooxygenase activation protein, zeta polypeptide

Chapter 1

Introduction

1.1 Overview

With over 10.9 million new cases of cancer diagnosed per annum, 6.7 million cancer-related deaths and 24.6 million persons living worldwide with cancer (Parkin *et al*, 2005), understanding the intricate nature of this disease is more imperative than ever.

Hepatocellular carcinoma (HCC) is uncommon in the UK, with an incidence rate of approximately 3,100 per annum. Though with a 5-year patient survival rate of only 5.4%, there are approximately 3,050 liver cancer-related deaths in the UK each year (*UK liver cancer statistics*, 2009). Additionally, the liver is a common site of invasion by metastatic tumours, with nearly half (48.2%) arising from colorectal cancers (Kasper *et al*, 2005). Colorectal carcinoma (CRC) is the second most common cancer in the UK, and a major contributor to cancer-related deaths due to the high frequency of liver metastasis (Bird *et al*, 2006). The 5-year survival rate for CRC patients as a whole is only 26 to 46.7%; this is reduced to just 4% in patients with inoperable tumours (Shimada *et al*, 2006).

Both HCCs and CRCs are notoriously difficult to treat, with the only curative treatment being surgical resection, which is only feasible in about 20% of patients (Burke & Allen-Mersh, 1996). Consequently further investigations into primary liver tumours and colorectal liver metastases are crucial to the view of identifying a more widely available treatment (Shimada *et al*, 2006).

Many researchers have identified metalloproteinases as mediators of pathological cancer cell invasion, with much research concentrated on matrix metalloproteinases (MMPs). More recently though the aberrant expression of specific members of the adamalysin sub-family of metalloproteinases has been described in numerous human cancers, e.g. breast, lung, brain and gastric cancers (Turner *et al*, 2009), but as yet has not been examined in relation to liver cancers.

Relevant aspects of liver physiology and primary and metastatic liver pathology will be discussed before focussing on the adamalysin family of proteolytic enzymes, whose dysregulated expression may facilitate the invasion of the liver by tumour cells.

1.2 The Microscopic Structure of the Liver

1.2.1 Liver Lobules

The four lobes of the liver are subdivided into thousands of hexagonal lobules (Figure 1.1), with each of these functional units measuring 0.8 to 1.5 mm in diameter (Crawford *et al*, 1998). Hepatic lobules are composed of a number of specific cell types, arranged into precise structures that allow the correct functioning of the liver as a whole. Each individual lobule is comprised of a vast number of single cell thick, polyhedral

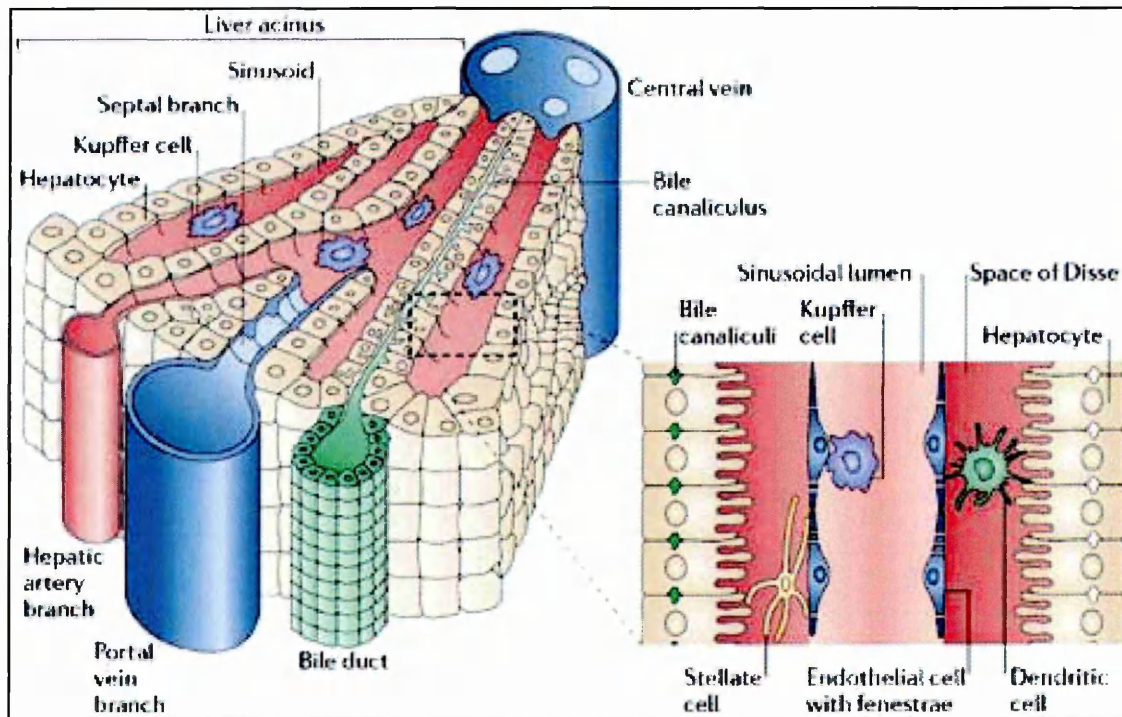


Figure 1.1: Microscopic structure of a hepatic lobule (Adams & Eksteen, 2006).

Functional hepatic lobules contain precise structures and cells that allow the liver to function correctly. At intrahepatic portal tracts (lobule corners), hepatic arteries terminate and portal veins form septal branches; both empty their contents into hepatic sinusoids. The fenestrated sinusoidal endothelium allows the flow of plasma into the space of Disse, which separates sinusoids from hepatocyte plates (see inset). Sinusoidal endothelium is interspersed with Kupffer cells that form part of the reticuloendothelial system. Single cell thick hepatocyte plates radiate from the central vein towards the edge of lobule, and have microvilli on their surface facing the sinusoidal endothelium and modifications forming bile canaliculi on their lateral faces. The space of Disse houses quiescent hepatic stellate cells (HSCs) that become fibrogenic upon liver damage.

hepatocyte columns, separated by the space of Disse, which radiate from the central vein (intrahepatic vein) to the edge of the lobule.

1.2.2 Hepatocytes

Hepatocytes are the main parenchymal cells of the liver, making up approximately 80% of the liver mass (Bowen, 1998). Consequently this cell type is involved in the majority of the liver's functions, including protein synthesis, protein storage, and detoxification, modification and excretion of endogenous and exogenous substances. Their cellular membrane abuts onto three compartments defined by morphological and functional features, i) the bile canaliculi, ii) the sinusoidal surface, and iii) the smooth intercellular fissure (Kuntz & Kuntz, 2005).

Approximately 12% of their lateral faces are modified to form bile canaliculi, which transport bile secreted by hepatocytes to bile ducts located at the intrahepatic portal tracts, then out of the liver (Bowen, 1998; Kuntz & Kuntz, 2005) (Figure 1.1 inset).

About 37% of the hepatocyte surface, that facing the sinusoidal endothelium, has an abundance of microvilli, providing a greater surface area in which to absorb the oxygen and nutrients present in the space of Disse ensuring their survival (Bowen, 1998; Kuntz & Kuntz, 2005).

The remaining 50% of the surface membrane of hepatocytes forms the smooth intercellular fissure, which is connected to the space of Disse. At this site the intercellular exchange between neighbouring hepatocytes is facilitated by gap junctions (maculae communicantes), whilst intermediate junctions (zonula adherens) and desmosomes (macula adherens) form the adhesion site between hepatocytes (Kuntz & Kuntz, 2005). Tight junctions (zonula occludens) are also present to prevent bile entering these fissures from the bile canalicula, allowing only the exchange of water and cations at these sites.

1.2.3 Endothelial Cells (ECs)

Hepatocyte plates are separated by EC-lined hepatic sinusoids, which are low pressure vascular channels supported by a reticulin network (collagen type III) (Sakakibara *et al*, 1985). These sinusoidal capillaries differ structurally from capillaries of other organs by the presence of small interspersed pores known collectively as the sieve plate, and larger pores known as fenestrae (Kuntz & Kuntz, 2005).

The fenestrated sinusoidal endothelium has no basement membrane and therefore allows the virtually unimpeded flow of nutrient-rich blood plasma from the septal branches of the hepatic portal vein into the space of Disse situated between the sinusoidal endothelium and hepatocytes (Adams & Eksteen, 2006). It functions to filter blood components, and regulate the exchange of fluid and material between the

sinusoids and hepatocytes (Kuntz & Kuntz, 2005). The plasma collecting in the space of Disse then flows back towards the intrahepatic portal tracts, and collects in lymphatic vessels to form a large fraction of the body's lymph (Bowen, 2003). Oxygen is delivered to hepatocytes in the same manner via the terminal branches of the hepatic artery (Adams & Eksteen, 2006).

1.2.4 Hepatic Stellate Cells (HSCs)

HSCs, also known as Ito cells, are pericytes resident in the space of Disse. Each cell has several protrusions from their cell body that wrap around the sinusoids. In their quiescent state their function is unclear, but lipid droplets in their cell body provide a storage facility for vitamin A (Iredale, 2001). Additionally, quiescent HSCs may act as liver-resident antigen-presenting cells that present lipid antigens to and stimulate the proliferation of natural killer (NK) cells (Winau *et al*, 2007).

When the liver is damaged, HSCs are converted into an activated state associated with the adoption of a myofibroblast-like phenotype; they lose their vitamin A and begin to secrete large amounts of interstitial collagens I, III (Benyon & Iredale, 2000) and IV, fibronectin and laminin (Kuntz & Kuntz, 2005). The over-expression of these extracellular matrix (ECM) components represents the final common pathway of the wound-healing response of the liver (Friedman, 1993). However, the continued secretion of collagens by HSCs has a detrimental effect upon the liver by contributing to pathological intralobular fibrosis and liver cirrhosis (Iredale, 2001).

The conversion of quiescent HSCs into contractile, fibrogenic HSCs capable of directed migration involves changes in their phenotypic profiles, characterised by the differing expression patterns of certain intracellular markers. Classically, α -smooth muscle actin was used as a marker for HSC activation in humans, but neural/neuroendocrine features also denote the conversion of quiescent to activated HSCs, including the expression of neural-cell adhesion molecule (N-CAM) and glial fibrillary protein (GFAP) (Morini *et al*, 2005).

Normally upon activation HSCs (together with activated Kupffer cells) begin to produce and secrete a number of metalloproteinases (Emonard *et al*, 1990), in particular MMP-1, -2 and its activating protease MMP-14 (Milani *et al*, 1992). Consequently these cell types have the ability to degrade interstitial collagens present in normal and fibrillar collagen matrix (Aimes & Quigley, 1995; Ohuchi *et al*, 1997) and balance the amount of neomatrix laid down in the healing process with degradation of the existing matrix.

When liver fibrosis occurs and as it progresses, HSCs also release tissue inhibitors of metalloproteinase (TIMP) 1 and 2, which act to decrease the interstitial collagenase activity of MMP-1 and -2 (Iredale, 2001). Further to this, HSC activation results in the

entry of HSCs into the growth cycle (Friedman, 1993). Consequently there is an increase in overall numbers of activated HSCs actively producing neomatrix, whilst simultaneously preventing matrix degradation through TIMP expression (Iredale, 2001).

1.2.5 Kupffer Cells

Numerous Kupffer cells, specialised macrophages resident only in the liver, populate the hepatic sinusoids and form part of the reticuloendothelial system, also known as the mononuclear phagocyte system (Haubrich, 2004). These cells are integral to the liver's primary function of cleansing the blood of foreign materials and toxic substances (Wheeler, 2003). Kupffer cells exist in a resting state, but become activated in the presence of foreign materials and begin to secrete an assortment of pro-inflammatory cytokines (Section 1.5), including tumour necrosis factor alpha (TNF- α) and several types of interleukin (IL). These cytokines regulate the functions of other immunological cells required to elicit an inflammatory response, which ultimately results in the removal of the offending toxic or foreign molecules and initiates the healing process (Wheeler, 2003).

Another role of Kupffer cells is the recycling of old red blood cells that are no longer functional. Kupffer cells break down the red blood cell by phagocytic action and split the haemoglobin molecule. The globin molecules are reutilised and the iron containing portion, haem, is further broken down into iron that is reused and bilirubin, which is excreted into bile for removal from the body (Szymanska & Schmidt-Pospula, 1979).

Activated Kupffer cells, like activated HSCs, produce and secrete MMPs (Emonard *et al*, 1990), and as such are involved in the degradation of liver ECM.

1.2.6 Pit Cells

Pit cells are a unique population of NK cells resident in hepatic sinusoids, with morphological, functional and immunophenotypical differences from blood NK cells. They comprise 43% of liver-associated lymphocytes, together with T-lymphocytes (30%) and B-lymphocytes (3%). They often adhere to ECs lining the sinusoid, and have direct contact with blood. The pseudopodia of pit cells are able to penetrate the fenestrated sinusoidal endothelium, enter the space of Disse and make contact with the microvilli of hepatocytes. This strategic location of pit cells means they represent a first line cellular defence against metastasising colon cancer cells (Luo *et al*, 2000).

Pit cells contain large granules and rod-cored vesicles, and possess spontaneous cytotoxic activity against tumour and foreign cell types, as well as necrosed cells (Kuntz & Kuntz, 2005); this activity can be augmented by several cytokines, including IL-2 (Robertson & Ritz, 1990). Additionally pit cells preferentially kill cells lacking major

histocompatibility complex (MHC) class I molecules, and can mediate antibody-dependent cellular cytotoxicity (ADCC) via CD16 (Luo *et al*, 2000).

1.2.7 Intrahepatic Portal Tracts

The intrahepatic portal tract located at the corner of each hexagonal lobule completes the lobular structure. These areas are a complex feature composed of branches of the hepatic portal vein, hepatic artery, bile ducts and nerve fibres.

1.2.8 Liver Extracellular Matrix (ECM)

Fibrous tissue within the liver is quantitatively very limited (~3%), however the liver ECM is of major importance both in liver physiology and pathology (Bedossa & Paradis, 2003). In addition to a network of connective fibrous tissue surrounding the liver, termed Glisson's capsule, ECM is restricted in normal liver to intrahepatic portal tracts, sinusoid walls (reticulin network) and central veins, and acts as part of the frontier between the blood flow and parenchyma (Bedossa & Paradis, 2003).

Hepatic ECM is composed of two major components, proteins and proteoglycans (PGs; Section 1.6.7), which provide not only structural support to the organ, but also modulate several major biological processes (Selden *et al*, 1999). The protein portion of hepatic ECM is composed of several molecular forms of collagen, predominantly types I, III, IV (Liu *et al*, 2006a), and V (Bedossa & Paradis, 2003). Collagen types I, III and V, which are fibrillar collagens, are mainly found in the intrahepatic portal tract and central vein wall (Martinez-Hernandez, 1984). In addition to these collagens, there are also non-collagenous components, such as fibrin, elastin, fibronectins, laminins and nidogens.

The reticulin network provides hepatic sinusoids with structural integrity by forming a low density, basement membrane-like material along the sinusoid wall (Martinez-Hernandez, 1984). Reticulin or reticular fibres is a histological term used to describe the scleroprotein fibril in liver ECM composed of collagen type III fibres. These fibres are often associated with other types of collagen, glycoproteins, PGs and glycosaminoglycans (GAGs) (Ushiki, 2002). Reticulin differs from regular collagenous fibres principally by the presence of a higher concentration of galactose, glucose, mannose and fructose sugars. Reticulin has a regular pattern in normal liver pathology, however when the liver becomes fibrosed this pattern is often disturbed.

The other major components of liver ECM, PGs, are a heterogeneous group of proteins containing GAG side chains (Selden *et al*, 1999). These highly glycosylated proteins form large complexes either with each other, hyaluronans (a non-sulphated GAG) or fibrous matrix proteins, such as collagen. These complexes regulate the movement of

molecules through the ECM, affect the activity and stability of proteins and signalling molecules within the ECM (Alberts *et al*, 2008) and also, due to the hyaluronan component, modulate cell proliferation and migration (Stern, 2004).

Although the main function of ECM remains the mechanical coherence and resistance of the liver, as is the case in other tissues, liver ECM also affects the function and morphology of hepatocytes and other liver sub-populations (Selden *et al*, 1999) and modulates the processes of cell proliferation, migration, differentiation, signalling, and gene expression. It facilitates these important processes by sequestering numerous growth factors, hormones, enzymes, and cytokines in their inactive forms, which upon treatment become activated and deliver messages that modify the cellular microenvironment (Bedossa & Paradis, 2003).

The correct quality and quantity of hepatic ECM is essential for the proper functioning of the liver. Even a slight alteration in the liver ECM will rapidly affect the structure and function of the liver. Major alterations in both the quality and quantity of hepatic ECM occur during the development and progression of liver fibrosis, with activated HSCs producing the majority of the fibrotic neomatrix. The process of liver fibrosis, even in its early stages, rapidly affects the structure and functions of the liver, due to the modification of ECM at the interface between blood flow and epithelial compartment (Bedossa & Paradis, 2003).

1.3 Tumour Invasion and Metastasis

The progression from a benign non-invasive tumour, which predominantly has a single clonal origin (Ki *et al*, 2007), to a malignant neoplasm capable of invading neighbouring tissues is a complex and multi-step process involving the generation of a heterogeneous population of tumour cells with characteristic properties (Turner *et al*, 2009; Gutman & Fidler, 1995). These hallmarks of cancer cells include the ability to proliferate independently of growth/anti-growth signals, to stimulate sustained angiogenesis, to degrade surrounding extracellular matrix, to modulate cellular adhesion and migration capabilities, and evade apoptosis (Hanahan & Weinberg, 2000; Thompson & Price, 2002).

The destructive processes involved in cell invasion and metastasis are not exclusive to cancer progression, but occur routinely during wound repair, vasculogenesis and axon outgrowth (Chang & Werb, 2001). However, these processes are less controlled in cancer cells. Invading malignant cells must interact with basement membranes or the ECM during dissemination. This involves three key processes: i) attachment of malignant cells to ECM, ii) proteolytic breakdown of ECM, and iii) migration of invading cells through damaged ECM (Ray & Stetler-Stevenson, 1994). The proteolysis events

orchestrating the destructive process of normal and non-malignant pathologies are controlled and self-limiting; those involved in tumour invasion appear to occur perpetually, with a loss of controlling mechanisms, which can result in the formation of secondary tumours (Chang & Werb, 2001; Duffy, 1992).

Malignant cells cross the basement membrane at least three times during metastasis to: i) escape their primary site, ii) infiltrate the vascular system, and iii) extravasate from the bloodstream into a target organ (Figure 1.2) (Ray & Stetler-Stevenson, 1994; Duffy, 1992). This is mediated by a number of different proteolytic enzymes, which could be released from the invading tumour (Duffy, 1992), stromal fibroblasts surrounding the tumour and localised inflammatory cells (macrophages and neutrophils) (Foda & Zucker, 2001). The highest activity levels of proteases involved in cancer dissemination are found at the invading front of the tumour, where degradation of normal tissue is occurring (Duffy, 1992).

1.4 Liver Cancer

1.4.1 HCC Incidence and Epidemiology

There are two main types of primary liver cancer, HCC and cholangiocarcinoma (bile duct cancer), with the latter accounting for only 10-25% of all primary liver cancers registered in Europe (Parkin *et al*, 2005). They have a combined incidence rate of 10 per 100,000 population in Europe (Bosch *et al*, 2004), which equates to ~50,000 new cases of primary liver cancer per annum, ~3100 of which occurred in the UK (*UK liver cancer statistics*, 2009). Unfortunately, the incidence of liver cancer is steadily increasing in many developed countries, including the UK (Bosch *et al*, 2004).

The cause of primary liver cancer is currently unknown; however there are a number of hepatic diseases that predispose the liver to tumour development including cirrhosis (90-95% of UK cases), hepatitis B virus or hepatitis C virus infection (>75% of cases worldwide), and some hereditary conditions e.g. haemochromatosis (Parkin *et al*, 2005; Ryder, 2003). So it is not surprising that in the Western world advancing age is also a risk factor of HCC development, which may reflect the long term nature of these underlying liver diseases (Ryder, 2003). The prevalence of liver cancer is also higher in males than females, with a ratio of 1.9:1 in Europe (Bosch *et al*, 2004).

The prognosis of this malignancy is poor, despite advances in the detection and diagnosis of liver cancer. The 5-year survival rate of primary liver cancer is 6.5% in Europe as a whole (Bosch *et al*, 2004), and slightly lower in the UK (5.4%), with ~3,050 liver cancer-related deaths in the UK each year (*UK liver cancer statistics*, 2009).

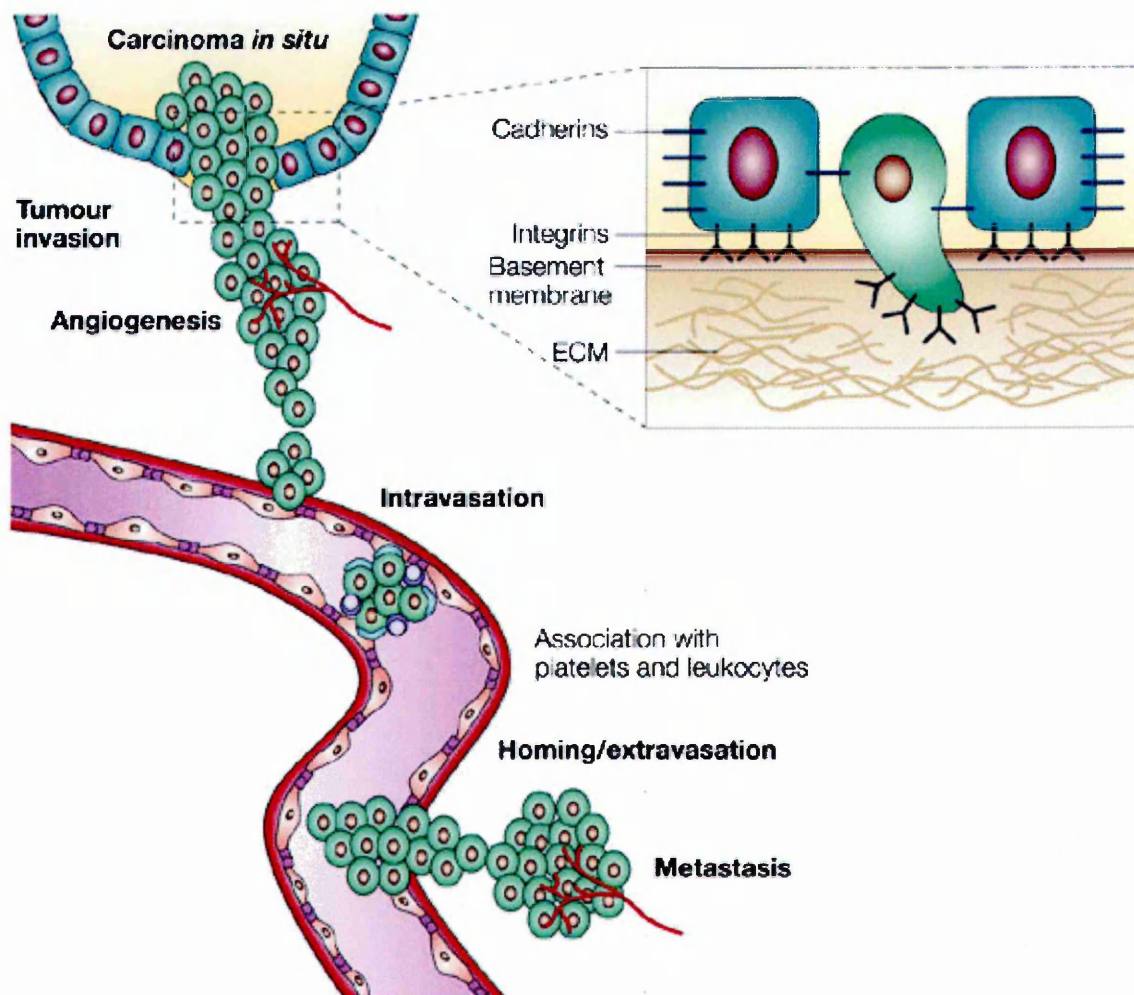


Figure 1.2: The metastatic cascade (Guo & Giancotti, 2004).

Malignant tumour cells detached from the tumour mass, penetrate the basement membrane, and invade the surrounding ECM. These cells can then enter the bloodstream via intravasation. Many malignant cells are eliminated at this stage by the action of immune cells. Once the target organ has been reached, tumour cells adhere to the endothelium of the blood vessel, extravasate into the target organ, and undergo proliferation to form metastatic tumours.

1.4.2 CRC Liver Metastases Incidence and Epidemiology

CRC is the third most common cancer worldwide, and the second most common cause of cancer death in the UK, with an incidence of approximately 57 per 100,000 population (Bird *et al*, 2006), which equates to approximately 28,000 new cases per annum in the UK (Burke & Allen-Mersh, 1996).

The prevalence of CRC is higher in males than females, with 60% of cases arising in males (Bird *et al*, 2006). These tumours primarily affect people of advanced age, with over 50% occurring in patients over the age of 70 years (McMillan & McArdle, 2007). Recent advances in the diagnosis and localised treatment of early stage CRC have resulted in the lives of many patients being saved (Yamasaki *et al*, 2007). However, the prognosis for patients with advanced CRC is still poor (Ki *et al*, 2007).

The prognosis and overall survival rate of a CRC patient is ultimately determined by tumour burden and the dissemination of the primary tumour throughout the patient, particularly to the liver. At the time of CRC diagnosis, 25% of patients have detectable liver metastases (synchronous metastases), and a further 25% will develop liver metastases during the course of their disease (metachronous metastases) (Bird *et al*, 2006). This liver metastasis is the major cause of death in CRC patients (Ki *et al*, 2007).

If no treatment was given to CRC patients with liver metastases the majority would not survive beyond 8 - 12 months, however prognosis is improved with the correct treatment. Treatment of patients with unilobular metastases extends their median survival to 24 months, whilst the treatment of patients with bilobular disease extends their median survival to 18 months. The 5-year survival rate of this malignancy is between 26 and 46.7% (Shimada *et al*, 2006).

1.4.3 CRC Progression to the Liver

The predilection for liver metastases in the course of CRC is thought to be due to the vast amount of blood flowing to the liver from the colon via the hepatic portal vein (Burke & Allen-Mersh, 1996). This volume of blood may contain breakaway tumour cells with newly acquired metastatic potential, providing them with the potential to permeate the entire organ via the extensive branching of the hepatic portal vein into intrahepatic portal tracts, which extend throughout the liver.

However, the mere presence of malignant cells is not enough to permit the colonisation of the liver; the establishment of nascent metastases requires the adhesion of circulating tumour cells to hepatic ECs within the hepatic sinusoid, followed by their growth and extravasation into the liver parenchyma (Bird *et al*, 2006). The metastatic potential of colorectal cells is linked to cell adhesion molecules (CAMs). Ordinarily, cadherin-catenin complexes present in adherin junctions anchor cells in position; a

down-regulation of these complexes can facilitate tumour cell detachment from the primary site. The subsequent over-expression of integrins and selectins may support the progression and development of tumours in distant tissues via the regulation of cell motility and angiogenesis (Paschos *et al*, 2009).

Heparin-like heparan sulphate PGs (HSPGs) present in the liver ECM are known to affect the clonal growth efficiency of hepatoma cell lines (Doerr *et al*, 1989). This may suggest that organ-specific PGs and their GAG side chains may be responsible for the regulation of autocrine growth factors in metastatic cells (Zvibel *et al*, 1991). In colorectal tumours, the EGF family of growth factors and their receptors play an essential role in the regulation of cellular proliferation, and the number of EGF receptors on colon cancer cells correlates with increased metastasis to the liver (Zvibel *et al*, 1991; Radinsky, 1995).

1.4.4 Liver Tumour Pathology

Liver metastases originating from colorectal adenocarcinomas can be divided histologically into three distinct sub-groups dependent upon their growth pattern, namely desmoplastic (42%), replacement (12%) and pushing (46%) (Figure 1.3). Usually only one growth pattern is observed in a single liver metastasis, and in patients with more than one metastasis, all metastases have the same growth pattern (Vermeulen *et al*, 2001). These differing growth patterns of liver tumours were initially described by Nakashima *et al* (1983) in relation to primary HCC.

Links between the growth patterns of primary CRCs and their liver metastases have since been made, such that primary CRCs with a pushing growth pattern are more likely to form liver metastases with a desmoplastic growth pattern ($P < 0.001$) and primary CRCs with an infiltrative growth pattern are more likely to form non-capsulated metastases ($P < 0.001$) (Rajaganeshan *et al*, 2007).

The characteristic features of each growth pattern are easily observed at the tumour-liver parenchyma interface by the analysis of two histological stains, haematoxylin and eosin (H & E) -stain, and Gordon-Sweet's reticulin-stain (Figure 1.3) (Vermeulen *et al*, 2001; Illemann *et al*, 2009).

The growth pattern of liver metastases can be used as a prognostic indicator of the outcome of disease (Okano *et al*, 2000). This may be due to the differing degrees of angiogenesis within tumours of different growth patterns, and/or the differing levels of sinusoidal co-option (Vermeulen *et al*, 2001). However, for all metastatic growth patterns there is an inverse correlation between microvessel density and tumour cell apoptosis, such that the higher the microvessel density, the less tumour cells undergo apoptosis, and the poorer the outcome for the patient (Rajaganeshan *et al*, 2007). It is

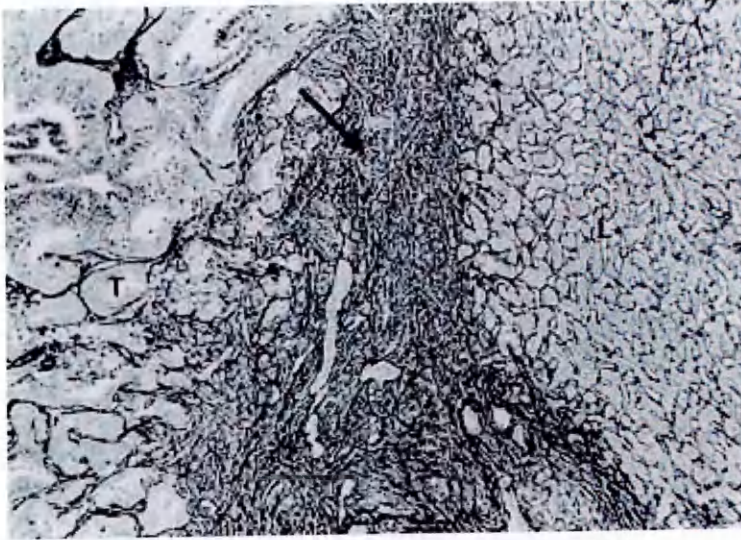
Figure 1.3: Gordon-Sweet's reticulin staining of CRC liver metastases with differing growth patterns (Vermeulen *et al*, 2001).

A) Demoplastic growth pattern. The arrow indicates the fibrotic capsule separating the tumour tissue (T) from the liver parenchyma (L). Liver architecture is not preserved in the metastasis.

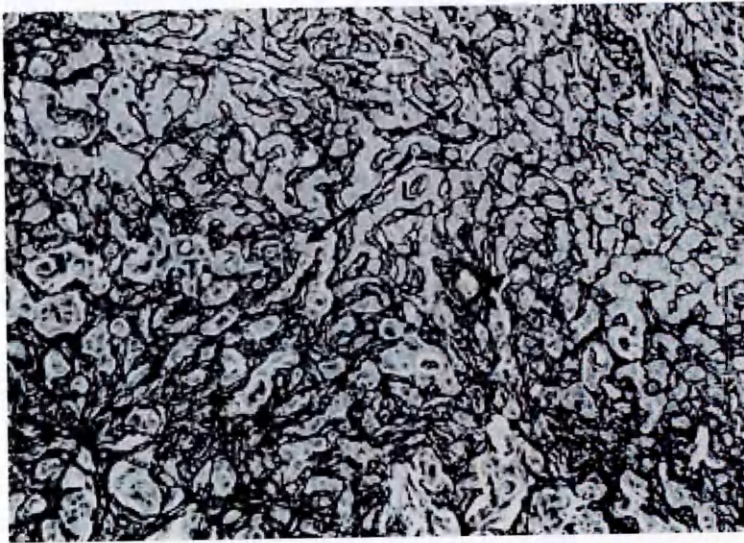
B) Replacement growth pattern. The arrows indicate the interface between the tumour tissue (T) and the liver parenchyma (L). Liver architecture is preserved in the metastasis, but there is a slight broadening of the cell plates and an increase in number of reticulin fibres separating the cell plates.

C) Pushing growth pattern. The arrows indicate the interface between the tumour tissue (T) and the liver parenchyma (L). The cell plates run in parallel with the circumference of the metastasis. Liver architecture is not preserved in the metastasis.

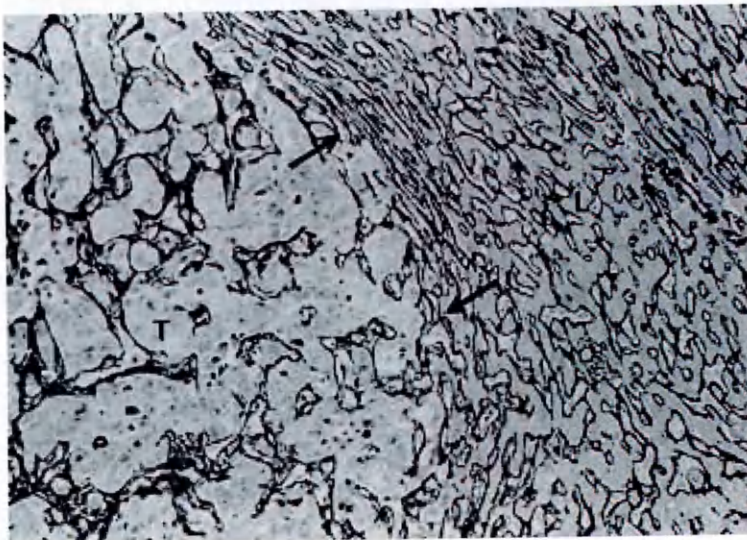
A)



B)



C)



not known if this also applies to HCCs.

Desmoplastic Growth Pattern

Liver metastases demonstrating a desmoplastic or encapsulated growth pattern are characterised by the accumulation of fibrillar collagens at the metastasis periphery (Figure 1.3A) (Conti *et al*, 2008). There is no contact between tumour cells and hepatocytes, as this dense reticulin positive desmoplastic stroma forms a capsule surrounding the tumour (Vermeulen *et al*, 2001; Illemann *et al*, 2009).

Present throughout this collagen-rich capsule is a dense lymphocytic infiltrate, indicating that metastatic CRC cells of this phenotype provoke an inflammatory response within the liver. Hence, the desmoplastic reaction may arise due to the classical wound healing response of activated HSCs (Conti *et al*, 2008). Interestingly, the dysregulated deposition of interstitial collagens within the desmoplastic capsule, particularly collagen type I, enhances CRC cell growth. Bile ducts and capillaries are also present in the rim of the newly formed stroma (Vermeulen *et al*, 2001).

As the tumour expands, liver cells at the tumour-liver interface collapse and disappear (Illemann *et al*, 2009), and consequently the liver architecture and reticulin pattern are not conserved within the metastasis (Vermeulen *et al*, 2001). Liver ECM breakdown by proteolytic enzymes may be essential to for the growth and expansion of liver metastases with a desmoplastic growth pattern (Illemann *et al*, 2009).

Liver metastases with this growth pattern are generally well-differentiated, and therefore classified as low grade tumours.

Replacement Growth Pattern

This category of CRC liver metastasis is characterised by the replacement of hepatocytes by tumour cells within the liver cell plates, resulting in the intimate cell-cell contact of tumour cells and hepatocytes (Figure 1.3B). The reticulin network of the liver parenchyma is conserved in this growth pattern, but a slight broadening of liver cell plates can occur, which is probably due to the slight increase in the number of reticulin fibres (Vermeulen *et al*, 2001).

No inflammation is evident at the periphery of replacement growth metastases, and there is an absence of desmoplasia in this location (Vermeulen *et al*, 2001; Stessels *et al*, 2004). However, due to minimal angiogenesis, characterised by a high tumour cell to EC proliferation ratio (Stessels *et al*, 2004), fibrosis and necrosis is frequently present at the centre of the metastasis (Vermeulen *et al*, 2001). Occasionally small glands are formed at the tumour-parenchyma interface, consisting of tumour cells at one side of the lumen and of liver cells at the other side (Vermeulen *et al*, 2001).

Liver metastases with this growth pattern generally have an intermediate degree of differentiation, and therefore classified as intermediate grade tumours.

Pushing Growth Pattern

Liver metastases with a pushing or sinusoidal growth pattern are characterised at the tumour-liver parenchyma interface by hepatocyte plates being pushed aside and made to run in parallel with the outer edge of the tumour (Figure 1.3C). Due to this, the liver architecture and consequently the reticulin pattern of the liver parenchyma are not conserved within these liver metastases (Vermeulen *et al*, 2001).

There is no accumulation of reticulin or desmoplastic stroma formation at the metastasis periphery, but a thin layer of reticulin fibres is present that acts to separate hepatocytes from tumour cells. A mild inflammatory infiltrate is nearly always present at the tumour-liver parenchyma interface (Vermeulen *et al*, 2001).

HCC cells with this expansion pattern grow in an infiltrating manner into the sinusoids at the tumour periphery, and compress the liver cell plates and eventually take their place (Nakashima *et al*, 1983). If liver metastases with a pushing growth pattern grow in the same manner, matrix degrading activity may not be required as they could use the pre-existing cavity of the sinusoid (Illemann *et al*, 2009).

Liver metastases with this growth pattern are generally anaplastic, and therefore classified as high grade tumours, and contain three times more proliferating ECs than desmoplastic and replacement patterns. They also show a strong correlation between EC and tumour cell proliferation, which is not evident in the other growth patterns (Vermeulen *et al*, 2001).

1.5 Cytokines

Cytokines are a diverse group of glycoproteins and low molecular weight peptides that predominantly act as extracellular messengers between cells (Dunlop & Campbell, 2000). They have many important roles within the human body, such as stimulating and regulating host immune responses to pathogens, activating signal transduction pathways that regulate cell growth, differentiation and cell death, and wound repair and healing. These processes can be hi-jacked by tumour cells to aid their growth and survival.

Cytokines are categorised to reflect their originally identified function, e.g. interferons (IFNs) were first identified by their ability to "interfere" with viral replication in host cells. However, due to the vast array of cytokines with differing origins and functions, it is simpler to group them according to their structure (Table 1.1) (Janeway *et al*, 2005).

Table 1.1: Cytokine categorisation, cell source and major functions.*

Family	Cytokine	Producer cells	Actions
Interferon (IFN)	IFN- α	Leukocytes, dendritic cells	Anti-viral; increased expression of MHC class I
	IFN- β	Fibroblasts	Anti-viral; increased expression of MHC class I
	IFN- γ	T-cells, NK cells	Anti-viral; increased expression of MHC class I & II and antigen processing components; macrophage activation; Immunoglobulin (Ig) class switching; suppression of T-helper 2 cells (T_H2)
Tumour necrosis factor (TNF family)	TNF- α (cachectin)	Macrophages, NK cells, T-cells	Local inflammation mediator, endothelial activation, induces other cytokines, increased expression of MHC class I
	TNF- β	T-cells, B-cells	Killing; endothelial activation
	CD40 ligand (CD40L)	T-cells, mast cells	B-cell activation; class switching
	Trail	T-cells, monocytes	Apoptosis of activated T-cells and tumour cells
Hematopoietins	IL-2 (T-cell growth factor)	T-cells	T-cell proliferation; NK cell activation
	IL-4 (B-cell growth factor)	T-cells, mast cells, basophils	B-cell activation; IgE switch; induces differentiation into CD4 T_H2 cells
	IL-6 (IFN- β_2)	T-cells, macrophages, ECs	T- & B-cell growth & differentiation, acute phase protein production, fever

*This table is not extensive and does not list all cytokines within families, nor does it show all of their functions.

Table 1.1 (continued): Cytokine categorisation, cell source and major functions.*

Family	Cytokine	Producer cells	Actions
Hematopoietins	LIF (leukaemia inhibitory factor)	Bone marrow stroma, fibroblasts	Maintains embryonic stem cells
Interleukin-10 (IL-10)	IL-10 (cytokine synthesis inhibitory factor)	T-cells, macrophages	Potent suppressant of macrophage functions
	IL-19	Monocytes	Induces IL-6 & TNF- α expression by monocytes
	IL-24 (MDA7)	Monocytes, T-cells	Inhibits tumour growth
Interleukin-12 (IL-12)	IL-12 (NK-cell stimulatory factor)	Macrophage, dendritic cells	Activates NK cells; induces CD4 T-cell differentiation into T _H 1-like cells
	IL-23	Dendritic cells	Induces proliferation of memory T-cells; increased IFN- γ production
Unassigned	TGF- β	Chondrocytes, monocytes, T-cells	Inhibits cell growth; anti-inflammatory; induces switch to IgA production, stimulates collagen & PG synthesis
	IL-1 α & IL-1 β	Macrophages, epithelial cells	Fever; T-cell activation; macrophage activation
	MIF (macrophage migration inhibitory factor)	T-cells; pituitary cells	Inhibits macrophage migration; stimulates macrophage activation; induces steroid resistance

*This table is not extensive and does not list all cytokines within families, nor does it show all of their functions.

Most cytokines are produced and secreted transiently by a range of cell types in response to stimuli, such as pathological and cellular stresses. Cytokines can either be secreted in their active forms or exist as a latent complex that requires activation. The tight regulatory control over cytokine release and activation ensures their presence only when required, thus preventing tissue damage.

Cytokines act on a range of target cells in a paracrine or autocrine manner via specific high-affinity cell surface receptors, making them potent biological molecules. Cytokine receptors are linked to intracellular second messenger signalling pathways (Dunlop & Campbell, 2000), which result in altered gene expression in the target cell. The actions of cytokines are redundant, multiple and pleiotropic, and as such understanding their integrated functioning is not easily achieved.

1.5.1 Interleukin-1 β (IL-1 β), Interleukin-6 (IL-6) and Tumour Necrosis Factor- α (TNF- α) in Cancer

There is growing evidence that inflammation is a factor in the development of cancer (Jung *et al*, 2003), with many pro-inflammatory cytokines being implicated in malignancies. Cytokines present in the tumour microenvironment have been shown to play a major role in the promotion of tumour growth by promoting cellular proliferation whilst attenuating apoptosis, and in the promotion of angiogenesis and tumour dissemination (Dranoff, 2004). However, there is no single cytokine common to all cancer patients (Dunlop & Campbell, 2000).

All cells normally present within the liver have the capacity to produce cytokines, but Kupffer cells are usually responsible for the initial induction of early-response cytokines (Simpson *et al*, 1997). Once cytokine production is induced, be it by Kupffer cells or malignant cells themselves, other cells in the liver can be stimulated to produce further cytokines resulting in an amplification of the inflammatory response (Simpson *et al*, 1997).

In the liver, IL-6 is released in response to TNF- α , usually following hepatic injury or surgery (Zimmers *et al*, 2003), this can increase hepatocyte proliferation which may contribute to HCC and metastatic liver tumour development (Sander *et al*, 2007). Further to this, many CRC patients have elevated serum and peritoneal concentrations of three pro-inflammatory cytokines, IL-1 β , IL-6 and TNF- α (Whitworth *et al*, 2006). The production of these cytokines is increased, both locally and systemically, after the surgical treatment of cancer patients (Kuninaka *et al*, 2000). The production of IL-1 β and TNF- α by Kupffer cells within the liver can also be induced by carcinoembryonic antigen (CEA), a tumour marker elevated in approximately 70% of patients with CRC and CRC liver metastases (Burke & Allen-Mersh, 1996, Simpson *et al*, 1997).

IL-1 β

IL-1 β is elevated in a number of cancers, including vulva, endometrium, prostate (Dunlop & Campbell, 2000) and breast cancers (Reed *et al*, 2009) where it has been linked to tumour growth, angiogenesis and invasiveness (Jung *et al*, 2003).

Jung *et al* (2003) have determined that IL-1 β induces a stabilised hypoxia-inducible factor- α (HIF- α) protein in normoxia, which stimulates vascular endothelial growth factor (VEGF) production and promotes angiogenesis. In a lung epithelial cell line (A549), IL-1 β treatment activates the phosphoinositide 3-kinase (PI3-K) / Akt pathway, which in turn activates a nuclear factor- κ B (NF κ B) dependent pathway and induces cyclooxygenase-2 (COX-2) production. COX-2 then mediates HIF-1 α up-regulation, which induces VEGF production, and via its interaction with its transmembrane tyrosine kinase receptor on ECs lining the lumen of blood vessels, promotes angiogenesis.

COX-2 is also known to initiate colon cancer progression, with IL-1 β treatment of a colon cancer cell line (CaCo-2) resulting in COX-2 induction and HIF-1 α elevation by the same mechanism as in A549 cells (Jung *et al*, 2003).

Epidemiological studies have suggested that the risk of development of certain cancers, including breast, colon, stomach, lung and oesophagus cancers, is reduced by the long-term administration of aspirin and non-steroidal anti-inflammatory drugs (NSAIDs) (Reed *et al*, 2009; Coussens & Werb, 2001). The chemopreventative effect of these drugs is related to their ability to inhibit COX-2, which converts arachidonic acid to prostaglandins to induce inflammatory reactions in damaged tissues (Coussens & Werb, 2001).

Cytokines may also be involved in tumour cell migration. IL-1 β produced by tumour cells promotes tumour cell adhesion at metastatic sites by increasing the intercellular adhesion molecule 1 (ICAM-1) from ECs to facilitate tumour cell adhesion (Lai *et al*, 1993). TNF- α has also been linked to the induction of adhesion molecules and the facilitation of metastatic cell adhesion (Simpson *et al*, 1997).

Many advanced stage cancer patients (90%) suffer from cachexia syndrome, which is associated with more than 20% of cancer-related deaths (Tisdale, 2002). Cachexia is a clinical consequence of a chronic, systemic inflammatory response, associated with pro-inflammatory cytokines including IL-1 β , IL-6 and TNF- α . This condition is characterised by abnormally low weight resulting from the depletion of host adipose tissue and skeletal muscle mass, coupled with the malnutrition of the patient due to the induction of anorexia and/or decreased food intake.

Increased IL-1 β serum levels are associated with the anorexic component of cachexia. IL-1 β induces the production of corticotropin-releasing hormone (CRH) in the hypothalamus, whilst suppressing the actions of the appetite stimulant neuropeptide Y (NPY) by stimulating expression of the hormone leptin, which blocks NPY release. Hence IL-1 β induces a negative feedback effect disrupting the NPY signalling pathway, resulting in the long-term inhibition of food intake (Tisdale, 2002).

IL-6

Increased serum levels of IL-6 are associated with poor prognosis of patients with gastric, prostate, ovarian and breast cancers and renal cell carcinoma (Chung & Chang, 2003). IL-6 is also elevated in HCC patients, with males having higher serum concentrations than females. Evidence from rodent models suggest that IL-6 is a gender-specific risk factor for HCC, such that oestrogens mediate the inhibition of IL-6 production by hepatic Kupffer cells, via interaction with the IL-6 expression activators NF κ B and CCAAT-enhancer-binding protein β , effectively reducing the risk of HCC development in females (Sander *et al*, 2007).

Serum IL-6 is also elevated in CRC patients (Ito & Miki, 1999), where it may be involved in malignant transformation and tumour progression (Chung & Chang, 2003). Furthermore, IL-6 levels are significantly higher in CRC patients with lymph node and liver metastases than in patients without metastases, indicating that serum IL-6 levels reflect the disease status of CRC patients (Chung & Chang, 2003).

Production of the soluble receptor of IL-6 (sIL-6R) is also elevated during the pathogenesis of colon cancer (Atreya & Neurath, 2005). This may be due to the up-regulation of a disintegrin and metalloproteinase 17 (ADAM17; Section 1.6.4) in colon cancer, which is known to release sIL-6R from the cell membrane (Becker *et al*, 2004). The combined effect of elevated IL-6 and sIL-6R is the increased formation of IL-6-sIL-6R complexes, which interact with the membrane protein glycoprotein 130 (gp130) and initiate the Janus kinases/signal transducer and activators of transcription (JAK/STAT) trans-signalling pathway that induces the increased expression and nuclear translocation of the cytoplasmic transcription factor STAT3 (Kishimoto *et al*, 1995; Heinrich *et al*, 2003). IL-6 treatment has been shown to induce the activation of STAT3 in primary hepatocytes and human hepatoma cells, which is likely to be due to the high levels of gp130 protein on hepatocytes (Gao, 2005).

STAT3 activates the transcription of a number of genes that are involved in the progression of the cell cycle and cellular proliferation and differentiation, including cyclin D1, c-myc, Jun B and c-Jun, anti-apoptotic genes such as bcl-xl and bcl-2, and acute-phase proteins, such as C-reactive protein and serum amyloid A (Atreya &

Neurath, 2005; Gao, 2005). Although the synthesis of hepatic acute-phase proteins are increased due to elevated IL-6 concentrations in CRC liver metastases patients, overall hepatic protein synthesis is reduced (Fearon *et al*, 1991).

The prolonged increase in serum IL-6 levels has been associated with the weight loss component of cachexia, particularly in renal cell carcinoma patients. IL-6 can directly up-regulate pathways of protein degradation, specifically the 26S proteasome and lysosomal proteolytic pathways, leading to protein degradation in skeletal muscle (Tisdale, 2002).

TNF- α

TNF- α is over-expressed in ovarian, breast, prostate, bladder and colorectal cancers, lymphomas and leukaemias, and is often associated with the expression of IL-1 β and IL-6 (Balkwill & Mantovani, 2001). Biopsy tissue from CRC patients indicate that messenger RNA (mRNA) for TNF- α is present in these tumours, but its expression is not limited to malignant tissue, as adjacent normal tissue can express a higher level of this cytokine (Naylor *et al*, 1990). ADAM17 is known to be the major mediator of TNF- α release from its position on the cell membrane (Section 1.6.3), and is often up-regulated in these tumour types (Wajant *et al*, 2003).

The role of TNF- α in cancer is not clear, but it can both stimulate and inhibit tumour formation (Sturm *et al*, 2003). Being a major mediator of inflammation, TNF- α can induce cell death at the site of inflammation and destroy tumour blood vessels when expressed locally in high doses. Conversely, TNF- α can induce angiogenic factors to aid tumour progression and dissemination (Balkwill & Mantovani, 2001; Naylor *et al*, 1990). Following liver injury Kupffer cells become activated and begin to secrete TNF- α , which stimulates the normally quiescent hepatocytes to proliferate (Cosgrove *et al*, 2008).

Over 30 TNF receptor (TNF-R) superfamily members have been identified and can be separated into death domain (DD)-containing and DD-absent receptors (Gaur & Aggarwal, 2003). The binding of TNF- α to the receptor TNF-R1, also known as death receptor (DR) 2, is able to signal cell death via the cytoplasmic domain of the receptor and subsequent recruitment of the DD-containing adaptor protein fas-associated protein with death domain (FADD) and caspase-8 and -10 (Wajant *et al*, 2003).

Similarly, the TNF superfamily member fas ligand (fasL) may regulate HSC survival via its association with fas receptor (fasR). HSCs express fasR or DR1 and respond to fasL by undergoing apoptosis. HSCs express fasL itself, which is cleaved by MMP-7 to yield a soluble cell signal, and may act in an autocrine manner to regulate their own

survival (Jamil & Iredale, 2006). FasL can also bind to decoy receptor (DcR) 3, rendering fasL inactive (Sheikh & Fornace, 2000).

However, the role of TNF- α in cellular apoptosis induction *in vivo* appears to be eclipsed by its role in the inflammatory process (Wajant *et al*, 2003). For example TNF- α , previously known as cachectin, activates skeletal muscle protein degradation in humans with cachexia syndrome, possibly by increasing ubiquitin gene expression in target cells. TNF- α also has the potential to induce catabolism of adipose tissue, a characteristic shared with IL-1 β . Similarly, TNF- α , like IL-1 β , is associated with the increased production of CRH resulting in suppression of food intake.

Furthermore, elevated serum levels of TNF- α in cancer patients correlates with a lower bitterness detection threshold than in control subjects. This may be a causative factor in the anorexic component of cachexia development, as altered taste perception is commonly associated with advanced cancer sufferers (Tisdale, 2002).

1.6 Metalloproteinases

Proteolytic enzymes or proteases occur naturally in all organisms and have many functions within the human body, including the facilitation of normal physiological invasion via the remodelling of the ECM environment; examples of which include wound repair, vasculogenesis and axon outgrowth (Chang & Werb, 2001). Tumourigenic invasion utilises a similar mechanism to physiological invasion, and involves many of the same proteases. There are currently five classes of proteases, i) serine, ii) aspartate, iii) cysteine, iv) threonine, and v) metallo- proteases, with members of each class implicated in the process of tumour invasion and metastasis (Table 1.2) (Nyberg *et al*, 2006).

Metalloproteinases are a class of protease enzymes found in bacteria, fungi and higher organisms, and are subdivided into two groups, i) exopeptidases, and ii) endopeptidases. Of particular interest in the pathological invasion of cancer cells are the endopeptidases, which catalyse the hydrolysis of non-terminal peptide bonds, especially those with hydrophobic residues (Creighton, 1993). Endopeptidases differ widely in sequence and structure, but most contain a catalytically active zinc atom, and as such belong to the metzincin superfamily of zinc-dependent proteases.

The metzincin superfamily is comprised of four subfamilies, the astacins, the matrixins (MMPs), the adamalysins (snake venom metalloproteinases (SVMPs) and ADAMs), and the serralysins (large bacterial proteinases) (Kaushal & Shah, 2000). Metalloproteinases are important in many aspects of normal development and physiology, ranging from cell proliferation, differentiation and remodelling of the ECM to vascularisation and cell migration (Chang & Werb, 2001). For these processes to

Table 1.2: Protease families involved in tumour invasion and metastases. (Adapted from Nyberg *et al*, 2006).

Serine Proteases	Metalloproteases	Other proteases
Cathepsins G & E	Matrixins: MMPs	Aspartate proteases: Cathepsins D & E
Chymase	Adamalysins: ADAMs, ADAMTSs & SVMPs	Cysteine proteases: Cathepsin B, H, K, L, M, N, O & S
Chymotrypsin	Astacins	Threonine proteases
Elastase	Serralysins	
Membrane-bound serine proteases, e.g. Matriptase		
Plasmin		
Plasminogen activators (Tumour-associated) trypsins		
Tryptase		
Human tissue kallikreins		

proceed correctly there is a delicate balance between MP action and their inhibition by endogenous TIMPs (Ray & Stetler-Stevenson, 1994); when this regulation is disrupted metalloproteinases can contribute to the pathology of disease, for example rheumatoid arthritis and cancer (Rundhaug, 2003; Zlokovic, 2006).

Crossing of the basement membrane by malignant cells during metastasis is mediated by a number of different proteolytic enzymes. The dysregulated expression of ADAMs and ADAMTSs has been reported in numerous human cancers, where, in many cases, they are implicated as positive regulators of cancer progression. The roles of the primary ECM remodelling enzymes, the MMPs, have been extensively reviewed in relation to cancer (Curran & Murray 1999; Duffy *et al*, 2000).

Proteolytically active ADAMs act as ectodomain sheddases, which release extracellular regions of membrane-bound proteins, e.g. adhesion molecules, growth factors, cytokines, chemokines and receptors, and certain ADAMTSs breakdown ECM PGs, e.g. aggrecan and versican (Section 1.6.7). Through these combined actions they are able to sculpt the tumour microenvironment and modulate key processes involved in cancer progression, including cell proliferation, migration and angiogenesis. Members of both groups of proteins can also act to inhibit or slow cancer progression; ADAMs can interact with specific integrins to elicit inhibitory effects on cancer dissemination, and certain ADAMTSs possess anti-angiogenic activity, which prevents the increase of tumour size.

1.6.1 A Disintegrin And Metalloproteinase (ADAM) Proteins

ADAMs are multi-domain, transmembrane proteins, forming one of four distinct subfamilies of the metzincin zinc-dependent protease superfamily, the adamalysins (Kaushal & Shah, 2000). They are expressed in a wide range of animal species, tissues and cell types, and have been implicated in sperm-egg fusion, spermatogenesis, neutrophil infiltration, platelet aggregation, neurogenesis, and cachexia (Condon *et al*, 2001), as well as a number of pathological conditions including Alzheimer's disease (Deuss *et al*, 2008), multiple sclerosis (Kieseier *et al*, 2003), and cancer (Rocks *et al*, 2008).

Over 29 ADAM proteins have been identified in humans to date (Roy *et al*, 2006), and these can be broadly grouped according to their distribution and functions. The first group termed the "ectodomain sheddases" (Nath *et al*, 2001) encompass ADAMs that are distributed throughout the body and have an active metalloproteinase domain (ADAMs 1, 8, 9, 10, 12, 15, 17, 19, 28, and 33). These enzymes are involved in the proteolysis of the ectodomains of membrane-anchored cytokines, growth factors and their receptors (Condon *et al*, 2001; Yamamoto *et al*, 1999), allowing cells to alter

responsiveness to their environment. The second group (ADAMs 11, 22 and 23) are predicted to have an inactive metalloproteinase domain, effectively limiting their function to adhesion/de-adhesion and cell fusion. The third group contains 13 ADAM proteins (ADAMs 2, 3, 5, 6, 7, 16, 18, 20, 21, 24, 25, 26, 29, 30 and 32), which are exclusively expressed in the male gonads (testis and epidermis), where some have a role in sperm maturation (Tousseyn *et al*, 2006). Of these ADAMs 20, 21 and 30 have known proteolytic activity and ADAMs 2, 3, 7 and 32 have a predicted inactive metalloproteinase domain.

1.6.2 ADAM domain structure

ADAM proteins are ~750 amino acids in length and have a characteristic 7 domain structure (Figure 1.4), namely, the prodomain, metalloproteinase, disintegrin-like, cysteine-rich, EGF-like, transmembrane and cytoplasmic tail domains (Primakoff & Myles, 2000). In addition, ADAM proteins are synthesised with an N-terminal signal peptide to direct them into the secretory pathway (Seals & Courtneidge, 2003).

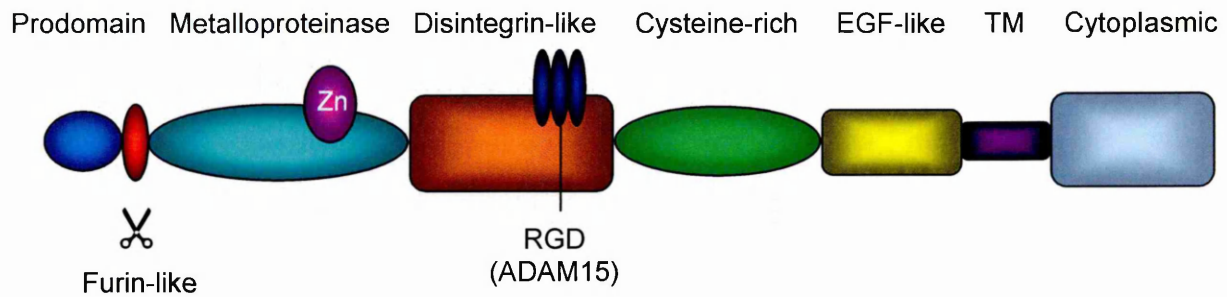
Prodomain

All ADAM proteins are synthesised as zymogens with the approximately 200 amino acid prodomain located at their N-terminus, which acts to maintain the latent, inactive state of the immature protein (Seals & Courtneidge, 2003). Activation of ADAM zymogens is facilitated in the trans-Golgi network by furin-like proprotein convertases, which remove the prodomain at a furin recognition site (RxxR sequence) (single letter amino acid code x is for any other amino acid), located between the prodomain and the metalloproteinase domain (Schlöndorff *et al*, 2000). Most ADAM proteins are thought to be activated by this process; however notable exceptions are ADAM8 and ADAM28 which can undergo autocatalytic activation (Schlomann *et al*, 2002; Howard *et al*, 2000).

Active ADAM enzymes have an essential zinc atom in their catalytic domain with which a conserved cysteine residue located within the prodomain preferentially interacts. This cysteine-zinc intramolecular complex blocks the active site resulting in an inactive enzyme conformation (Van Wart & Birkedal-Hansen, 1990). A cysteine switch occurs upon activation of the enzyme (furin cleavage), which breaks the cysteine-zinc interaction and results in the formation of a mature length protein with an unobstructed, active catalytic site (Rocks *et al*, 2008).

The prodomain has a secondary function in the proper folding of ADAM proteins, in particular the metalloproteinase domain, as ADAM proteins synthesised without a prodomain are proteolytically inactive (Loechel *et al*, 1999; Milla *et al*, 1999; Anders *et al*, 2001).

ADAM



ADAMTS

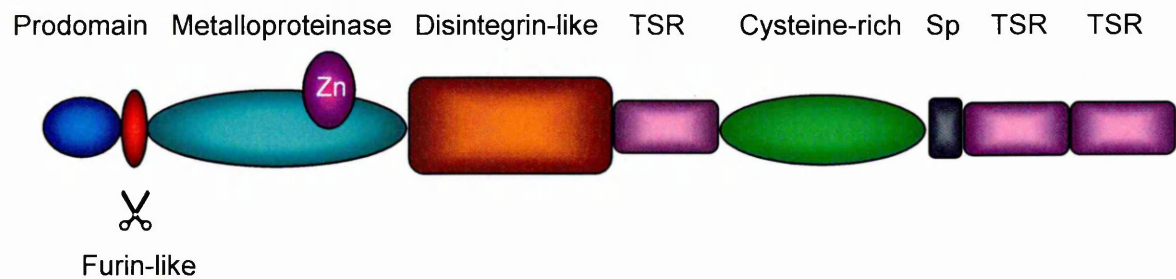


Figure 1.4: Domain structures of ADAM and ADAMTS proteinases.

ADAM proteins consist of seven common domains, namely the prodomain, metalloproteinase, disintegrin-like, cysteine-rich, epidermal growth factor (EGF)-like, transmembrane (TM) and cytoplasmic tail domains. ADAM15 is the only ADAM protein with the RGD motif characteristic of true disintegrin proteins. ADAMTS proteins also contain the prodomain, metalloproteinase, disintegrin-like and cysteine-rich domains, but remaining domains are comprised of variable numbers of thrombospondin repeats (TSRs) and a spacer domain (Sp). They may also contain additional domains unique to individual ADAMTSs, e.g. gon and CUB (not shown). Most ADAM and ADAMTS zymogens are processed by furin-like proprotein convertases at a furin recognition site (furin-like), and converted to mature length proteins.

Furthermore, the prodomain is necessary for proper transit of ADAM proteins through the secretory pathway, as a form of the soluble splice variant of ADAM12 (ADAM12-S) lacking the prodomain is retained in the early endomembrane system. However, when both the prodomain and metalloproteinase domains were absent from the protein constructs, the protein was secreted from the cell (Loechel *et al*, 1999). Taken together these data suggest that the prodomain ensures correct folding of the metalloprotease domain during synthesis, allowing proper transit through the secretory pathway (Seals & Courtneidge, 2003).

Metalloproteinase Domain

The metalloproteinase domain of ADAM proteins (~200 amino acids) contains the active site consensus sequence HExxHxxGxxHD (Mężyk *et al*, 2003). A tetrahedral coordination sphere is formed by the three histidine residues binding an essential zinc ion, and the glutamic acid residue acting as a catalytic support for the required water molecule (Fox & Bjarnason, 1996). The glycine residue allows a turn in the peptide backbone, which together with an essential downstream methionine residue located in a methionine-turn motif (Seals & Courtneidge, 2003) completes the active site structure and ensures that the hydrolytic processing of proteins can occur. Members of the metzincin superfamily have significant conservation within their catalytic sites, but characteristic structural differences of individual proteins may determine their specificity for substrates and/or proteinase inhibitors (Stöcker *et al*, 1995). Alterations in the active site consensus sequence of a number of ADAM proteins e.g. ADAMs 2, 3, 22 and 23 (Tousseyn *et al*, 2006) renders them proteolytically inactive (Rocks *et al*, 2008).

Disintegrin-Like Domain

The disintegrin-like domain of ADAM proteins (60 to 90 amino acids) has sequence similarity to the SVMPs. But unlike SVMPs, ADAM proteins are not true disintegrin proteins, as they usually lack an RGD consensus sequence (Fox & Bjarnason, 1996). This motif allows disintegrins to interact with integrins from different cell systems (Lu *et al*, 2007), including platelet integrins (Seals & Courtneidge, 2003). ADAM15 is the only ADAM protein known to have an RGD-motif (Lu *et al*, 2007); the remainder contain an xCD-motif in their disintegrin-like domains, which has also been identified as an integrin-binding motif (McLane *et al*, 1998). Additionally, a number of ADAM proteins, e.g. ADAMs 1, 2, 3, 9 & 12, contain an Rx₆DEVF sequence in this domain, which binds readily to α 9 β 1 integrins. ADAM10 and 17 lack this aspartic acid containing sequence and consequently cannot bind α 9 β 1 integrins (Eto *et al*, 2002).

Cysteine-Rich Domain

Little is known about the function of the cysteine-rich domain of ADAM proteins (~160 amino acids), but in ADAM12 for example, it interacts with cell surface HSPGs, such as syndecan, to mediate cell-cell or cell-matrix attachment (Iba *et al*, 2000). Interestingly, the disintegrin-like domain of ADAM12 is not involved in cell adhesion (Iba *et al*, 1999), suggesting that the cysteine-rich domain compensates for its dysfunctional disintegrin-like domain. The cysteine-rich domains of ADAM1 and ADAM12 contain a putative fusogenic peptide suggesting a role in cell-cell fusion (Huovila *et al*, 1996); however at this time this function remains hypothetical.

Epidermal Growth Factor (EGF) -Like Domain

The 40 amino acid EGF-like domain of ADAM proteins contains six cysteine residues, and may allow ADAM proteins to interact with chaperones involved in biosynthesis (Lu *et al*, 2007). Little else is known of the functions of this domain.

Transmembrane Domain

The majority of ADAM proteins are type I membrane proteins, and as such are anchored to the cell surface via a transmembrane domain located near the C-terminus of the protein. Proteins present in this location are mature length proteins, many of which are catalytically active. However, some ADAM proteins (e.g. ADAMs 11, 12, 17 & 28) have alternative splice forms, which are altered upstream of the transmembrane domain and are consequently present as soluble, secreted forms (Lu *et al*, 2007).

Cytoplasmic Tail Domain

The cytoplasmic tail domain of ADAM proteins is highly variable in both length (40 to 250 amino acids) and sequence, and contains specialised motifs with hypothesised involvement in the signal transduction between the interior and exterior of the cell and vice versa. The most frequently occurring motif in this domain, PxxP, acts as a binding site for Src homology (SH) 3 domain-containing proteins, such as signalling adaptors and enzymes, and allows protein-protein interactions at a site other than a catalytic site. Many human ADAMs contain this motif, including ADAMs 7, 8, 9, 10, 12, 15, 17, 19, 22, 29 and 33 (Seals & Courtneidge, 2003; Lu *et al*, 2007).

Some ADAM proteins, e.g. ADAM12 and 15, also contain potential serine-threonine and/or tyrosine kinase phosphorylation sites in their cytoplasmic tails (Seals & Courtneidge, 2003). These sites may function as ligands for SH2 domain-containing binding proteins, in addition to providing an adaptor function allowing the assembly of protein complexes required for ADAMs to execute their functional activity (Lu *et al*, 2007).

1.6.3 ADAM17 Functions

ADAM17 was first identified as the major proteinase responsible for the processing of membrane-bound pro-TNF- α into its soluble active form (TNF- α), from which it gained its alternative name TNF- α converting enzyme (TACE) (Black *et al*, 1997). Since then the role of ADAM17 in the proteolytic cleavage of the ectodomain of a wide range of membrane-bound precursors has been extensively studied (Sunnarborg *et al*, 2002). These substrates include a number of growth factors, cytokines, receptors and adhesion molecules, as summarised in Table 1.3 (Mezyk *et al*, 2003; Lee *et al*, 2003; Plumb *et al*, 2006; Edwards *et al*, 2008).

ADAM17 can be up-regulated in response to various cytokines, e.g. IL-1 β , TNF- α , TGF- β 1 and IFN- γ (Roy *et al*, 2006), with TGF- β 1 and TNF- α inducing ADAM17 activation in hepatocytes, which releases epidermal growth factor receptor (EGFR) ligands to activate EGFR signalling (Murillo *et al*, 2005). The up-regulation of ADAM17 has been associated with pathologies such as cancer (Vázquez *et al*, 1999; Ringel *et al*, 2006; Wiseman & Werb, 2002), rheumatoid arthritis (Yamamoto *et al*, 1999; Schlöndorff *et al*, 2000) and multiple sclerosis (Plumb *et al*, 2006).

ADAM17 has a well established function in the EGFR signalling pathway, which has a critical role in normal development (Sahin *et al*, 2004). This signalling pathway has also been identified in the development and progression of a number of cancers (Fischer *et al*, 2003; Borrel-Pagès *et al*, 2003), including ovarian cancer development (Tanaka *et al*, 2005), glioma cell invasiveness (Zheng *et al*, 2007) and HCC growth and invasiveness (Ding *et al*, 2004).

EGFR signal trans-activation is primarily achieved via ectodomain shedding of the EGFR ligand membrane precursors in part by ADAM17 (Sunnarborg *et al*, 2002). The direct treatment of EGFR by ligand binding results in the dimerisation and subsequent phosphorylation of the two receptor molecules. This creates phosphotyrosine docking sites to activate intracellular signalling cascades, such as mitogen-activated protein kinases (MAPKs), the PI3-K/Akt pathway and modulation of ion channels (Fischer *et al*, 2003).

Membrane-bound EGFR ligands are also capable of EGFR signalling; however this can only occur in an autocrine or juxtacrine manner. The production of soluble EGFR ligands allows the additional signalling modes of paracrine or endocrine signalling to occur (Sahin *et al*, 2004).

ADAM17 also possesses α -secretase activity, as do ADAM9 and ADAM10, which can increase cellular proliferation via the cleavage of amyloid precursor protein (APP) (Section 1.6.4). However the down-regulation of ADAM17 by siRNA does not affect

Table 1.3: ADAM17 substrates (Adapted from Mezyk *et al*, 2003; Plumb *et al*, 2006; Edwards *et al*, 2008).

Growth factors / Cytokines / Chemokines	EGF-like ligands	Receptors	Cell adhesion molecules (CAMs)	Others
Colony stimulating factor-1 (CSF-1)	Amphiregulin	ACE2/SARS-CoV receptor	Activated leukocyte CAM (ALCAM)	Amyloid precursor protein (APP)
CxCL16	Angiotensin II	CD30 (TNFRSF8)	L1-CAM	CD40
Fractalkine (Cx ₃ CL1)	Betacellulin	Growth hormone receptor	L-selectin	CD44
TNF- α	Epigen	IL-1R2	N-CAM	Cellular prion protein (PrP ^o)
TNF-related activation-induced cytokine / Receptor activator of nuclear factor- κ B ligand (TRANCE/RANKL)	Epiregulin	IL-6R	Nectin-4	Collagen XVII
	ErbB4/HER4	IL-15R	Vascular CAM-1 (VCAM-1)	Delta-like ligand-1 (DLL1)
	Heparin-binding EGF-like growth factor (HB-EGF)	Macrophage colony-stimulating factor receptor (M-CSF-R)		Desmoglein-2
	Neuregulins	Neuronal pentraxin receptor (NPR)		JAM-A

Table 1.3 (continued): ADAM17 substrates.

Growth factors / Cytokines / Chemokines	EGF-like ligands	Receptors	Cell adhesion molecules (CAMs)	Others
	Transforming growth factor- α (TGF- α)	Neurotrophin receptor (p75NTR)		Kit ligand-1 and -2
		Notch1		Klotho
		TNF-R1 (p55TNFR)		Lymphocyte-activation gene 3 (LAG-3)
		TNF-R2 (p75TNFR)		MHC-class I related chain A/B (MICA/MICB)
		TrkA neurotrophin receptor		Mucin-1 (MUC1)
		Vacuolar sorting protein receptor (VPS10-p)		Pre-adipocyte factor-1 (Pref-1)
		Protein tyrosine phosphatase (PTP) –LAR		Semaphorin 4D

cellular proliferation of pancreatic ductal adenocarcinoma (PDAC) cells *in vitro*, but their invasive behaviour is notably reduced (Ringel *et al*, 2006).

1.6.4 ADAM17 in Cancer

Many ADAM proteins, including ADAM17, have been implicated in the development and/or progression of cancer (Table 1.4).

ADAM17 and Cancer Cell Proliferation

Physiological cell proliferation is tightly regulated and responsive to the specific needs of the human body. However, when these controls become defective in a cell, it can grow and divide in an unregulated manner forming a mass of cells with no physiological function, a tumour (Lodish *et al*, 2000). The speed at which primary and metastatic tumours develop depends largely on the rate of cell proliferation within the tumour, and the rate of cell death (Begg & Steel, 2002).

The over-expression of certain proteolytically active ADAM proteins has been associated with the increased proliferative capacity of a number of tumour types, via the cleavage of growth factors or cell surface proteins, examples of which include ADAM9 (Arribas & Bech-Serra, 2006), 10, 12 and 17 (Rocks *et al*, 2008). In particular, ADAM17 influences tumour cell proliferation when over-expressed in breast (Wiseman & Werb, 2002), ovary (Tanaka *et al*, 2005), kidney (Roemer *et al*, 2004), colon (Vázquez *et al*, 1999), prostate (Karan *et al*, 2003) and primary HCC (Itabashi *et al*, 2008).

ADAM17 has α -secretase activity (Asai *et al*, 2003), and as such can shed a non-amyloidogenic fragment of APP from the cell surface generating soluble APP (sAPP); ADAM9, 10 (Lammich *et al*, 1999), and 19 (Tanabe *et al*, 2007) also possess α -secretase activity. The enhanced secretion of sAPP in explant cultures of anaplastic astrocytomas and glioblastomas has been shown to correlate to the malignancy of tumours (Nakagawa *et al*, 1999). This may be due to the proliferation-promoting effect of sAPP, as demonstrated in skin keratinocyte (Hoffmann *et al*, 2000), rat thyroid epithelial (Pietrzik *et al*, 1998) and colon carcinoma (Meng *et al*, 2001) cell lines. Hence the over-expression of ADAMs with α -secretase activity by tumours, in conjunction with sAPP could result in the increased proliferation of tumour cells.

However, Ko *et al* (2007) have demonstrated that an ADAM10 anti-sense oligonucleotide reduced both the expression of this enzyme and the growth of an oral squamous cell carcinoma cell line OECM1, which ordinarily has elevated expression of APP and ADAM10, without changes in sAPP. This might suggest mechanisms that do not involve sAPP in the cell growth-promoting activity of α -secretases.

Table 1.4: Aberrant ADAM protein expression in human cancers and their functions.

ADAM	Proteolytic activity	Functions in cancers	Expression in cancers*
ADAM8	Yes	Promotes cell migration and invasion.	Brain (Wildeboer <i>et al</i> , 2006), Kidney (Roemer <i>et al</i> , 2004), Lung (Ishikawa <i>et al</i> , 2004), Pancreas (Valkovskaya <i>et al</i> , 2007), Prostate (Fritzsche <i>et al</i> , 2006)
ADAM9	Yes	Promotes cell proliferation, adhesion and invasion.	Breast (O'Shea <i>et al</i> , 2003), Kidney (Fritzsche <i>et al</i> , 2008), Liver (Tannapfel <i>et al</i> , 2003), Lung (Shintani <i>et al</i> , 2004), Pancreas (Grützmann <i>et al</i> , 2004), Skin (Zigrino <i>et al</i> , 2005), Stomach (Carl-McGrath <i>et al</i> , 2005)
ADAM10	Yes	Promotes cell growth, proliferation and migration.	Colon (Gavert <i>et al</i> , 2007), Oral cavity (Ko <i>et al</i> , 2007), Ovary, Uterus (Fogel <i>et al</i> , 2003), Prostate (McColloch <i>et al</i> , 2004), Stomach (Yoshimura <i>et al</i> , 2002)
ADAM12	Yes	Promotes cell growth, proliferation and invasion. $\alpha 4\beta 1$ binding inhibits cell migration.	Bladder (Fröhlich <i>et al</i> , 2006), Bone (Tian <i>et al</i> , 2002), Brain (Kodama <i>et al</i> , 2004), Breast, Colon (Iba <i>et al</i> , 1999), Liver (Le Pabic <i>et al</i> , 2003), Lung (Rocks <i>et al</i> , 2006), Stomach (Carl-McGrath <i>et al</i> , 2005)

* Up-regulated expression of ADAM proteins in cancers, unless otherwise stated.

↓ Down-regulated expression.

Table 1.4 (continued): Aberrant ADAM protein expression in human cancers and their functions.

ADAM	Proteolytic activity	Functions in cancers	Expression in cancers*
ADAM15	Yes	Promotes cell growth and angiogenesis. $\alpha V\beta 3$ binding inhibits cell migration.	Breast, Prostate (Kuefer <i>et al</i> , 2006), Lung (Schütz <i>et al</i> , 2005), Ovary (Nath <i>et al</i> , 2001), Stomach (Carl-McGrath <i>et al</i> , 2005)
ADAM17	Yes	Promotes cell growth, proliferation and angiogenesis. $\alpha 5\beta 1$ binding inhibits cell migration.	Brain (Zheng <i>et al</i> , 2007), Breast (Wiseman & Werb, 2002), Colon (Vázquez <i>et al</i> , 1999), Kidney (Roemer <i>et al</i> , 2004), Liver (Itabashi <i>et al</i> , 2008), Ovary (Tanaka <i>et al</i> , 2005), Pancreas (Ringel <i>et al</i> , 2006), Prostate (Karan <i>et al</i> , 2003)
ADAM19	Yes	Promotes cell proliferation. $\alpha 5\beta 1$ or $\alpha 9\beta 1$ binding inhibits cell migration.	Brain (Wildeboer <i>et al</i> , 2006), Kidney (Roemer <i>et al</i> , 2004)
ADAM23	No	Promotes cell growth and migration.	Brain (Cal <i>et al</i> , 2000)
		Promotes cell migration.	↓ Breast (Costa <i>et al</i> , 2004)
ADAM28	Yes	Promotes cell proliferation.	Breast (Mitsui <i>et al</i> , 2006), Kidney (Roemer <i>et al</i> , 2004), Lung (Ohtsuka <i>et al</i> , 2006)

* Up-regulated expression of ADAM proteins in cancers, unless otherwise stated.

↓ Down-regulated expression.

ADAM17 could also increase tumour cell proliferation via the release of angiotensin II (Ang II; an EGF-like ligand), which triggers EGFR signal transactivation (Itabashi *et al*, 2008). Ang II has a fundamental role as a vasoconstrictor controlling cardiovascular function and renal homeostasis, but also acts as a potent growth factor of vascular smooth muscle cells and certain cancer cell lines (Itabashi *et al*, 2008). Similarly, amphiregulin (another EGFR ligand) is released by ADAM17 (Sahin *et al*, 2004) and enhances proliferation of cancer cells (Rocks *et al*, 2008).

ADAM17 and Cancer-Associated Angiogenesis

The process of angiogenesis, whereby new blood vessels are formed from pre-existing vasculature, appears to provide the primary form of vascularisation within a tumour and is the rate-limiting step in cancer progression (Handsley & Edwards, 2005). Angiogenesis has two clear functions in cancer progression; the first and most apparent role in this pathology is to provide the tumour with its own blood supply (Carmeliet & Jain, 2000). The new vascular network supplies nutrients and oxygen throughout the tumour mass, enabling it to grow beyond the critical 2mm sphere of an avascular tumour (Lodish *et al*, 2000). The second, more subtle role for neoplastic angiogenic vasculature is to provide a route for dissemination of tumour cells to different sites of the body via the process of metastasis (Handsley & Edwards, 2005).

An increasing number of ADAM proteins have been linked to angiogenesis, at least indirectly, with potential roles in the modulation of angiogenic factors and the release of membrane-bound angiogenic inhibitors (Handsley & Edwards, 2005).

ADAM17 is over-expressed in a number of human cancers, including PDAC (Ringel *et al*, 2006), breast (Wiseman & Werb, 2002) and colon carcinomas (Vázquez *et al*, 1999), where a role as a positive regulator in tumour-associated angiogenesis has been established (Blanchot-Jossic *et al*, 2005).

The combined approach of immunohistological and mRNA analysis applied by Blanchot-Jossic *et al* (2005) showed that ADAM17 is over-expressed in both its pro and active forms in neoplastic and ECs within primary colon carcinomas relative to paired normal colonic mucosa. They also demonstrated that phosphorylated EGFR (*P*-EGFR) was significantly up-regulated in most colon carcinomas compared with paired normal mucosa. Although the relatively weak over-expression of *P*-EGFR did not correlate with ADAM17 over-expression, EGFR protein was co-expressed with ADAM17 in cancer cells and ECs present in the tumour mass.

This indicated that ADAM17-mediated EGFR activation is involved in tumour-mediated angiogenesis, as the downstream signalling cascade of EGFR is involved in a number of essential angiogenic processes such as cell migration, adhesion and proliferation.

However, the ADAM family of proteins show redundancy in substrate specificity, and ADAMs 9, 10, 12, and 15 have also been shown to shed EGFR ligands from the cell surface in response to stimulants (Sahin *et al*, 2004), hence any of these may also be capable of EGFR-mediated angiogenesis (Roy *et al*, 2006).

Further evidence of ADAM protein involvement in the positive regulation of angiogenesis was gleaned using *in vitro* models of angiogenesis. The human mammary epithelial cell line HMEC-1 expresses both ADAM17 and ADAM15, and treatment with the ADAM-specific inhibitor GL129471 inhibited the major processes involved in angiogenesis, namely migration, adhesion and proliferation, and the formation of capillary tubules (Trochon *et al*, 1998). The same angiogenic responses could also be inhibited in ECs by blocking the interaction between the disintegrin-like domain of ADAM15 and the angiogenic integrin $\alpha 5\beta 1$ in humans (Trochon-Joseph *et al*, 2004).

ADAM10 and ADAM17 are involved in the ligand-dependent activation of the Notch signalling pathway. This is a two-step process of controlled proteolysis in which the first cleavage is performed by ADAM10 or ADAM17 (Huovila *et al*, 2005). The involvement of Notch in cancer depends on the cellular context and it has been proposed that it can act either in a tumour promoting or a tumour suppressive fashion. Oncogenic signals of Notch have, for example, been reported in breast epithelium, melanocytes and T-cell acute lymphoblastic leukaemia (Stylianou *et al*, 2006). Through its effects on gene expression, cancer processes modulated by Notch include suppression of p53, angiogenesis and cell adhesion (Lefort *et al*, 2007). However, it has also been reported that conditional Notch1 knockout mice develop cutaneous lesions that resemble basal cell carcinoma (Lefort *et al*, 2007).

ADAM17 and Cancer Cell Adhesion and Migration

Cell migration is a complex sequential process necessary for physiological development, tissue repair and regeneration. It is also the process that drives the metastasis of cancer cells. Cell migration is aided by the integrin family of adhesion molecules, which promote stable interactions between cells and the ECM, as well as functioning as signalling molecules initiating intracellular signals that regulate certain cell behaviours including cell migration (Arribas & Bech-Serra, 2006).

A number of ADAM proteins interact with cell surface integrins via their disintegrin-like domain, and it is possible that these interactions influence cell migration during cancer progression. Evidence suggests that the interaction of ADAM17 with $\alpha 5\beta 1$ integrin can inhibit Chinese hamster ovary (CHO) cell migration; other examples of this include the

interactions of ADAM12 with $\alpha 4\beta 1$, ADAM15 with $\alpha V\beta 3$, and ADAM19 and ADAM33 with both $\alpha 5\beta 1$ and $\alpha 9\beta 1$ (Arribas & Bech-Serra, 2006; Huang *et al*, 2005).

The mechanisms by which these inhibitory effects are mediated may vary, but are as yet poorly understood. However, ADAM15 over-expression in ovarian cancer disturbed the pro-migratory interaction of $\alpha V\beta 3$ integrin with vitronectin, which resulted in reduced cellular adhesion to vitronectin and the consequent reduction in random cellular motility (Nath *et al*, 2001).

Conversely, other ADAM proteins can promote cell migration via integrin interaction, and may therefore aid tumour cell invasion. Activated HSCs, commonly known as liver stromal cells, secrete the soluble splice variant of ADAM9 (ADAM9-S), which can localise to the surface of colon carcinoma cells via an interaction between $\alpha 6\beta 4$ and $\alpha 2\beta 1$ integrins on the tumour cell and the disintegrin domain of ADAM9-S. Its localisation to the cell surface can promote the invasion of colon carcinoma cells *in vitro* by the degradation of laminin and other ECM components (Mazzocca *et al*, 2005), but further investigation is required to determine whether this effect is also observed *in vivo*. This highly invasive phenotype has also been demonstrated in a variety of cell lines (Arribas & Bech-Serra, 2006).

Interestingly, recent crystallographic studies have revealed that the disintegrin domain of ADAMs, which supposedly interacts with integrins, is inaccessible for protein binding. The hyper-variable region of the cysteine-rich domain has been proposed as a potential protein-protein association region (Takeda *et al*, 2006).

1.6.5 A Disintegrin and Metalloproteinase with Thrombospondin Motif (ADAMTS) Proteins

ADAMTSs are multi-domain, extracellular proteins, belonging to the same subfamily of metzincin proteins as the ADAMs, the adamalysins (Kaushal & Shah, 2000). Although they are secreted proteinases, they usually bind to ECM components, such as HSPGs (Section 1.6.7) (Porter *et al*, 2004). There are 19 ADAMTSs, numbered 1-10 and 12-20 (ADAMTS-11 is the same protein as ADAMTS-5) with known functions in ECM processing, organogenesis, haemostasis (Porter *et al*, 2004), and angiogenesis (Porter *et al*, 2005). They can be divided into four sub-divisions depending upon their structural characteristics and activities (Jones & Riley, 2005).

The first division contains ADAMTS-1, -4, -5, -8, -9, -15 and -20, which possess the ability to cleave members of hyaluronan or lectican family of large aggregating PGs, including aggrecan, versican, neurocan, and brevican (Bandtlow & Zimmermann, 2000), and are therefore known as hyaluronanases. These enzymes can also be classed as glutamyl endopeptidases (GEPs), as they cleave proteins at the carboxyl end of

glutamate residues. All ADAMTSs in this division can cleave aggrecan, with the exception of ADAMTS-20, which originally led them to be known as aggrecanases.

The second group containing ADAMTS-2, -3 and -14, are known as pro-collagen N-propeptidases; ADAMTS-2 is able to cleave type I, II and III procollagens, ADAMTS-3 processes type II procollagen peptides, and ADAMTS-14 (a homologue of ADAMTS-2) functions as the major type I procollagen N-propeptidase in tendons.

The third group contains only ADAMTS-13; this proteinase is responsible for the cleavage of the large multimeric von Willebrand factor (vWF) precursor. The remaining ADAMTS proteins are grouped into a category known as 'others', which can be subgrouped into four pairs based on their structural features; these are ADAMTS-6 and -10, ADAMTS-7 and -12, ADAMTS-16 and -18, and ADAMTS-17 and -19.

1.6.6 ADAMTS Domain Structure

ADAMTSs share considerable structural similarities with ADAMs with four domains of similar type, the prodomain, metalloproteinase domain, disintegrin-like domain and cysteine-rich domain (Section 1.6.2). ADAMTSs also contain additional characteristic domains, including thrombospondin type-I repeats (TSRs) (Tucker, 2004), a spacer domain and several C-terminal domains unique to particular ADAMTSs (Figure 1.4).

Prodomain

Like ADAMs, ADAMTSs are synthesised as zymogens, however after proteolytic processing at the N-terminus to remove the signal sequence and prodomain, they are secreted from cells, indicating that the prodomain has a specific function in the intracellular retention of the inactive ADAMTSs. Whilst for most ADAMTSs the removal of the prodomain is an important step in their activation, ADAMTS-13 is enzymatically active when this region is still attached (Majerus *et al*, 2003).

As for ADAMs, the main enzyme involved in the removal of the prodomain is furin. However, the prodomain of ADAMTS-4 can be removed in a cell line that does not express furin (Wang *et al*, 2004); therefore other enzymes may also be involved.

Metalloproteinase Domain

ADAMTSs possess a metalloproteinase domain with a zinc binding module of the sequence HExxHxxGxxHD similar to that in ADAM proteins, which is responsible for the proteolytic activity of these enzymes.

Disintegrin-Like Domain

The disintegrin-like domain of ADAMTSs is 25-45% similar to that of SVMPs, however none of the ADAMTSs contain an RGD motif and their interactions with integrins have not been reported (Kaushal & Shah, 2000).

Cysteine-Rich Domain

The highly homologous cysteine-rich domain contains ten conserved cysteines (Kaushal & Shah, 2000), but little is known about its functional role.

Spacer Domain

The spacer domain is the least homologous of all the domains and it comprises an N-terminal part in which several hydrophobic amino acids are conserved and a C-terminal section which is highly variable.

ADAMTSs may also undergo C-terminal processing post-translationally within this domain, which can alter their localisation and substrate specificity. This controlled proteolysis has been shown for ADAMTS-1, ADAMTS-4, ADAMTS-8 and ADAMTS-9. The relationship between C-terminal processing, localisation and biological activity of ADAMTS-4 is well characterised. The conversion of the full-length 75 kDa form to 60 kDa and 50 kDa species results in changes in the pattern of cleavage of aggrecan and the range of substrates degraded. Additionally, ECM binding is altered, such that the 75 kDa isoform associates with ECM, whilst shorter forms with truncated spacer regions do not (Kashiwagi *et al*, 2004).

Thrombospondin Repeats (TSRs)

Sandwiched between the disintegrin-like and cysteine-rich domains is the central TSR, which is very similar in amino acid sequence in all ADAMTSs. Whereas the TSRs closer to the C-terminus differ much more in sequence, but can include a CVSTCG motif that binds to the CD36 cell surface receptor or a motif known to interact with sulphatide and heparin (Cal *et al*, 2002). Members of the ADAMTS family have a different number of C-terminal TSRs, e.g. ADAMTS-4 lacks a C-terminal TSR motif, while ADAMTS-9 and ADAMTS-20 have 14 C-terminal TSRs.

In several ADAMTSs the TSRs and spacer domain together are involved in the binding of ECM. Similarly, the TSR which precedes the spacer and cysteine-rich domain in ADAMTS-4 is important in its binding to sulphated GAGs linked to aggrecan (Cal *et al*, 2002).

Unique C-Terminal Domains

Some ADAMTSs have unique C-terminal domains. ADAMTS -2, -3, -10, -12, -14, -17 and -19 have a protease and lacunin (PLAC) domain (Somerville *et al*, 2004). ADAMTS-13 is characterised by the presence of two complement subcomponents C1r/C1s/embryonic sea urchin protein Uegf (CUB) domains which also occur in proteases of the astacin family (a subfamily of the metzincins) (Zheng *et al*, 2001). The CUB domain is present in several extracellular and plasma membrane bound proteins.

The long isoform of ADAMTS-9 and ADAMTS-20 have a gon domain that was originally discovered in an ADAMTS involved in the development of gonads in *Caenorhabditis elegans* (Somerville *et al*, 2003). ADAMTS-7 and ADAMTS-12 contain a mucin domain which is located between their C-terminal TSRs (specifically between repeats 3 and 4 out of seven) (Somerville *et al*, 2004), and C-terminal processing of ADAMTS-12 occurs within this domain.

1.6.7 ADAMTS-1, -4 and -5 Protein Functions

Belonging to the hyalactanase group of ADAMTS proteins, ADAMTS-1, -4 and -5 are able to cleave hyalactans, a group of CSPGs that bind non-covalently to hyaluronan present on cell surfaces and in the ECM (Bandtlow & Zimmermann, 2000). They differ structurally at their C-termini, such that ADAMTS-1 has two TSRs, ADAMTS-4 has none and ADAMTS-5 has one; this may confer substrate specificity to these proteinases and account for their differing substrate spectra.

PGs are glycoproteins with at least one sulphated GAG side chain bound covalently to the core protein (Zimmermann & Dours-Zimmerman, 2008). PGs are major ECM components providing structural support to cells, and can be characterised by the disaccharide units of their GAG side chains into chondroitin sulphate (CS), HS, and keratan sulphate (KS) PGs (Bandtlow & Zimmermann, 2000).

Additional roles have been implicated for PGs from *in vitro* studies, in which a variety of ligands, including growth factors, CAMs, enzymes and enzyme inhibitors, bind to PGs. This may indicate that PGs mediate the bio-availability of these ligands (Bandtlow & Zimmermann, 2000).

The hyalactans, also known as lecticans, are a family of secreted CSPGs, namely aggrecan, versican, brevican and neurocan, which participate in the formation of ECM (Bandtlow & Zimmermann, 2000). All lecticans have highly conserved terminal globular regions; the N-terminal globular domain binds to the core protein-free GAG hyaluronan (a core protein-free non-sulphated polymer of glucosamine and glucuronic acid), and the C-terminal globular domain has a unique lectin domain flanked by an EGF and complement regulatory protein (CRP) -like domain, indicating a role in carbohydrate binding (Jones *et al*, 2003; Yamaguchi, 2000). However, their interglobular domains or intermediate CS-attachment domains have substantial variation in sequence, length and number of CS side chains; this region is highly sensitive to proteolysis (Viapiano & Matthews, 2006).

ADAMTS-4 and -5 are the classical aggrecanases (Zimmermann and Dours-Zimmerman 2008), and extensive research has been performed into the role of these, and ADAMTS-1, in arthritic diseases, such as rheumatoid arthritis and osteoarthritis,

due to their ability to cleave aggrecan, the major CSPG of cartilage. ADAMTS-1, -4 and -5 cleave aggrecan at a site distinct from MMP cleavage, E³⁷³-A³⁷⁴, located within the GAG-binding domain (Kuno *et al*, 2000; Tortorella *et al*, 2000; Abbaszade *et al*, 1999). Since these early studies, further cleavage sites have been identified or proposed for all three enzymes, namely E¹⁶⁶⁷-G¹⁶⁶⁸, E¹⁴⁸⁰-G¹⁴⁸¹, E¹⁵⁴⁵-G¹⁵⁴⁶, E¹⁸¹⁹-A¹⁸²⁰, and E¹⁹¹⁹-L¹⁹²⁰, all located within the GAG-binding domain of aggrecan (Flannery, 2006).

Versican is a major CSPG present in developing blood vessels, and is synthesised by arterial smooth muscle cells (Wight & Merrilees, 2004). There are 4 splice variants of versican (V0, V1, V2 and V3), and ADAMTS-1 and -4 are able to cleave V1/V0 versican at the E⁴⁴¹-A⁴⁴²/E¹⁴²⁸-A¹⁴²⁹ bonds (Jönsson-Rylander *et al*, 2005). Brevican is mainly restricted to neural tissues (Yamaguchi, 2000), and is processed by ADAMTS-4 and -5 at the E³⁹⁵-S³⁹⁶ bond (Held-Feindt *et al*, 2006). Similarly, neurocan is restricted to neural tissues (Yamaguchi, 2000).

Aside from their proteolytic functions, ADAMTS-1 and -5 may also confer anti-angiogenic properties via their central TSRs (Section 1.6.8).

1.6.8 ADAMTS-1, -4 and -5 and Cancer

Many ADAMTS proteins are dysregulated during cancer progression (Table 1.5), including ADAMTS-1, -4 and -5.

ADAMTS-1 and -5 and Cancer-Associated Angiogenesis

Until recently all proteinases were considered to be positive regulators of tumoral angiogenesis. However, four members of the ADAMTS family (ADAMTS-1, -5, -8 and -12) have recently been shown to have anti-angiogenic properties.

ADAMTS-1 (METH-1) and ADAMTS-8 (METH-2) exhibit potent angio-inhibitory activity *in vitro* (Roy *et al*, 2006), by acting independently to inhibit bovine VEGF (bVEGF) - induced vascularisation in the rabbit corneal pocket assay, and to inhibit VEGF-induced angiogenesis in the chick chorioallantoic membrane assay (CAM assay) (Vázquez *et al*, 1999).

The anti-angiogenic activity of ADAMTS-1 has been mapped to the three TSRs in the proteins C-terminus, with recombinant and proteolytic fragments containing these repeats also exhibiting angio-inhibitory activity in the rabbit corneal pocket and chick CAM assays (Vázquez *et al*, 1999). However, mutational analyses have revealed that although TSRs are necessary for the inhibition of angiogenesis, they alone are not sufficient to bring about this response *in vivo*. The spacer domain must be present in combination with the TSRs of the protein to elicit an anti-tumour response (Kuno *et al*, 2004).

Table 1.5: Aberrant ADAMTS protein expression in human cancers and their functions.

ADAMTS	Proteolytic activity	Functions in cancers	Expression in cancers*
ADAMTS-1	Yes	Promotes cell invasion and angiogenesis.	Breast (Porter <i>et al</i> , 2006)
		Down-regulation of this anti-angiogenic protein permits angiogenesis.	↓ Breast (Porter <i>et al</i> , 2004), ↓ Lung (Rocks <i>et al</i> , 2006), ↓ Liver, ↓ Pancreas (Masui <i>et al</i> , 2001)
ADAMTS-4	Yes	Promotes cell invasion.	Brain (Held-Feindt <i>et al</i> , 2006)
ADAMTS-5 or ADAMTS-11	Yes	Promotes cell invasion.	Brain (Held-Feindt <i>et al</i> , 2006)
ADAMTS-8	Yes	Undetermined.	Lung (Dunn <i>et al</i> , 2004)
		Down-regulation of this anti-angiogenic protein permits angiogenesis.	↓ Brain (Dunn <i>et al</i> , 2006)
ADAMTS-13	Yes	Undetermined.	↓ Brain (Oleksowicz <i>et al</i> , 1999)
ADAMTS-15	Yes	Predicator of prolonged survival.	Breast (Porter <i>et al</i> , 2006)
		Down-regulation is a predicator of poor prognosis.	↓ Breast (Porter <i>et al</i> , 2006)
ADAMTS-18 or ADAMTS-21	Yes	Tumour suppressor.	Oesophagus (Jin <i>et al</i> , 2007)

* Up-regulated expression of ADAMTS proteins in cancers, unless otherwise stated.

↓ Down-regulated expression.

Furthermore, a GWQRRL/TVECRD motif common to the first C-terminal TSR of both ADAMTS-1 and -8, but absent from all other ADAMTS proteins, may play an important role in the angio-inhibitory action of these proteins (Porter *et al*, 2005). C-terminal processing of ADAMTS-1 from its 87 kDa full length form to a 64 kDa form lacking the terminal TSR domain and part of the spacer domain reduces its angio-inhibitory effect (Rodríguez-Manzanaque *et al*, 2000).

The sequestration of VEGF₁₆₅ by ADAMTS-1 and -8 may provide a mechanism by which they execute their anti-angiogenic activity (Handsley & Edwards, 2005). VEGF₁₆₅ is one of the most specific mediators of tumour angiogenesis, with suppression of VEGF signalling causing the inhibition of angiogenesis and an associated reduction of tumour burden. Conversely, the over-expression of VEGF and its receptor VEGF receptor 2 (VEGFR2) results in the increased invasion and metastasis of human cancers (Luque *et al*, 2003).

Luque *et al* (2003) have shown that ADAMTS-1 can bind to VEGF₁₆₅ and form a stable complex, but it cannot bind to the splice variant of VEGF lacking a heparin-binding domain in its C-terminal (VEGF₁₂₁). Interestingly, the TSRs of ADAMTS-1 and -8 contain the consensus sequence WSxWS, which also binds heparin (Vázquez *et al*, 1999). So it is likely that heparin or another HSPG, such as syndecan, acts as a chaperone between ADAMTS-1 and VEGF₁₆₅, resulting in the reduced bioavailability of VEGF, and consequent inhibition of VEGFR2 phosphorylation. This leads to decreased EC proliferation and angiogenesis (Luque *et al*, 2003). However, the functional inactivation of VEGFR2 due to the binding of ADAMTS-1 to VEGF₁₆₅ is reversible, and dissociation of the complex results in an active growth factor and the subsequent phosphorylation of VEGFR2 (Luque *et al*, 2003; Iruela-Arispe *et al*, 2003).

In order to overcome the anti-angiogenic actions of ADAMTS-1 and -8, many tumour types have been found to down-regulate their expression. For example ADAMTS-1 is down-regulated in mammary (Porter *et al*, 2004), hepatocellular and pancreatic carcinomas (Masui *et al*, 2001), and ADAMTS-8 in brain tumours (Dunn *et al*, 2006).

In contrast, the over-expression of full-length ADAMTS-1 in TA₃ mammary carcinoma, Lewis lung carcinoma (Liu *et al*, 2006b), and CHO cell lines (Kuno *et al*, 2004) was found to promote angiogenesis and invasion. This must suggest that C-terminal processing, and consequently the proteolytic status of ADAMTS-1 determines its effect on tumour metastasis *in vivo* (Rocks *et al*, 2008; Liu *et al*, 2006b).

Another potential anti-angiogenic ADAMTS protein is ADAMTS-5, and although the function of full-length ADAMTS-5 in angiogenesis is presently unknown, the first TSR of ADAMTS-5 functions as an angiogenesis inhibitor *in vitro* (Sharghi-Namini *et al*, 2008).

Synthetic and recombinant forms of the centrally located ADAMTS-5 TSR, but not the C-terminal TSR, inhibited EC tubule formation on Matrigel, a consequence of reduced cell-matrix attachment and increased EC apoptosis.

The first TSR peptide of ADAMTS-5 also inhibited EC proliferation in the presence and absence of VEGF, which normally stimulates EC proliferation; although this did not contribute significantly to the decrease in EC tube-like structures. However, unlike other known anti-angiogenic proteins, the first TSR peptide of ADAMTS-5 promotes the migration of ECs; it is hypothesised that this increased motility may decrease the ability of ECs to form organised tubules (Sharghi-Namini *et al*, 2008).

Llamazares *et al* (2007) provided extensive evidence that ADAMTS-12 functions as an angio-inhibitory protein.

ADAMTS-4 and -5 and Cancer Progression

A number of ADAMTS proteins have been implicated in the progression of cancer, but a specific role in this progression has yet to be elucidated. These include ADAMTS-4, -5, -8, -13 and -15.

Human glioblastomas are the most common type of brain tumours, and also the most difficult to treat effectively due to their infiltrative invasion of surrounding normal neural tissue (Viapiano *et al*, 2008). The ECM can modulate cellular movement, as is the case for glioblastomas (Nutt *et al*, 2001), which consistently up-regulates the ECM protein brevican, a neural-specific CSPG, also known as brain enriched hyaluronan binding protein (BEHAB). In normal brain tissue brevican inhibits cell and neurite motility, but its over-expression in glioblastomas dramatically enhances tumour growth and invasion *in vitro* and *in vivo* (Viapiano *et al*, 2008).

An up-regulation of brevican cleavage products has also been observed in human glioblastomas (Viapiano *et al*, 2005), with the N-terminal fragment containing a hyaluronan-binding domain causing increased invasive behaviour of tumours *in vivo* (Zhang *et al*, 1998). Hu *et al* (2008) have since shown that cleaved brevican promotes EGFR activation, increases the expression of adhesion molecules, and promotes the secretion of fibronectin and the accumulation of fibronectin microfibrils on the cell surface. Furthermore, the N-terminal cleavage fragment of brevican binds to fibronectin to promote glioblastoma cell motility in cultured cells and surgical glioblastoma samples (Hu *et al*, 2008).

Brevican is cleaved at a single site (E³⁹⁵-S³⁹⁶) by the hyalactanases ADAMTS-4 and -5, and although both proteinases are present in normal brain tissue, their production is increased in proliferating glioblastoma cells *in situ*, compared to cultured human glioblastoma cells (Held-Feindt *et al*, 2006). These data have led to the conclusion that

ADAMTS-4 and -5 may contribute to the highly invasive behaviour of malignant glioblastomas, via the processing of brevican.

1.6.9 *Tissue Inhibitors of Metalloproteinases (TIMPs)*

The proteolytic activities of ADAM17, ADAMTS-1, 4 and -5 are tightly regulated by the endogenous TIMP3 (Nagase *et al*, 2006); thus ensuring that these enzymes can perform their normal physiological functions without becoming pathological. The remaining three TIMP proteins (TIMP1, 2, and 4) result in varying degrees of ADAM17, ADAMTS-1, 4 and -5 inhibition. TIMPs are expressed by a variety of cell types and are present in most tissue types and bodily fluids (Lambert *et al*, 2004).

TIMPs are between 184 and 194 amino acids in length, and divided into an N-terminal and a C-terminal domain, with the N-terminal domain providing their inhibitory action (Nagase *et al*, 2006). TIMP1, 2 and 4 are present in a soluble form (Lambert *et al*, 2004), whereas the N-terminal domain of TIMP3 binds tightly to sulphated GAGs (Hashimoto *et al*, 2004). Therefore through its interaction with cell membrane HSPGs, e.g. syndecan, TIMP3 may inhibit membrane-bound ADAM proteins, such as ADAM17 (Hashimoto *et al*, 2004), whilst its interaction with ECM CSPGs, e.g. aggrecan, may enable TIMP3 to inhibit extracellular ADAMTS proteins, such as ADAMTS-1, -4 and -5 (Lambert *et al*, 2004).

TIMP3 was shown to be the major *in vivo* regulator of ADAM17 following the partial hepatectomy of TIMP3 null mice. In these mice liver regeneration was impaired due to abnormal inflammation, with elevated TNF- α release, thus suggesting that ADAM17 is one of the major targets of TIMP3 *in vivo* (Mohammed *et al*, 2004). TIMP-1 and -4 are very poor inhibitors of ADAM17, whilst TIMP2 does not inhibit ADAM17 activity at all (Nagase *et al*, 2006).

A number of studies have documented the effective inhibition of ADAMTS-4 and -5 by TIMP3 (Hashimoto *et al*, 2001; Kashiwagi *et al*, 2001). With regards to ADAMTS-4, TIMP1 and 2 showed weak aggrecanase inhibition, with very weak inhibition by TIMP4 (Hashimoto *et al*, 2001). Similarly, Kashiwagi *et al* (2001) demonstrated that the N-terminal domain of TIMP3 is a strong inhibitor of ADAMTS-4 and -5. In contrast they found no inhibition of these enzymes by TIMP1 or 2, and ADAMTS-4 but not ADAMTS-5 inhibition by TIMP4. α_2 -macroglobulin (α_2m) is also an endogenous inhibitor of ADAMTS-4 and -5 (Tortorella *et al*, 2004). In addition TIMP3 inhibits ADAMTS-1 activity, although activity is not completely blocked, this is also true of TIMP2 (Rodríguez-Manzaneque *et al*, 2002).

Interestingly, the dysregulated expression of TIMPs has been observed at various stages of cancer progression. For example, the down-regulation of TIMP1 and 2

expression is associated with increased invasiveness of tumour cells, whilst their over-expression leads to reduced tumour growth and metastasis formation in tumours of various origins (Lambert *et al*, 2004). As previously described (Section 1.5.1) cytokines can also be dysregulated in cancer, and some of these cytokines have been found to regulate the expression of TIMPs. This may provide a mechanism for controlling the proteolytic activity of enzymes under TIMP control. For example when the pro-inflammatory cytokines IL-1 β and TNF- α are applied simultaneously to brain ECs, TIMP3 expression is almost completely blocked (Bugno *et al*, 1999).

1.7 Conclusions

Surgical resection is currently the only curative treatment of liver tumours, but this treatment option is only available to a minority of patients. Hence a need exists for the development of more widely available, effective treatment of liver tumours. Many published investigations implicate adamalysin family members in the development and progression of human tumours. It is therefore feasible that one or more of these family members may also aid the development and/or progression of tumours within the liver.

An investigation into the expression of these proteolytic enzymes is necessary to determine whether they are expressed within the liver and to ascertain whether they are aberrantly expressed by liver tumours to aid tumour colonisation of the liver and/or tumour dissemination. This may ultimately enable the development of novel liver cancer treatments.

Liver tumours with a desmoplastic reaction express higher levels of proteolytic enzymes than liver tumours with other growth patterns; these include well-differentiated HCCs and 42% of colorectal liver metastases. There are currently no commercially available cell lines derived from colorectal liver metastases, but many well-differentiated HCC cell lines are readily available, e.g. HepG2 and HuH-7. These would therefore be appropriate *in vitro* models in which to investigate adamalysin expression in liver tumours.

1.8 Aims and Objectives of the Study

Hypothesis

ADAM17 and ADAMTS-1, -4 and -5 are important mediators of tumour cell invasion and metastasis of the liver.

Overall aim

To determine the potential role of ADAM17 and ADAMTS-1, -4 and -5 in tumour cell invasion and metastasis of the liver.

Specific Objectives

- To determine the production and modulation of ADAM17 and ADAMTS-1, -4 and -5, and their endogenous inhibitor TIMP3, in human hepatoma and stellate cell lines at the mRNA and protein level, and their production at the mRNA level in total RNA extracts of normal adult and foetal liver.
- To determine the effect of pro-inflammatory cytokines on the proliferation of human hepatoma and stellate cell lines.
- To determine the production and release of fractalkine from human hepatoma cells as an indicator of sheddase activity and the role of ADAM17 in this process. Fractalkine may also have a role in invasion and metastatic processes having a role in angiogenesis.
- To determine the levels of cell surface ADAM17 on human hepatoma cells in response to cytokine treatment, which has the potential to increase sheddase activity.

Chapter 2

Materials and Methods

Unless otherwise stated, all experimental methods were performed at ambient temperature (~20°C) and at atmospheric pressure (~100 kPa).

2.1 Materials

2.1.1 Manufacturers of Reagents

Abcam Inc, 332 Cambridge Science Park, Cambridge, UK

Mouse Monoclonal Antibody to GAPDH (ab8245); Mouse Monoclonal Antibody to Hepatoctye Specific Antigen, clone OCH1E5 (ab49432); Rabbit Polyclonal Antibody to ADAM17 (ab2051); Rabbit Polyclonal Antibody to ADAMTS-1 - Carboxyterminal end (ab39194); Rabbit Polyclonal Antibody to ADAMTS-4 - Carboxyterminal end (ab28285); Rabbit Polyclonal Antibody to ADAMTS-5 - Carboxyterminal end (ab39202); Rabbit Polyclonal Antibody to TIMP3 (ab2169); Rabbit Polyclonal Antibody to TIMP3 - Loop 1 (ab39184).

ABgene Ltd, ABgene House, Blenheim Road, Epsom, Surrey, UK

ABsolute™ QPCR SYBR® Green Fluorescein Mix, 2X (AB-1219).

Amersham Biosciences, Part of GE Healthcare UK Ltd, Amersham Place, Little Chalfort, Amersham, Buckinghamshire, UK

ECL Plus Western Blotting Detection Reagents (RPN2132).

Becton Dickinson UK Ltd, Between Towns Road, Cowley, Oxford, UK

FACS Flow™ (342003); FACS Lysing Solution, 10X (349202); IntraSure™ Kit (641776).

Bio-Rad Laboratories Ltd, Bio-Rad House, Maxted Road, Hemel Hempstead, Hertfordshire, UK

iScript™ cDNA Synthesis Kit (170-8891).

Carl Zeiss Ltd, Woodfield Road, Welwyn Garden City, Hertfordshire, UK

Immersion Oil for fluorescence microscopy (518F).

Chemicon Europe Ltd, Part of Millipore, The Science Centre, Eagle Close, Chandlers Ford, Hampshire, UK

Mouse Monoclonal Antibody to Glial Fibrillary Acidic Protein (GFAP), clone GA5 (MAB3402); Rabbit Polyclonal Antibody to TACE/ADAM17 (AB19027); TACE, C-Terminal Control Peptide (AG909).

Chivers Ireland Ltd, Coolock, Dublin, Republic of Ireland

Marvel Original Dried Skimmed Milk Powder.

Dako UK Ltd, Cambridge House, St Thomas Place, Ely, Cambridgeshire, UK

Rabbit Polyclonal to Mouse Immunoglobulin G (IgG) Horseradish Peroxidase Conjugate (P0161).

Fisher Scientific, Part of Thermo Fisher Scientific, Bishop Meadow Road, Loughborough, Leicestershire, UK

Acetic Acid Glacial, Laboratory Reagent Grade (A/0360/PB17); Acetone, Laboratory Reagent Grade (A/0560/17); Methanol, HPLC Grade (M/4056/17); Anhydrous Propan-2-ol, Analytical Reagent Grade (P/7500/17).

Invitrogen Ltd, 3 Fountain Drive, Inchinnan Business Park, Paisley, Renfrewshire, UK

Custom Oligonucleotide Primers; Gibco™ DMEM Low Glucose (31885-023); Gibco™ DMEM High Glucose with GlutaMAX (61965-026); Gibco™ Dulbecco's PBS without CaCl₂ and MgCl₂, 1X (14190-094); Gibco™ Dulbecco's PBS without CaCl₂ and MgCl₂, 10X (14200-067); Gibco™ Foetal Calf Serum (10106-169); Gibco™ Fungizone® Antimycotic (15290-026); Gibco™ L-Glutamine 200mM, 100X (25030-024); Gibco™ Pen Strep (15070-063); Gibco™ Sodium Pyruvate Solution, 100mM (11360-039); Gibco™ 0.05% Trypsin-EDTA, 1X (25300-062); Molecular Probes® Alexa Fluor® 488 Goat Polyclonal Antibody to Rabbit IgG (A11008); Molecular Probes® Alexa Fluor® 488 Rabbit Polyclonal Antibody to Mouse IgG (A11059); Molecular Probes® Alexa Fluor® 568 Goat Polyclonal Antibody to Mouse IgG (A11004); NuPAGE® Antioxidant (NP0005); NuPAGE® 10% Bis-Tris Gel 1.0mm x 10 wells (NP302BOX); NuPAGE® LDS Sample Buffer, 4X (NP0007); NuPAGE® MOPS SDS Running Buffer, 20X (NP0001); NuPAGE® Sample Reducing Agent, 10X (NP0009); NuPAGE® Transfer Buffer, 20X (NP0006); SeeBlue® Plus2 Pre-stained Standard (LC5925); UltraPure™ Agarose (15510-019).

PeproTech EC Ltd, PeproTech House, 29 Margravine Road, London, UK

Recombinant Human IL-1-β (200-01B); Recombinant Human IL-6 (220-06); Recombinant Human TNF-α (300-01A).

Perbio Science UK Ltd, Unit 9, Atley Way, North Nelson Industrial Estate, Cramlington, Northumberland, UK

Dharmacon DharmaFECT 4 Transfection Reagent (T-2004-02); Dharmacon ON-TARGET plus human ADAM17 SMART pool (L-003453-00); Dharmacon ON-TARGET plus human GAPD CONTROL pool (D-001830-10-05); Dharmacon ON-TARGET plus Non-targeting pool (D-001810-10-05); Dharmacon siRNA Buffer, 5X (B-002000-UB-100); Pierce Restore™ Plus Western Blot Stripping Buffer (46430).

Promega UK Ltd, Delta House, Southampton Science Park, Southampton, UK

Blue/Orange 6X Loading Dye (G1881); 25bp DNA Step Ladder (G4511); Magnesium Chloride Solution, 25 mM (A3511).

R & D Systems Europe Ltd, Barton Lane, Abingdon, Oxfordshire, UK

DuoSet[®] ELISA Development System, Human CX₃CL1/Fractalkine (DY365); Mouse IgG₁ Isotype Control, fluorescein conjugate (IC002F); Mouse Monoclonal Antibody to CX3CL1/Fractalkine (MAB3651); Mouse Monoclonal Antibody to Human TACE, Cytosolic (MAB2129); Mouse Monoclonal Antibody to Human TACE, fluorescein conjugate (FAB9301F); Mouse Monoclonal Antibody to Human TIMP3 (MAB973).

Santa Cruz, Bergheimer Str 89/11, 69115 Heidelberg, Germany

Rabbit Polyclonal TACE (H-170) IgG (sc-25782).

Sigma-Aldrich Company Ltd, The Old Brickyard, New Road, Gillingham, Dorset, UK

Albumin from Bovine Serum (A3059); Bicinchoninic Acid Solution (B9643); BioChemika DEPC-treated Water (95284); Brilliant Blue R (B0149); Cell Dissociation Solution, 1X, Non-Enzymatic (C5914); Cell Growth Determination Kit, MTT Based (CGD-1); CelLytic[™]-M Mammalian Cell Lysis/Extraction Reagent (C2978); Chloroform (C2432); Copper(II) Sulphate Pentahydrate 4% Solution (C2284); Dimethyl Sulfoxide (D2650); Deoxyribonuclease I (DNase I), Amplification Grade (AMP-D1); ECACC HepG2 Cell Line (85011430); Ethanol for Molecular Biology (E7148); Fluka Tri Reagent[™] (93289); Goat Polyclonal Antibody to Rabbit IgG (whole molecule), Horseradish Peroxidase Conjugate (A9169); Hydrochloric Acid, 37% (H-7020); Minimal Essential Medium Eagle with Earle's Salts (M2279); MEM Non-Essential amino acid solution, 100X (M7145); Paraformaldehyde (P6148); 1, 10-Phenanthroline Monohydrate (P9375); Ponceau S Solution (P7170); Propidium Iodide (P4170); Protease Inhibitor Cocktail for general use (P2714); 2-Propanol, for Molecular Biology, minimum 99% (I9516); Rabbit Polyclonal Antibody to Actin (20-33) (A5060); Sulphuric Acid, ACS Reagent (320501); SYBR[®] Green I (S9430); Trichloroacetic acid, SigmaUltra, minimum 99% (T9159); Tris-Borate-EDTA Buffer, 10X (T4415); Tris Buffered Saline, 10X (T5912); Tween[®] 20 (P1379).

Stratagene Europe, Gebouw California, Hogehilweg 15, 1101 CB Amsterdam Zuidoost, The Netherlands

MVP[™] Total RNA, Human Liver (540017); MVP[™] Total RNA, Human Foetal Liver (540173).

Vector Laboratories Ltd, 3 Accent Park, Bakewell Road, Orton Southgate, Peterborough, UK

VECTASHIELD Mounting Medium with DAPI (H-1200).

2.1.2 Manufacturers of Consumables

Amersham Biosciences, Part of GE Healthcare UK Ltd, Amersham Place, Little Chalfont, Amersham, Buckinghamshire, UK

Hybond-C Extra Nitrocellulose Membrane, 20 cm X 3 m (RPN203E).

Becton Dickinson UK Ltd, Between Towns Road, Cowley, Oxford, UK

Disposable 21-Gauge Needle (SZR-175-530R); Falcon 5 mL Polystyrene Round Bottom Tubes (352054); Plastipak™ 20 mL Sterile Syringes (BD300629).

Bio-Rad Laboratories Ltd, Bio-Rad House, Maxted Road, Hemel Hempstead, Hertfordshire, UK

iQ 96-well PCR plates (223-9441); Optical Quality Sealing Tapes (223-9444).

Fisher Scientific, Part of Thermo Fisher Scientific, Bishop Meadow Road, Loughborough, Leicestershire, UK

Azo Wipe®, Bactericidal Wipes (Hyg-231-001T); Disposable Centrifuge Tube, 15 mL (05-539-12), and 50 mL (05-539-8); Cover Glass 22 x 50 mm, 0.13-0.17 mm thick (102250); Filter paper (FAB-OFF-330W); Improved Neubauer Haemocytometer (MNK-510-020J); Lab-Tek II 8-well Chamber Slide with cover (TKT-210-916Y); Microcentrifuge Tubes, 1.5 mL with Cap (FB74031); Nalgene® Cryo 1°C Freezing Container (CRY-120-010T); Nalgene® 2 mL Cryogenic Vials (CRY-100-021F); Nunclon™ Delta Surface Cell Culture Flasks, T25 (156367) and T75 (156472); Nunclon™ Delta Surface Cell Culture Plates with lid, 6-Well (140675), 24-Well (142475) and 96-Well (167008); Pechiney Plastic Packaging Parafilm M Laboratory Wrapping Film (13-374-10); Pipette Tips, 10 µL Crystal (FB34521), 200 µL Yellow (FB34531) and 1000 µL Blue (FB31611); Pipettes, Sterile, 5 mL (13-676-10H), 10 mL (13-676-10J) and 25 mL (13-676-10K); Rexam Medical Autoclave Indicator Tape (AUY-170-030P); Semperit Medium Nitrile, Powder-free, Disposable Gloves (SAR-265-050G); Wash Bottle (03-409-22C); Weigh boats, Small (FB50333), Medium (FB50335) and Large (FB50337).

R & D Systems Europe Ltd, Barton Lane, Abingdon, Oxfordshire, UK

Clear 96-Well Microplate (DY990).

Sarstedt Ltd, Boston Road, Beaumont Road, Beaumont Leys, Leicester, UK

0.20 µm filter, sterile (83.1826.001); Microcentrifuge Tubes, 0.5 mL with Cap (72.699).

Sigma-Aldrich Company Ltd, The Old Brickyard, New Road, Gillingham, Dorset, UK

0.6mL Clear-View Snap-Cap Microtubes (T2566); QuickDraw™ Blotting Paper (P6928).

Starlab (UK) Ltd, Tanners Drive, Blakelands, Milton Keynes, UK

1-10 μ L Graduated Filter Tips, Sterile (S1121-3810); 1-20 μ L Bevelled Filter Tips, Sterile (S1120-1810); 1-200 μ L Graduated Filter Tips, Sterile (S1120-8810); 101-1000 μ L Extended Length Filter Tips, Sterile (S1122-1830)

VWR International Ltd, Hunter Boulevard, Magna Park, Lutterworth, Leicestershire, UK

BD Falcon Cell Scraper, 25 cm Handle/1.8 cm Blade (353086).

Whatman International Ltd, Springfield Mill, James Whatman Way, Maidstone, Kent, UK

Lens Cleaning Tissue (2105 862).

2.1.3 Manufacturers of Equipment

Amersham Pharmacia Biotech, Part of GE Healthcare UK Ltd, Amersham Place, Little Chalfont, Amersham, Buckinghamshire, UK

Electrophoresis Power Supply, EPS 301.

Anachem Ltd, Anachem House, Charles Street, Luton, Bedfordshire, UK

Gilson Pipetman, P2, P10, P20, P100, P200 and P1000.

Applied Biosystems, Lingley House, Birchwood Boulevard, Warrington, Cheshire, UK

Primer Express[®] Software V2.

Becton Dickinson UK Ltd, Between Towns Road, Cowley, Oxford, UK

FACSCalibur Flow Cytometer with Cell Quest Pro Software.

Bio-Rad Laboratories Ltd, Bio-Rad House, Maxted Road, Hemel Hempstead, Hertfordshire, UK

iCycler iQ[™] Real-Time Detection System; Mini-Protean III Electrophoresis Cell; Mini-Sub[®] Cell GT for Agarose Gel Electrophoresis.

Carl Zeiss Ltd, Woodfield Road, Welwyn Garden City, Hertfordshire, UK

LSM 510 Laser Scanning Confocal Microscope with LSM 510 Software V3.2 SP2.

Epson (UK) Ltd, Maylands Avenue, Hemel Hempstead, Hertfordshire, UK

Epson Expression 1680 Pro Scanner.

Eurofins MWG Operon, Worples Road, Raynes Road, London, UK

Primus Thermo Cycler.

Fisher Scientific, Part of Thermo Fisher Scientific, Bishop Meadow Road, Loughborough, Leicestershire, UK

Fisherbrand Hydrus 300 pH meter; Stirring Hotplate; Stuart Scientific Blood Tube Rotator, SB1.

Forma Scientific, BOX 649, Marietta, Ohio, USA

CryoMed Cell Dewar.

Grant Instruments (Cambridge) Ltd, Shepreth, Cambridgeshire, UK

Digital dry block heating system, QBD2; Universal Unstirred Water Bath, SUB14.

Heracus Instruments, Kandro Laboratories Products, Germany

HERAsafe Class II Microbiological Safety Cabinet; HERAcell Incubator.

Invitrogen Ltd, 3 Fountain Drive, Inchinnan Business Park, Paisley, Renfrewshire, UK

Novex XCell *SureLock*™ Mini Cell for electrophoresis.

Labtech International Ltd, Acorn House, The Broyle, Ringmer, East Sussex, UK

Nanodrop® ND-1000 Spectrophotometer.

Leica Microsystems (UK) Ltd, Davy Avenue, Knowlhill, Milton Keynes, Buckinghamshire, UK

Light Microscope with Xli Camera and XLiCAP Imaging Software.

Mettler-Toledo Ltd, Boston Road, Beaumont Leys, Leicester, UK

Analytical Balance, AB104-S.

MSE (UK) Ltd, Worsley Bridge Road, Lower Sydenham, London, UK

MicroCentaur Benchtop Centrifuge, MSB010.CX2.5.

Microsoft Corporation, Redmond, Washington, USA

Microsoft Office Excel 2007.

Perkin Elmer LAS (UK) Ltd, Chalfont Road, Seer Green, Beaconsfield, Buckinghamshire, UK

Wallac Victor² 1420 Multilabel Counter with Wallac 1420 Manager Software V 3.0.

Primer Design Ltd, Millbrook Technology Campus, Second Avenue, Southampton, Hampshire, UK

geNorm Software.

Scientific Laboratory Supplies, Wilford Industrial Estate, Ruddington Lane, Wilford, Nottingham, UK

Clifton Cyclone Vortex Mixer; Integra Biosciences Pipetboy acu.

SPSS® Inc, Chicago, Illinois, USA

Statistical Package for Social Sciences (SPSS) 15.0 for Windows.

Thermo Scientific, Part of Thermo Fisher Scientific, Bishop Meadow Road, Loughborough, Leicestershire, UK

Sorvall Benchtop Centrifuge, RT7 PLUS.

TEW Electric Heating Equipment Co. Ltd, Nan Kang Road, Taipei, Taiwan, Republic of China

Impulse Sealer, TISH-300.

Ultra Violet Products Ltd, Trinity Hall Farm Estate, Nuffield Road, Cambridge, UK

Bio-Imager with Labworks Image Acquisition & Analysis Software V4.

USF Elga Ltd, High Street, Lane End, High Wycombe, Buckinghamshire, UK

Maxima Water Purification System.

2.2 Cell Culture

Three adherent liver cell lines were utilised in this study, HepG2, HuH-7 and LX-2. HepG2 cells are a human well-differentiated HCC cell line derived from a biopsy taken during the hepatic lobectomy of a 15-year old Caucasian male from Argentina in 1975 (Aden *et al*, 1979). These transformed hepatocytes have an epithelial-like morphology, but tend to form islands of cells when cultured *in vitro*.

HuH-7 cells (a gift from Prof. M. Harris, Leeds University, Leeds, UK) are a human well-differentiated HCC cell line isolated on day 28 of the primary cell culture of hepatocytes derived from the surgical removal of the hepatoma of a 57-year old Japanese male in 1982 (Nakabayashi *et al*, 1982). Like the HepG2 cell line, HuH-7 cells have an epithelial-like morphology, but form a monolayer in culture.

LX-2 cells (a gift from Dr. N.C. Bird, Royal Hallamshire Hospital, Sheffield University, Sheffield, UK), are a human activated HSC line obtained from normal liver tissue (Xu *et al*, 2005). The isolated HSCs were transfected with the plasmid pRSVTag that encodes the SV40 large T antigen, which confers immortality, and a single transfected clone was used to establish the LX-1 cell line. The LX-2 cell line was then established by selecting for a subline of LX-1 cells that were able to grow under reduced serum conditions. The LX-2 cell line has a retinoid phenotype typical of stellate cells, and a

98.7% gene expression similarity to primary HSCs as determined by microarray analysis (Xu *et al*, 2005).

All cell culture procedures were carried out under aseptic conditions in a Class II Microbiological Safety Cabinet. Cell lines were grown in the appropriate complete culture medium (Table 2.1) in plasticware (T25 or T75 cell culture flasks, or 6-, 24- or 96-well plates) in a cell incubator with a humidified atmosphere maintained at 37°C and buffered with 5% carbon dioxide.

2.2.1 Recovery of Cryofrozen Cells

Long-term culture of the cell lines was initiated by recovery of cryofrozen cells. Ampoules containing 1 mL of 1×10^6 cells/mL cryofrozen cells were left at room temperature for approximately 1 minute, and then transferred to a 37°C water bath for 1-2 minutes until fully thawed. To decrease the risk of contamination ampoules were never fully immersed in the water bath and wiped with bactericidal wipes prior to opening. The contents of the ampoules were transferred into T25 flasks containing the appropriate, pre-warmed, complete cell culture medium (9 mL) and incubated in a cell incubator.

After 1-2 hours cells were observed under a light microscope at 100X magnification (10X ocular lens and 10X objective lens) for the attachment to the substratum. If attachment had occurred, medium was replaced to remove the toxic dimethyl sulfoxide (DMSO), which was used as a cryoprotector to prevent crystal formation in the cells when freezing. If attachment had not occurred, cells were left overnight to adhere to the substratum before replacement of the medium.

2.2.2 Cell Harvesting and Serial Passage of Cells

Long-term culture of adherent cell lines was achieved by serial passages of sub-confluent monolayers of cells. Spent cell culture medium was aspirated from cell culture flasks and cells washed twice with 5 mL or 10 mL (for T25 or T75 respectively) Dulbecco's phosphate buffered saline (DPBS) without calcium and magnesium, to remove remaining medium. To detach the cells from the substratum 1.5 mL or 3 mL (for T25 or T75 respectively) of 0.05% trypsin/0.53 mM ethylenediaminetetraacetic acid (EDTA) solution was added to the washed cells and incubated in a cell incubator for 5 minutes.

An equal volume of pre-warmed complete culture medium to trypsin/EDTA was added to the detached cells, mixed by gentle pipetting, and then transferred to a sterile 15 mL centrifuge tube. Suspended cells were centrifuged at 200 x g for 5 minutes to pellet the cells, and supernatant aspirated from the harvested cells to remove the trypsin/EDTA containing medium which is detrimental to cell growth.

Table 2.1: Cell lines utilised in this study, and their appropriate complete culture medium composition.

Cell Line	Cell Type	Origin	Obtained from	Culture Medium
HepG2	Hepatocytes from a well differentiated HCC	Human 15 year-old Caucasian male	European Collection of Cell Cultures (ECACC), UK	500 mL Minimal essential medium (MEME) with Earle's salts 10% (v/v) Heat inactivated foetal calf serum 1% (v/v) Penicillin / Streptomycin (50 Units/mL / 50 µg/mL) 1% (v/v) L-Glutamine (2 mM) 1% (v/v) Non-essential amino acids
LX-2	Activated HSCs from a normal liver	Human	Dr. N.C. Bird, Sheffield University, Sheffield, UK	500 mL Dulbecco's modified Eagle's medium (DMEM), high glucose, GlutaMax 10% (v/v) Heat inactivated foetal calf serum 1% (v/v) Penicillin / Streptomycin (50 Units/mL / 50 µg/mL) 1% (v/v) Fungizone Antimycotic (2.5 µg/mL amphotericin B) 1% (v/v) Sodium Pyruvate (1 mM)
HuH-7	Hepatocytes from a well differentiated HCC	Human 57 year-old Japanese male	Prof. M. Harris, Leeds University, Leeds, UK	500 mL DMEM, 1g glucose, pyruvate, L-Glutamine 10% (v/v) Heat inactivated foetal calf serum 1% (v/v) Penicillin / Streptomycin (50 Units/mL / 50 µg/mL) 1% (v/v) L-Glutamine (2 mM)

Cells were re-suspended in a known volume of fresh pre-warmed culture medium, and counted (Section 2.2.3) at this time if required for experimental procedures, or 1 mL of the suspended cells were decanted into a clean, sterile T25 or T75 culture flask and mixed by gentle pipetting with 9 mL or 19 mL pre-warmed complete culture medium, respectively. Culture flasks were placed in a cell incubator and observed after 1-2 hours under a light microscope at 100X magnification (10X ocular lens and 10X objective lens) for reattachment of cells to the substratum.

2.2.3 Cell Counting

Harvested cells were re-suspended in a known volume of culture medium, from which the cell density was calculated using an improved Neubauer haemocytometer. Briefly, a quartz coverslip was placed over the counting chamber forming a void with a depth of 0.1 mm. 10 μ L cell suspension was introduced into this void via capillary action and viewed under a light microscope at 100X magnification. The number of cells in the central and four corner squares of the counting chamber grid were counted; this represents a surface area of 0.2 mm² or a volume of 0.02 mm³. From this the number of cells per mL was calculated using the following equation:

$$\text{Cell concentration per mL} = \text{Total Cell Count in 5 squares} \times 5 \times 10^4$$

2.2.4 Cytokine Treatment of Cells

For qRT-PCR analysis cells were seeded into 24-well plates at a density of 1×10^5 cells/well in a volume of 1 mL complete cell culture medium. Cells were allowed to adhere for 24 hours in a cell incubator, after which spent medium was aspirated from cells. Cells were washed twice with DPBS to remove all traces of serum from the complete culture medium, which may influence the experiment.

Cytokines were diluted to working concentrations of 0.001 mg/mL, 0.01 mg/mL and 0.1 mg/mL in sterile water (IL-1 β and TNF- α) or 5 mM acetic acid (IL-6) and stored at -20°C until required.

Cells were treated in triplicate wells with 1 ng/mL, 10 ng/mL or 100 ng/mL of IL-1 β , IL-6 or TNF- α in 1 mL of serum-free medium and incubated in a cell incubator for 24 hours. As a control for IL-1 β and TNF- α treatment, untreated cells were incubated for 24 hours in 1 mL of serum-free medium. As a control for IL-6 treatment, cells were incubated for 24 hours with 1 μ L 5 mM acetic acid in 1 mL of serum-free medium, to ensure that any effect of IL-6 treatment was due to the cytokine and not the dissolving acetic acid.

Subsequently spent medium was aspirated from the treated cells and cells were washed twice with DPBS. 0.33 mL Tri Reagent was added to each well of treated cells

and the triplicate samples were pooled. Total RNA was extracted from the treated cell lysates according to the manufacturers' protocol (Section 2.3.1).

Four independent experiments were performed to allow statistical analysis.

Minor alterations were made to this method to allow western blot analysis. Cells were seeded into 6-well plates at a density of 5.4×10^5 cells/well in a volume of 3 mL complete cell culture medium. Cells were treated with 1 ng/mL, 10 ng/mL or 100 ng/mL of IL-1 β , IL-6 or TNF- α in 3 mL of serum-free medium and incubated in a cell incubator for 48 hours. Supernatant was removed from cells and stored at -80°C for analysis by enzyme-linked immunosorbant assay (ELISA) for shed fractalkine (Section 2.6). Cells were lysed by the application of 500 μ L of supplemented CellLytic-M and protein extracted according to the manufacturers' protocol (Section 2.4.1). The remainder of the procedure was unaltered.

2.2.5 Short Interfering RNA (siRNA) Transfection

RNA interference (RNAi) is an evolutionally conserved phenomenon in eukaryotes, which represents a unique form of post-transcriptional gene silencing.

Post-transcriptional gene silencing was performed by the use of lipid-mediated siRNA transfection of HepG2 cells according to the manufacturers' protocol.

HepG2 cells were seeded into a 96-well plate at an optimum density of 1×10^4 cells/well in 100 μ L antibiotic-free, complete culture medium. Cells were allowed to adhere for 24 hours in a cell incubator, after which spent medium was aspirated from cells. Cells were washed twice with DPBS to remove all traces of serum from the complete culture medium, which may have influenced the experiment.

Cells were transfected in triplicate wells for mRNA analysis and 10-wells for protein analysis, with a control siRNA (ON-TARGETplus GAPDH control pool or ON-TARGETplus non-targeting pool), or siRNA for the target gene (ON-TARGETplus ADAM17 SMART pool). Untreated control samples containing antibiotic- and serum-free culture medium were used for a baseline reference. GAPDH siRNA was selected for the HepG2 experimental system as this positive control siRNA typically reduces GAPDH expression by 91% when measured at the mRNA level 24 hours after transfection with 100 nM siRNA.

For each lipid-mediated siRNA transfection, 5 μ L of appropriate 2 μ M siRNA solution was added to 5 μ L antibiotic- and serum-free culture medium and mixed gently. In a separate tube, 0.4 μ L DharmaFECT 4 transfection reagent was added to 9.6 μ L antibiotic- and serum-free culture medium and mixed gently. Both tubes were incubated for 5 minutes before being combined, mixed gently and incubated for a

further 20 minutes. 80 μL antibiotic- and serum-free culture medium was then added to the transfection mix, for a total volume of 100 μL transfection medium.

Spent culture medium was removed from the cultured cells and 100 μL of the appropriate transfection medium added. Cells were incubated in a cell incubator for 48 hours for mRNA analysis and 72 hours for protein analysis.

After the appropriate time, supernatant was removed from cells, and stored at -80°C for analysis by enzyme-linked immunosorbant assay (ELISA) for shed fractalkine (Section 2.6). Cells were lysed as appropriate with a total volume of 250 μL Tri Reagent per 3-wells for mRNA analysis or 500 μL CellLytic-M supplemented with 10% protease inhibitor cocktail and 10 mM 1, 10-phenanthroline per 10-wells for protein analysis according to the manufacturers' protocols (Sections 2.3.1 and 2.4.1 respectively).

At least three independent experiments were performed to allow statistical analysis.

2.2.6 Cellular Proliferation Assay

Cellular proliferation was examined using the MTT based cell growth determination kit (Figure 2.1) according to the manufacturers' protocol.

Cells were seeded into 96-well plates at 2.5×10^4 cells/well in 250 μL complete culture medium and allowed to adhere for 24 hours in a cell incubator. A standard curve of cells was also seeded. Spent medium was aspirated and cells washed twice with 250 μL DPBS. Triplicate wells were treated with 250 μL of cytokines (Section 2.2.4) or serum-free medium for the standard curve, and left to incubate in a cell incubator for 24, 48 or 72 hours.

5 mg/mL MTT solution was aseptically added to triplicate wells of experimental samples and duplicate wells of the standard curve in an amount equal to 10% of the culture volume, and incubated for 3 hours in a cell incubator. Spent medium was carefully removed, and resultant MTT formazan crystals dissolved in MTT solvent (0.1 N HCl in anhydrous isopropanol; acidified isopropanol) in a volume equal to the original culture volume by gentle agitation and trituration.

The absorbance of the reaction solutions were measured at 570 nm in a Wallac Victor² plate reading spectrophotometer, and cells counted (Section 2.2.3) from the remaining repeat of the standard curve. From these data a standard curve of cell numbers was produced and cell numbers in the experimental samples determined using linear regression analysis of the form:

$$y = mx + c$$

y = absorbance; **m** = gradient; **x** = protein concentration; **c** = y intercept

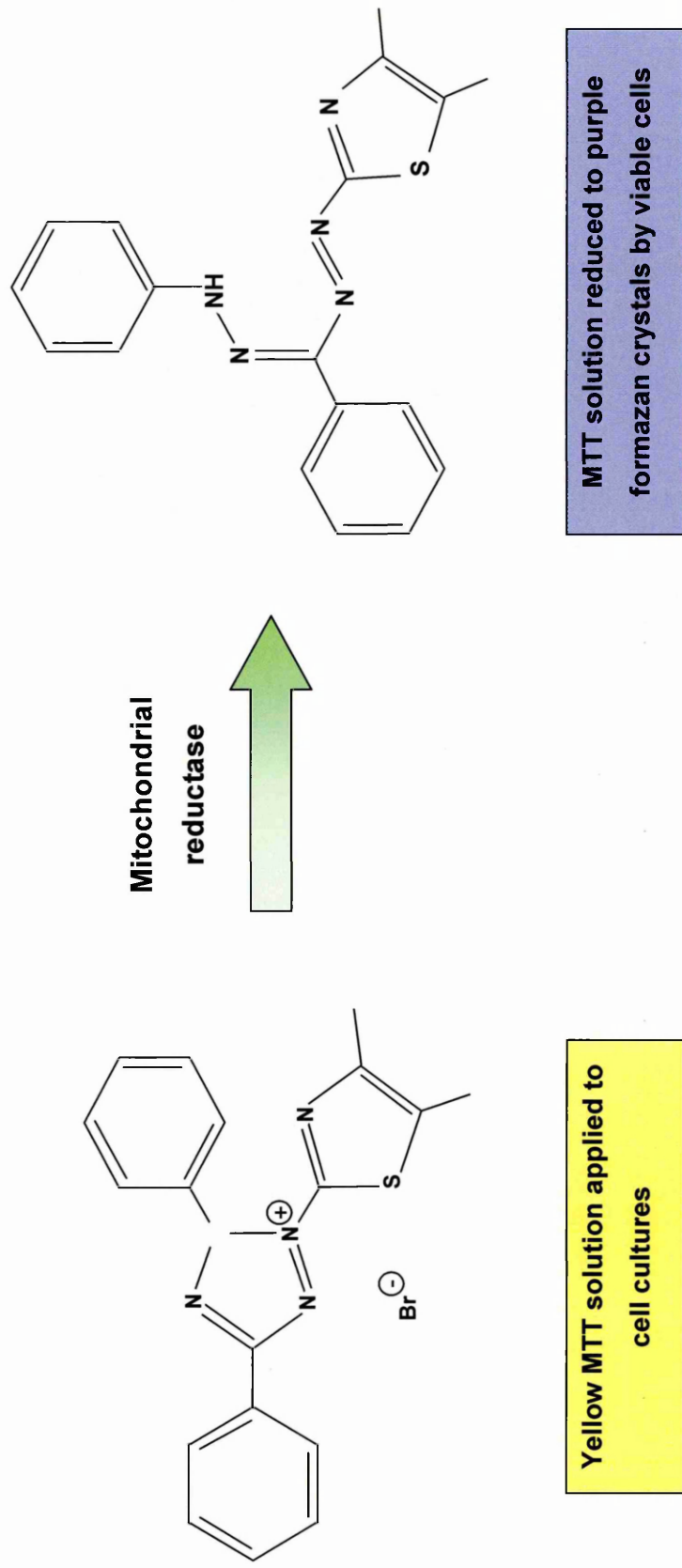


Figure 2.1: Colorimetric MTT based cellular proliferation assay method.

Yellow MTT solution is applied to cultured cells, and reduced by mitochondrial reductase to insoluble purple formazan crystals in living cells. The formazan crystals are then solubilised by acidified isopropanol, and the absorbance of the resultant coloured solution determined. This together with a standard curve of cell numbers allows the number of viable cells within an experimental culture to be ascertained.

Minor alterations were made to this method to accommodate specific conditions required for successful siRNA transfection. HepG2 cells were seeded at 1.0×10^4 cells/well in 100 μ L/well antibiotic-free complete culture medium. In place of cytokine treatment, cells were subjected to siRNA transfection as described in Section 2.2.5 and left to incubate for 24, 48, 72 or 96 hours. The remainder of the procedure was unaltered.

Four independent experiments were performed to allow statistical analysis.

2.3 Quantitative Real-Time (Reverse Transcription) - Polymerase Chain Reaction (qRT-PCR)

qRT-PCR is the standard method commonly used to detect and quantify gene expression. Following the reverse transcription of RNA into complementary DNA (cDNA), PCR is used to amplify the target DNA molecule, which is quantified in real-time by the accumulation of fluorescence after each amplification cycle.

2.3.1 Total RNA Extraction

Total RNA was extracted from cell cultures using Tri Reagent according to the manufacturers' protocol. Briefly, monolayer cells were lysed to form an homogenous cell lysate in an appropriate volume of Tri Reagent (1 mL per 10cm² culture flask) and transferred into 1.5 mL microcentrifuge tubes. 0.2 mL of chloroform was added to samples, mixed vigorously and left to stand for 10 minutes.

Samples were centrifuged at 12,000 x g for 15 minutes at 4°C and the aqueous phase was collected and added to 0.5 mL isopropanol for RNA precipitation. After 10 minutes the samples were centrifuged at 12,000 x g for 10 minutes at 4°C. The resultant RNA pellets were washed with 75% ethanol, centrifuged at 7,500 x g for 5 minutes at 4°C, and then re-suspended in 10 μ L diethyl pyrocarbonate (DEPC)-treated water. Extracted total RNA was stored at -80°C until required. All volumes stated are those required per 1 mL Tri Reagent used in sample preparation, and were adjusted accordingly to accommodate different start volumes of Tri Reagent.

Total RNA from human adult and foetal livers was obtained from Stratagene Europe.

2.3.2 Deoxyribonuclease I (DNase I) Treatment of RNA

Extracted total RNA was subjected to DNase I treatment using a DNase I amplification grade kit according to the manufacturers' protocol, in order to degrade any double or single stranded DNA contamination. Briefly, 8 μ L of extracted RNA was added to a 0.5 mL RNase-free PCR tube, together with 1 μ L of 10X reaction buffer and 1 μ L of amplification grade DNase I, the contents was mixed and allowed to stand for 15 minutes at room temperature.

1 μL of stop solution was then added to inactivate the DNase I prior to heating at 70°C for 10 minutes to denature the DNase I and the RNA. DNase I treated total RNA was stored at -80°C until required. All volumes stated are those required per 8 μL total RNA, and were adjusted accordingly to accommodate different start volumes of total RNA.

2.3.3 Agarose Gel Electrophoresis of Total RNA

The integrity and purity of DNase I treated total RNA was confirmed by the presence of two sharp bands on 1% agarose gels after electrophoresis with SYBR green I staining. The 2 bands were approximately 5 kb and 2 kb in size and represented the 28S and 18S ribosomal RNA (rRNA) molecules respectively; these were present in a 2:1 ratio of 28S:18S rRNA.

To prepare agarose gels 50 mL 1% agarose solution (0.5 g agarose in 50 mL 1X TBE buffer) was heated to melt the agarose, and allowed to cool slightly before being poured into a clean gel tray. A 15-well comb was inserted into the agarose solution and the gel was left to set for approximately 15 minutes.

Agarose gels were placed into an electrophoresis tank containing 1X TBE buffer and the well-forming comb removed prior to loading. A maximum volume of 2 μL of DNase I treated total RNA, mixed with 2 μL blue/orange loading dye and 1.5 μL SYBR green I dye, was loaded per well of the agarose gel.

Electrophoresis was carried out at a constant 100 volts (V) for 15 minutes. An image of the agarose gel was captured on a Bio-Imager system using the LabWorks 4 software package programmed for RNA/DNA gel capture.

2.3.4 RNA Quantification

The concentration of RNA ($\text{ng}/\mu\text{L}$) within a given sample of DNase I treated total RNA was quantified using the Nanodrop[®] ND-1000 spectrophotometer programmed for RNA measurements, according to the manufacturers' protocol.

Briefly, 1.2 μL DEPC-treated water was applied to the base measurement pedestal and the top measurement pedestal lowered into place. A measurement column of liquid was formed between the ends of the two optical fibres located in the measurement pedestals, and a spectrum of measurements taken between 200 nm and 350 nm. These initial absorbance measurements were used to blank the instrument and give a baseline measurement. 1.2 μL total RNA sample was then applied to the base pedestal and the absorbance measurement process repeated, resulting in the determination of RNA concentration (A260) and purity (A280 and A230).

2.3.5 cDNA Synthesis

cDNA was synthesised from intact DNase I treated total RNA using the iScript™ cDNA synthesis kit according to the manufacturers' protocol.

Briefly, 4 µL of 5X iScript reaction mix, 1 µL of iScript reverse transcriptase, 1 µg DNase I treated total RNA, and variable nuclease-free water to a total volume of 20 µL were mixed in an RNase-free PCR tube on ice. The reaction mix was placed in a PCR thermocycler with the following conditions: 25°C for 5 minutes, followed by 42°C for 30 minutes, then 85°C for 5 minutes. The synthesised cDNA was cooled to 4°C prior to storage at -20°C until required.

2.3.6 qRT-PCR

Forward and reverse PCR primers were created for each of the target genes of interest using Primer Express® software (Haddock *et al*, 2006) (see Table 2.2 for full gene name, function and primer sequence).

PCR reactions were prepared on ice and performed in a volume of 20 µL, containing 10 µL 2X Absolute QPCR SYBR Green Fluorescein mix (product contains ThermoStart™ DNA polymerase, dNTPs (dATP, dCTP, dGTP and dTTP), proprietary reaction buffer containing MgCl₂ and enhancers, SYBR Green I dye and fluorescein), 1 µL 12.5 pmol/µL of each of the forward and reverse oligonucleotide primers for the gene of interest, 1 µL 25mM MgCl₂, 4.5 µL RNase-free water and 2.5 µL cDNA template. Reactions were performed in duplicate and four independent experiments were performed to allow statistical analysis.

Amplification was carried out in a Bio-Rad iCycler, Multicolor Real-Time PCR Detection System using the following programme: 2 minutes at 50°C, 15 minutes at 95°C, 40 cycles of 15 seconds at 95°C, then 1 minute at 60°C. Reactions were then subjected to 30 seconds at 95°C, 30 seconds at 50°C, then 45 cycles of 10 seconds starting at 50°C with an increase of 1°C per cycle, enabling melt curve data collection.

Amplification data were plotted for each qRT-PCR reaction and used to calculate cycle threshold (CT) values, from which the difference in threshold cycles for target and reference, known as delta cycle threshold (Δ CT), was computed by use of the equation below.

$$\Delta\text{CT} = \text{Target CT value} - \text{Reference CT value}$$

The expression level of each target could then be calculated (Livak & Schmittgen, 2001), assuming the primer efficiencies of the target and reference genes were approximately 100% (equation below).

Table 2.2: qRT-PCR target gene information, including primer sequences.

Gene abbreviation / Gene name	NCBI accession number	Function	Primer sequence (5' -3')	Position		Primers*	Product size (bp)
ADAM17 / A disintegrin and metalloproteinase 17	NM_003183.3	Enzyme that cleaves several cell-surface proteins, including TNF- α membrane-bound precursor, fractalkine and IL-1 receptor type II	ACGAAAGCGAGTACACTGCAAA	472		D	98
			ATCATCATCTCTTATGTGGCTAGAA	569			
ADAMTS-1 / A disintegrin and metalloproteinase with thrombospondin motifs 1	NM_006988.3	Enzyme that cleaves aggrecan at the '1938- Glu-Leu-1939' site. Also has angiogenic inhibitor activity	GCACTGCAAGGCGTAGGAC	945		D	89
			AAGCATGGTTTCCACATAGCG	1034			
ADAMTS-4 / A disintegrin and metalloproteinase with thrombospondin motifs 4	NM_005099.4	Enzyme that cleaves aggrecan at the '392- Glu- Ala-393' site	TCACTGACTTCCTGGACAATGG	1641		D	80
			GGAAAGTCACAGGCAGATGCA	1721			

*Localisation of forward and reverse primer in different exons (D).

Table 2.2 (continued): qRT-PCR target gene information, including primer sequences.

Gene abbreviation / Gene name	NCBI accession number	Function	Primer sequence (5'-3')	Position	Primers*	Product size (bp)
ADAMTS-5 / A disintegrin and metalloproteinase with thrombospondin motifs 5	NM_007038.3	Enzyme that cleaves aggrecan at the '392-Glu-Ala-393' site	CACTGTGGCTCACGAAATCG	1340	D	92
			CGCTTATCTTCTGTGGAACCAAA	1432		
TIMP3 / Tissue inhibitor of metalloproteinases 3	NM_000362.4	Protein that forms a complex with metalloproteinases, irreversibly inactivating them	TCCGAGAGTCTCTGTGGCCCTTA	1447	D	95
			GCACAGCCCCGGTGACATCT	1542		

*Localisation of forward and reverse primer in different exons (D).

Target expression level = $2^{-(\Delta CT)}$

The amplification data were also used to compute the difference in threshold cycles for the target control and target sample, known as delta cycle threshold of target gene ($\Delta CT_{\text{target}}$), by use of the equation below. A delta cycle threshold of reference gene ($\Delta CT_{\text{reference}}$) was calculated in a similar manner, substituting target CT values with reference CT values (equation below).

$$\Delta CT_{\text{target}} = \text{Control CT value} - \text{Sample CT value}$$

A negative $\Delta CT_{\text{target}}$ value indicates decreased target gene expression, whereas a positive $\Delta CT_{\text{target}}$ value denotes an increase in target gene expression.

To determine the fold change in the target gene an adapted form of the Northern formula (below) was applied, where efficiency relates to the efficiency of the primer pair used (Section 2.3.8).

$$\text{Expression change of target} = E^{\Delta CT_{\text{target}}}$$

An Efficiency $E^{\Delta CT_{\text{target}}}$ ($E^{\Delta CT_{\text{target}}} > 1$) indicates a fold increase in the target gene expression, conversely an $E^{\Delta CT_{\text{target}}} < 1$ signifies the fold decrease in target gene expression.

The Pfaffl equation (below) was used to calculate the relative expression ratio of a target gene in relation to an adequate reference gene (Pfaffl, 2001). A relative expression ratio > 1 indicates a fold increase in the target gene expression after normalisation against a reference gene, conversely a relative expression ratio < 1 signifies the fold decrease in target gene expression after normalisation against a reference gene.

$$\text{Relative expression ratio} = \frac{(\text{Efficiency}_{\text{target}})^{\Delta CT_{\text{target}}}}{(\text{Efficiency}_{\text{reference}})^{\Delta CT_{\text{reference}}}}$$

In addition to melt curve analysis, correct PCR product amplification was verified by agarose gel electrophoresis as Section 2.3.3, but with the following alterations. A maximum volume of 10 μL of PCR product mixed with 2 μL blue/orange loading dye, was loaded per well of the 2.5% agarose gel containing 5 μL ethidium bromide. Samples were run concurrently with 6 μL of a 25 bp DNA ladder to allow product size to be calculated. Electrophoresis was carried out at a constant 100 V for 45 minutes.

2.3.7 Selection of Housekeeping Genes for qRT-PCR

To ensure accurate gene expression measurements, results from qRT-PCR experiments were normalised against a reference gene unaffected by experimental

conditions. Eight commonly used housekeeping genes (β -actin, β_2m , GAPDH, HRPT1, RPL_{13A}, SDHA, UBC and YHWAZ) (see Table 2.3 for full gene name, function and primer sequence) were tested for their suitability in this role. Primer sequences for the potential housekeeping genes were obtained from published sequences (Vandesompele *et al*, 2002).

The housekeeping genes were subjected to qRT-PCR (Section 2.3.6), and discounted as suitable reference genes if there was no product amplification, if product amplification was too high, or if the melting temperature (T_m) of the gene product and the no template control (NTC) product were the same.

geNorm software was then utilised to select the two most stable housekeeping genes for each experimental system from the remaining housekeeping genes. geNorm analysis required the transformation of CT values obtained from qRT-PCR into relative quantification data, prior to input into the geNorm program. The ΔCT method was used to transform the data; ΔCT values were calculated by subtracting the highest CT value from all other CT values measured for each gene, then the equation $2^{(-\Delta CT)}$ was applied to each data point.

The geNorm applet determined the average expression stability measure (M) of each reference gene, and the stepwise exclusion of the least stable gene (highest M value) enabled the two most stable reference genes within each experimental system to be identified. Reference genes in an ideal system have an M <1.5.

2.3.8 Standard Curve Method

The standard curve method was used to establish the efficiency of nine primer pairs. Ideally, the efficiency of each primer pair should be 100%, such that the template is doubled during the exponential phase of each cycle, this is denoted by a slope of -3.32; the correlation coefficient should be 1.00, indicating a strong decreasing linear dependence between variables. However, a good qRT-PCR reaction should have an efficiency between 90 and 110%, which corresponds to a slope between -3.58 and -3.10, with a correlation coefficient close to 1.00.

cDNA from an appropriate cell line was subjected to a two-fold dilution series with ddH₂O, followed by qRT-PCR using the standard curve program on the iCycler, to generate a standard curve from the resultant data.

2.4 Western Blotting

Western blotting is an immunological technique used to detect and quantify a specific protein in a protein extract, cell lysate or tissue homogenate (Figure 2.2). It uses gel electrophoresis to fractionate denatured proteins by the length of their polypeptide

Table 2.3: qRT-PCR housekeeping gene information, including primer sequences.

Gene abbreviation / Gene name	NCBI accession number	Function	Primer sequence (5'-3')	Position	Primers*	Product size (bp)
β-actin / Beta actin	NM_001101.2	Cytoskeletal structural protein	CTGGAACGGTGAAAGGTGACA	1348	S	140
			AAGGGACTTCCTGTAAACAATGCA	1487		
β₂m / Beta-2-microglobulin	NM_004048.2	Beta-chain of MHC class I molecules	TGCTGTCTCCATGTTTGATGATCT	589	S	86
			TCTCTGCTCCCCACCTCTAAGT	674		
GAPDH / Glyceraldehyde-3-phosphate dehydrogenase	NM_002046.3	Oxidoreductase in glycolysis and gluconeogenesis	TGCACCACCAACTGCTTAGC	556	D	87
			GGCATGGACTGTGGTCATGAG	642		
HPRT1 / Hypoxanthine phosphoribosyl-transferase 1	NM_000194.2	Purine synthesis in salvage pathway	TGACACTGGCAAAAACAATGCA	578	D	94
			GGTCCTTTTCACCAGCAAGCT	671		

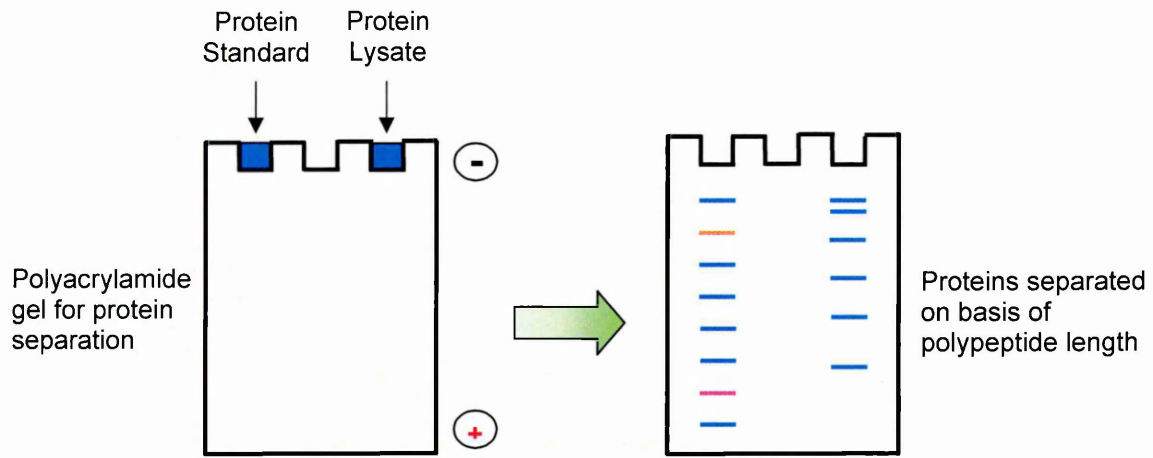
*Localisation of forward and reverse primer in different exons (D) or the same exon (S). [§] A single-exon gene.

Table 2.3 (continued): qRT-PCR housekeeping gene information, including primer sequences.

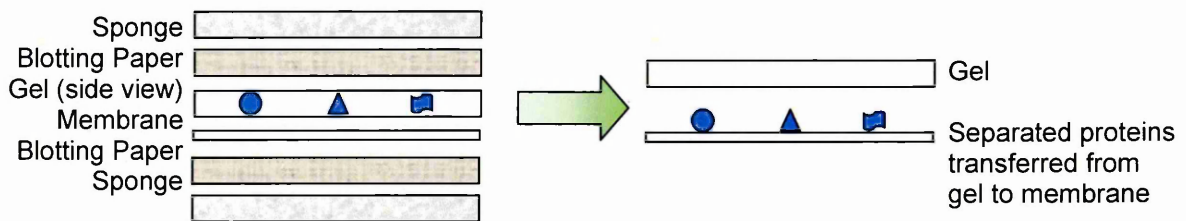
Gene abbreviation / Gene name	NCBI accession number	Function	Primer sequence (5'-3')	Position	Primers*	Product size (bp)
RPL _{13A} / Ribosomal protein L13a	NM_012423.2	Structural component of the large 60S ribosomal subunit	CCTGGAGGAGAAGAGGAAAGAGA	487	D	126
			TTGAGGACCTCTGTGTATTTGTCAA	612		
SDHA / Succinate dehydrogenase complex, subunit A	NM_004168.2	Electron transporter in the TCA cycle and respiratory chain	TGGGAACAAGAGGGCATCTG	229	D	86
			CCACCACTGCATCAAATTCATG	314		
UBC / Ubiquitin C	M26880.1	Protein degradation	ATTGGGTCGCGGTTCTTG	53	D	167
			TGCCTTGACATTCTCGATGGT	219		
YWHAZ / Tyrosine 3-monooxygenase / tryptophan 5-monooxygenase activation protein, zeta polypeptide	NM_003406.3	Signal transduction by binding to phosphorylated serine residues on a variety of signalling molecules	ACTTTTGGTACATTGTGGCTTCAA	1145	S [§]	94
			CCGCCAGGACAAACCAGTAT	1238		

*Localisation of forward and reverse primer in different exons (D) or the same exon (S). [§] A single-exon gene.

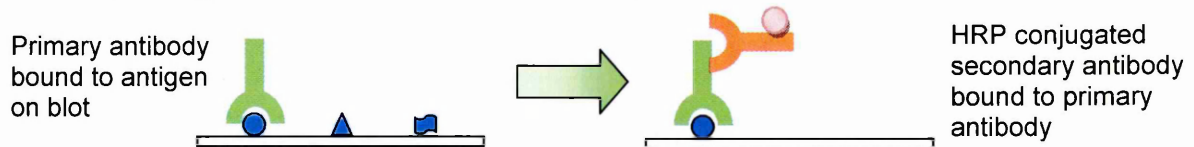
A) SDS-PAGE



B) Western blotting



C) Immunoprobng



D) Chemiluminescent Immunodetection

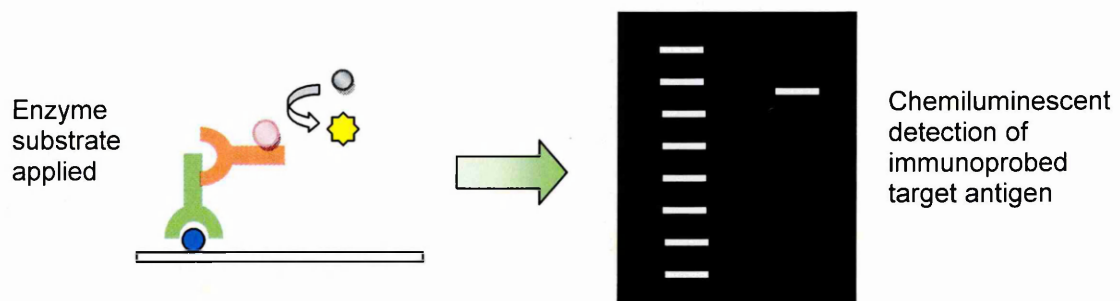


Figure 2.2: Western blotting method.

A) Proteins denatured by SDS are fractionated by gel electrophoresis, **B)** and electroblotted onto a membrane. **C)** Blots are immunoprobng with primary antibodies specific to the target protein, followed by a horseradish peroxidase-linked secondary antibody. **D)** The target protein is visualised by application of enzyme substrate to produce luminescence proportionate to the amount of protein present.

chain, which are then transferred onto a nitrocellulose membrane (NCM) and probed with primary antibodies specific to the target protein. A horseradish peroxidase (HRP) - linked secondary antibody directed against the species-specific portion of the primary antibody in conjunction with a chemiluminescent reagent allows the visualisation of the protein. The amount of luminescence produced is proportionate to the amount of protein present.

2.4.1 Protein Extraction

Following cytokine treatment of cells (Section 2.2.4), protein lysates were prepared by the application of CellLytic-M supplemented with protease inhibitor cocktail (10%) and 10 mM 1, 10-phenanthroline (8.5 mL CellLytic-M, 1 mL protease inhibitor cocktail, 500 μ L 200 mM 1, 10-phenanthroline), according to the manufacturers' protocol. Briefly, monolayer cells were lysed in an appropriate volume of supplemented CellLytic-M. Samples were incubated with agitation for 15 minutes to form an homogenous cell lysate.

To increase total protein yield, cells were scraped from the substratum prior to the collection of the cell lysate. Samples were centrifuged at 12,000 x g for 15 minutes to pellet cellular debris, and protein-containing supernatants transferred into chilled tubes. Protein samples were stored at -80°C until required.

2.4.2 Bicinchoninic Acid (BCA) Assay for Protein Determination

Protein samples were subjected to protein determination by use of the BCA protein assay kit according to the manufacturers' protocol. Briefly, bovine serum albumin (BSA) protein standards of different concentrations ranging from 0.1 mg/mL - 20 mg/mL were prepared, with dilutions made in supplemented CellLytic-M. The required volume of BCA working reagent was prepared by mixing 50 parts of the BCA solution with 1 part copper (II) sulphate pentahydrate 4% solution. 200 μ L of the BCA working reagent was added to 20 μ L of the BSA standards in triplicate and the unknown protein samples in duplicate in a 96-well plate, mixed and allowed to incubate at ambient temperature for 30 minutes.

The absorbance of the reaction solutions were measured at 570 nm in a Wallac Victor² plate reading spectrophotometer. From these data a standard curve was produced and protein concentrations of the experimental samples determined using linear regression analysis of the form:

$$y = mx + c$$

y = absorbance; **m** = gradient; **x** = protein concentration; **c** = y intercept

2.4.3 Trichloroacetic Acid (TCA) Precipitation of Protein

Protein lysates were precipitated using TCA according to the manufacturers' protocol, to allow the concentration of protein samples. Briefly, 50 μ L (1/10 volume) 100% TCA (w/v) was added to each 500 μ L cell lysate sample, vortexed for 15 seconds, placed on ice for 15 minutes, then centrifuged at 14,000 x g for 10 minutes. Following the removal of the supernatant, the resultant protein pellets were washed twice by the addition of 50 μ L acetone, mixing and centrifugation at 14,000 x g for 5 minutes. Protein pellets were air dried for 60 minutes at room temperature, prior to re-suspension in 50 μ L DPBS (sample concentration factor = 10X).

2.4.4 Sodium Dodecyl Sulphate Polyacrylamide Gel Electrophoresis (SDS-PAGE)

Protein samples (6 μ g/lane) were fractionated under reducing conditions on pre-cast NuPage 10% Bis-Tris gels, using the sodium dodecyl sulphate polyacrylamide gel electrophoresis (SDS-PAGE) Laemmli system (Laemmli, 1970).

Protein samples were prepared by adding 50 μ L protein lysate to 25 μ L NuPage LDS sample buffer, 10 μ L mL NuPage sample reducing buffer and 15 μ L dH₂O. All protein samples were reduced by heating to 100°C for 5 minutes in a heating block.

Pre-cast mini gels were placed into a Novex electrophoresis tank containing NuPage MOPS SDS running buffer (25 mL 20X NuPage MOPS SDS running buffer, 475 mL dH₂O, 250 μ L NuPage anti-oxidant), and the well-forming comb removed prior to loading. 6 μ g of protein was loaded per well, and electrophoresis carried out at a constant 125 V for approximately 90 minutes.

Protein samples were run concurrently with SeeBlue Plus 2 pre-stained standard, which contained protein standards of known molecular mass.

2.4.5 Coomassie Blue Staining of Protein

To verify the correct running and equal loading of protein samples, fractionated proteins in SDS-PAGE gels were immersed in Coomassie Brilliant Blue stain (1% Brilliant Blue R, 60% dH₂O, 30% methanol, 10% glacial acetic acid) for 2 hours with gentle agitation. Gels were rinsed in destain (60% dH₂O, 30% methanol, 10% glacial acetic acid), and then left overnight in destain with gentle agitation to remove excess stain from the gel. An image of the gel was captured by use of a general purpose scanner.

2.4.6 Protein Electroblothing

Alternatively, fractionated proteins were transferred onto Hybond-C Extra nitrocellulose membrane, 0.45 μ m pore size, according to the method of Towbin *et al* (1979). A piece

of NCM was soaked for 10 minutes in transfer buffer (84.95% dH₂O, 10% methanol, 5% 20X NuPage transfer buffer, 0.05% NuPage anti-oxidant), along with 2 pieces of Quickdraw blotting paper and 2 pieces of sponge per mini gel.

The transfer cassette was assembled whilst fully submerged to ensure no air bubbles were formed between each layer; bubbles would interfere with transfer. One sponge was placed on the opened transfer cassette, a piece of blotting paper was placed on top of the sponge followed by the NCM, the gel, a further piece of blotting paper and the final sponge. The cassette was closed and placed in the transfer chamber containing transfer buffer, ensuring the NCM was closest to the anode.

Protein transfer from SDS-PAGE gel to NCM was carried out at a constant 100 V for 60 minutes on ice. To verify the transfer process had occurred correctly, blots were briefly immersed in Ponceau S Red to temporarily visualise proteins, then rinsed under running water to remove the stain.

2.4.7 Immunoprobng

Electroblotted proteins were subjected to immunoprobng of the protein of interest. Prior to probng with antibodies, blots were blocked for 90 minutes with gentle agitation, in 5% blocking buffer (5% non-fat milk powder, 100 mL Tris-buffered saline (TBS), 0.05% polyoxyethylene sorbitan monolaurate (Tween-20)); Tween-20 acts as a stringent blocking agent to reduce non-specific binding of antibodies to the NCM.

Blots were incubated overnight at 4°C with the primary antibody diluted to an appropriate concentration in TBS with 0.05% Tween-20 (TBS-T) with or without non-fat milk powder (Table 2.4). For negative controls, primary antibody was omitted from the blots. Unbound antibody was removed from the blot by washing three times for 10 minutes each in TBS-T, with gentle agitation.

HRP-conjugated secondary antibodies diluted to an appropriate concentration in blocking buffer (Table 2.4) were placed onto the blots and incubated for 2 hours with gentle agitation. To eliminate excess secondary antibody, blots were washed twice in TBS-T for 5 minutes each with agitation, then once in TBS for 5 minutes with agitation.

2.4.8 Chemiluminescent Immunodetection

Chemiluminescent immunodetection of immunoprobed blots was carried out using the ECL Plus Chemiluminescence detection system, according to manufacturers' instructions.

Briefly, blots were placed onto a sheet of transparent plastic, ensuring they did not dry out, and the chemiluminescent substrate solution (2 mL Reagent A, 50 µL Reagent B) was applied evenly to the surface of the blot and allowed to develop for 5 minutes.

Table 2.4: Summary of primary and secondary antibodies used for western blotting.

Primary Antibody			Secondary Antibody			
Immunogen	Concentration / Working dilution	Reactivity	Clonality	Immunogen	Concentration / Working dilution	Clonality / Conjugate
TACE/ADAM17 - amino acids 807-823 (AB19027)	3.34 µg/mL / 1 in 300 in 5.0% blocking buffer	Human, Mouse and Rat	Rabbit polyclonal	Rabbit IgG- (A9169)	0.2225 ng/mL / 1 in 80000 in 5.0% blocking buffer	Goat polyclonal / HRP
TACE - H-170 - amino acids 235-404 (sc-25782)	3.34 µg/mL / 1 in 300 in TBS-T	Human, Mouse and Rat	Rabbit polyclonal	Rabbit IgG- HRP (A9169)	0.2225 ng/mL / 1 in 80000 in 2.5% blocking buffer	Goat polyclonal / HRP
ADAMTS-1 - amino acids 920-967 (ab39194)	3.34 µg/mL / 1 in 300 in TBS-T	Human	Rabbit polyclonal	Rabbit IgG- HRP (A9169)	0.2225 ng/mL / 1 in 80000 in 0.01% blocking buffer	Goat polyclonal / HRP
ADAMTS-4 - amino acids 790-837 (ab28285)	3.34 µg/mL / 1 in 750 in TBS-T	Human	Rabbit polyclonal	Rabbit IgG- HRP (A9169)	0.2225 ng/mL / 1 in 80000 in 0.1% blocking buffer	Goat polyclonal / HRP

Table 2.4 (continued): Summary of primary and secondary antibodies used for western blotting.

Immunogen	Primary Antibody			Secondary Antibody		
	Concentration / Working dilution	Reactivity	Clonality	Immunogen	Concentration / Working dilution	Clonality / Conjugate
ADAMTS-5 - amino acids 850-890 (ab39202)	1.00 µg/mL / 1 in 1000 in TBST	Human	Rabbit polyclonal	Rabbit IgG-HRP (A9169)	0.2225 ng/mL / 1 in 80000 in 2.5% blocking buffer	Goat polyclonal / HRP
TIMP3 - amino acids unknown (MAB973)	1.0 µg/mL / 1 in 500 in TBS-T	Human	Mouse monoclonal	Mouse IgG (P0161)	1 in 1000 in 1% blocking buffer	Rabbit polyclonal / HRP
GAPDH - amino acids unknown (ab8245)	0.1 µg/mL / 1 in 5000 in 5% blocking buffer	Broad reactivity	Mouse monoclonal	Mouse IgG (P0161)	1 in 1000 in 5% blocking buffer	Rabbit polyclonal / HRP
Actin - amino acids 20-33 (A5060)	11.8 µg/mL / 1 in 1000 in 5.0% blocking buffer	Broad reactivity	Rabbit polyclonal	Rabbit IgG (A9169)	0.2225 ng/mL / 1 in 80000 in 5.0% blocking buffer	Goat polyclonal / HRP

Excess chemiluminescent substrate solution was removed from the blot prior to covering with a further clean piece of transparent plastic to form a membrane sandwich ready for luminography.

An image of the blot was captured on the UVP Bio-Imager system using the Labworks 4 software package programmed for western blot capture. The molecular mass of the visualised target protein was calculated relative to the protein standards.

Labworks 4 software was also utilised to perform single band density analysis (densitometry). Using the 1D gel toolbar, uniform width lanes were drawn onto the blot and adjusted to surround the band of interest. Ensuring the band was centralised in the lane, the integrated optical density (IOD) was calculated using the background correction option 'Joining Valleys' (20%). This was subtracted from each lane profile prior to IOD calculation.

Analysis of an internal reference protein (actin) in each protein sample allowed the normalisation of the IOD from each protein of interest. The generation of relative IODs enabled comparisons to be made across multiple samples. Normalisation of data was achieved using the following equation:

Relative IOD = IOD of protein of interest – IOD of internal control protein

2.4.9 Stripping of Western Blot Membrane

Primary and secondary antibodies were removed from the blots using Restore™ Plus Western Blot Stripping Buffer according to the manufacturers' protocol.

Briefly, blots were washed for 5 minutes in TBS-T with agitation, incubated with a sufficient volume of stripping buffer to cover the blot for 5 minutes with agitation, and then washed for a further 5 minutes in TBS-T with agitation. Blots were re-blocked and probed for actin, which was used as an internal reference protein to allow normalisation between samples; method as described in Sections 2.4.7 and 2.4.8.

2.5 Immunocytochemistry (ICC)

ICC is an immunological technique used to detect specific antigens in cultured cells by the use of antibodies (Figure 2.3). A primary antibody specific to the antigen is applied to the cells and later a secondary antibody directed against a species-specific portion of the primary antibody is applied. The secondary antibody is conjugated to a fluorochrome, consequently the location of the primary antibody and the bound antigen can be visualised using laser scanning confocal microscopy or fluorescent microscopy.

Cells were seeded into 8-well chamber slides at a density of 1×10^5 cells/well in 400 μ L complete cell culture medium and allowed to adhere for 24 hours in a cell incubator. After this time, spent medium was aspirated and cells were washed twice with DPBS to

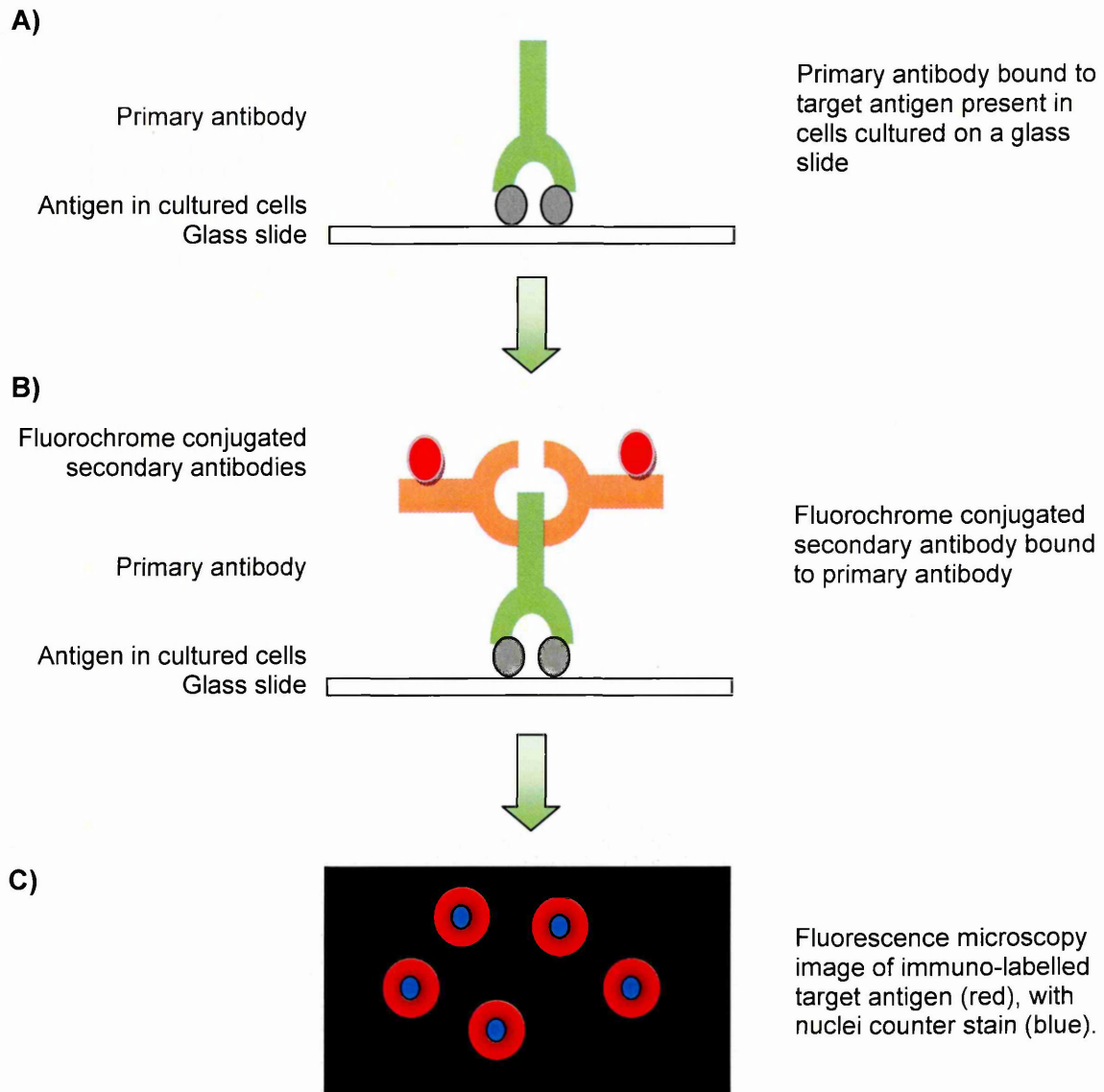


Figure 2.3: Immunocytochemistry (ICC) method.

A) Cells are cultured on a chamber slide, and immunoprobed with primary antibodies specific to the target protein. **B)** A fluorochrome conjugated secondary antibody directed against a species-specific portion of the primary antibody is then applied. **C)** The target antigen is visualised using a fluorescence or confocal microscope. Cells can be counter stained to allow the visualisation of the cell nuclei.

remove all traces of serum from the complete culture medium, which may influence the experiment

Cells were treated with 1 ng/mL, 10 ng/mL or 100 ng/mL of IL-1 β , IL-6 or TNF- α in 400 μ L of serum-free medium and incubated in a cell incubator for 48 hours. As a control for IL-1 β and TNF- α treatment, untreated cells were incubated for 48 hours in 400 μ L of serum-free medium. As a control for IL-6 treatment, cells were incubated for 48 hours with 1 μ L/mL 5 mM acetic acid in 400 μ L of serum-free medium, to ensure that any effect of IL-6 treatment was due to the cytokine and not the dissolving acetic acid.

Subsequently spent medium was removed from the treated cells and cells washed twice with 200 μ L DPBS per well for 5 minutes with gentle agitation. Cells were fixed for 10 minutes with either 200 μ L 4% paraformaldehyde (PFA) (4 $^{\circ}$ C) to visualise cell surface antigens or 200 μ L acetone (-20 $^{\circ}$ C) to permeabilise cells and therefore visualise intracellular antigens.

Fixative was removed from all samples; cells fixed with 4% PFA were washed three times with 200 μ L DPBS per well for 5 minutes each with gentle agitation. Whereas acetone fixed samples were allowed to air dry for 10 minutes, followed by one wash with 200 μ L DPBS per well for 5 minutes with gentle agitation.

Cell preparations were incubated overnight at 4 $^{\circ}$ C with the primary antibody diluted to an appropriate concentration in DPBS (Table 2.5). For negative controls, primary antibody was omitted from the well. Primary antibody was aspirated from the wells and unbound antibody removed by washing three times for 5 minutes each in 200 μ L DPBS, with gentle agitation.

Fluorochrome conjugated secondary antibodies diluted to an appropriate concentration in DPBS (Table 2.5) were applied to the cell preparations and incubated for 1 hour with gentle agitation, in a darkened humidified chamber. Following aspiration of the secondary antibody, cell preparations were washed three times in DPBS for 5 minutes each with gentle agitation in darkness, to eliminate excess secondary antibody whilst preserving antibody fluorescence.

Chambers were removed from the slide and a cell nuclei counter-stain applied to the cells. A coverslip was applied to the slide and the sealed into place with nail varnish. ICC slides were visualised and imaged on a laser scanning confocal microscope at 630X magnification with oil, using the LSM 510 software.

Minor alterations were made to this methodology to accommodate specific conditions required for successful siRNA transfection. HepG2 cells were seeded at 1.0×10^4

Table 2.5: Summary of primary and secondary antibodies used for ICC.

Primary Antibody			Secondary Antibody			
Immunogen	Concentration / Working dilution	Reactivity	Clonality	Immunogen	Concentration / Working dilution	Clonality / Conjugate
TACE - H-170 - amino acids 235-404 (sc-25782)	20 µg/mL / 1 in 50 in DPBS	Human, Mouse, Rat	Rabbit polyclonal	Rabbit IgG (A11008)	4.0 µg/mL / 1 in 500 in DPBS	Goat polyclonal / Alexa Fluor® 488
ADAMTS-1 - amino acids 920-967 (ab39194)	20 µg/mL / 1 in 50 in DPBS	Human	Rabbit polyclonal	Rabbit IgG (A11008)	4.0 µg/mL / 1 in 500 in DPBS	Goat polyclonal / Alexa Fluor® 488
ADAMTS-4 - amino acids 790-837 (ab28285)	20 µg/mL / 1 in 50 in DPBS	Human	Rabbit polyclonal	Rabbit IgG (A11008)	4.0 µg/mL / 1 in 500 in DPBS	Goat polyclonal / Alexa Fluor® 488
ADAMTS-5 - amino acids 850-890 (ab39202)	20 µg/mL / 1 in 50 in DPBS	Human	Rabbit polyclonal	Rabbit IgG (A11008)	4.0 µg/mL / 1 in 500 in DPBS	Goat polyclonal / Alexa Fluor® 488

Table 2.5 (continued): Summary of primary and secondary antibodies used for ICC.

Immunogen	Primary Antibody			Secondary Antibody		
	Concentration / Working dilution	Reactivity	Clonality	Immunogen	Concentration / Working dilution	Clonality
TIMP3 - amino acids unknown (ab2169)	0.2 µg/mL / 1 in 50 in DPBS	Human, Mouse	Rabbit polyclonal	Rabbit IgG (A11008)	4.0 µg/mL / 1 in 500 in DPBS	Goat polyclonal / Alexa Fluor® 488
Fractalkine - amino acids unknown (MAB3651)	2.5 µg/mL / 1 in 200 in DPBS	Human	Mouse monoclonal	Mouse IgG (A11059)	4.0 µg/mL / 1 in 500 in DPBS	Rabbit polyclonal / Alexa Fluor® 488
Hepatocyte Specific Antigen - amino acids unknown (ab49432)	Undetermined / 1 in 50 in DPBS	Human	Mouse monoclonal	Mouse IgG (A11004)	4.0 µg/mL / 1 in 500 in DPBS	Goat polyclonal / Alexa Fluor® 568
GFAP - amino acids unknown (MAB3402)	5 µg/mL / 1 in 200 in DPBS	Human, Porcine, Chicken, Rat	Mouse monoclonal	Mouse IgG (A11004)	4.0 µg/mL / 1 in 500 in DPBS	Goat polyclonal / Alexa Fluor® 568

cells/well in 100 μL /well antibiotic-free complete culture medium. In place of cytokine treatment, cells were subjected to siRNA transfection as described in Section 2.2.5 and left to incubate for 72 hours. The remainder of the procedure was unaltered.

2.6 Enzyme-Linked Immunosorbant Assay (ELISA)

ELISA is used to detect the presence of and quantify the amount of a specific antigen within a sample by the use of antibodies against the antigen of interest (Figure 2.4). The DuoSet human CX₃CL1/Fractalkine ELISA kit was used according to the manufacturers' protocol, to determine the amount of fractalkine shed from the surface of HepG2 cells into the supernatant.

Briefly, 100 μL mouse anti-human fractalkine capture antibody (4.0 $\mu\text{g}/\text{mL}$ in DPBS) was applied per well of a 96-well microplate, the plate was sealed and left to incubate overnight. Capture antibody was aspirated and each well washed three times with wash buffer (0.05% Tween 20 in DPBS). To ensure the complete removal of liquid after each wash, the plate was inverted and blotted against clean paper towels. Plates were then blocked with 300 μL reagent diluents (1% BSA in DPBS) for 1 hour, this was then aspirated and the plate washed three times with wash buffer, as described above. 100 μL sample (HepG2 conditioned medium) or fractalkine standards in reagent diluent were applied per well, covered with an adhesive strip and left to incubate for 2 hours, this was then aspirated and the plate washed three times with wash buffer, as described above. 100 μL biotinylated mouse anti-human fractalkine detection antibody (500 ng/mL in reagent diluent) was applied per well, covered with a new adhesive strip and left to incubate for 2 hours, this was then aspirated and the plate washed three times with wash buffer, as described above.

100 μL streptavidin-HRP (1 part in 100 parts reagent diluent) was applied per well, covered with an adhesive strip and left to incubate for 20 minutes (avoiding direct sunlight). 50 μL stop solution (2 N H₂SO₄) was applied to each well, and mixed by gentle tapping. Finally, the absorbance of the reaction solutions were measured at 450 and 570 nm in a spectrophotometer, and the A₅₇₀ readings subtracted from A₄₅₀ readings to correct for plate imperfections. From these data a standard curve was produced and the concentration of soluble fractalkine present in the experimental samples determined using linear regression analysis of the form:

$$y = mx + c$$

y = absorbance; **m** = gradient; **x** = protein concentration; **c** = y intercept

When the treatment under investigation was known to alter the proliferative capacity of the cell line, the amount of soluble fractalkine was quantified relative to the protein

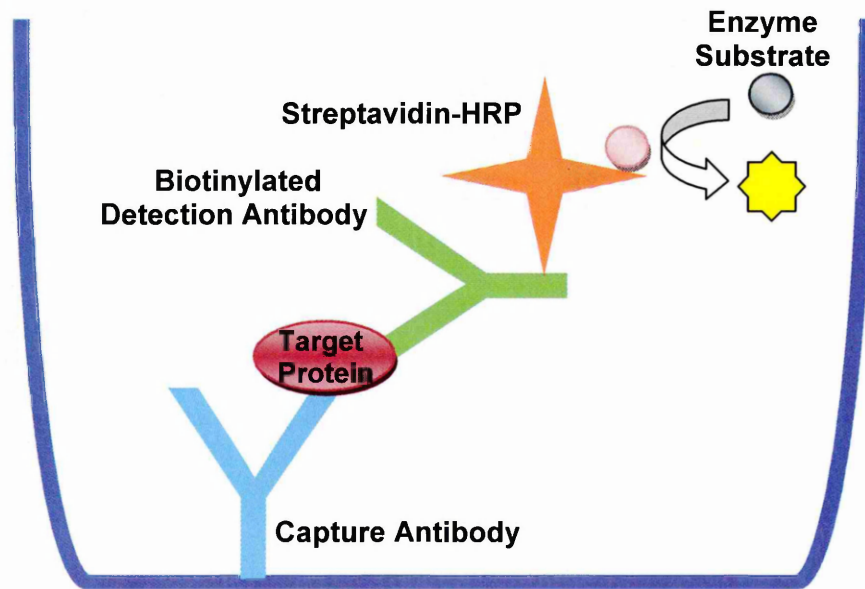


Figure 2.4: The sandwich ELISA method.

A monoclonal capture antibody against a target protein is attached to the walls of a microtiter plate, prior to the addition of a test sample. If target protein is present in the sample, it binds to the capture antibody. A biotinylated detection antibody that also recognises the target protein is then applied to each well, followed by streptavidin tetrameric protein conjugated with HRP reporter enzyme, which binds avidly to biotin. Enzyme substrate is then added and a colour change occurs to reveal the presence if enzyme-labelled antibody bound to target protein. This colour change is measured on a plate reading spectrophotometer.

content of each well from which the supernatant was collected as determined by the BCA assay (Section 2.4.2). Resultant data were presented in the form of concentration of fractalkine (ng)/mg protein. When cellular proliferation was unaltered by treatment, soluble fractalkine was expressed in the form of ng/mL of fractalkine.

At least three independent experiments were performed to allow statistical analysis.

2.7 Flow Cytometry

HepG2 cells were seeded into T25 flasks at 1.4×10^6 cells/flask in 3 mL complete culture medium and allowed to adhere for 24 hours in a cell incubator. Spent medium was aspirated and cells washed twice with DPBS. Flasks were treated with 100 ng/mL IL-1 β , IL-6 or TNF- α in 3 mL of serum-free medium (Section 2.2.4) and incubated in a cell incubator for 24 hours.

Subsequently spent medium was aspirated and cells washed twice with DPBS. Non-enzymatic cell dissociation solution (2 mL) was added to each flask of cells and allowed to act for 10 minutes in a cell incubator. Cells were transferred into 15 mL centrifuge tubes, centrifuged at 200 x g for 5 minutes to pellet the cells, and supernatant aspirated from the harvested cells.

Cells were re-suspended in 2 mL of chilled DPBS containing 1% foetal calf serum (FCS) to prevent non-specific binding of the primary antibody and left to incubate for 5 minutes prior to cell counting (Section 2.2.3). Samples were centrifuged at 200 x g for 5 minutes, supernatant decanted and cells re-suspended in the residual volume. Cells were re-suspended to a density of 1.0×10^6 cell/mL in chilled DPBS containing 1% FCS, and 200 μ L of each cell suspension (1×10^5 cells) aliquoted into six separate flow cytometry tubes; three tubes for cell surface antigen detection and three tubes for intracellular antigen detection. Cells were then pelleted by centrifugation at 200 x g for 5 minutes, supernatant decanted and cells re-suspended in the residual volume.

For cell surface antigen labelling, 10 μ L FITC-conjugated ADAM17 antibody or FITC-conjugated isotype control antibody were added to separate tubes, mixed by gentle agitation and incubated in the dark at 4°C for 30 minutes. The third tube was used as an unlabelled control. 1 mL chilled DPBS containing 1% FCS was added to each tube, mixed by gentle agitation, incubated in the dark for 5 minutes, and then centrifuged at 200 x g for 5 minutes. Supernatant was decanted and cells re-suspended in 300 μ L of DPBS containing 1% FCS. Immediately before flow cytometric analysis, 25 μ L of 100 μ g/mL propidium iodide was added to the ADAM17- and isotype control-labelled samples to allow viable cells to be identified.

For intracellular antigen labelling, the IntraSure kit was used according to the manufacturers' protocol. Briefly, 50 μ L reagent A was added to the each sample, vortexed thoroughly and incubated in the dark for 5 minutes to fix the cells. 1 mL FACS lysing solution was then added, vortexed thoroughly and incubated in the dark for 10 minutes to permeabilise the cells. Samples were centrifuged at 200 x g for 5 minutes and supernatant decanted. 25 μ L reagent B was applied to each sample to further permeabilise the cells, and 10 μ L of FITC-conjugated ADAM17 antibody or FITC-conjugated isotype control antibody were added to separate tubes, mixed by gentle agitation and incubated in the dark at 4°C for 30 minutes. The third tube was used as an unlabelled control. 1 mL chilled DPBS containing 1% FCS was added to each tube, mixed by gentle agitation, incubated in the dark for 5 minutes, and then centrifuged at 200 x g for 5 minutes. Supernatant was decanted and cells re-suspended in 300 μ L 1% PFA in the dark for 30 minutes to re-fix the cells. Samples were then analysed using the flow cytometer.

To determine whether ADAM17 protein was present in HepG2 cells, a fluorescence index (FI) for each set of samples was calculated using the equation below.

$$\text{Fluorescence Index} = \frac{\text{Antibody Fluorescence}}{\text{Isotype Control Fluorescence}}$$

A FI >1 indicates specific antibody staining, whereas a FI <1 signifies no specific antibody staining.

Three independent experiments were performed to allow statistical analysis.

2.8 Statistical Analyses

Statistical analysis of experimental data was performed using Statistical Package for Social Sciences (SPSS) 15.0 for Windows, unless otherwise stated. Appropriate statistical tests were selected following consultation with a statistician (Dr. R. Jackson, Sheffield Hallam University, Sheffield, UK).

The one-sample Kolmogorov-Smirnov test was used to test the normality of the data (Zar, 1999); the mean, variance, skewness and kurtosis were also examined. If the distribution of the data was not normal (i.e. significant Kolmogorov-Smirnov test ($P < 0.05$), and skewness and kurtosis statistics more or less than 0), logarithmic, square root or negative reciprocal transformations were performed, then one-sample Kolmogorov-Smirnov test and skewness and kurtosis statistics were repeated on the new variables, until normality of data was achieved.

One-way analysis of variance (ANOVA) was applied to the normalised data to analyse variation within an experiment, and test the null hypothesis that there is no variation

between the treatment and control groups (Zar, 1999). If the ANOVA rejected the equality of the means ($P < 0.05$), Levene's test was used to test for homogeneity of variances. If variances were found to be equal ($P > 0.05$) a 2-sided Dunnett's test was used for post hoc pairwise analysis, if unequal variances were found ($P < 0.05$) a Dunnett's T3 test was used. The Dunnett's post hoc tests specifically compare the means of treatment groups against the mean of a control group, to identify treatment groups which are significantly different to the control group (Zar, 1999).

When data could not be transformed into a normal distribution, the non-parametric Kruskal-Wallis test was applied to the data to analyse variation within an experiment (Zar, 1999); the null hypothesis was the same as for the ANOVA, i.e. there is no variation between the treatment and control groups. This test uses the ranks of the data rather than the raw data values to calculate the statistic. The Kruskal-Wallis test rejected the equality of the means when $P < 0.05$.

The student's t-test was performed using Microsoft® Office Excel 2007, to assess whether the means of two groups were statistically different from each other when only two independent experiments were performed (Zar, 1999). The null hypothesis states that there is no variation between the treatment and control groups, and the equality of the means was rejected when $P < 0.05$.

Chapter 3

Proliferative Responses and Modulation of ADAM17, ADAMTS-1, -4, -5 and TIMP3 mRNA in Liver Cell Lines by IL-1 β , IL-6 and TNF- α

3.1 Introduction

This chapter describes investigations of the *in vitro* effects of three pro-inflammatory cytokines (IL-1 β , IL-6 and TNF- α), which are often up-regulated in CRC and HCC patients, on the proliferative capacity of two human HCC cell lines, HepG2 and HuH-7, and one human activated HSC line, LX-2, and the modulation of ADAM17, ADAMTS-1, -4, -5 and TIMP3 gene expression in these cell lines.

3.1.1 Cell Culture

The culture of mammalian cells *in vitro* is a fundamental technique that facilitates the investigation of cell behaviour under defined conditions. Modification of these conditions, for example by addition of a specific cytokine or down-regulation of a specific gene, allows the effect of that variable to be examined on cell behaviour and compared to normal physiological (basal) cell behaviour. The most common types of cell culture are primary and secondary (cell lines), each of which has distinct advantages to the researcher.

Primary cultures contain cells separated and purified directly from mammalian tissues, and as such usually contain heterogeneous cell populations. Primary cell cultures generate physiologically relevant data as they closely correspond to the parent cell types and mimic the *in vivo* state of the tissue of origin. However, primary cells can only be utilised over a limited number of sub-cultures (passages) before they die or become altered from the parent phenotype.

Secondary cultures consist of immortalised cells which can be grown indefinitely and this can result in alteration from the parent cell genotype/phenotype. However, as most mammalian cell line cultures contain a homogenous (clonal) population of cells, consistent and reproducible data can be collected from secondary cell cultures.

3.1.2 Cell Viability and Proliferation

It is often important to know the effect a treatment has on the viability and proliferation of a cellular population. These factors can be effectively assessed by use of the colorimetric MTT metabolic activity assay, in which MTT is reduced by mitochondrial reductase into insoluble formazan crystals by viable cells. Absorbance measurements obtained after the solubilisation of formazan crystals allows the number of viable cells within an experimental culture to be ascertained when used in conjunction with a standard curve of cell numbers.

3.1.3 The Principle of qRT-PCR

qRT-PCR is widely used to detect and quantify gene expression. It involves reverse transcription of RNA into cDNA followed by PCR to amplify the target cDNA molecule,

which is quantified in real-time by accumulation of fluorescence after each amplification cycle.

Two distinct types of detection chemistries are used in qRT-PCR, namely probe- or non-probe based chemistries. Probe-based detection methods are termed specific, as they utilise amplicon-specific fluorescent probes that only generate a fluorescent signal when hybridised to their complementary target. Whereas non-probe detection methods rely on fluorescent dyes that intercalate with double-stranded DNA, unbound dye exhibits little fluorescence in solution, but as DNA polymerisation proceeds the dye binds to nascent DNA resulting in an increase in the fluorescence signal. Verification of the PCR product is then required in which a melt curve (dissociation curve) of the amplicon is generated that plots fluorescence as a function of temperature. This step is unnecessary for specific probe-based assays.

There are two established methods of PCR product quantification, relative and absolute. Relative quantification determines changes in the mRNA expression of a target gene across multiple samples and expresses it relative to an internal reference gene, such as a housekeeping gene. Several mathematical algorithms have been developed to produce the corrected relative expression ratio; these include relative quantification without primer amplification efficiency correction, e.g. the comparative CT method (Livak & Schmittgen, 2001), and relative quantification with primer amplification efficiency correction, e.g. the PffafI method (PffafI, 2001).

In order for the former model to be valid, the primer amplification efficiencies of the target and reference genes must be approximately equal, which is not always the case. However, differences in primer amplification efficiencies are taken into consideration in the latter model, making it the more superior model of relative quantification. It is generally considered that relative quantification is adequate for investigating physiological changes in gene expression levels, though care must be taken to select a reference gene that is not affected by the treatment under investigation, or results may be misleading.

Absolute quantification uses a standard curve of CT values, generated from a dilution series of an external standard with known initial target copy number, to determine the absolute quantity of mRNA from a target gene within an unknown sample. The reliability of this method depends heavily on the accuracy of the standards. The strategy of absolute quantification is commonly used to quantify viral or tumour load in bodily fluids (Bustin & Mueller, 2005).

Advances in the technologies surrounding qRT-PCR have led to this technique having increasing importance not only in research, but also in clinical applications. However,

some inherent problems still exist with this method, and reliable quantitative data can only be obtained when each step of the experimental protocol is properly validated.

3.1.4 Specific Objectives

- To determine the parental origin of the three cell lines (HepG2, HuH-7 and LX-2) utilised throughout these studies, by observing cell morphology and cellular markers.
- To establish appropriate controls for each of the cytokine treatments (IL-1 β , IL-6 and TNF- α) used.
- To determine the proliferative effect of each cytokine treatment on each of the three cell lines under investigation.
- To optimise the method of qRT-PCR for the detection of ADAM17, ADAMTS-1, -4, -5 and TIMP3 gene expression.
- To determine the modulating effect of each cytokine treatment on the gene expression of ADAM17, ADAMTS-1, -4, -5 and TIMP3 in each of the three cell lines under investigation.

3.2 Results

3.2.1 Cell Line Characterisation

All *in vitro* experiments in this study were performed on three human liver cell lines, HepG2, HuH-7 and LX-2, so it was necessary to validate the parental origin of these cell lines. The combination of phase contrast microscopy and ICC for cell markers confirms the phenotypes of these cells are consistent with their expected parental phenotype.

Phase contrast microscopy demonstrated that both well-differentiated HCC cell lines HepG2 and HuH-7 displayed an epithelial-like morphology, but with obvious differences in their growth patterns. HepG2 cells formed islands of cells with some areas of highly confluent cells and other areas with no cell coverage (Figure 3.1A), whereas HuH-7 cells formed a uniform monolayer of cells (Figure 3.1B). LX-2 cells also formed a monolayer in culture, but in contrast to HepG2 and HuH-7 cells they had a myofibroblast-like phenotype with protrusions emanating from the main body of the cell (Figure 3.1C).

Cells from each cell line were subjected to immunofluorescent ICC (Section 2.5) following acetone fixation to allow the intracellular staining of two cell markers, hepatocyte specific antigen and GFAP (Figure 3.1). Negative controls were also performed in which the primary antibody was omitted from the staining procedure. See Section 5.2.1 for the optimisation of this technique.

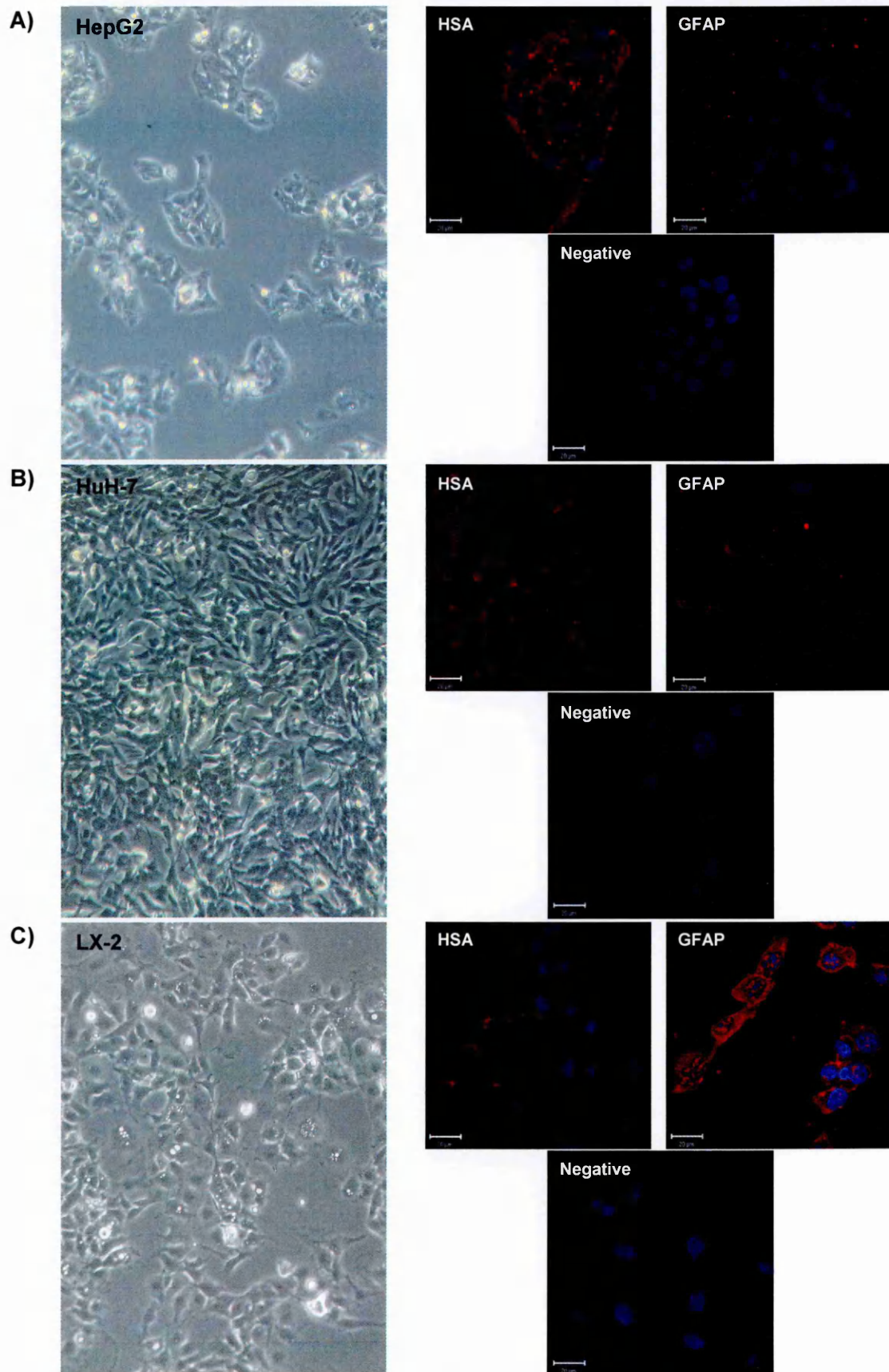


Figure 3.1: Cultured **A)** HepG2, **B)** HuH-7 and **C)** LX-2 cells imaged by phase contrast microscopy (100X), and following ICC for hepatocyte specific antigen (HSA) and GFAP (both red). Nuclei stained with DAPI (blue) in all images. Scale bar is 20 μm .

The characteristic granular cytoplasmic staining of hepatocyte specific antigen was visualised in both the HepG2 and HuH-7 cell lines, but was absent from LX-2 cells. This indicates that HepG2 and HuH-7 cells were derived from hepatocytes, but LX-2 cells were not. Conversely, staining for GFAP revealed that HepG2 and HuH-7 cells had minimal intracellular staining for this neural cell marker. However, LX-2 cells, which were derived from activated HSCs with a neural origin, demonstrate intense GFAP staining.

3.2.2 Establishing Appropriate Controls for Cytokine Treatments

Throughout these investigations an untreated control sample (serum-free medium only) was used for the comparison of IL-1 β and TNF- α treated samples, as these cytokines were dissolved in sterile distilled water as recommended by the manufacturer. An acetic acid-containing control sample (1 μ L 5mM acetic acid in 1 mL serum-free medium) was used to allow comparisons of IL-6 treated samples, as this cytokine was dissolved in 5 mM acetic acid according to the manufacturers' instructions. To establish the effect of the presence of acetic acid in the cell culture media, pH measurements were taken of the serum-free media and acetic acid-containing serum-free media for each cell line after 0, 3, 6 and 24 hours in a cell incubator.

The pH measurements of all samples indicate that they were weak alkaline solutions (Table 3.1), that underwent minor decreases in pH over the 24 hour time course, with a maximum decrease of 0.42 (HuH-7 controls) and a minimum of 0.3 (HepG2 untreated control). No differences in pH were observed between the HuH-7 and LX-2 untreated and acetic acid-containing serum-free media samples at any time point. However, a slight increase in pH was observed at all time points in the acetic acid-containing HepG2 control sample in comparison to the untreated serum-free control sample, ranging from 0.09 immediately after the addition of acetic acid to 0.02 after 24 hours.

3.2.3 Proliferative Responses of HepG2, HuH-7 and LX-2 Cell Lines to IL-1 β , IL-6 and TNF- α

To determine whether the pro-inflammatory cytokines studied (IL-1 β , IL-6 and TNF- α) altered the proliferation rate of HepG2, HuH-7 or LX-2 cells, cells were incubated for 24, 48 or 72 hours with an appropriate concentration of each cytokine. Following this, the cell number of each cell population was determined using the MTT assay (Section 2.2.6). A standard curve of actual cell numbers was used to convert the absorbance reading of metabolic activity into a cell number.

Each experiment included triplicate samples for each time point, and was performed four times to confirm trends found. IL-1 β and TNF- α treated cells were compared to an

Table 3.1: pH measurements of untreated and acetic acid-containing serum-free cell culture media used as control samples for cytokine treatment experiments.

Time point (hours)	HepG2 serum-free media		Huh-7 serum-free media		LX-2 serum-free media	
	Untreated (pH)	Acetic acid-containing (pH)	Untreated (pH)	Acetic acid-containing (pH)	Untreated (pH)	Acetic acid-containing (pH)
0	7.62	7.71	8.01	8.01	7.95	7.95
1	7.41	7.46	7.74	7.74	7.73	7.73
3	7.36	7.39	7.66	7.66	7.67	7.67
6	7.35	7.38	7.64	7.64	7.64	7.64
24	7.32	7.34	7.59	7.59	7.59	7.59

untreated control sample, whereas IL-6 treated cells were compared to an acetic acid-containing control sample.

HepG2 Cells

The numbers of viable HepG2 cells following cytokine treatment with 1, 10 or 100 ng/mL of IL-1 β , IL-6 and TNF- α are shown in Figure 3.2. At the 24 hour time point, 10 ng/mL IL-1 β treated HepG2 cells were considerably increased compared to the control cells (P=0.039). An inverse concentration dependent increase in cell number was observed at both the 48 and 72 hour time points following IL-1 β treatment, such that 1 ng/mL IL- β treated samples had the highest cell number (mean value of 4.89×10^4 and 8.30×10^4 cells/well respectively) and 100 ng/mL treated samples had the lowest number of cells (mean of 3.66×10^4 and 6.35×10^4 cells/well). When compared to the control sample, 1 ng/mL IL- β caused statistically significant increases in cell numbers at both the 48 and 72 hour time points (P=0.039 and P=0.008 respectively), as did 10 ng/mL IL- β after 72 hours (P=0.016).

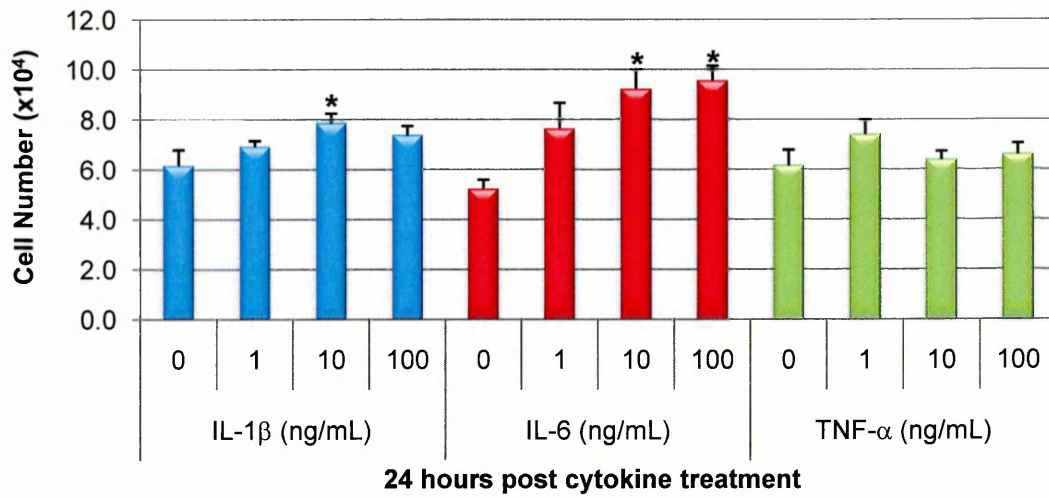
A concentration dependent increase in HepG2 cell number was observed following 24 hours of IL-6 treatment, with a significant increase observed with 10 and 100 ng/mL as compared to the control (P=0.015 and P=0.014 respectively). IL-6 treatment for the extended time points of 48 and 72 hours did not result in differences in cell number when compared to the appropriate control.

TNF- α treatment of HepG2 cells did not alter cell number after 24 hours with any of the concentrations investigated. However after 48 hours of treatment with 1 ng/mL TNF- α , HepG2 cell numbers were increased significantly in comparison to the control (P=0.007). After 72 hours of application, TNF- α caused comparable increases in cell numbers that were statistically different to the control sample for all concentrations tested (P=0.025, P=0.024 and P=0.004 respectively).

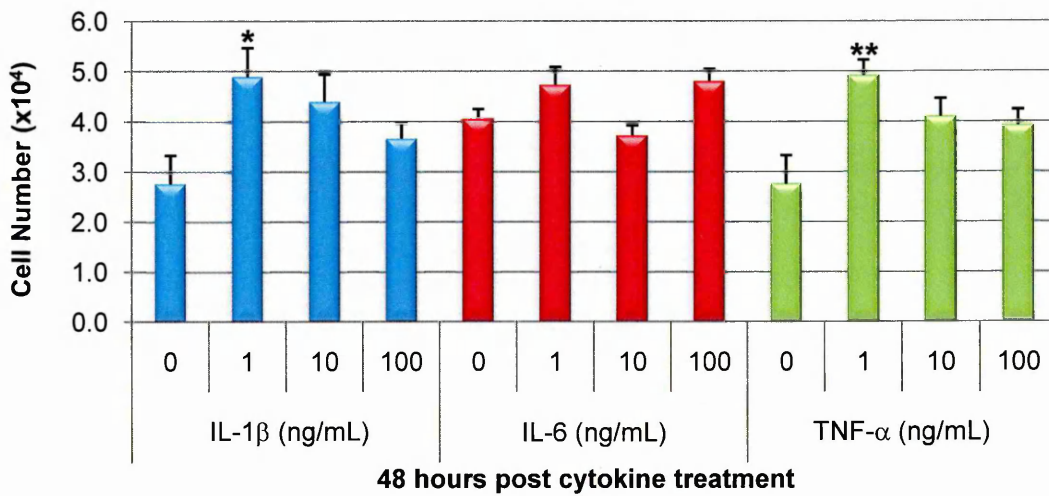
HuH-7 Cells

The numbers of viable HuH-7 cells following cytokine treatment with 1, 10 or 100 ng/mL of IL-1 β , IL-6 and TNF- α are shown in Figure 3.3. At the 24 hour time point, 100 ng/mL of IL-1 β resulted in a statistically significant increase (P=0.038) in the number of HuH-7 cells from a mean value of 1.62×10^4 cells/well to 2.87×10^4 cells/well. This increase was not statistically significant at the later time points of 48 and 72 hours. Minor increases in cell numbers were observed at the 48 and 72 hour time points with 1 and 10 ng/mL of IL-1 β , but these were not statistically different to their controls.

A)



B)



C)

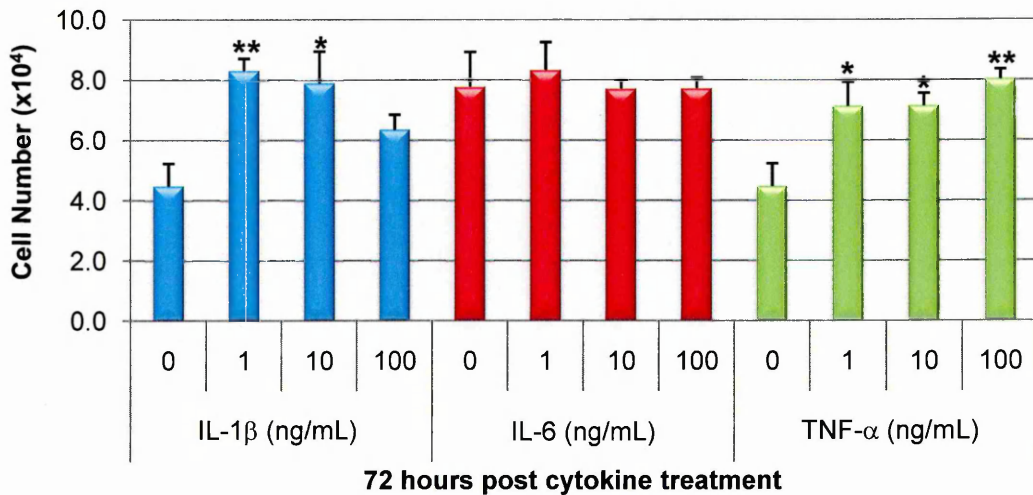


Figure 3.2: Viable HepG2 cell numbers following treatment for **A)** 24 hours, **B)** 48 hours, and **C)** 72 hours with varying concentrations of IL-1 β , IL-6 or TNF- α . Data presented as mean \pm SEM. Significant difference from control, * P<0.05, ** P<0.01 (ANOVA with Dunnett's test; n=4).

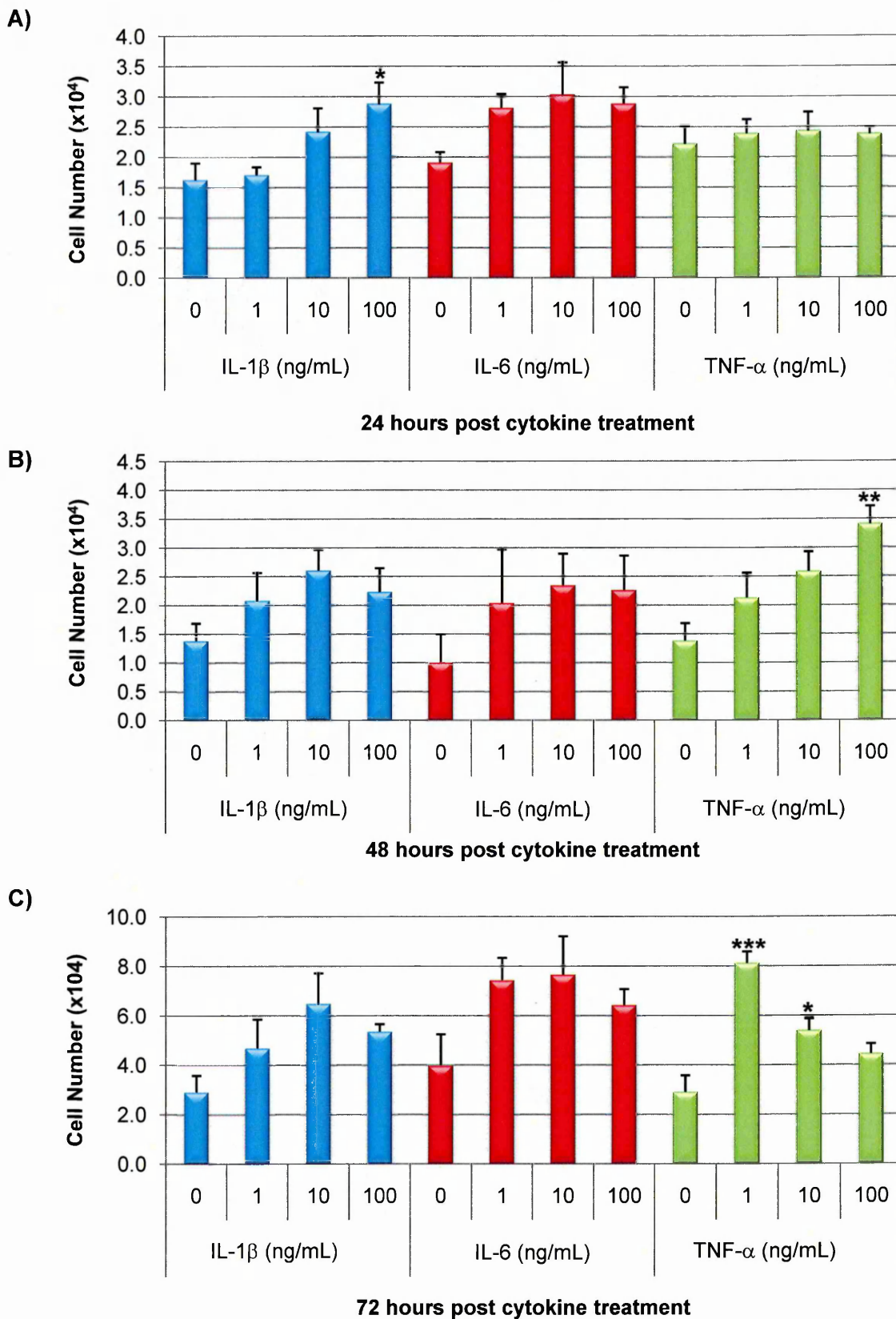


Figure 3.3: Viable HuH-7 cell numbers following treatment for **A)** 24 hours, **B)** 48 hours, and **C)** 72 hours with varying concentrations of IL-1 β , IL-6 or TNF- α . Data presented as mean \pm SEM. Significant difference from control, * P<0.05, ** P<0.01, *** P<0.001 (ANOVA with Dunnett's test; n=4).

IL-6 treatment of HuH-7 cells resulted in an approximately equal increase in cell numbers with 1, 10 and 100 ng/mL, however these changes were not statistically different from the control samples.

No differences were observed in HuH-7 cell numbers after 24 hours treatment with TNF- α at any of the concentrations examined. However at the 48 hour time point, concentration dependent increase of cell number was recorded with increasing concentration of TNF- α , culminating in a statistically significant increase of cells ($P=0.008$) in 100 ng/mL treated samples (a mean value of 3.41×10^4 cell/well compared to 1.38×10^4 cell/well for the control).

Cell numbers were also increased at the 72 hour time point, but in an inverse manner with increasing concentration of TNF- α . Such that 1 ng/mL TNF- α treated samples had the highest cell number (mean value of 8.11×10^4 cells/well) and 100 ng/mL treated samples had the lowest (mean of 4.44×10^4 cells/well). This equated to statistically significant increases of cell number in 1 and 10 ng/mL TNF- α treated samples compared to the control ($P=0.0001$ and $P=0.012$ respectively).

LX-2 Cells

The numbers of viable LX-2 cells following cytokine treatment with 1, 10 or 100 ng/mL of IL-1 β , IL-6 and TNF- α are shown in Figure 3.4. There were no statistically significant changes in cell number with any of the cytokine treatments at any time point when compared to the appropriate control. However, a trend of reduced cell number is observed with treatments of 1 and 100 ng/mL TNF- α at all three time points; these changes were not statistically different to the untreated controls.

3.2.4 qRT-PCR optimisation

qRT-PCR optimisation is paramount in obtaining good, reliable results. Initially a standard PCR protocol was tested; this had a 15 minute hot start at 95°C to activate the enzyme, followed by 40 cycles of 15 seconds at 95°C for denaturation, 15 seconds at 58°C for primer annealing and 30 seconds at 72°C for polymerisation (elongation). The use of a hot start enzyme prevents unspecific amplification due to weak unspecific binding of primers during PCR setup. The amplification cycles were followed by melt curve data collection, consisting of 30 seconds denaturation, followed by 45 cycles of 10 seconds starting at 50°C and increasing by 1°C with each cycle.

Standard curve data generated using the above protocol indicated very poor primer efficiencies for all genes tested (β -actin, HRPT1, YWHAZ, ADAM17, ADAMTS-1, ADAMTS-4, ADAMTS-5 AND TIMP3), with no product amplification seen in many cases. An adjustment of the primer annealing temperature to 60°C and a subsequent

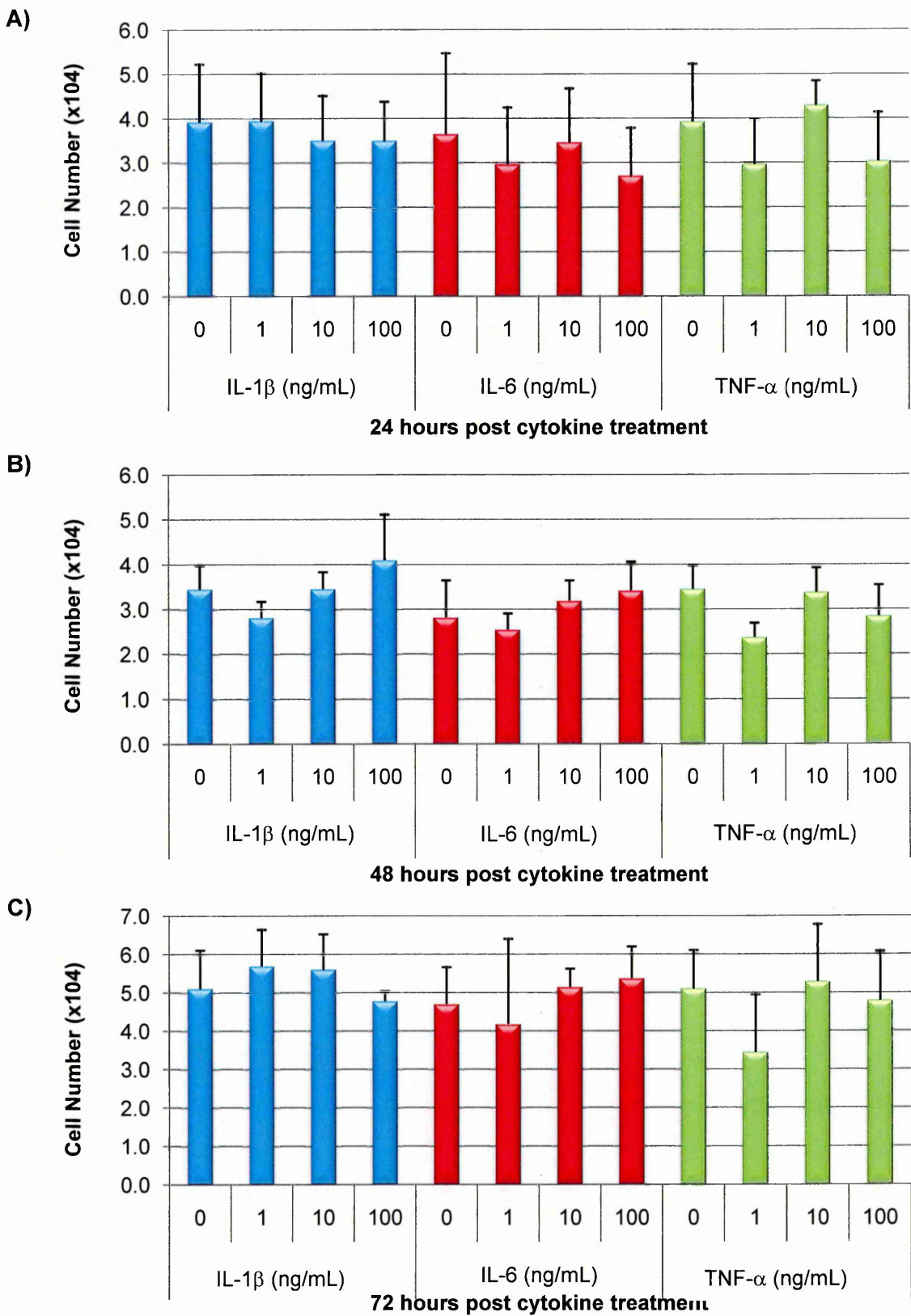


Figure 3.4: Viable LX-2 cell numbers following treatment for **A)** 24 hours, **B)** 48 hours, and **C)** 72 hours with varying concentrations of IL-1 β , IL-6 or TNF- α . Data presented as mean \pm SEM. There were no significant differences in the data (ANOVA with Dunnett's test; n=4).

increase of the number of amplification cycles to 45 proved to have little effect.

The initial qRT-PCR protocol was further adapted and resulted in a highly efficient protocol suitable for all genes of interest. Prior to the 15 minute hot start at 95°C, a 2 minute step at 50°C was added to ensure nothing (in particular the primers) had precipitated out of the reaction mix. 40 cycles of 15 seconds at 95°C (denaturation) and 1 minute at 60°C (polymerisation) followed the hot start. The melt curve data collection and analysis step remained unchanged.

The reaction volume was optimised using HepG2 cDNA under the same reaction conditions, but with varying total reaction volumes (25 µL, 20 µL and 15 µL) (Table 3.2). Observation of the CT values from two housekeeping gene transcripts indicated that reaction volumes of 25 µL and 20 µL gave comparable results (mean CT variation of 0.3 for HPRT1 and 0.1 for YWHAZ). Whereas reduced reaction volumes of 15µL generated minor detrimental effects on the data (mean CT variation of 0.55 for HPRT1 and 0.7 for YWHAZ). Hence, a reaction volume of 20 µL was selected for use in all qRT-PCR experiments.

To further increase the reliability of the results obtained from the qRT-PCR experiments concerning mRNA expression of specific genes within a system, extracted total RNA was treated with DNase I to degrade any contaminating genomic DNA (Figure 3.5; Section 2.3.1 - 2.3.2). The presence of DNA in a qRT-PCR could potentially be amplified and influence the results obtained, due to the sensitivity of the technique.

3.2.5 Selection of housekeeping gene transcripts

Eight widely used housekeeping gene transcripts (β -actin, β_2m , GAPDH, HPRT1, RPL_{13A}, SDHA, UBC, and YWHAZ) were considered for their suitability to act as reference genes for the normalisation of qRT-PCR experiments (Section 2.3.7). Each of these internal control transcripts belongs to a different functional class (Table 2.3), which significantly reduces the chance that the genes might be co-regulated (Vandesompele *et al*, 2002).

From the eight potential reference gene transcripts, five were discarded after preliminary qRT-PCR experiments performed in the HepG2 experimental system (Table 3.3). β_2m was excluded due to the lack of PCR product amplification in the conditions used; CT values of the experimental samples and the negative controls were comparable. SDHA and UBC were discounted as they had the same T_m as the experimental samples and NTC, thus it was not possible to determine if specific product or a contaminant was amplified without performing agarose gel electrophoresis of the samples. Finally, GAPDH and RPL_{13A} were eliminated as reference transcripts

Table 3.2: qRT-PCR data comparing different reaction mix volumes.

Gene	25 μ L			20 μ L			15 μ L		
	CT 1	CT 2	Mean	CT 1	CT 2	Mean	CT 1	CT 2	Mean
HRPT1	22.9	21.0	21.95	22.1	22.4	22.25	23.1	22.5	22.8
YWHAZ	20.5	20.1	20.30	20.0	20.8	20.40	21.0	21.2	21.1

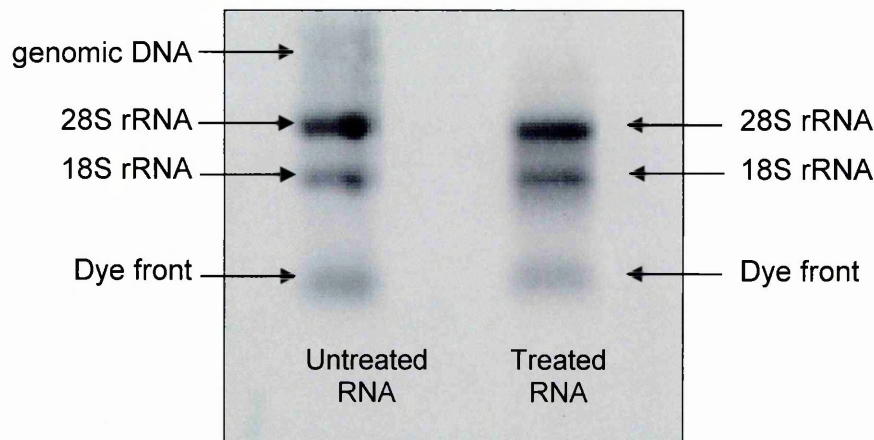


Figure 3.5: Comparison of untreated total RNA to DNase I treated total RNA by agarose gel electrophoresis.

Both total RNA samples subjected to agarose gel electrophoresis were intact and of good integrity, demonstrated by the presence of the 28S and 18S rRNA subunits. The untreated total RNA sample (left) was contaminated with genomic DNA, seen as a high molecular weight species above the 28S rRNA band. Conversely, the total RNA sample subjected to DNase I treatment (right) had no genomic DNA contamination, due to the degrading action of DNase I. This is a negative image of the agarose gel.

Table 3.3: Suitability of reference gene transcripts for the normalisation of qRT-PCR experiments.*

Gene	Sample 1		Sample 2		Sample 3		Negative control		Conclusion
	CT	T _m (°C)	CT	T _m (°C)	CT	T _m (°C)	CT	T _m (°C)	
β-actin	24.2	89	24.0	89	23.9	90	34.1	80	Suitable
β ₂ m	32.9	78	33.1	78	33.0	78	30.7	79	Not detected
GAPDH	13.9	86	15.3	86	14.0	86	>40	77	Too highly expressed
HRPT1	20.4	85	20.8	85	20.7	85	30.6	81	Suitable
RPL _{13A}	13.7	85	13.4	85	14.2	85	35.5	79	Too highly expressed
SDHA	25.7	82	25.7	82	25.7	82	31.0	80	Comparable T _m for product and NTC**
UBC	22.0	87	22.0	87	22.0	87	33.9	87	Comparable T _m for product and NTC
YWHAZ	22.5	84	21.4	84	21.0	84	34.1	78	Suitable

* Data obtained from the HepG2 cell line.

** NTC = No template control.

due to their high expression levels; the low CT value would act to skew the data resulting in inaccurate quantification of the RNA of interest.

The remaining three housekeeping gene transcripts, β -actin, HRPT1 & YWHAZ, were all good candidates for use as reference transcripts in the HepG2 cell line; they are from different functional groups, each have a different T_m for the specific product and negative controls allowing contamination to be easily identified, and all are expressed at moderate levels decreasing the possibility of skewed data.

For each experimental system, the expression stability measure (M) of the two most stable genes was determined using the geNorm applet (Section 2.3.7). These were then used as reference gene transcripts for that particular system allowing the normalisation of other transcripts within that system. Reference gene transcripts in an ideal system have an M-value less than 1.5; the lower the M-value the higher the reference transcripts stability.

The first experimental system tested was HepG2 cells treated with varying concentrations (1 ng/mL, 10 ng/mL or 100 ng/mL) of IL-1 β , IL-6 and TNF- α . The CT values obtained from each qRT-PCR experiment were converted into relative quantification data and subjected to geometric averaging by geNorm. Of the three housekeeping genes assessed, YWHAZ was the least stably expressed gene. After the stepwise elimination of YWHAZ, the M-value of the two most stably expressed genes for this experimental system, β -actin and HRPT1, was 0.703 (Table 3.4), indicating their suitability as reference gene transcripts for this system.

The second experimental system tested was HuH-7 cells treated in the same manner as the HepG2 experimental system. After data conversion and geNorm analysis, the two most stably expressed housekeeping genes tested were HRPT1 and YWHAZ, with the least stable being β -actin. The stepwise omission of β -actin resulted in an M-value of 0.905 for HRPT1 and YWHAZ (Table 3.4), demonstrating that these two gene transcripts are ideal reference transcripts for this system.

The final experimental system tested was LX-2 cells treated as above. Following qRT-PCR data transformation and entry into geNorm, the least stably expressed gene was YWHAZ. Stepwise removal of this gene yielded an M-value of 0.527 for β -actin and HPRT1 (Table 3.4). Therefore, β -actin and HPRT1 are ideal reference gene transcripts for this system.

Table 3.4 indicates some variance in stability of reference gene expression between independent experiments within each system. However, in all cases the M-values were less than 1.5, indicating their suitability as reference genes within these systems.

Table 3.4: geNorm analysis from the HepG2, HuH-7 and LX-2 experimental systems, indicating the generated M-values for each independent experiment.

Cell Line	Reference genes	Cytokine Treatment	Independent Experiment M-values	Mean M-Values	
HepG2	β -actin & HPRT1	IL-1 β	0.325	0.616	
			0.575		
			0.888		
			0.676		
			IL-6	0.636	0.775
				1.100	
				0.642	
				0.723	
			TNF- α	0.357	0.717
				1.077	
				0.165	
				1.269	
Overall Mean M-value				0.703	
HuH-7	HPRT1 & YWHAZ	IL-1 β	1.074	0.885	
			1.020		
			1.217		
			0.229		
			IL-6	---	0.767
				0.703	
				0.887	
				0.712	
			TNF- α	1.183	0.916
				1.094	
				0.989	
				0.397	
Overall Mean M-value				0.905	

Table 3.4 (continued): geNorm analysis from the HepG2, HuH-7 and LX-2 experimental systems, indicating the generated M-values for each independent experiment.

Cell Line	Reference genes	Cytokine Treatment	Independent Experiment M-values	Mean M-Values
LX-2	β -actin & HPRT1	IL-1 β	0.414	0.382
			0.347	
			0.132	
			0.633	
		IL-6	0.737	0.671
			0.563	
			0.900	
			0.485	
		TNF- α	0.259	0.528
			0.773	
			0.366	
			0.712	
Overall Mean M-value				0.527

3.2.6 Primer Efficiencies

After qRT-PCR optimisation and housekeeping transcripts selection, the amplification efficiency of eight primer pairs was assessed. cDNA from an appropriate cell line was subjected to a two-fold dilution series with ddH₂O, followed by qRT-PCR using the standard curve method (Section 2.3.8). The primer efficiency of the housekeeping transcripts, β -actin, HRPT1 and YWHAZ, were tested using cDNA from the HepG2 cell line; THP-1 (human acute monocytic leukaemia cell line) cDNA was used for ADAM17 and TIMP3; and ADAMTS-1, -4 and -5 were assessed using cDNA from U373 cells (human glioblastoma-astrocytoma cell line).

Table 3.5 summarises the primer efficiencies obtained for each primer pair, along with the correlation coefficient and the slope of the line, whilst Figure 3.6 shows the actual standard curve plots generated following qRT-PCR using the standard curve method. The primer efficiencies for the genes tested ranged between 94.4% (ADAMTS-5) and 100% (β -actin), with correlation coefficients of not less than 0.929 (ADAMTS-5) and not more than 0.996 (YWHAZ).

Although this is only a moderately small difference in efficiencies, it was decided that the Pfaffl method of quantification would be more suitable than the $\Delta\Delta$ CT method (comparative CT method); the $\Delta\Delta$ CT method assumes the amplification efficiencies of the target and the control gene are approximately equal, whereas the Pfaffl method allows quantification of genes when their efficiencies are unequal (Section 2.3.6).

3.2.7 qRT-PCR Products

To verify that only the expected qRT-PCR product was amplified in each reaction, amplification and melt curve data, together with agarose gel electrophoresis of the qRT-PCR products were examined (Sections 2.3.3 & 2.3.6).

qRT-PCR amplification data presented in graphical form allowed PCR product amplification to be tracked throughout cycling, and consequently the determination of CT values for each sample. Figure 3.7 illustrates the amplification curves generated after qRT-PCR for each of the selected housekeeping gene transcripts (β -actin, HPRT1 and YWHAZ) and transcripts of interest (ADAM17, ADAMTS-1, -4, -5 and TIMP3) in duplicate, together with their NTC.

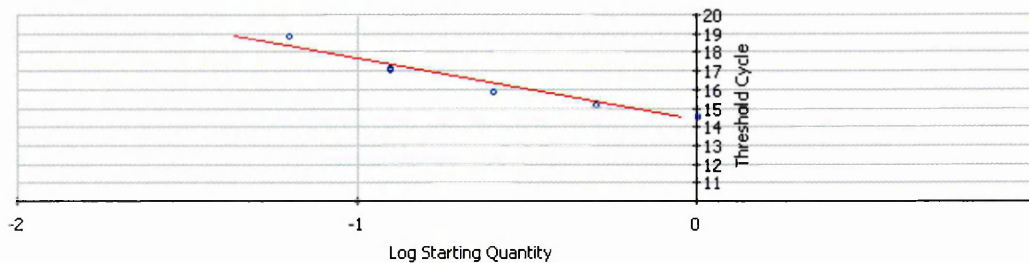
In all cases the duplicate samples showed a sigmoidal growth curve with a CT value of not more than 0.3 cycles difference, demonstrating the accuracy of this technique. The CT values of the experimental samples were in most cases more than 10 cycles (and not less than 4 cycles) lower than the CT value for the NTC, indicating that product is being amplified in the experimental samples. NTCs should not generate a CT value

Table 3.5: qRT-PCR primer efficiencies for each primer pair, including correlation coefficient, slope of line and cDNA source.

Gene	Primer efficiency (%)	Correlation coefficient	Slope	cDNA source
β-actin	100	0.980	-3.321	HepG2 (Hepatoma)
HRPT1	98.9	0.961	-3.349	HepG2 (Hepatoma)
YWHAZ	99.9	0.996	-3.325	HepG2 (Hepatoma)
ADAM17	97.7	0.968	-3.379	THP-1 (Leukaemia)
ADAMTS-1	99.0	0.991	-3.347	U373 (Astrocytoma)
ADAMTS-4	95.0	0.949	-3.447	U373 (Astrocytoma)
ADAMTS-5	94.4	0.929	-3.464	U373 (Astrocytoma)
TIMP3	99.1	0.961	-3.344	THP-1 (Leukaemia)

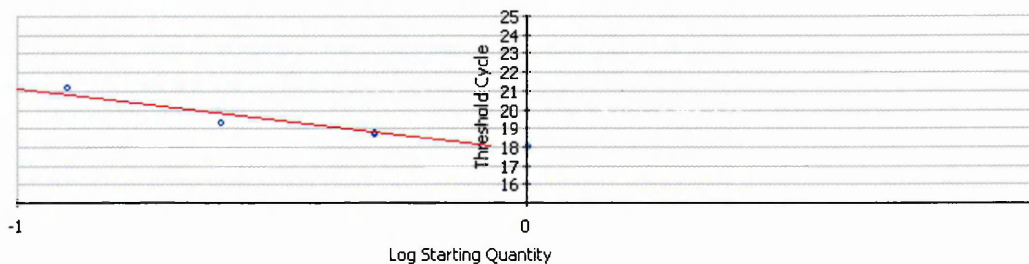
A) β -actin

Correlation Coefficient: 0.980 Slope: -3.321 Intercept: 14.338 $Y = -3.321 X + 14.338$
PCR Efficiency: 100.0 %



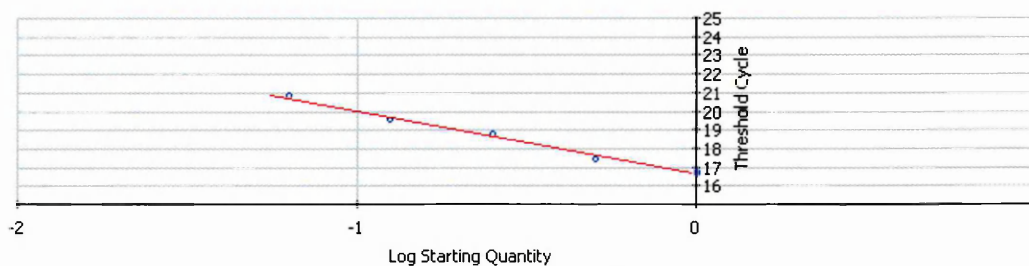
B) HPRT1

Correlation Coefficient: 0.961 Slope: -3.349 Intercept: 17.822 $Y = -3.349 X + 17.822$
PCR Efficiency: 98.9 %



C) YWHAZ

Correlation Coefficient: 0.996 Slope: -3.325 Intercept: 16.703 $Y = -3.325 X + 16.703$
PCR Efficiency: 99.9 %



D) ADAM17

Correlation Coefficient: 0.968 Slope: -3.379 Intercept: 24.412 $Y = -3.379 X + 24.412$
PCR Efficiency: 97.7 %

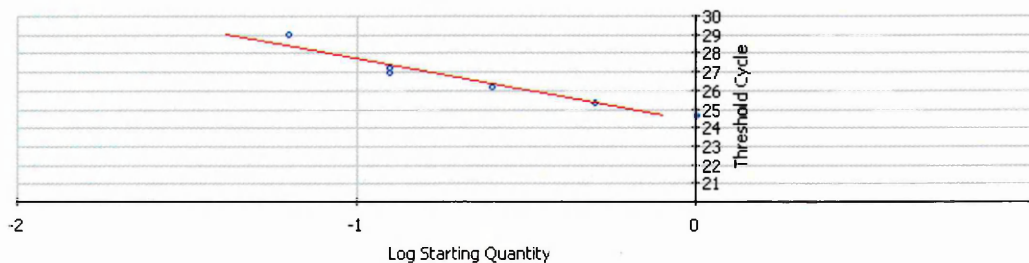
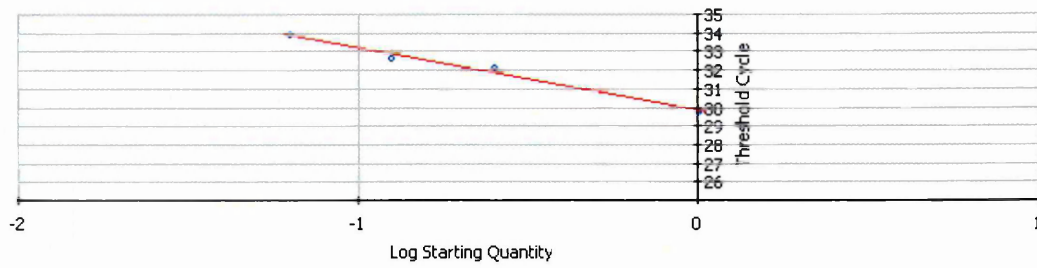


Figure 3.6: Standard curve plots generated from qRT-PCR data showing the PCR primer pair efficiencies for **A) β -actin**, **B) HPRT1**, **C) YWHAZ** and **D) ADAM17**.

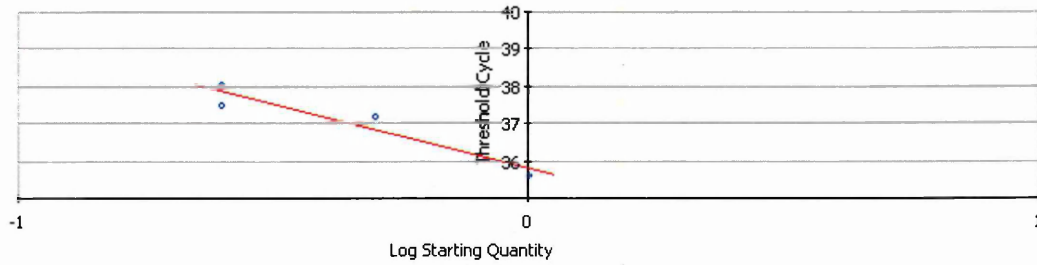
E) ADAMTS-1

Correlation Coefficient: 0.991 Slope: -3.347 Intercept: 29.892 $Y = -3.347 X + 29.892$
PCR Efficiency: 99.0 %



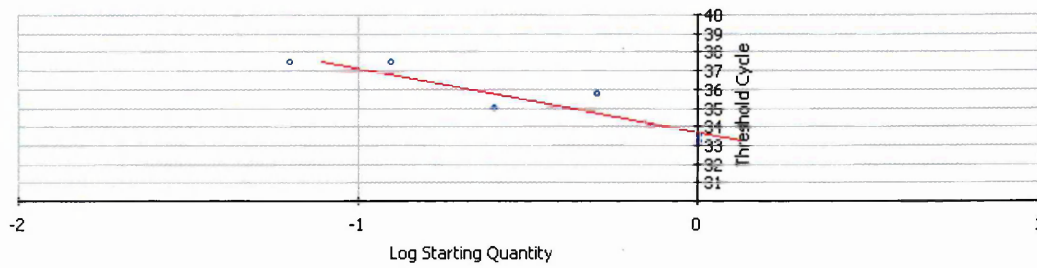
F) ADAMTS-4

Correlation Coefficient: 0.949 Slope: -3.447 Intercept: 35.820 $Y = -3.447 X + 35.820$
PCR Efficiency: 95.0 %



G) ADAMTS-5

Correlation Coefficient: 0.929 Slope: -3.464 Intercept: 33.726 $Y = -3.464 X + 33.726$
PCR Efficiency: 94.4 %



H) TIMP3

Correlation Coefficient: 0.961 Slope: -3.344 Intercept: 22.293 $Y = -3.344 X + 22.293$
PCR Efficiency: 99.1 %

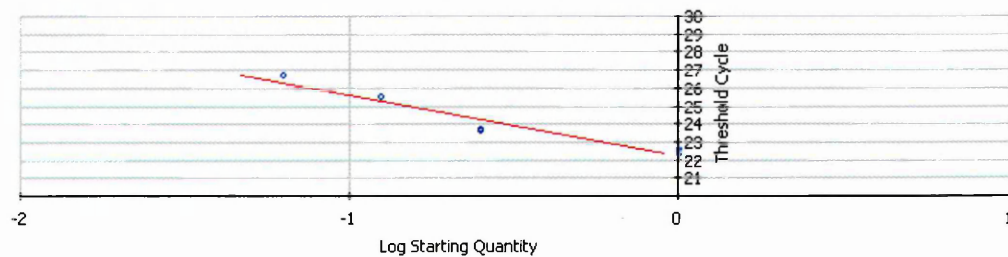


Figure 3.6 (continued): Standard curve plots generated from qRT-PCR data showing the PCR primer pair efficiencies for **E) ADAMTS-1**, **F) ADAMTS-4**, **G) ADAMTS-5** and **H) TIMP3**.

due to the absence of template; this was the case for β -actin, ADAM17, ADAMTS-1 and TIMP3. However CT values were obtained from NTCs for HPRT1, YWHAZ, ADAMTS-4 and ADAMTS-5; this was due to primer dimer formation (explanation below).

PCR products have a unique T_m dependent upon their DNA base composition, thus melt curve analysis (Figure 3.7) allowed the verification of correctly amplified fragments. All duplicate samples demonstrated a single peak in fluorescence indicative of the amplification of a single product. Whereas, the NTC for each primer pair either generated no peak (β -actin and ADAM17), a slight peak (ADAMTS-1, ADAMTS-4 and TIMP3) or a peak of fluorescence notably different to the specific PCR product (HPRT, YWHAZ and ADAMTS-5).

Melt curve analysis also determined that primer dimers were formed in all samples probed for HPRT1, YWHAZ, ADAMTS-4 and ADAMTS-5, with a shoulder to the left of the product specific peak of the same T_m in both experimental samples and their NTC. Thus explaining the pseudo-amplification observed in HPRT1, YWHAZ, ADAMTS-4 and ADAMTS-5 primer pair NTCs.

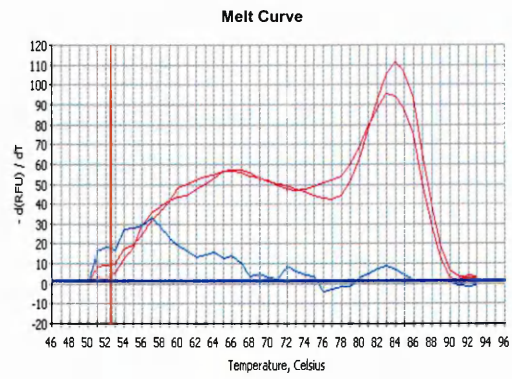
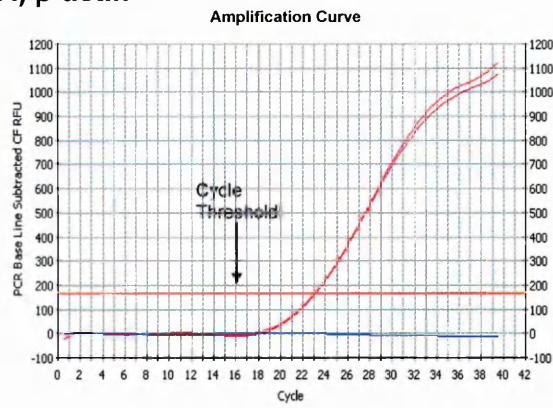
Agarose gel electrophoresis of qRT-PCR products further confirmed the specificity of each set of primer pairs (Figure 3.8). In all cases the amplified product size correlated with the expected band size from cDNA, indicating there was no genomic DNA contamination and that only specific product was amplified. No band was evident in any NTC, again demonstrating there was no amplification in NTCs.

3.2.8 Gene expression in adult and foetal liver samples

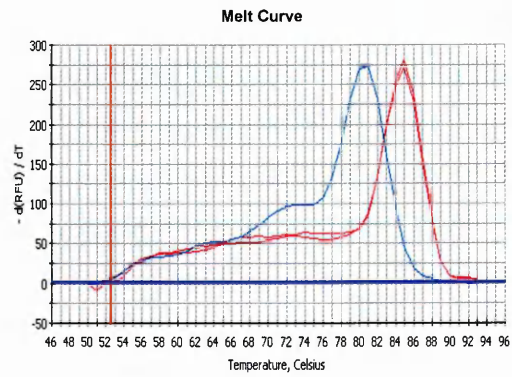
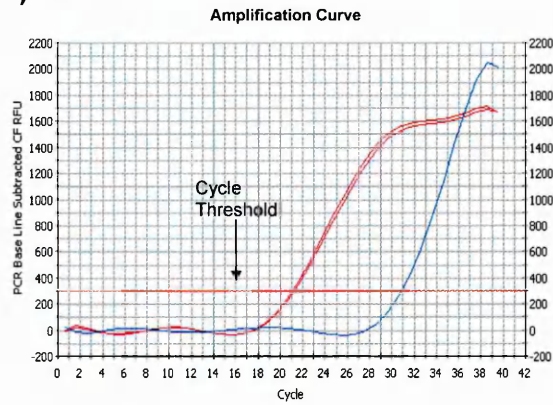
qRT-PCR was performed on reverse-transcribed total RNA obtained from the normal livers of an adult and foetus (Stratagene, The Netherlands), to determine the presence of ADAM17, ADAMTS-1, -4, -5 and TIMP3 at the level of gene expression. $2^{-\Delta CT}$ values were calculated from the qRT-PCR data with normalisation against YWHAZ, most stable housekeeping gene transcripts for these samples (adult liver M-value of 0.341 and foetal liver M-value of 0.890).

All genes of interest were expressed in both adult and foetal liver samples. Examination of $2^{-\Delta CT}$ values for both adult and foetal liver samples (Figure 3.9) indicated that of the genes of interest, TIMP3 was the most highly expressed gene, followed by moderate levels of ADAMTS-1, ADAMTS-5 and ADAM17. ADAMTS-4 gene expression was only detected at very low levels in both adult and foetal liver samples.

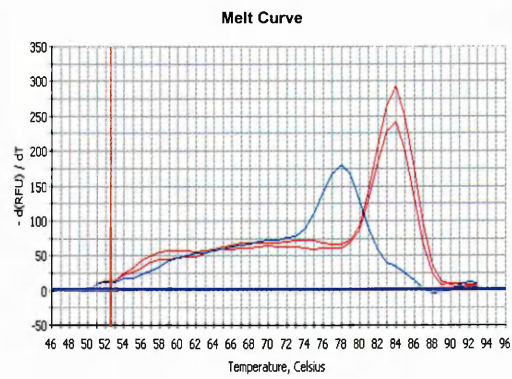
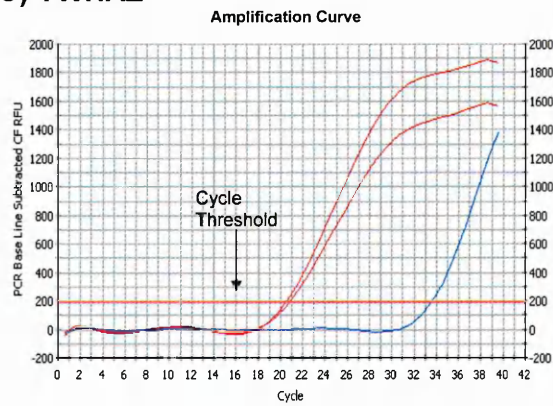
A) β -actin



B) HPRT1



C) YWHAZ



D) ADAM17

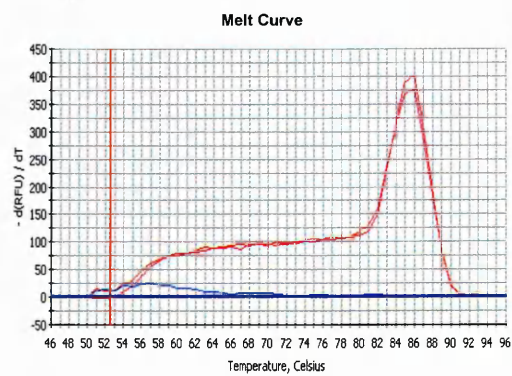
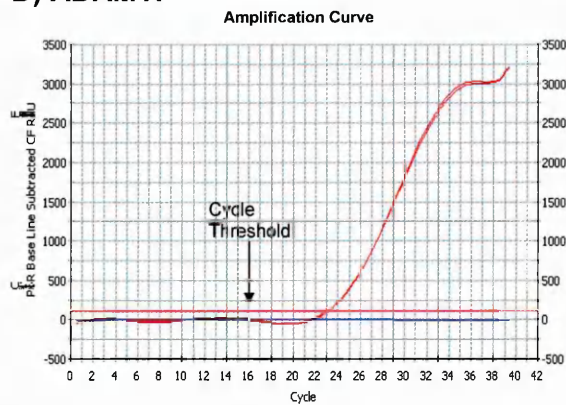
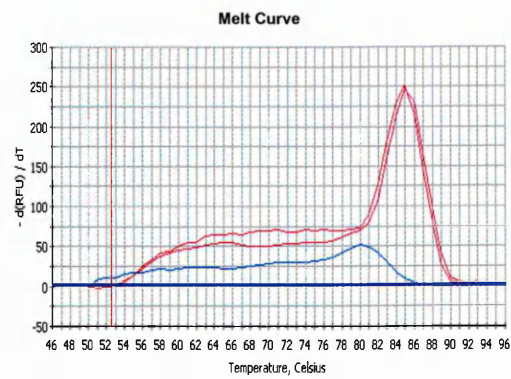
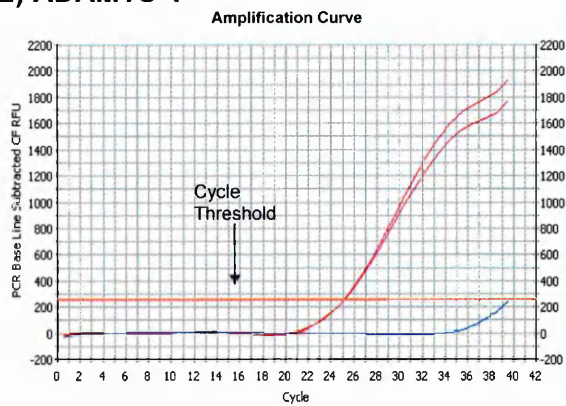
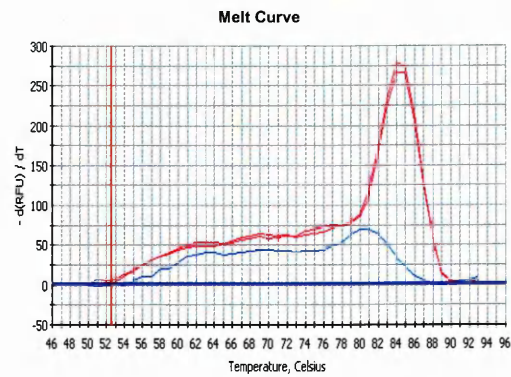
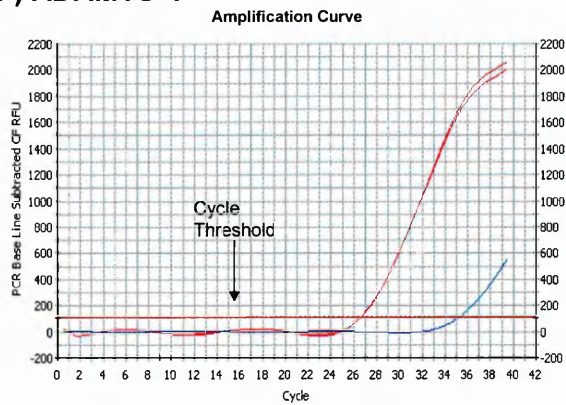


Figure 3.7: Amplification and melt curves generated from qRT-PCR data for **A)** β -actin, **B)** HPRT1, **C)** YWHAZ and **D)** ADAM17 (red) and NTC (blue).

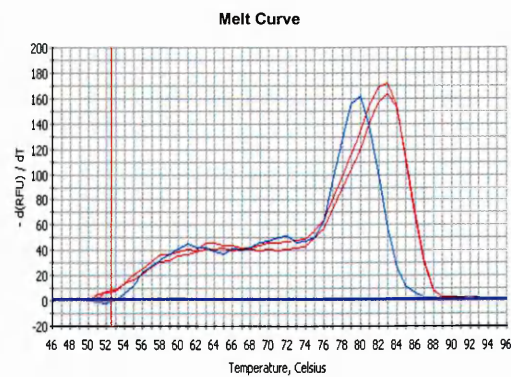
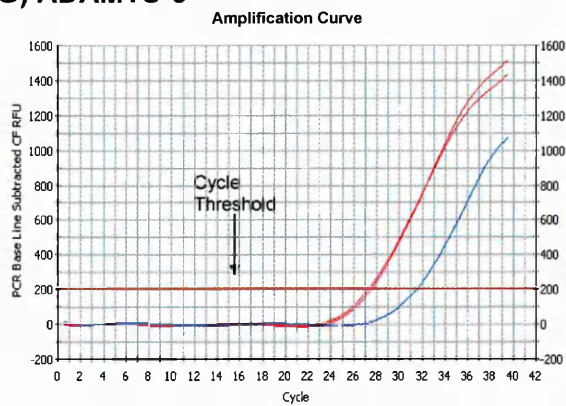
E) ADAMTS-1



F) ADAMTS-4



G) ADAMTS-5



H) TIMP3

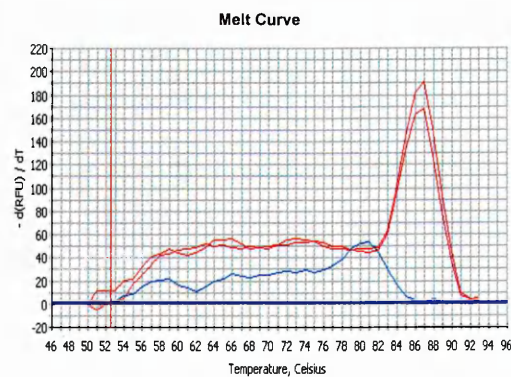
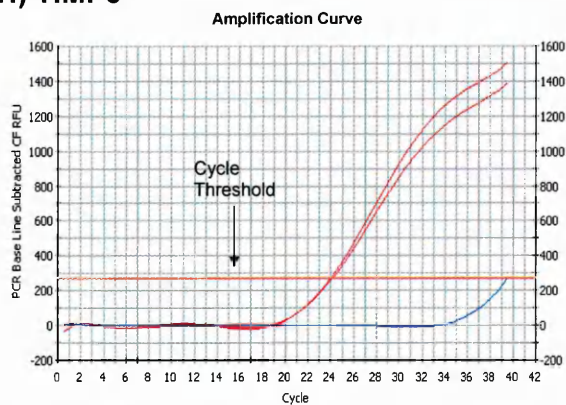


Figure 3.7 (continued): Amplification and melt curves generated from qRT-PCR data for E) ADAMTS-1, F) ADAMTS-4, G) ADAMTS-5 and H) TIMP3 (red) and NTC (blue).

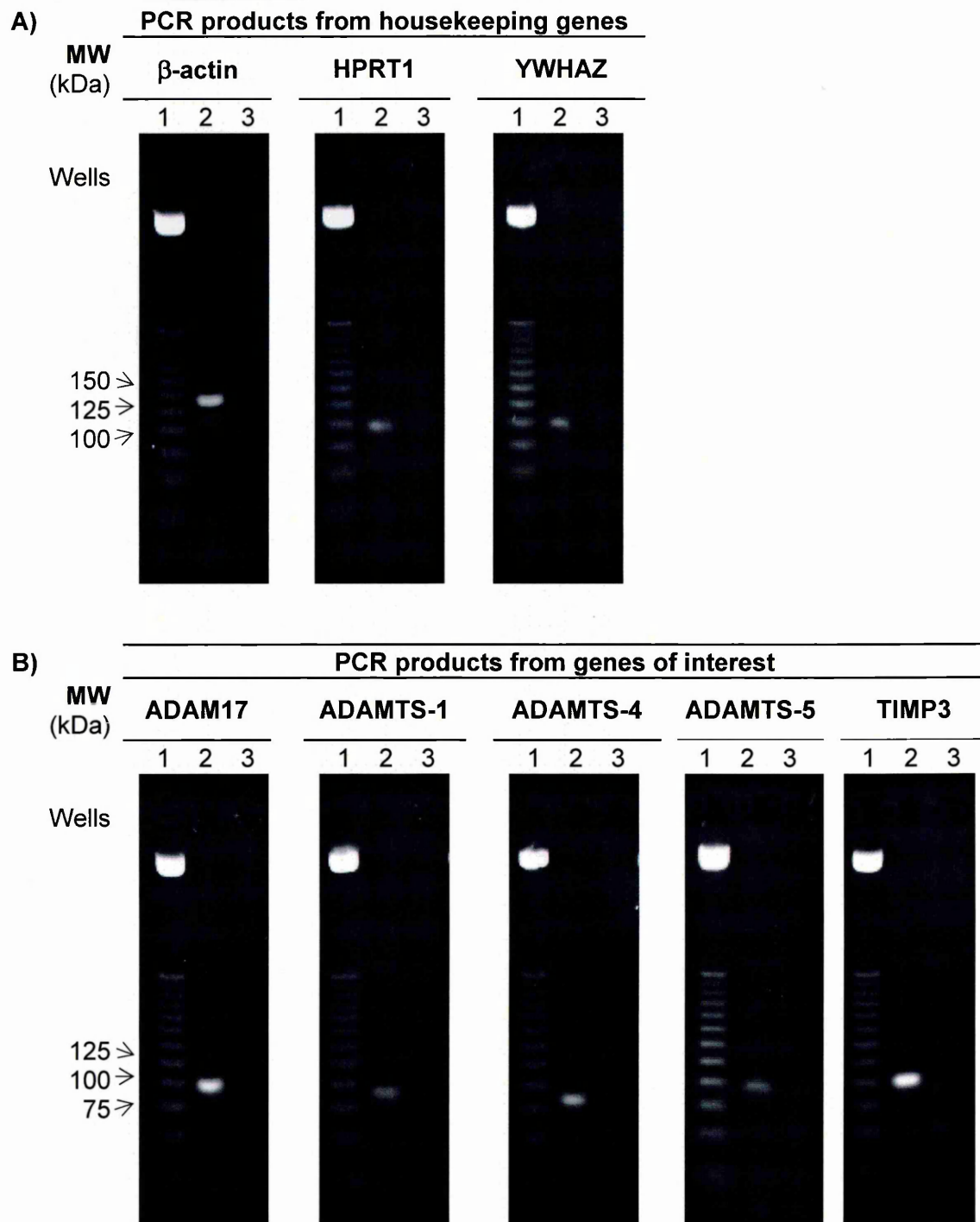


Figure 3.8: Agarose gel electrophoresis of the qRT-PCR products generated for **A)** the housekeeping genes, β -actin (140 bp), HPRT1 (94 bp) and YWHAZ (94 bp), and **B)** the genes of interest, ADAM17 (98 bp), ADAMTS-1 (89 bp), -4 (80 bp), -5 (92 bp) and TIMP3 (95 bp). Where 1 represents 25 bp marker, 2 signifies specific amplified product, and 3 denotes the NTC.

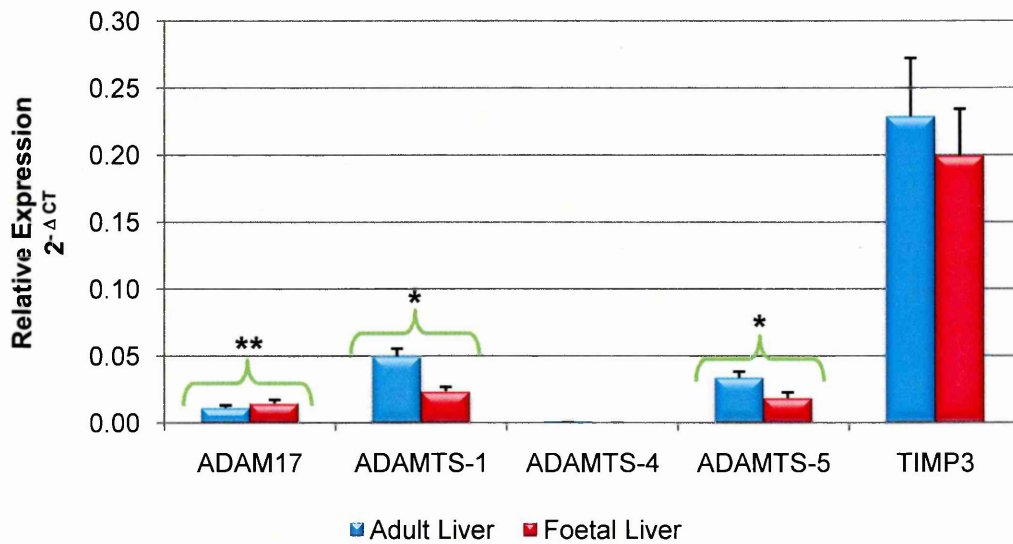


Figure 3.9: ADAM17, ADAMTS-1, ADAMTS-4, ADAMTS-5 and TIMP3 mRNA expression in normal foetal liver samples compared to normal adult liver samples. Data presented as mean \pm SEM. Significant difference of foetal liver from adult liver samples, * $P < 0.05$, ** $P < 0.001$ (Students T-test; $n=4$).

ADAM17 was expressed at a slightly higher level in the foetal liver sample than in the adult liver sample ($P=0.009$). Whereas all other genes of interest had lower gene expression in the foetal liver compared to the adult liver sample, with significance reached for ADAMTS-1 ($P=0.010$) and ADAMTS-5 gene expression ($P=0.017$).

3.2.9 Modulation of Gene Expression by IL-1 β , IL-6 and TNF- α

The pro-inflammatory cytokines IL-1 β , IL-6 and TNF- α were applied separately to each of the cell lines under investigation (HepG2, HuH-7 or LX-2) for 24 hours, after which qRT-PCR was performed to assess the influence of these treatments on the gene expression of ADAM17, ADAMTS-1, -4, -5 and TIMP3. The resultant data were quantified using the Pfaffl method, with normalisation against two suitable housekeeping gene transcripts as determined by geNorm analysis (Section 3.2.5).

Each experiment included triplicate wells of samples that were pooled to minimise well-to-well variation and reactions were performed in duplicate. Four independent experiments were performed to confirm trends found. IL-1 β and TNF- α treated cell were compared to an untreated control sample, whereas IL-6 treated cells were compared to an acetic acid-containing control sample.

Sample preparation

Following cytokine treatment, total RNA was extracted from each sample, and treated with DNase I to degrade any contaminating genomic DNA (Sections 2.3.1 - 2.3.3). Samples were subjected to agarose gel electrophoresis (Figure 3.10), where it was determined, by the presence of both 28S and 18S rRNA subunits, that all samples contained intact, high quality RNA. The absence of genomic DNA was also established.

The DNase I treated total RNA was quantified spectrophotometrically (Section 2.3.4), as bases in nucleic acids absorb UV light with an absorption peak of 260 nm. Additional absorbance readings at 280 nm (A_{280}) and 230 nm (A_{230}) were used to determine the RNA purity and presence of contaminants. An absorbance A_{260}/A_{280} ratio of 2.0 indicates a pure RNA preparation, with a range of 1.8-2.0 being acceptable. An absorbance A_{260}/A_{280} ratio of <1.8 indicates the presence of protein contaminants. Similarly, an absorbance A_{260}/A_{230} ratio of <1.0 indicates contamination of the RNA preparation by chaotropic salts and phenol, with a value close to 2.0 indicative of no contaminants. In all cases the A_{260}/A_{280} and A_{260}/A_{230} ratios were within an acceptable range.

Total RNA (1 μ g) from each sample was then reverse transcribed and the resulting cDNA used as template in qRT-PCR experiments (Sections 2.3.5 – 2.3.6).

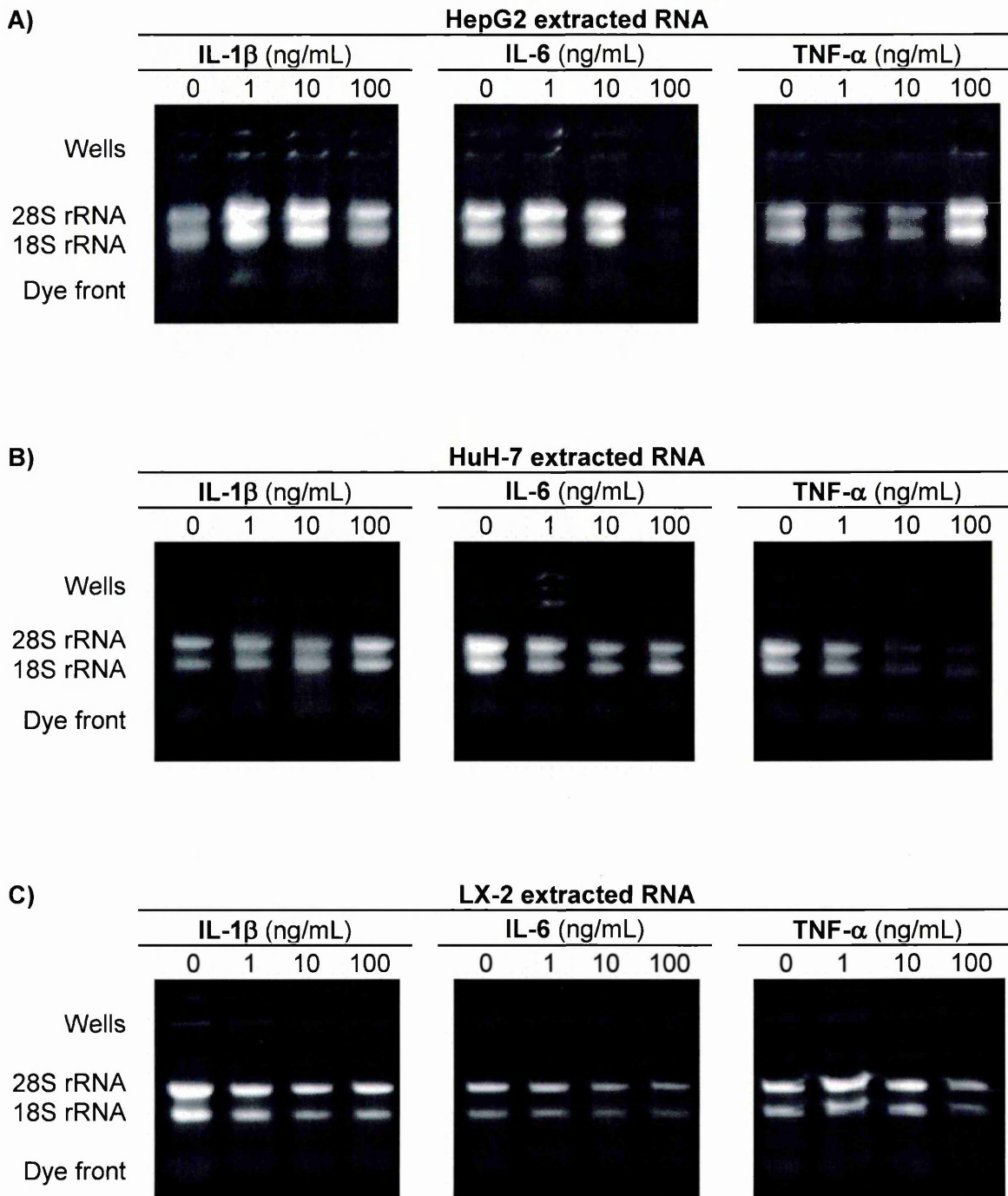


Figure 3.10: Agarose gel electrophoresis of DNase I treated RNA samples extracted from **A)** HepG2, **B)** HuH-7, and **C)** LX-2 cells following 24 hours of treatment with varying concentrations of IL1- β , IL-6 or TNF- α .

The HepG2 experimental system

The examination of $2^{-\Delta CT}$ values for normalised untreated HepG2 samples (Figure 3.11A) indicates that of the five genes of interest, TIMP3 was the most highly expressed gene ($2^{-\Delta CT}=5.327$), followed by ADAM17 ($2^{-\Delta CT}=0.097$) and ADAMTS-1 ($2^{-\Delta CT}=0.079$). ADAMTS-4 gene expression was only detected at low levels ($2^{-\Delta CT}=0.014$) and ADAMTS-5 was not expressed at a detectable level in any HepG2 sample, untreated or treated.

Modulations of the expression of ADAM17, ADAMTS-1, -4, -5 and TIMP3 in the HepG2 experimental system following 24 hours of cytokine treatment with 1, 10 or 100 ng/mL of IL-1 β , IL-6 and TNF- α is shown in Figure 3.12. qRT-PCR data obtained from HepG2 cells were normalised against β -actin and HPRT1, to ensure the accurate quantification.

IL-1 β treatment of HepG2 cells did not cause significant changes in the expression of ADAM17 or TIMP3 in comparison to untreated control cells. However, moderate increases in ADAMTS-1 gene expression were observed with 1, 10 and 100 ng/mL of IL-1 β (2.79-fold ($P=0.002$), 5.44-fold ($P=0.0001$) and 4.51-fold ($P=0.0001$) increases respectively), yielding a concentration dependent response with a peak at 10 ng/mL. A concentration dependent response curve was also observed for ADAMTS-4, but with smaller increases in gene expression, again peaking with 10 ng/mL of IL-1 β treatment. However, a statistically significant albeit small increase in ADAMTS-4 gene expression was only achieved following 100 ng/mL of treatment (1.80-fold increase; $P=0.023$).

IL-6 treatment of HepG2 cells did not affect the expression of ADAM17, ADAMTS-4 or TIMP3 in comparison to the control sample. However, a concentration dependent increase in ADAMTS-1 gene expression occurred after treatment with 1, 10 and 100 ng/mL IL-6, yielding a 28.03-fold increase in expression after 100 ng/mL of treatment ($P=0.001$).

The gene expression of ADAM17, ADAMTS-1 ADAMTS-4 and TIMP3 in HepG2 cells was not significantly altered following TNF- α treatment. Although 10 and 100 ng/mL of treatment did result in 3.64-fold and 2.82-fold increases of ADAMTS-1 respectively, and although these increases were at a higher level than those seen after IL-1 β treatment, they were not deemed to be statistically significant due to their large SEM. Similarly, 10 ng/mL TNF- α resulted in a 5-fold increase in ADAMTS-4 expression; significance was not reached due to the large SEM even though the increase was larger than that seen after IL-1 β treatment.

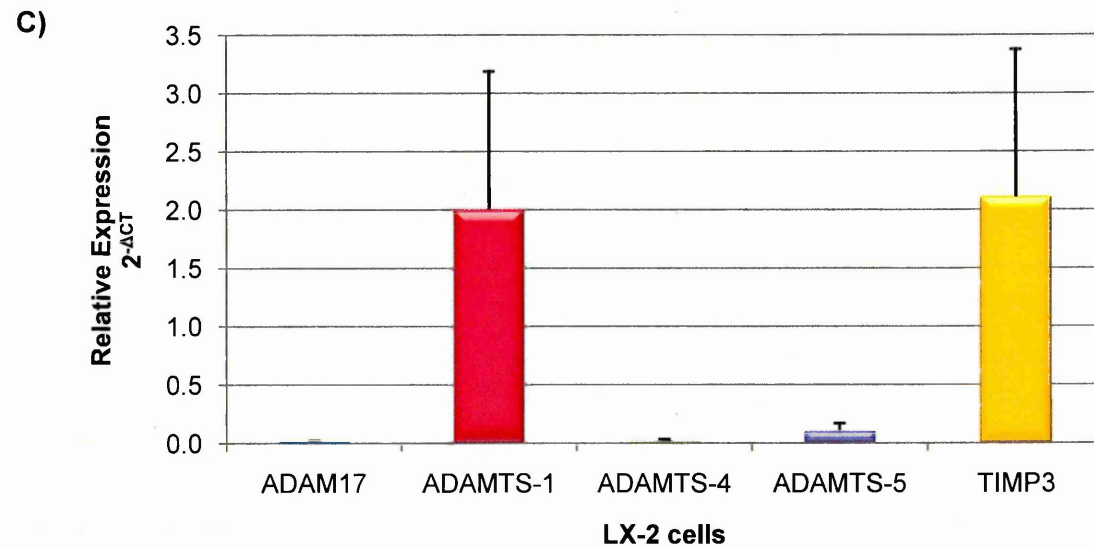
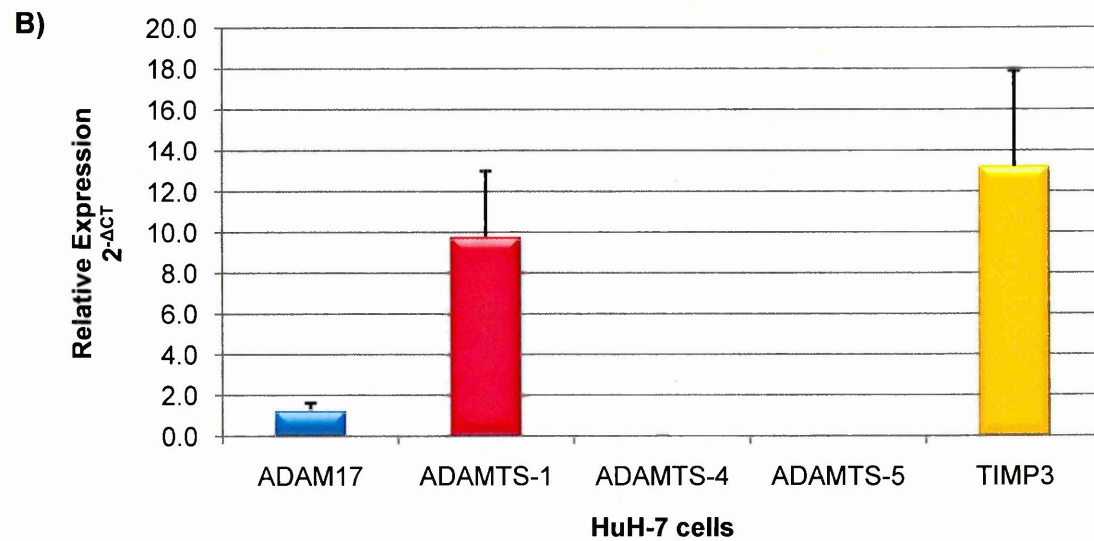
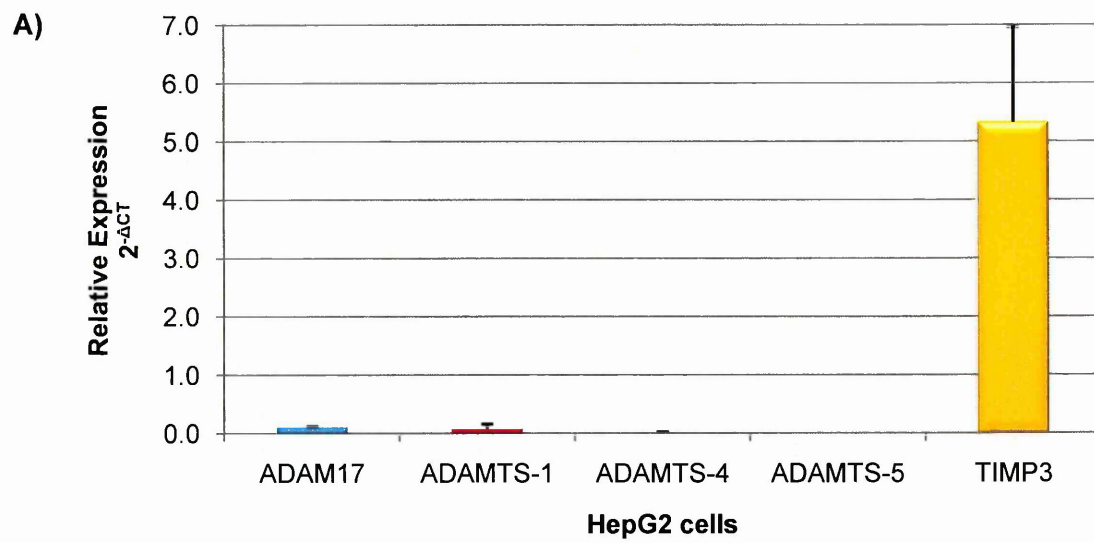


Figure 3.11: ADAM17, ADAMTS-1, ADAMTS-4, ADAMTS-5 and TIMP3 mRNA expression in **A)** HepG2, **B)** HuH-7 and **C)** LX-2 cells. Data presented as mean \pm SEM. (n=12).

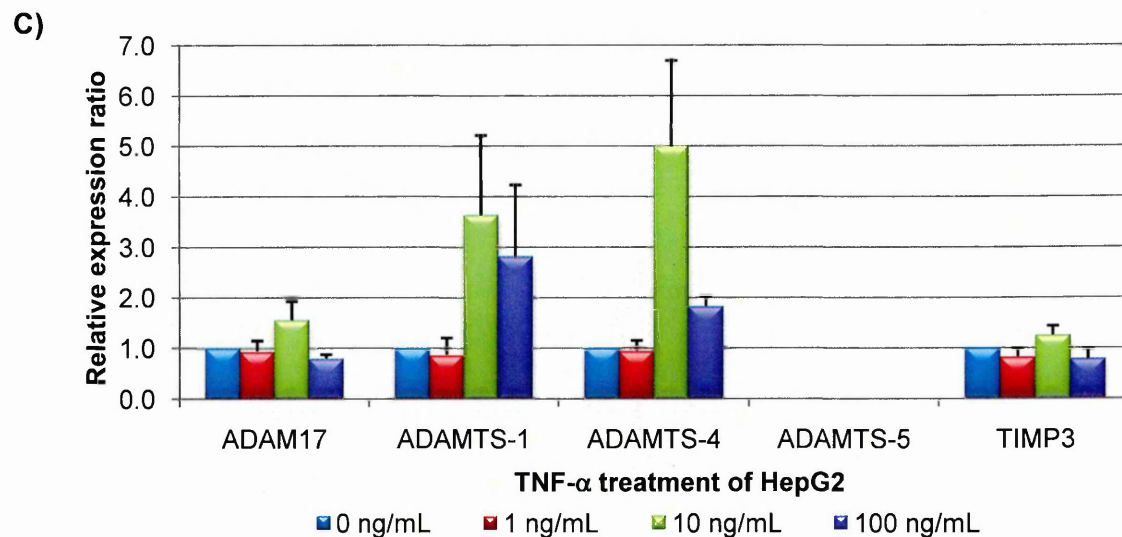
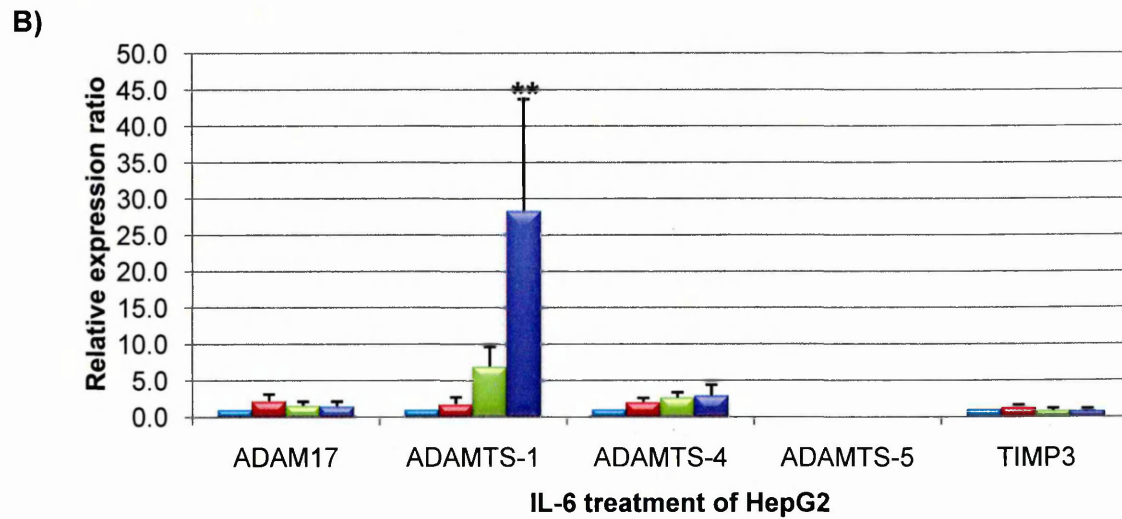
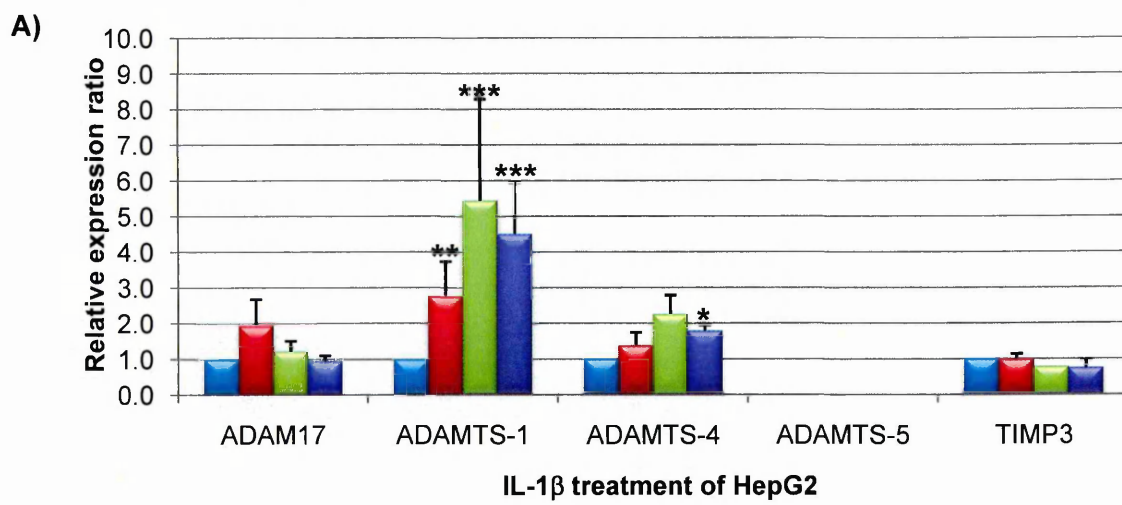


Figure 3.12: ADAM17, ADAMTS-1, ADAMTS-4, ADAMTS-5 and TIMP3 mRNA expression in HepG2 cells following 24 hours of treatment with varying concentrations of **A)** IL-1 β , **B)** IL-6 or **C)** TNF- α . Data presented as mean \pm SEM. Significant difference from control, * $P < 0.05$, ** $P < 0.01$, *** $P < 0.001$ (ANOVA with Dunnett's test; $n = 4$).

The HuH-7 experimental system

The $2^{-\Delta CT}$ values for normalised untreated HuH-7 samples (Figure 3.11B) show that amongst the genes of interest, TIMP3 and ADAMTS-1 were both highly expressed ($2^{-\Delta CT}=13.211$ and $2^{-\Delta CT}=9.795$ respectively), and ADAM17 was expressed at intermediate levels ($2^{-\Delta CT}=1.243$). ADAMTS-4 and ADAMTS-5 were only detected at very low levels at the gene level ($2^{-\Delta CT}=0.022$ and $2^{-\Delta CT}=0.011$), with ADAMTS-4 being detected in 25% of the control samples and ADAMTS-5 detected in 50% of them.

Modulation of ADAM17, ADAMTS-1, -4, -5 and TIMP3 at the gene expression level by varying concentrations (1, 10 or 100 ng/mL) of IL-1 β , IL-6 and TNF- α is shown in Figure 3.13. qRT-PCR data obtained from the HuH-7 experimental system were normalised against HPRT1 and YWHAZ, to ensure the accurate quantification.

IL-1 β treatment of HuH-7 cells did not result in any statistically significant modulations in the gene expression of ADAM17, ADAMTS-1, ADAMTS-4 or TIMP3. ADAMTS-5 was not detected in any of these samples. Similarly, IL-6 treatment did not produce any significant alterations in expression of the genes of interest.

TNF- α treatment did not alter the gene expression of ADAM17, ADAMTS-1, -4 or -5. However, TIMP3 gene expression was slightly down-regulated following 10 and 100 ng/mL of TNF- α treatment in a concentration dependent manner (1.88-fold ($P=0.049$) and 2.45-fold ($P=0.006$) decreases respectively).

The LX-2 experimental system

The $2^{-\Delta CT}$ values for normalised untreated LX-2 samples (Figure 3.11C) showed that TIMP3 was the most highly expressed gene of interest ($2^{-\Delta CT}=2.109$), followed by ADAMTS-1 ($2^{-\Delta CT}=2.002$), ADAMTS-5 ($2^{-\Delta CT}=0.098$) and ADAMTS-4 ($2^{-\Delta CT}=0.018$). The lowest level of gene expression was observed for ADAM17 ($2^{-\Delta CT}=0.014$).

The effect of IL-1 β , IL-6 and TNF- α treatment on the expression of ADAM17, ADAMTS-1, -4, -5 and TIMP3 in LX-2 cells is shown in Figure 3.14. qRT-PCR data obtained from the LX-2 experimental system were normalised against β -actin and HPRT1, to ensure accurate quantification.

IL-1 β treatment of LX-2 cells did not cause significant differences in the gene expression of ADAM17, ADAMTS-5 or TIMP3, with the exception of increases in ADAM17 expression following 1 ng/mL of treatment and TIMP3 following 100 ng/mL. Treatment of cells with 1 ng/mL of IL-1 β resulted in the small increases of ADAMTS-1 and ADAMTS-4 (2.05-fold ($P=0.022$) and 1.96-fold ($P=0.047$) increases respectively). Further increases were also observed in the expression of ADAMTS-4 following 10 and 100 ng/mL of treatment, although significance was not reached.

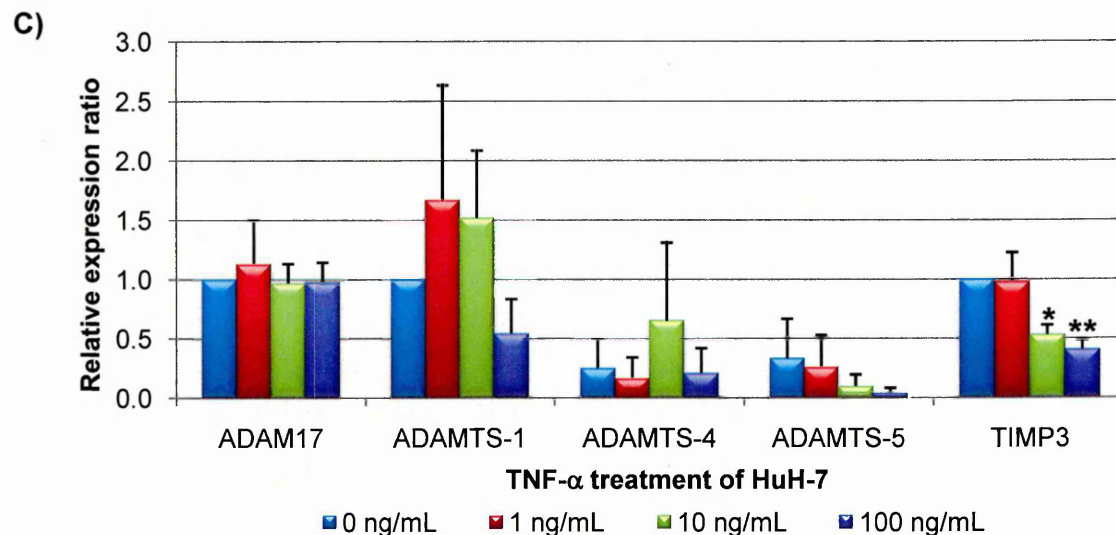
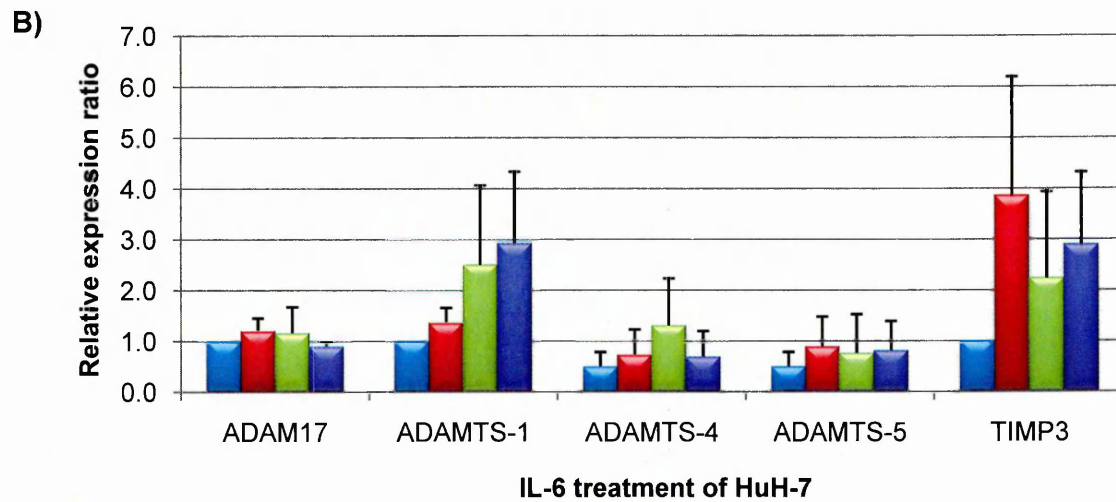
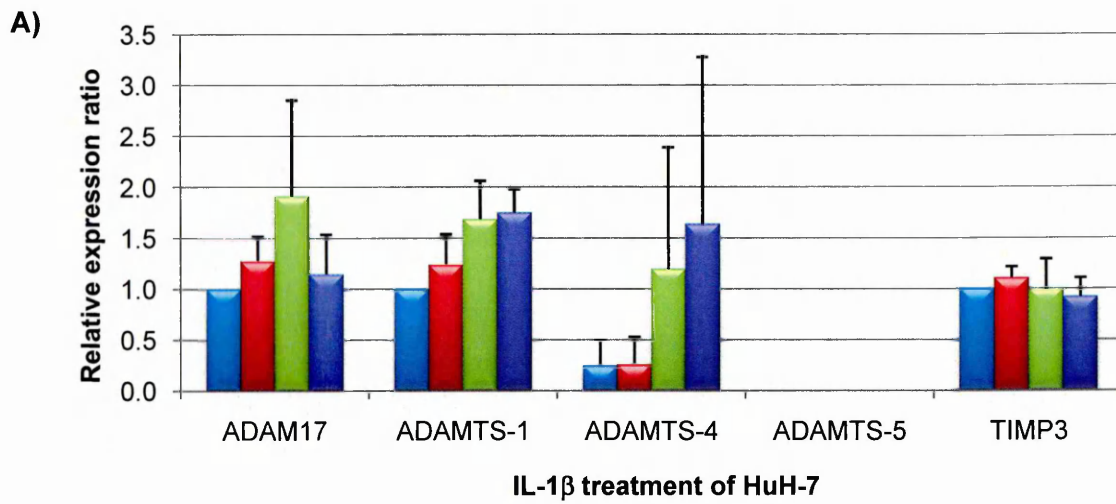


Figure 3.13: ADAM17, ADAMTS-1, ADAMTS-4, ADAMTS-5 and TIMP3 mRNA expression in HuH-7 cells following 24 hours of treatment with varying concentrations of **A)** IL-1 β , **B)** IL-6 or **C)** TNF- α . Data presented as mean \pm SEM. Significant difference from control, * P<0.05, ** P<0.01 (ANOVA with Dunnett's test; n=4). Some controls < 1, as not detected in all samples.

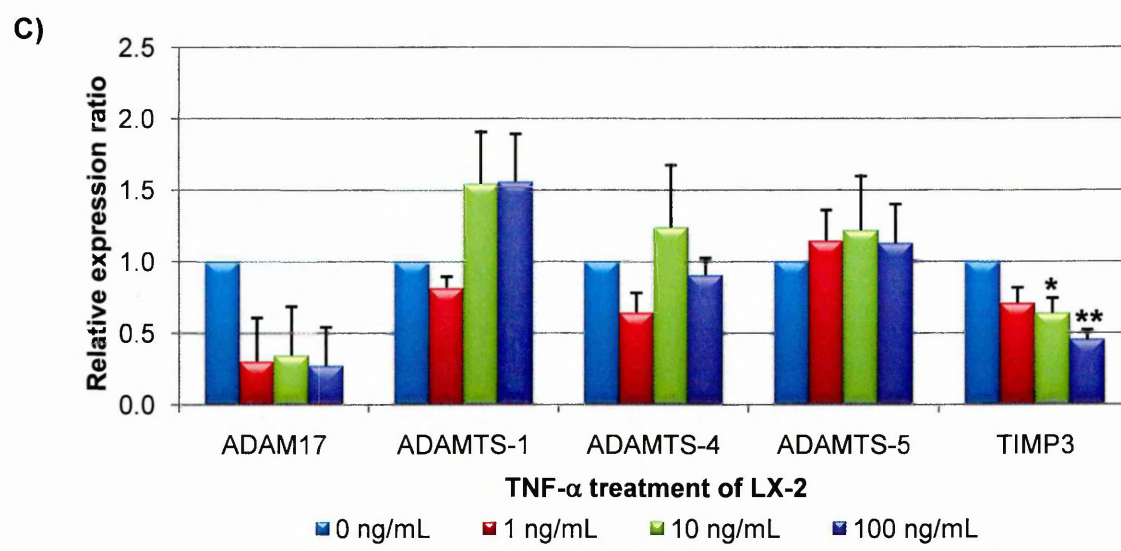
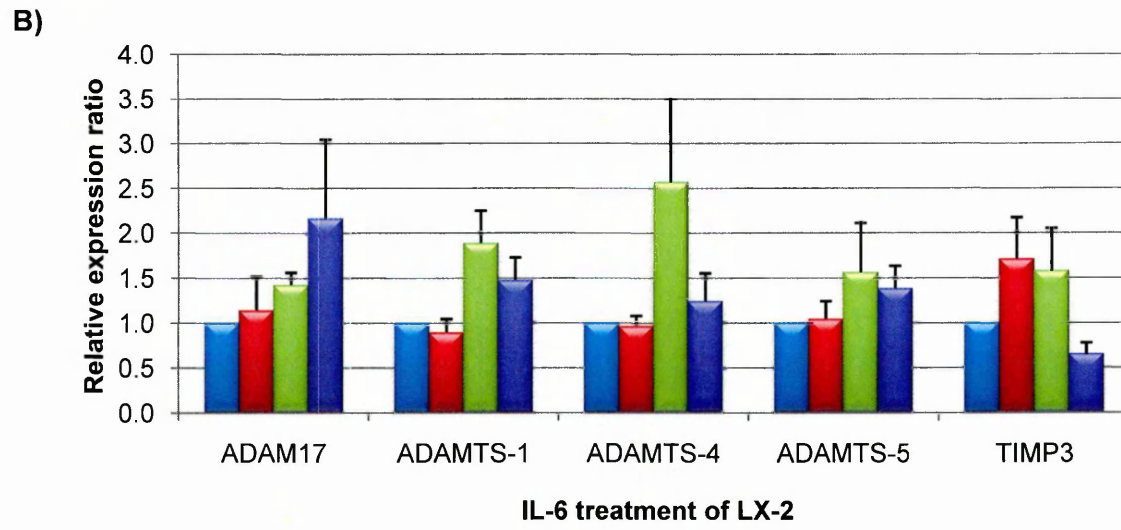
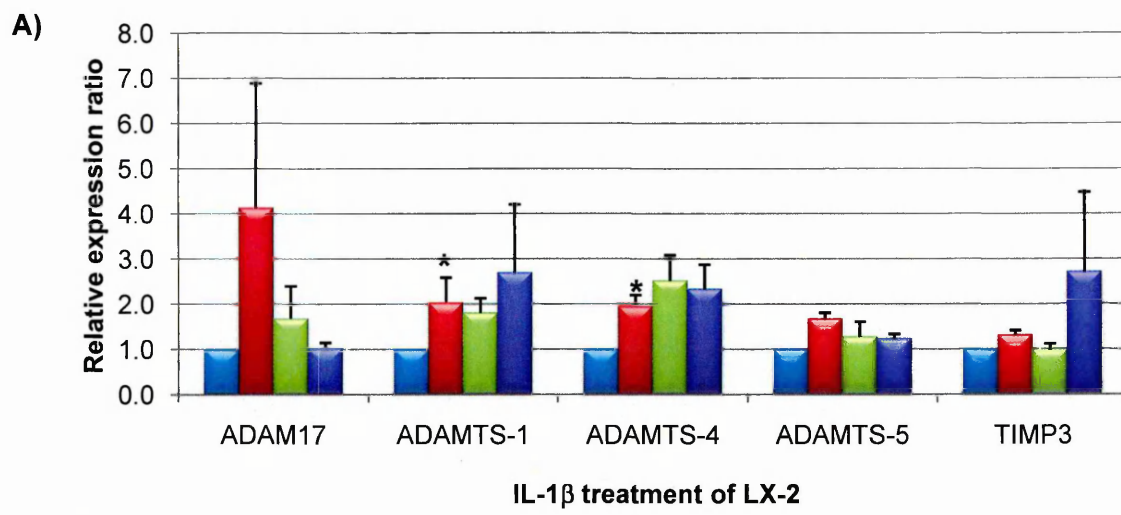


Figure 3.14: ADAM17, ADAMTS-1, ADAMTS-4, ADAMTS-5 and TIMP3 mRNA expression in LX-2 cells following 24 hours of treatment with varying concentrations of **A)** IL-1 β , **B)** IL-6 or **C)** TNF- α . Data presented as mean \pm SEM. Significant difference from control, * P<0.05, ** P<0.01, *** P<0.001 (ANOVA with Dunnett's test; n=4).

Application of IL-6 to LX-2 cells did not result in any significant changes in the expression of any of the genes of interest, however a minimal decrease in ADAMTS-1 was observed with 1 ng/mL of treatment (0.10-fold decrease) and slight increases with 10 and 100 ng/mL (1.89-fold and 1.48-fold increases respectively). A small concentration dependent increase in ADAM17 gene expression was also observed, which did not reach significance.

TNF- α treatment of LX-2 cells did not cause significant changes in the gene expression of ADAMTS-1, -4 or -5. ADAM17 gene expression was down-regulated following TNF- α treatment at all concentrations tested, however these decreases were not significant due to their large SEM. A concentration dependent decrease in the gene expression of TIMP3 was observed following TNF- α treatment. A minor decrease in TIMP3 expression was observed in comparison to the control following 1 ng/mL of TNF- α (1.41-fold decrease), with 10 and 100 ng/mL resulting in significant down-regulation of this gene (1.57-fold (P= 0.026) and 2.21-fold (P=0.002) decreases respectively).

3.2.10 Summary of Results

The results presented in this chapter are summarised in Table 3.6.

Table 3.6: Summary of the results presented in Chapter 3.

		Cell Lines		
		HepG2	HuH-7	
		Epithelial-like Islands of cells	Epithelial-like Monolayer	
		Myofibroblast-like Monolayer	LX-2	
Morphology	IL-1 β	↑ 10 ng/mL (24 hours) ↑ 1 ng/mL (48 hours) ↑ 1 & 10 ng/mL (72 hours)	↑ 100 ng/mL (24 hours)	Cytokines no effect
	IL-6	↑ 10 & 100 ng/mL (24 hours)	Cytokines no effect	Cytokines no effect
	TNF- α	↑ 1 ng/mL (48 hours) ↑ 1, 10 & 100 ng/mL (72 hours)	↑ 100 ng/mL (48 hours) ↑ 1 & 10 ng/mL (72 hours)	Cytokines no effect
Cellular Proliferation	Controls	TIMP3 > ADAM17 > ADAMTS-1 > ADAMTS-4; No ADAMTS-5 detected	TIMP3 > ADAMTS-1 > ADAM17 > ADAMTS-4 > ADAMTS-5	TIMP3 > ADAMTS-1 > ADAMTS-5 > ADAMTS-4 > ADAM17
	IL-1 β	↑ 1, 10 & 100 ng/mL ADAMTS-1 ↑ 100 ng/mL ADAMTS-4	Cytokines no effect	↑ 1 ng/mL ADAMTS-1 & -4
	IL-6	↑ 100 ng/mL ADAMTS-1	Cytokines no effect	Cytokines no effect
mRNA Expression	TNF- α	Cytokines no effect	↓ 10 & 100 ng/mL TIMP3	↓ 10 & 100 ng/mL TIMP3

3.3 Discussion

The objectives of these investigations were to verify the hepatic origin of the HepG2, HuH-7 and LX-2 cell lines, determine the proliferative effect of the pro-inflammatory cytokines IL-1 β , IL-6 and TNF- α on these cells, and determine if these treatments modulate the gene expression of ADAM17, ADAMTS-1, -4, -5 and TIMP3.

3.3.1 Characterisation of the Cell Lines HepG2, HuH-7 and LX-2

The first objective of this study was to confirm the parental origin of the adherent cell lines HepG2, HuH-7 and LX-2 used throughout this study. Phase contrast microscopy permitted the morphological comparison of the cultured cells to documentation detailing their growth characteristics. Additionally, ICC was used to demonstrate the presence of cell specific markers in each of the three liver cell lines. These evaluations were necessary to establish that the cell line phenotypes had not been substantially altered from their parental phenotype by serial passage.

HepG2 and HuH-7 cell lines were derived over a quarter of a century ago from well-differentiated HCCs developed from malignant hepatocytes (Aden *et al*, 1979; Nakabayashi *et al*, 1982), whereas LX-2 cells were established recently from human activated HSCs by Xu *et al* (2005). The visible characteristics of each cell line observed under phase contrast microscopy were as previously described. Specifically, both hepatoma cell lines had an epithelial-like morphology, although easily observed differences in their *in vitro* growth patterns were evident, such that cultured HepG2 cells formed islands of cells and HuH-7 cells a monolayer. LX-2 cells also grew in a monolayer, but had a distinct myofibroblast-like phenotype characteristic of activated HSCs.

Hepatocyte specific antigen is an uncharacterised antigen present in adult and foetal hepatocytes and the majority of malignant hepatocytes forming hepatomas. HepG2 and HuH-7 cells, but not LX-2 cells displayed the granular cytoplasmic staining characteristic of this antigen, substantiating the claim that both HepG2 and HuH-7 cells were derived from transformed hepatocytes, and LX-2 cells had a different cellular origin. Similarly, LX-2 cells, but not HepG2 or HuH-7 cells stained positive for neural cell marker GFAP characteristic of activated HSCs, authenticating the claim that LX-2 cells were derived from this cell type, and HepG2 and HuH-7 cells were not.

3.3.2 IL-1 β , IL-6 and TNF- α Differentially Increase Cellular Proliferation of Hepatoma Cell Lines, but Not the Activated Hepatic Stellate Cell Line

The second objective in this study was to determine the proliferative responses of HepG2, HuH-7 and LX-2 cells to treatment with pro-inflammatory cytokines, IL-1 β , IL-6

and TNF- α , thought to be important in HCC and CRC progression and tumour growth within the liver (Section 1.5.1).

The cytokines studied had no proliferative effect on the activated HSC line LX-2 at any time point. However, statistically significant increases in cell number were observed in the two hepatoma cell lines, HepG2 and HuH-7, although these changes were not consistent between the cell lines.

IL-1 β treatment significantly increased HepG2 and HuH-7 cell numbers at the 24 hour time point as compared to controls. This effect was observed at two further time points for HepG2 cells, but not for HuH-7 cells. This cytokine therefore has differential effects on the growth of these cell lines, which may reflect underlying genetic differences between these HCC cell lines.

IL-6 treatment did not alter HuH-7 cell proliferation. However, a concentration-dependent increase in cellular proliferation was observed in HepG2 cells after 24 hours; this effect was diminished at later time points of 48 and 72 hours. This suggests that IL-6 acts in the short term to promote HepG2 cell proliferation, possibly by activation of the JAK/STAT pathway and subsequent activation of STAT3 and transcription of a number of cell cycle genes including cyclin D (Section 1.5.1), an effect also observed in primary hepatocytes (Gao, 2005).

Conversely, TNF- α had no proliferative effect on either HepG2 or HuH-7 cells at the 24 hour time point, but significant increases in cell number were observed at the later time points of 48 and 72 hours in both cell lines. This indicates that TNF- α can act to promote tumour formation, possibly by the induction of angiogenic factors (Balkwill & Mantovani, 2001).

3.3.3 IL-1 β , IL-6 and TNF- α Differentially Modulate the Gene Expression of ADAM17, ADAMTS-1, -4, -5 and TIMP3 in Liver Cell Lines

The major objective addressed in this chapter was the modulation of expression of four proteolytic enzymes, ADAM17 and ADAMTS-1, -4 and -5, and their major endogenous inhibitor TIMP3 in HepG2, HuH-7 and LX-2 cell lines by the cytokines IL-1 β , IL-6 and TNF- α .

Previous researchers have documented the increased expression of ADAM17 mRNA in HCC as compared to paired non-cancerous liver tissue (Ding *et al*, 2004), and the increased expression of ADAM17 and TIMP3 mRNA in CRC as compared to normal colonic mucosa (Blanchot-Jossic *et al*, 2005; Powe *et al*, 1997; Zeng *et al*, 2001). Conversely, ADAMTS-1 mRNA was found to be decreased in HCCs, compared to cirrhotic liver (Masui *et al*, 2001). However, the expression of the other proteolytic

genes of interest have not been examined in CRC, HCC or normal liver tissue.

Following the optimisation and validation of the qRT-PCR method for the detection of ADAM17, ADAMTS-1, -4, -5 and TIMP3 gene transcripts, it was determined that all of these genes were expressed in non-cancerous adult and foetal liver tissue at a moderate level, with the exception of ADAMTS-4 which had low level expression. The differential expression of these genes was also observed in HepG2, HuH-7 and LX-2 cells, with moderate levels present unless otherwise stated below. HepG2 cells expressed low levels of ADAMTS-1 mRNA, and ADAMTS-5 mRNA was not detected; HuH-7 cells expressed ADAMTS-4 and -5 mRNA at very low and sometimes undetectable levels; LX-2 cells had low ADAMTS-4 mRNA expression and very low ADAM17 mRNA levels.

In each of the experimental systems tested, including the normal adult and foetal liver samples, comparable levels of TIMP3 gene expression were observed, at a higher level than the other genes examined. This is contradictory to data presented by Powe *et al* (1997) and later by Zeng *et al* (2001), in which they described TIMP3 mRNA to be increased in CRC compared to normal colon mucosa. These differences may result from the fact that paired tumour and non-tumour samples were used in their investigation, but due to the use of cell lines this was not possible in these investigations.

It was possible to modulate the expression of the 5 genes of interest by cytokine treatment in the three experimental cell lines investigated; these modulations were generally minor and differed between the cell lines. IL-1 β treatment of HepG2 cells resulted in the overall increase of ADAMTS-1 ($P=0.0001$) and -4 ($P=0.040$) mRNA yielding a concentration dependent response peaking at 10 ng/mL. A concentration dependent increase in ADAMTS-1 mRNA was also observed following IL-6 treatment of these cells ($P=0.004$), with a maximum fold increase of 28.03. These findings are in contrast to the down-regulation of ADAMTS-1 mRNA observed in hepatocellular, pancreatic and mammary carcinomas (Porter *et al*, 2004; Masui *et al*, 2001). Furthermore, TNF- α treatment of HepG2 cells yielded an overall increase in ADAMTS-4 expression when compared to the control group of cells ($P=0.003$).

Although minor modulation of gene expression was observed in the HuH-7 cell line following cytokine treatment, the only statistically significant modulation occurred following TNF- α application when a concentration dependent decrease in TIMP3 gene expression was observed ($P=0.007$). The same trend in TIMP3 mRNA down-regulation was also observed in LX-2 cells following TNF- α treatment ($P=0.005$). This reduction in the endogenous inhibitor of the proteolytic enzymes studied could permit their uninhibited action and consequently aid tumour progression.

Similarities between the LX-2 and the HepG2 cell lines were also observed, such that IL-1 β increased ADAMTS-4 gene expression yielding a concentration dependent response peaking at 10 ng/mL of treatment (P=0.001), and IL-6 increased ADAMTS-1 gene expression (P=0.037).

ADAM17 mRNA was not modulated by cytokine treatment in any of the cell lines investigated. However, it was expressed at a higher level in the two hepatoma cell lines than the normal activated HSC line, indicating it may play a fundamental role in the transformation of hepatocytes cells from normal to malignant, and later in other aspects of cancer development and progression (Section 1.6.4). For example, activation of the EGFR signalling pathway via ADAM17-mediated cleavage of EGFR ligands can result in tumour associated-angiogenesis (Vázquez *et al*, 1999) and enhanced tumour cell proliferation (Itabashi *et al*, 2008).

Similarly, ADAMTS-5 mRNA was not modulated by cytokine treatment in these cell lines. However, this gene was expressed at a moderate level in the non-cancerous liver cell line LX-2, but was undetectable in HepG2 cells and only present at very low levels in HuH-7 cells. This may indicate that ADAMTS-5 mRNA expression is eliminated or greatly reduced in hepatic tumours in order to decrease the presence of the anti-angiogenic ADAMTS-5 protein. This could increase the ability of the tumour to form neovasculature to aid tumour growth.

If the observed modulations in mRNA are reflected in changes at the protein level, these data could suggest that tumour cell invasion of the liver is influenced by the decreased expression of the inhibitor TIMP3 and anti-angiogenic protein ADAMTS-5, and the simultaneous increased proteolytic actions of ADAM17 and ADAMTS-1, and -4. These combined effects may allow the cancer cell to sculpt a pathway through the liver ECM and adhere to a site distant from the primary tumour and undergo angiogenesis to form a metastatic colony.

3.4 Summary

These data presented in this chapter illustrate the expected phenotypic characteristics of the liver cell lines HepG2, HuH-7 and LX-2, and their differential proliferative responses to cytokine treatments. Furthermore, preliminary investigations indicate that mRNA for ADAM17, ADAMTS-1, -4, -5 and TIMP3 were detected in non-cancerous adult and foetal liver tissue. These data also demonstrate the differential expression and modulation of these genes in each of the cell lines investigated with key findings being the very low expression levels of ADAMTS-5 in the hepatoma cell lines and the concentration dependent down-regulation of TIMP3 following TNF- α treatment in both the HuH-7 hepatoma cell line, and LX-2 activated hepatic stellate cell line.

Chapter 4

Modulation of ADAM17, ADAMTS-1, -4, -5 and TIMP3 Protein in Liver Cell Lines by IL-1 β , IL-6 and TNF- α

4.1 Introduction

This chapter describes the *in vitro* expression and modulation of ADAM17, ADAMTS-1, -4, -5 and TIMP3 proteins by the cytokines IL-1 β , IL-6 and TNF- α in three previously characterised liver cell lines, HepG2, HuH-7 and LX-2. This investigation also allowed the proteolytic status of these proteins to be determined.

4.1.1 Immunodetection of Proteins

Western blotting is a valuable technique used by researchers to determine the presence of specific proteins, after fractionation, by the use of antibodies directed against the protein of interest (Section 2.4). Monoclonal or polyclonal antibodies can be utilised in this method, with each type having distinct advantages.

Monoclonal antibodies are directed against individual epitopes, and can be consistently produced from single hybridoma clones. Hybridoma cells are generated by the fusion of myeloma cells and spleen cells from the host, usually a mouse, immunised with a specific antigen. Each successful hybrid cell is assayed for antigen specificity of the synthesised antibody, and stable and productive clones are selected for application. This process is time consuming and costly, and due to their very specific nature, even a small change in the antigen's epitope structure can reduce antibody function (Lipman *et al*, 2005).

In comparison, polyclonal antibodies are directed against several epitopes on a single antigen, and consequently often more effective at detecting specific antigens than monoclonal antibodies. Polyclonal antibodies are generated by the immunisation of multiple animals, e.g. rabbits, with a single antigen, such that polyclonal antibodies to this antigen are produced by a large number of B-cells. This is a rapid process, and consequently less expensive than monoclonal antibody production. However, the avidity of the polyclonal antibody for its antigen may alter over time, and antibody productivity is limited by the lifespan and size of the producing animal.

In addition to selecting a suitable antibody, the method of protein extraction is also very important, particularly when studying proteins capable of auto-cleavage, e.g. ADAM17. The addition of broad spectrum hydroxamate-based metalloproteinase inhibitors, such as 1, 10-phenanthroline and batimastat (BB-94), greatly reduces the mature form of ADAM17 cleaving its own cytoplasmic tail by the chelation of its essential zinc ion, allowing the examination of mature ADAM17 protein (Schlöndorff *et al*, 2000).

4.1.2 Specific Objectives

- To optimise the western blotting method for the detection of ADAM17, ADAMTS-1, -4, -5 and TIMP3 proteins.
- To establish an appropriate method of protein extraction to allow the full length ADAM17 form to be studied.
- To determine the modulating effect of IL-1 β , IL-6 or TNF- α treatments on the expressions of ADAM17, ADAMTS-1, -4, -5 and TIMP3 in each of the three cell lines under investigation.

4.2 Results

4.2.1 Western Blotting Optimisation

Western blot optimisation is essential to ensure the immunodetection of the fractionated protein of interest. A previously described western blotting protocol (personal communication, Dr. G. Haddock, Sheffield Hallam University, Sheffield, UK) was initially used to detect ADAM17 protein in samples extracted using the Tri-Reagent method from HepG2 cells. This protocol consisted of running 6 μ g of protein sample per lane (as determined by BCA) on a 10% Bis-Tris precast gel for approximately 1.5 hours at 125 V under reducing conditions. Fractionated proteins were transferred onto NCM by electroblotting for 1 hour at 100V on ice and subsequently blocked with 5% blocking buffer for one hour at room temperature.

Blots were immunoprobed with 1 ng/mL (1:1000 dilution) of polyclonal ADAM17 antibody (ab2051, Abcam) in 5% blocking buffer, followed by 0.3956 ng/mL (1:45000 dilution) of goat anti-rabbit IgG HRP-conjugated antibody (A9169, Sigma-Aldrich) in 5% blocking buffer. The detection of actin protein was used as a positive control to determine that the blot was performed correctly; 11.8 μ g/mL (1:1000 dilution) polyclonal actin antibody and 0.3956 ng/mL (1:45000 dilution) goat anti-rabbit IgG antibody, both in 5% blocking buffer. A negative control was also performed where the primary antibody was omitted from the immunoprobng procedure (0.3956 ng/mL secondary antibody in 5% blocking buffer only) to determine if any non-specific binding of the secondary antibody had occurred.

The same non-specific band pattern was observed with the ADAM17 and actin primary antibodies; a smear (62 kDa) was also present on all blots including the negative control (data not shown). Therefore the membrane blocking time was increased from 1 hour to 1.5 hours to eliminate the binding of the primary antibody to non-specific proteins, and the secondary antibody concentration was decreased to 0.2225 ng/mL (1 in 80000 dilution) to eliminate the background binding of the secondary antibody to the

membrane. Additionally, to ensure ADAM17 detection the primary antibody concentration was increased to 1 in 500, as reported by Plumb *et al* (2006).

Two methods of protein extraction were compared to ensure that post-lysis protein degradation was minimal. This study was performed in two cell lines, HepG2 and hCMEC/D3 (human cerebral microvascular endothelial cell line) cells, in collaboration with Dr. L.A. Hurst to eliminate any worker error. Figure 4.1 illustrates that ADAM17 is present in both cell lines, but with different band patterns in each. When protein was extracted with Tri Reagent, a doublet of 98 and 88 kDa was detected in both cell lines, however when protein was extracted using CelLytic supplemented with 10% protease inhibitor cocktail and 10 mM 1, 10-phenanthroline only the 98 kDa band was present. Hence supplemented CelLytic proved to be the better method of protein collection for this study.

A number of antibodies were tested for their suitability in the detection of ADAM17 (ab2051, Abcam; AB19027, Chemicon; MAB2129, R & D; sc-25782, Santa Cruz), with the latter being selected as it resulted in consistent band detection. Similarly, a number of TIMP3 antibodies were tested for the detection of this inhibitor (ab2169 & ab39184, Abcam; MAB973, R & D); the latter was selected as it was the only antibody that detected TIMP3 in the collected samples. This monoclonal TIMP3 antibody did result in some non-specific staining, however the predominant 30 kDa band was of an appropriate molecular mass for glycosylated TIMP3 protein. ADAMTS-1, -4 and -5 antibodies previously validated by Haddock *et al* (2006) were used for the study of these enzymes. In all cases the primary antibody concentration and blocking for the primary and secondary antibodies were adjusted to ensure specific protein detection (Table 2.4).

4.2.2 Modulation of Protein Expression by IL-1 β , IL-6 and TNF- α

Various concentrations (1, 10 and 100 ng/mL) of the pro-inflammatory cytokines IL-1 β , IL-6 and TNF- α were applied separately to each of the cell lines under investigation (HepG2, HuH-7 or LX-2) for 48 hours, and western blot analysis was performed to assess the effect of these treatments on the levels of ADAM17, ADAMTS-1, -4, -5 and TIMP3. This technique also allowed changes in the processed and degraded forms of each protein to be observed. The obtained data were quantified using IOD analysis, with normalisation against the internal control protein actin represented by a 42 kDa band. Each band was examined individually and the combined band densities (total protein data) displayed on the relative quantification plots.

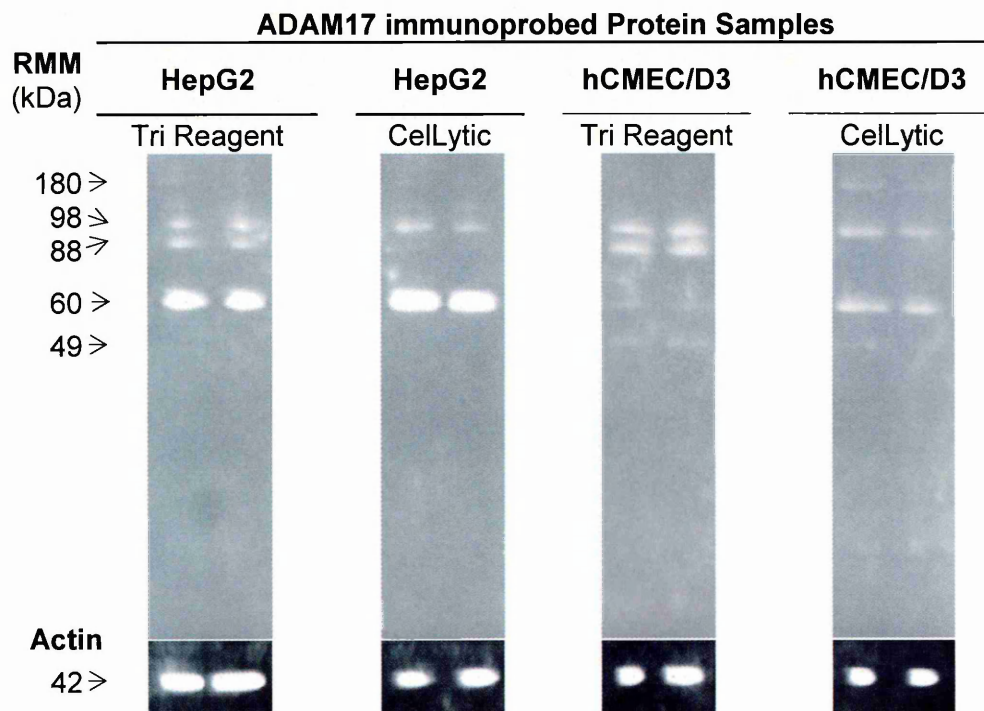


Figure 4.1: ADAM17 immunoprobed (AB19027, Chemicon) western blot of SDS-PAGE fractionated HepG2 and hCMEC/D3 duplicate protein samples following extraction with Tri Reagent or supplemented Cellytic methods. Equal loading of protein samples (6 μ g) was verified by actin immunoprobng.

The negative control for each immunoblot demonstrated no staining, indicating there was no non-specific binding of the secondary antibodies to the membrane itself or to the protein samples (data not shown).

Each experiment was only performed once in each cell line, and should therefore be regarded as preliminary data. Hence the significance of any modulations seen could not be assessed. IL-1 β and TNF- α treated cells were compared to an untreated control sample, whereas IL-6 treated cells were compared to an acetic acid-containing control sample.

Sample Preparation

Following cytokine treatment, cells were lysed and protein extracted from each sample in the presence of protease inhibitors to prevent the degradation of the protein samples (Section 2.4.1). Protein concentration was determined by BCA assay before SDS-PAGE under reducing conditions and Coomassie blue staining (Sections 2.4.2 – 2.4.5; Figure 4.2), which verified the equal loading of all protein samples. The Coomassie stains demonstrated no alterations in band patterns after cytokine treatment, although they were subtly different in each cell line tested.

The HepG2 Experimental System

The modulation of ADAM17, ADAMTS-1, -4, -5 and TIMP3 levels following 48 hours of treatment with 1, 10 or 100 ng/mL of IL-1 β , IL-6 or TNF- α in the HepG2 experimental system was investigated by western blotting. Initial observations of the immunoprobed blots indicated that each protein of interest was present in the HepG2 cell line, and that these proteins were present at different levels and in different forms.

The ADAM17 blot (Figure 4.3A) showed multiple bands ranging in size from 58 kDa to 210 kDa. The 210 kDa band may indicate dimerisation of ADAM17 protein or a highly glycosylated form. The 130 kDa band probably represents ADAM17 zymogen, with active ADAM17 at 110 kDa. The lower molecular weight bands (66 and 58 kDa) may be processed or degraded ADAM17 protein.

Total band intensity analysis of ADAM17 protein (Figure 4.3B) revealed a slight decrease after IL-1 β treatment at all concentrations tested, whereas a large fold increase was evident following IL-6 treatment, this included the concentration dependent increase in active (110 kDa) ADAM17 (data not shown), as determined by intensity analysis. Total ADAM17 protein was also increased following treatment with 1 ng/mL of TNF- α , although treatment with higher concentrations of this cytokine had no effect on total ADAM17 protein level. Again there was a concentration dependent increase in the 110 kDa active band of ADAM17 with this treatment (data not shown), as identified through densitometric analysis.

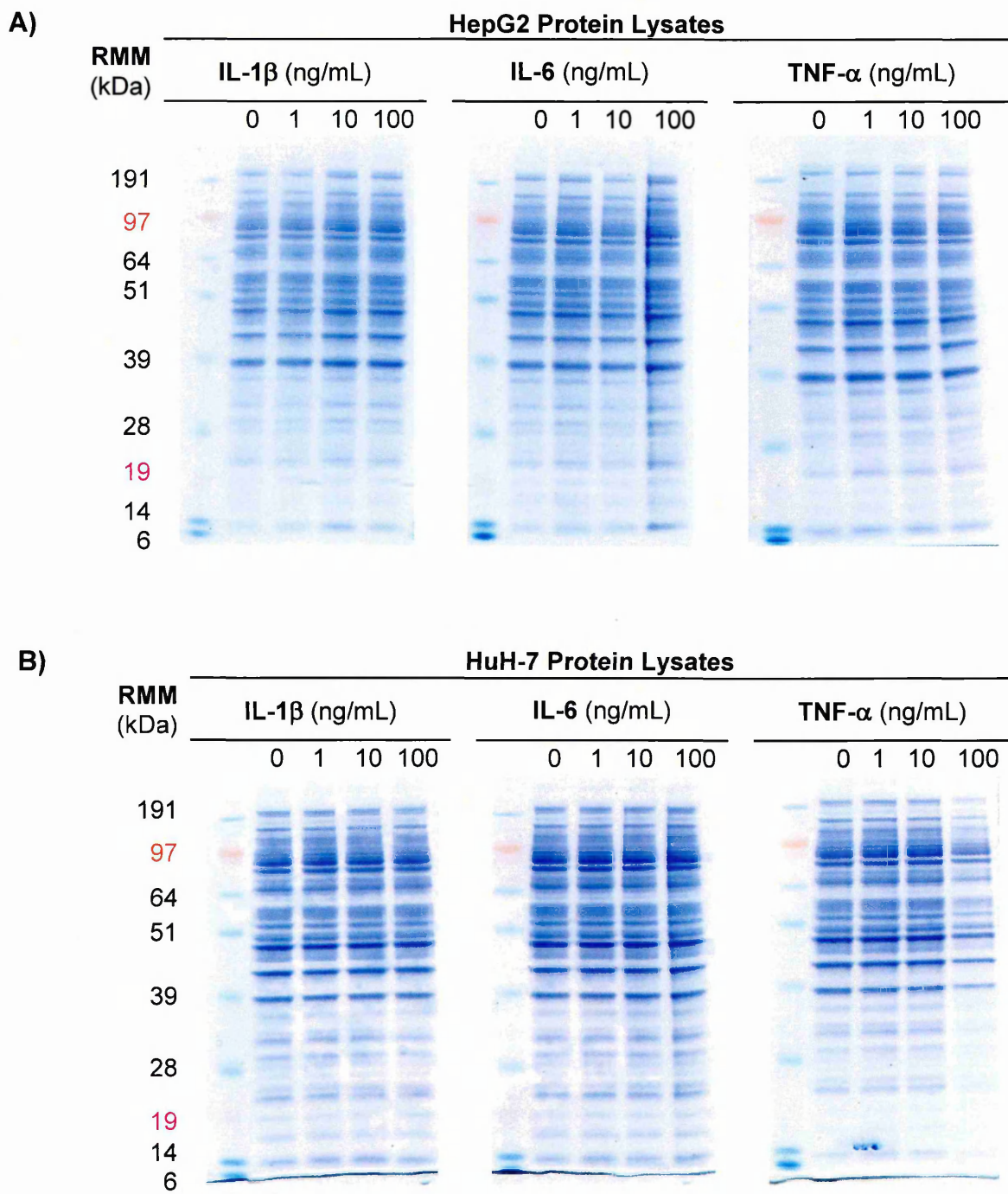


Figure 4.2: Coomassie stain of SDS-PAGE fractionated **A)** HepG2 and **B)** HuH-7 and LX-2 protein lysates following 48 hours of treatment with varying concentrations of IL1- β , IL-6 or TNF- α . Equal loading of protein samples (6 μ g) was verified.

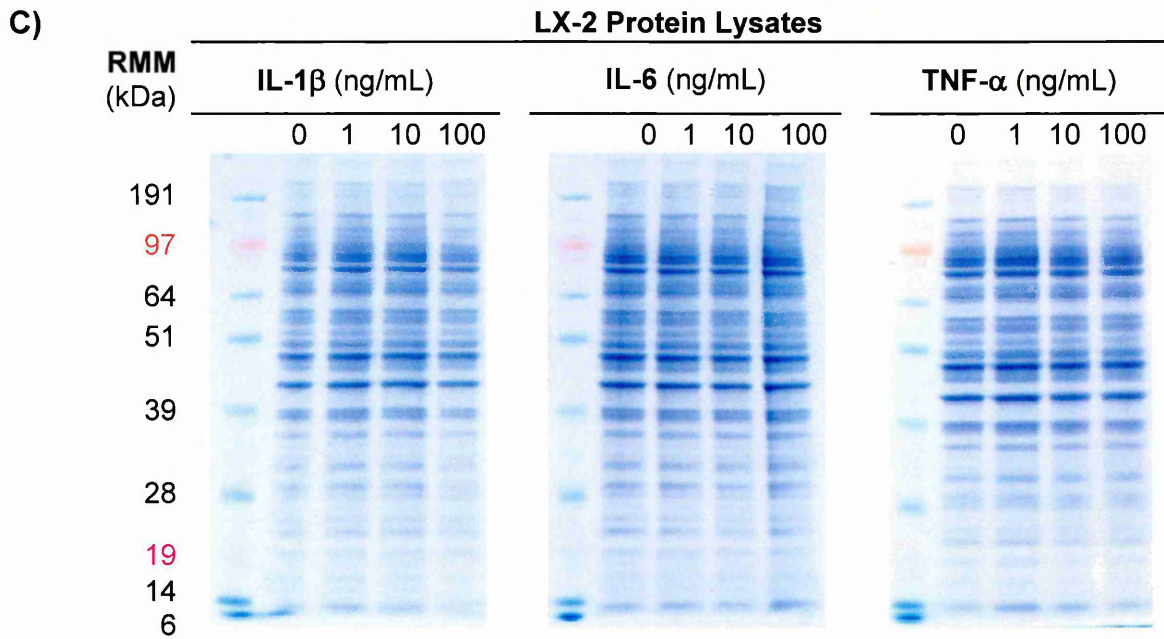


Figure 4.2 (continued): Coomassie stain of SDS-PAGE fractionated **C)** LX-2 protein lysates following 48 hours of treatment with varying concentrations of IL1- β , IL-6 or TNF- α . Equal loading of protein samples (6 μ g) was verified.

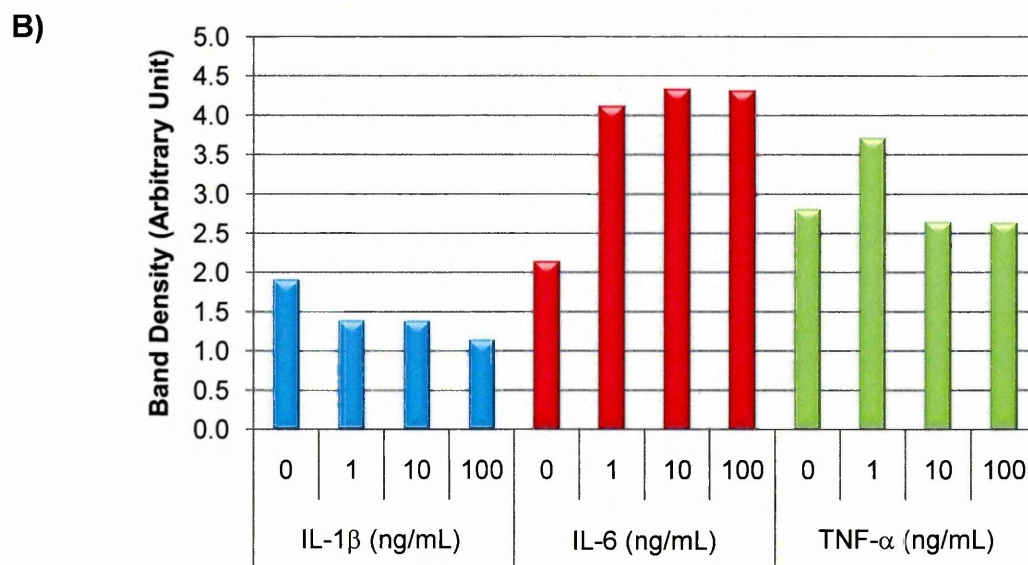
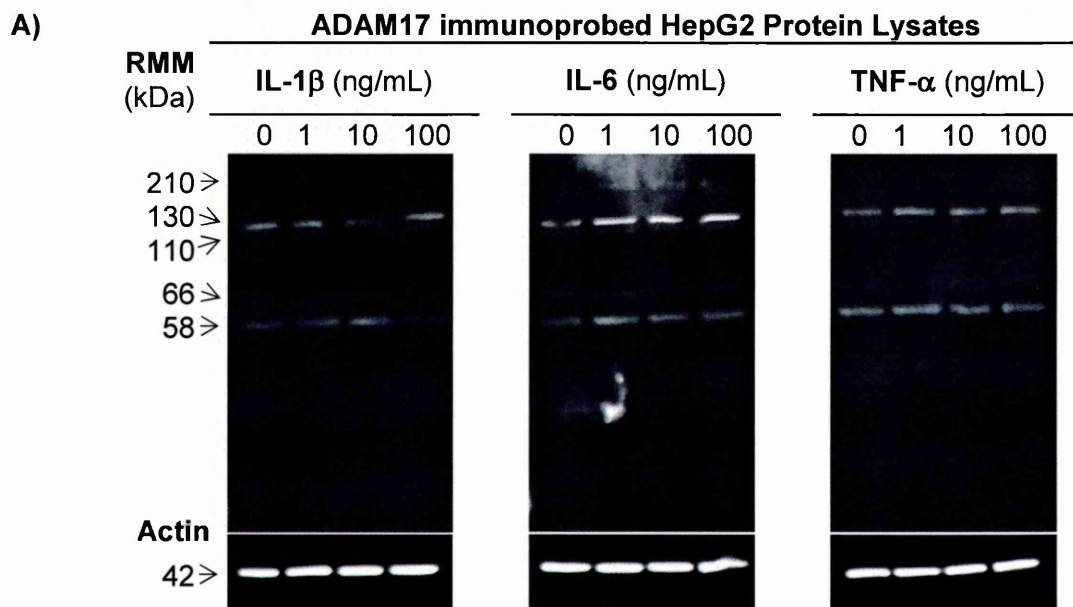


Figure 4.3: A) ADAM17 immunoprobed western blot of SDS-PAGE fractionated HepG2 protein lysates following 48 hours of treatment with varying concentrations of IL1- β , IL-6 or TNF- α . Equal loading of protein samples (6 μ g) was verified by actin immunoprobing. **B)** Relative quantification of total ADAM17 protein after actin normalisation. (n=1).

Figure 4.4A shows the blot for ADAMTS-1 with multiple bands present. Zymogen was only detected in the IL-1 β treated samples (110 kDa), however full length active ADAMTS-1 (87 kDa) and a predominant band representing the truncated active form of ADAMTS-1 (60 kDa) were evident. The 50, 48 and 42 kDa bands may represent C-terminally processed forms or breakdown products of ADAMTS-1.

Figure 4.4B demonstrates the reduced amount of ADAMTS-1 protein following 1 and 10 ng/mL of IL-1 β treatment as determined by densitometry; this decrease was also evident following 1 and 100 ng/mL IL-6 treatments. Whereas, application of 10 ng/mL of TNF- α increased total ADAMTS-1 protein expression, with increases observed in both active forms (87 and 60 kDa) of this protein.

The immunoblot for ADAMTS-4 (Figure 4.5A) showed the zymogen (110 kDa), predominant 64 kDa active form, and a C-terminally processed isoform of this active form (53 kDa). The other bands visible at 82, 60 and 49 kDa may represent other forms of this protein.

Densitometric analysis of ADAMTS-4 total protein (Figure 4.5B) revealed very small decreases after 1 and 10 ng/mL of IL-1 β , but an increase following 100 ng/mL of treatment. However, the active 64 kDa form of this protein was subject to a concentration dependent decrease following this treatment (data not shown). This same trend in overall protein was observed following IL-6 treatment. Whereas moderate decreases of ADAMTS-4 protein levels were seen after 10 and 100 ng/mL TNF- α .

The ADAMTS-5 probed blot (Figure 4.6A) indicated a predominant band of 120 kDa representing zymogen, with a faint band also evident at 110 kDa. Active ADAMTS-5 was present (70 kDa), as was a breakdown product (48 kDa).

ADAMTS-5 protein was shown by band intensity analysis (Figure 4.6B) to decrease slightly following 1 ng/mL of IL-1 β treatment, with a greater decrease observed after 10 and 100 ng/mL of treatment. IL-6 treatment of 1 and 100 ng/mL caused minor increases in ADAMTS-5 protein, whilst 10 ng/mL decreased this protein. Little modulation of ADAMTS-5 protein was observed following TNF- α treatment, although a concentration dependent increase in active ADAMTS-5 (70 kDa) was observed with this treatment, peaking with 10 ng/mL (data not shown).

TIMP3 protein was evident as a 30 kDa band on the immunoblot (Figure 4.7A). This protein was shown by densitometry (Figure 4.7B) to decrease in response to IL-1 β treatment in a concentration dependent manner with the maximum effect at 10 ng/mL. Variable increases in TIMP3 protein were observed following IL-6 treatment with the

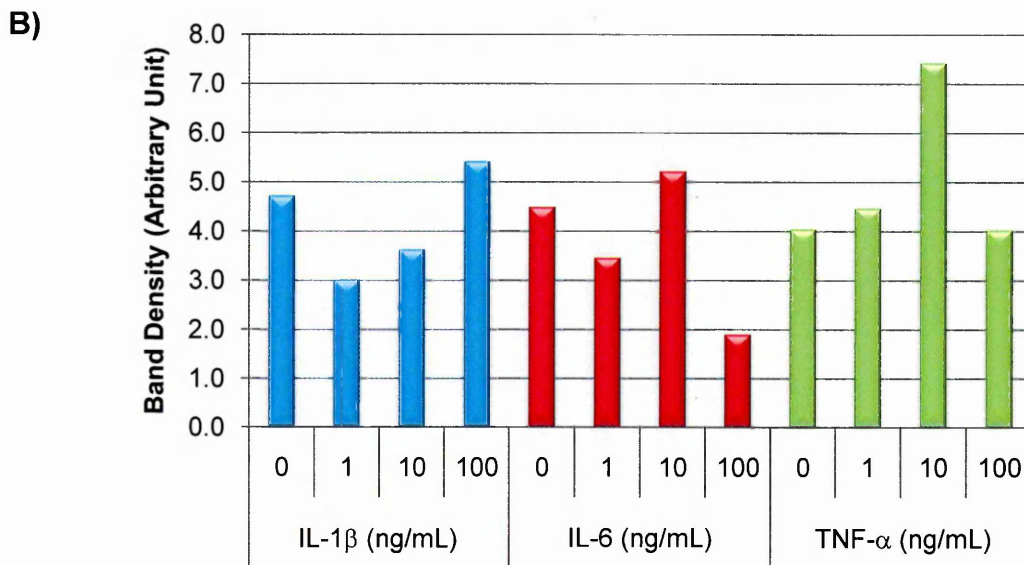
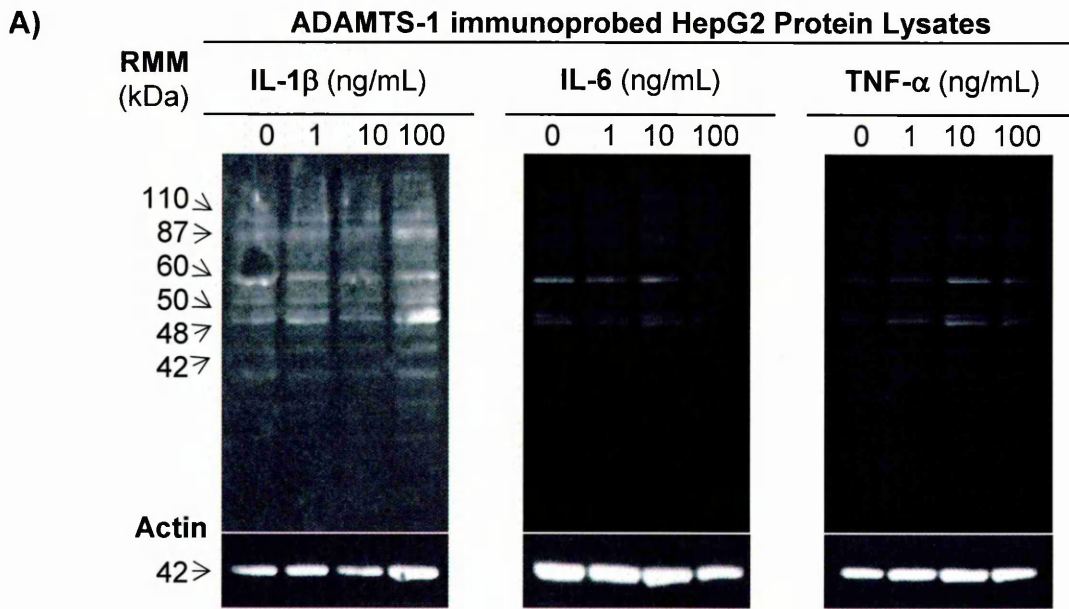


Figure 4.4: ADAMTS-1 immunoprobed western blot of SDS-PAGE fractionated HepG2 protein lysates following 48 hours of treatment with varying concentrations of IL1- β , IL-6 or TNF- α . Equal loading of protein samples (6 μ g) was verified by actin immunoprobing. **B)** Relative quantification of total ADAMTS-1 protein after actin normalisation. (n=1).

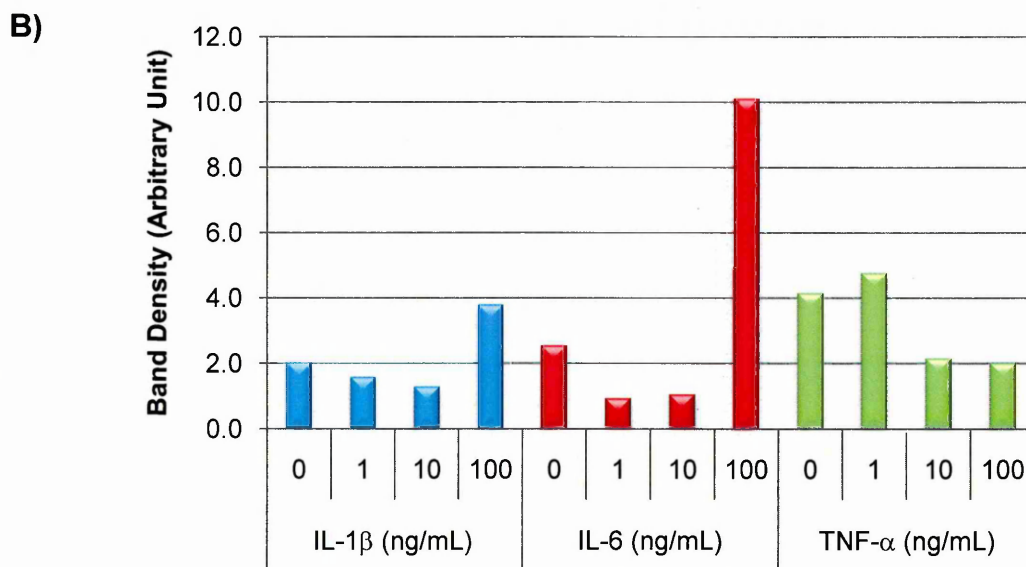
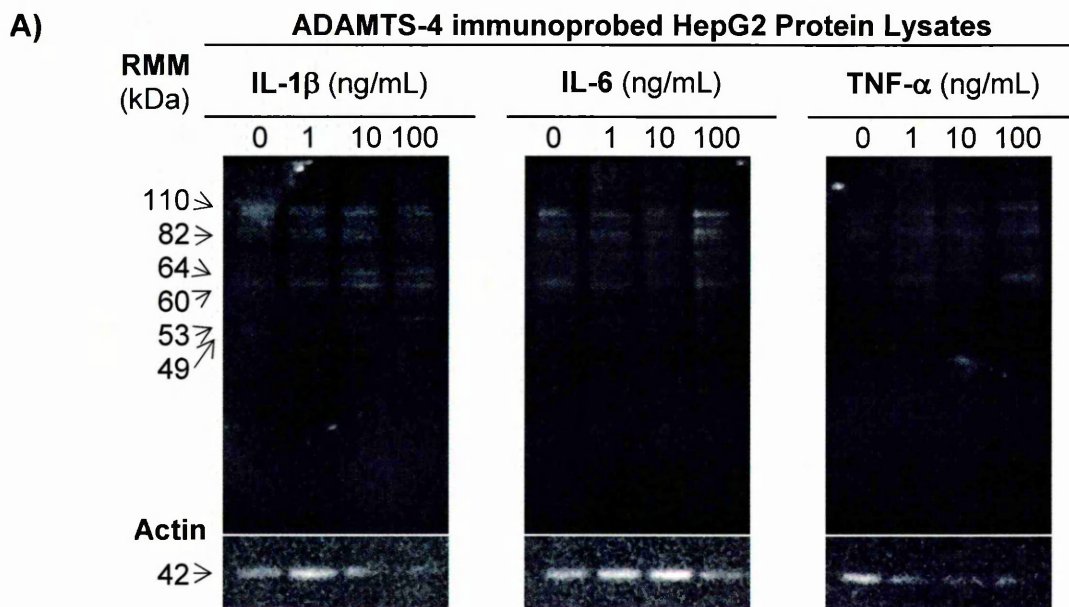


Figure 4.5: ADAMTS-4 immunoprobed western blot of SDS-PAGE fractionated HepG2 protein lysates following 48 hours of treatment with varying concentrations of IL1- β , IL-6 or TNF- α . Equal loading of protein samples (6 μ g) was verified by actin immunoprobing. **B)** Relative quantification of total ADAMTS-4 protein after actin normalisation. (n=1).

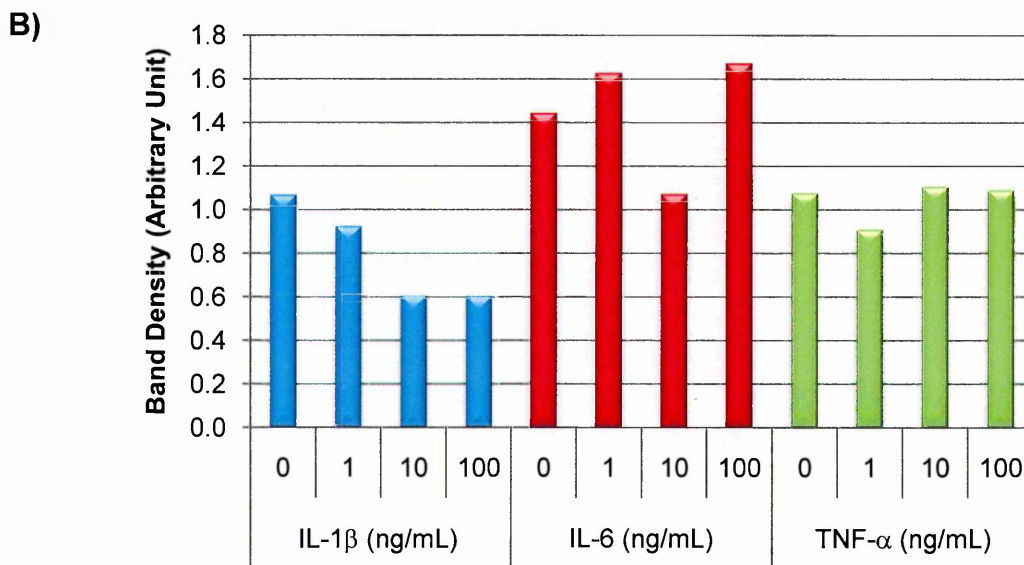
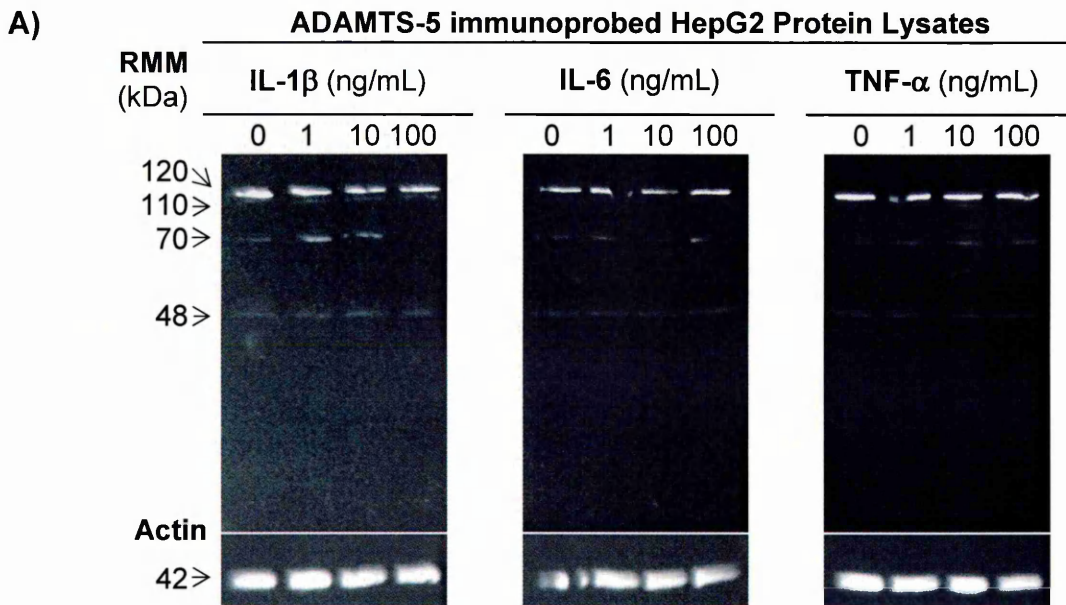


Figure 4.6: ADAMTS-5 immunoprobed western blot of SDS-PAGE fractionated HepG2 protein lysates following 48 hours of treatment with varying concentrations of IL1- β , IL-6 or TNF- α . Equal loading of protein samples (6 μ g) was verified by actin immunoprobing. **B)** Relative quantification of total ADAMTS-5 protein after actin normalisation. (n=1).

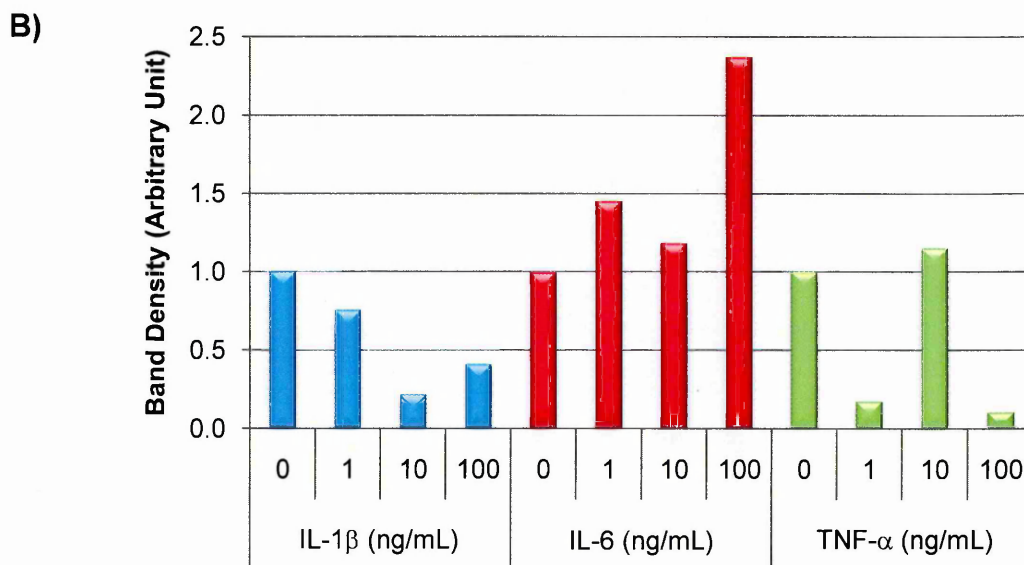
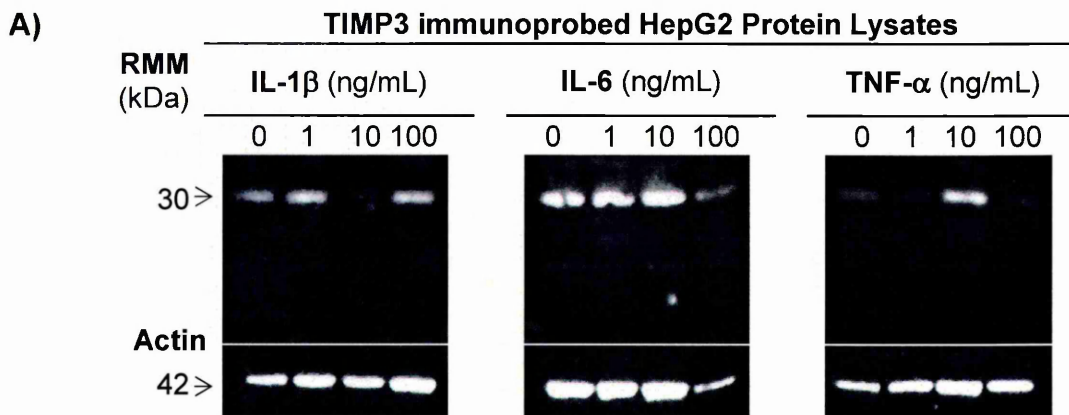


Figure 4.7: TIMP3 immunoprobed western blot of SDS-PAGE fractionated HepG2 protein lysates following 48 hours of treatment with varying concentrations of IL1- β , IL-6 or TNF- α . Equal loading of protein samples (6 μ g) was verified by actin immunoprobing. **B)** Relative quantification of total TIMP3 protein after actin normalisation. (n=1).

maximal effect seen after 100 ng/mL of treatment. Large decreases in TIMP3 protein were observed after 1 and 100 ng/mL of TNF- α treatment, although 10 ng/mL had no effect.

The HuH-7 Experimental System

Western blotting for ADAM17, ADAMTS-1, -4, -5 and TIMP3 proteins demonstrated that each protein of interest was present in HuH-7 protein lysates in different forms. Differential modulations of these proteins following 48 hours of treatment with 1, 10 or 100 ng/mL of IL-1 β , IL-6 or TNF- α were also observed.

ADAM17 was present on the blot (Figure 4.8A) as three predominant bands representing zymogen (130 kDa) and processed forms (66 and 58 kDa), and a further, lesser band representative of active ADAM17 (110 kDa).

Densitometry of total ADAM17 protein (Figure 4.8B) revealed minor decreases following 1 and 10 ng/mL of IL-1 β . Moderate decreases were evident after 1 and 10 ng/mL of IL-6 treatment, with a lesser decrease with 100 ng/mL. Conversely, total ADAM17 protein was increased following treatment with 100 ng/mL of TNF- α ; this was accompanied by a concentration dependent increase in active ADAM17 (110 kDa), peaking with 10 ng/mL of treatment (data not shown).

ADAMTS-1 zymogen was not present on the blot immunoprobed for ADAMTS-1 (Figure 4.9A); however a clear band at 87 kDa demonstrates active ADAMTS-1. The bands of 50, 48 and 42 kDa may represent processed forms or breakdown products of ADAMTS-1.

Densitometry (Figure 4.9B) indicates that ADAMTS-1 protein was reduced after 10 ng/mL of IL-1 β treatment. This protein was also decreased following 10 and 100 ng/mL of IL-6. Slight increases of ADAMTS-1 protein were observed after application of 1 and 10 ng/mL of TNF- α , but 100 ng/mL resulted in a decrease in this protein.

The ADAMTS-4 immunoblot (Figure 4.10A) allowed the visualisation of zymogen (110 kDa), active form (64 kDa), and a C-terminally processed isoform of this active form (53 kDa). Other possible forms of ADAMTS-4 can be seen at 82, 60 and 49 kDa.

Total ADAMTS-4 protein band intensity analysis (Figure 4.10B) highlighted an increase of this protein following application of 1 ng/mL of IL-1 β , with minimal effects at the other concentrations tested. IL-6 treatment yielded a minor increase in ADAMTS-4 protein after 1 ng/mL of treatment, with moderate decreases with 10 and 100 ng/mL. However, a concentration dependent increase in active ADAMTS-4 (64 kDa), peaking with 10 ng/mL, was seen following IL-1 β and IL-6 treatments (data not shown). A slight increase of ADAMTS-4 protein occurred with 100 ng/mL of TNF- α treatment.

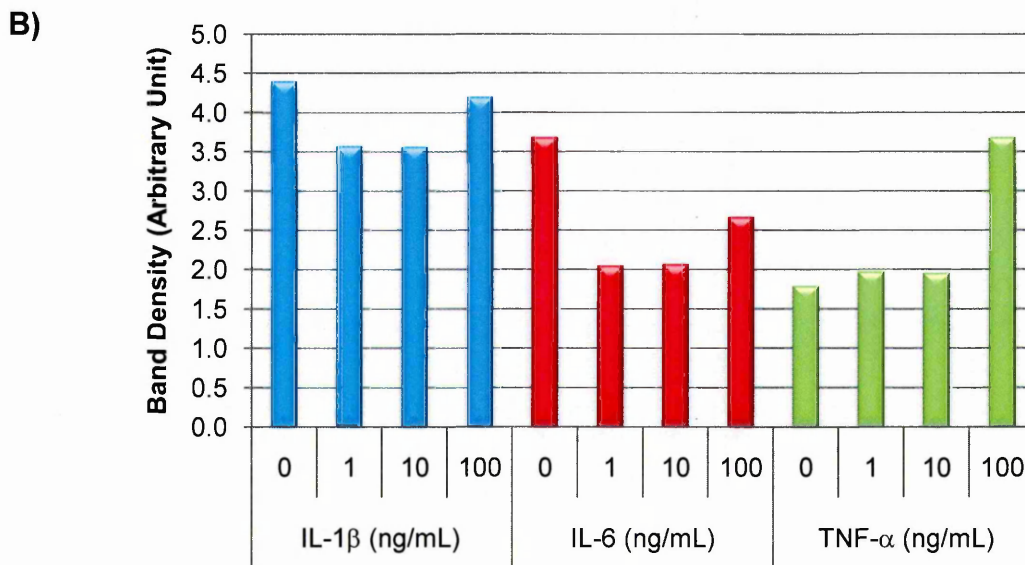
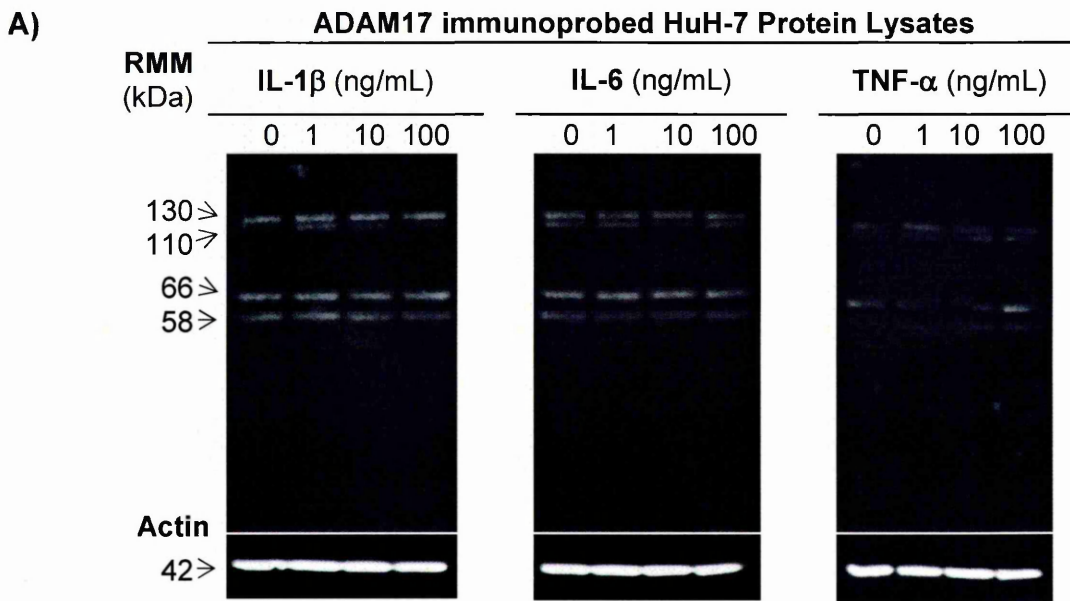


Figure 4.8: ADAM17 immunoprobed western blot of SDS-PAGE fractionated HuH-7 protein lysates following 48 hours of treatment with varying concentrations of IL1- β , IL-6 or TNF- α . Equal loading of protein samples (6 μ g) was verified by actin immunoprobeing. **B)** Relative quantification of total ADAM17 protein after actin normalisation. (n=1).

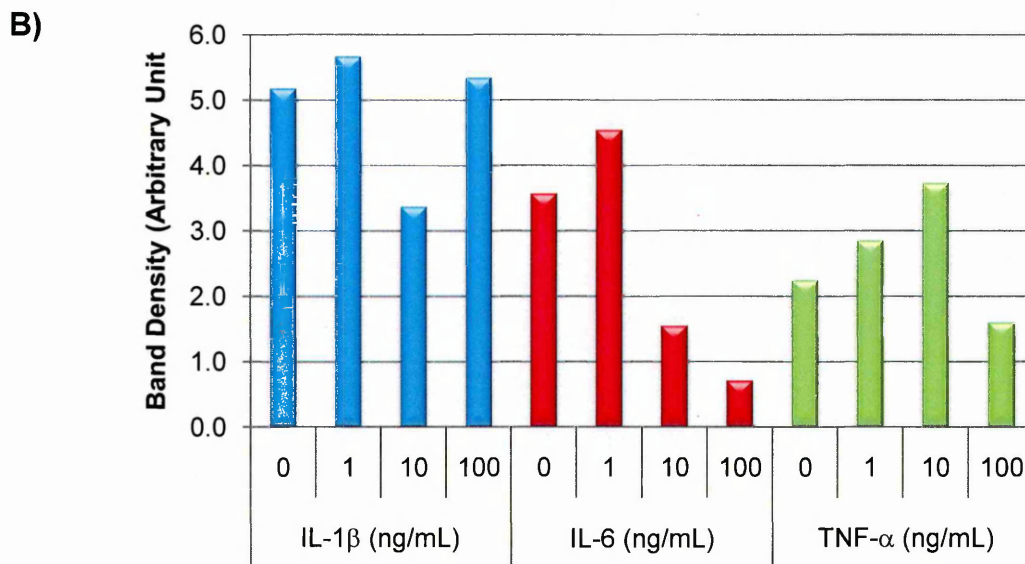
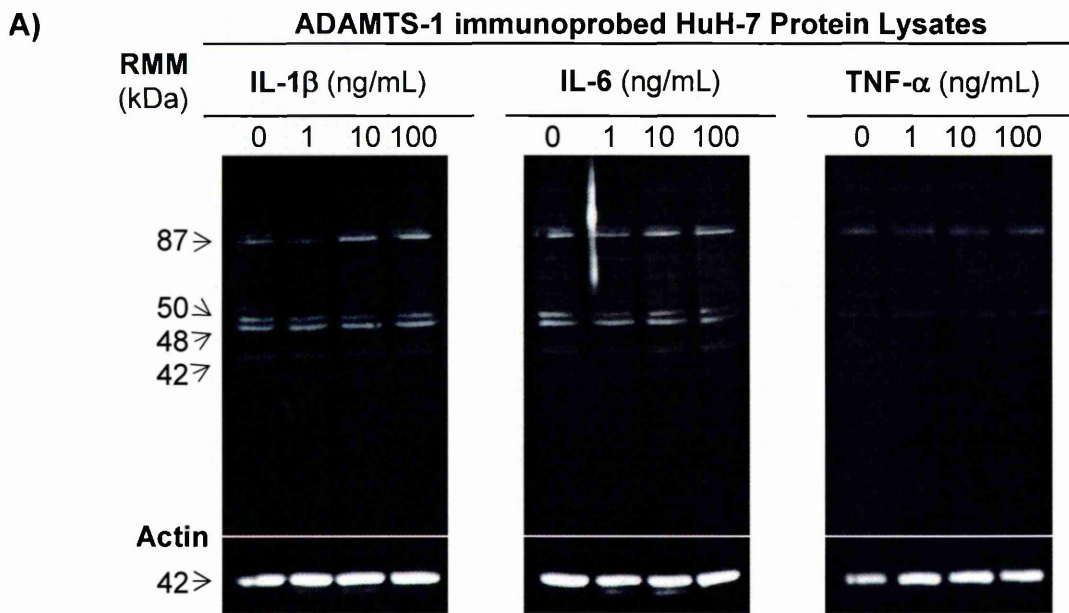


Figure 4.9: ADAMTS-1 immunoprobed western blot of SDS-PAGE fractionated HuH-7 protein lysates following 48 hours of treatment with varying concentrations of IL1- β , IL-6 or TNF- α . Equal loading of protein samples (6 μ g) was verified by actin immunoprobing. **B)** Relative quantification of total ADAMTS-1 protein after actin normalisation. (n=1).

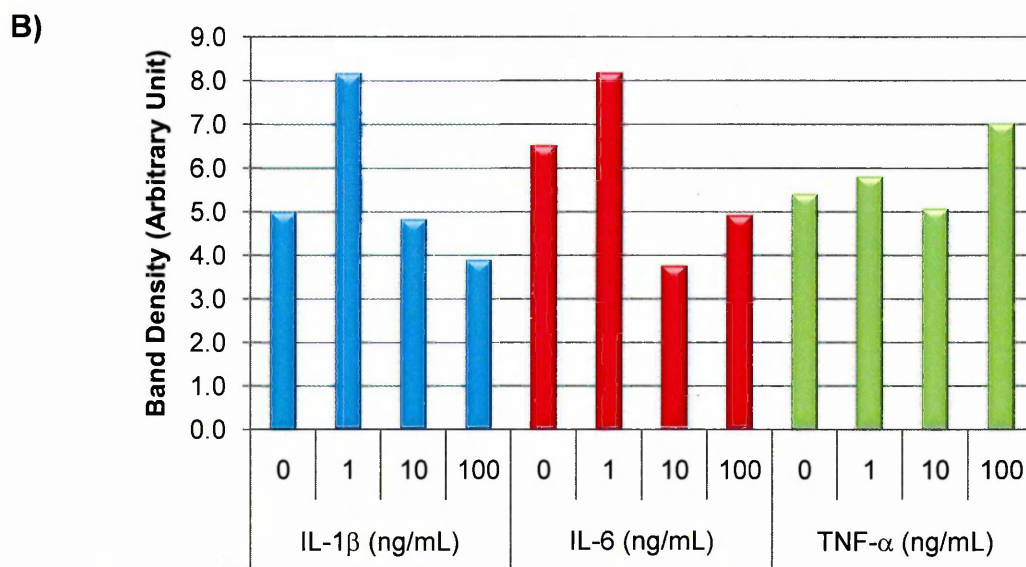
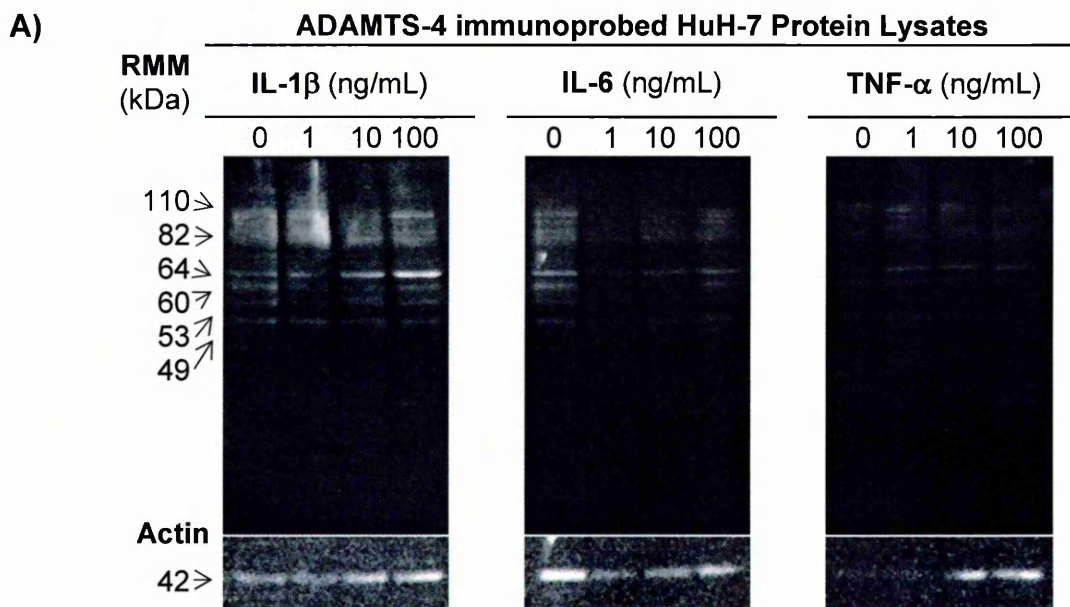


Figure 4.10: ADAMTS-4 immunoprobed western blot of SDS-PAGE fractionated HuH-7 protein lysates following 48 hours of treatment with varying concentrations of IL1- β , IL-6 or TNF- α . Equal loading of protein samples (6 μ g) was verified by actin immunoprobing. **B)** Relative quantification of total ADAMTS-4 protein after actin normalisation. (n=1).

The blot for ADAMTS-5 protein (Figure 4.11A) showed a predominant band representative of zymogen (120 kDa), with a faint band at 110 kDa. Active ADAMTS-5 protein was present as a 70 kDa band.

Densitometry of ADAMTS-5 (Figure 4.11B) showed that IL-1 β treatment caused little modulation of this protein, whereas 100 ng/mL of IL-6 resulted in a marked increase in ADAMTS-5 protein expression. Treatment with TNF- α had variable effects on ADAMTS-5 levels; 1 ng/mL of treatment marginally increased its expression, and 10 and 100 ng/mL caused minor decreases in ADAMTS-5 protein expression.

A 30 kDa band on the immunoblot represented TIMP3 protein (Figure 4.12A). Band intensity analysis (Figure 4.12B) demonstrated a minor increase and a moderate decrease in protein expression following 1 and 100 ng/mL of IL-1 β treatment respectively. Variable modulations were obtained following IL-6 treatment, such that increases in TIMP3 protein were observed following 1 and 100 ng/mL and a slight decrease was seen after 10 ng/mL of treatment. A concentration dependent increase in TIMP3 protein was seen with TNF- α treatment, peaking at 10 ng/mL.

The LX-2 Experimental System

The modulation of ADAM17, ADAMTS-1, -4, -5 and TIMP3 proteins in the LX-2 experimental system following 48 hours of cytokine treatment with 1, 10 or 100 ng/mL of IL-1 β , IL-6 and TNF- α was assessed by western blot analysis. Each protein of interest was present in the LX-2 cell line at different levels and in various forms.

The blot probed for ADAM17 (Figure 4.13A) indicated the presence of the 130 kDa zymogen, but not the 110 kDa active form. Three processed or degraded forms of ADAM17 protein (66, 58 and 39 kDa) were also evident.

Densitometry of total ADAM17 protein (Figure 4.13B) revealed minor increases following 1 and 10 ng/mL of IL-1 β . A minor increase was evident after 1 ng/mL of IL-6 treatment, with moderate decreases after 10 and 100 ng/mL. Total ADAM17 protein was decreased following treatment with 1 and 10 ng/mL of TNF- α , but increased after 100 ng/mL.

When probed for ADAMTS-1 (Figure 4.14A) the 110 kDa zymogen was not present on the blot, although a faint band at 165 kDa may represent a glycosylated form of the zymogen. The 87 kDa band indicates the presence of active ADAMTS-1 protein, with a truncated active form of ADAMTS-1 (60 kDa) also evident. Degraded or highly processed forms of ADAMTS-1 protein may be present as 50, 48 and 42 kDa bands.

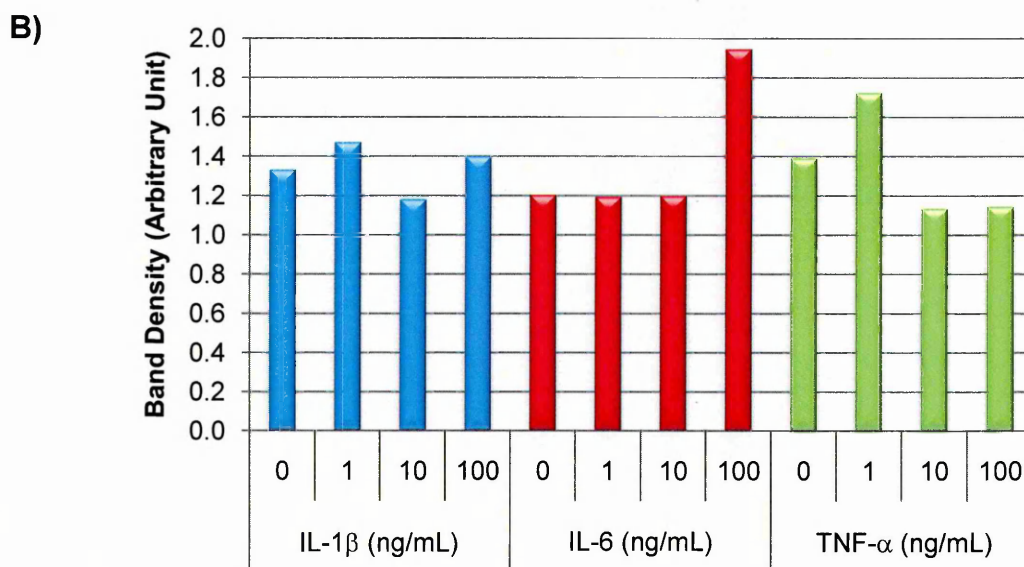
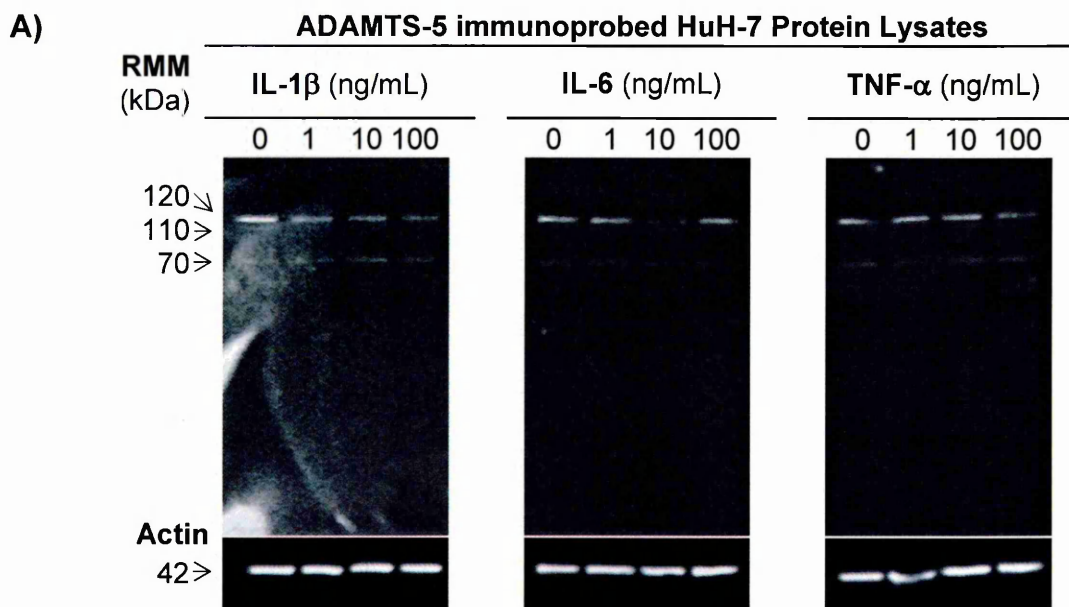


Figure 4.11: ADAMTS-5 immunoprobed western blot of SDS-PAGE fractionated HuH-7 protein lysates following 48 hours of treatment with varying concentrations of IL1- β , IL-6 or TNF- α . Equal loading of protein samples (6 μ g) was verified by actin immunoprobing. **B)** Relative quantification of total ADAMTS-5 protein after actin normalisation. (n=1).

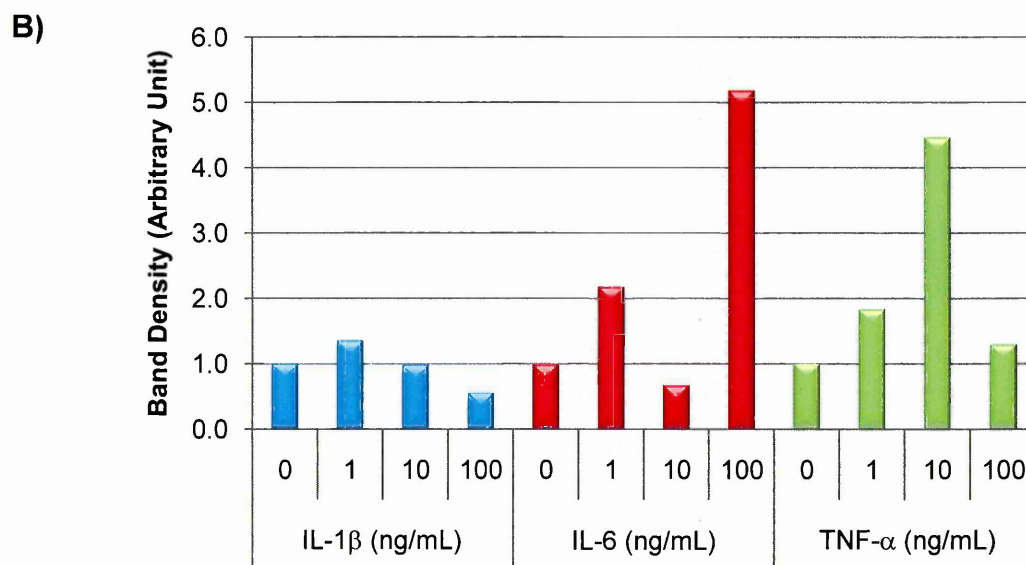
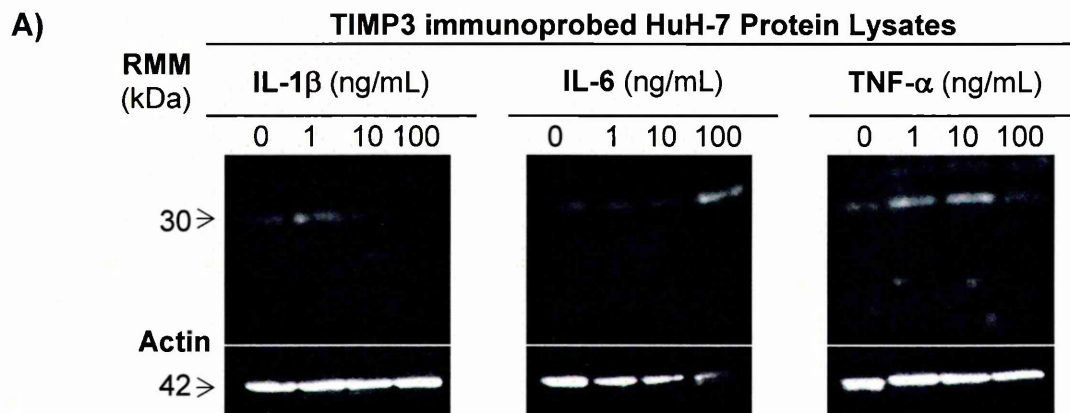


Figure 4.12: TIMP3 immunoprobed western blot of SDS-PAGE fractionated HuH-7 protein lysates following 48 hours of treatment with varying concentrations of IL1- β , IL-6 or TNF- α . Equal loading of protein samples (6 μ g) was verified by actin immunoprobing. **B)** Relative quantification of total TIMP3 protein after actin normalisation. (n=1).

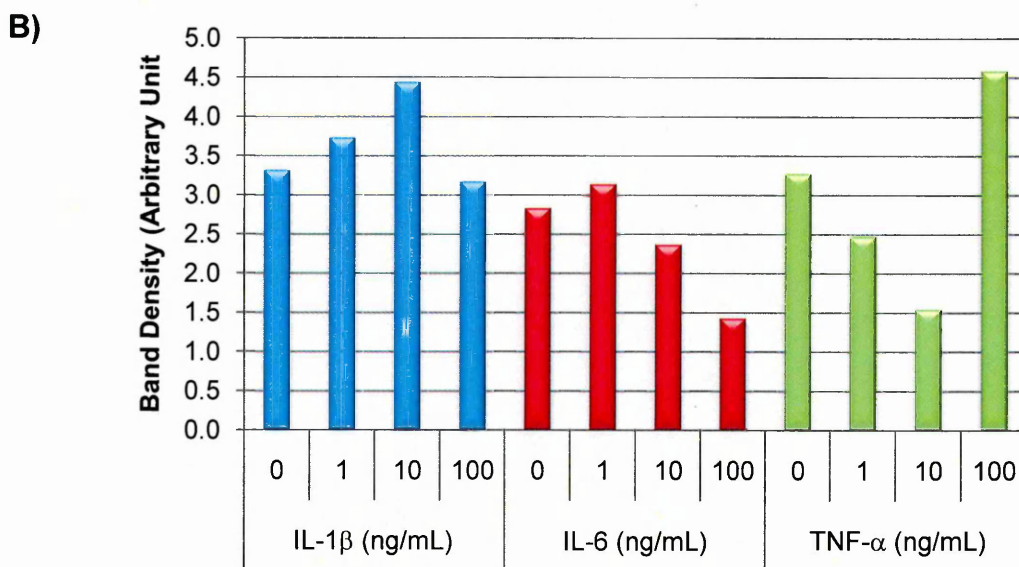
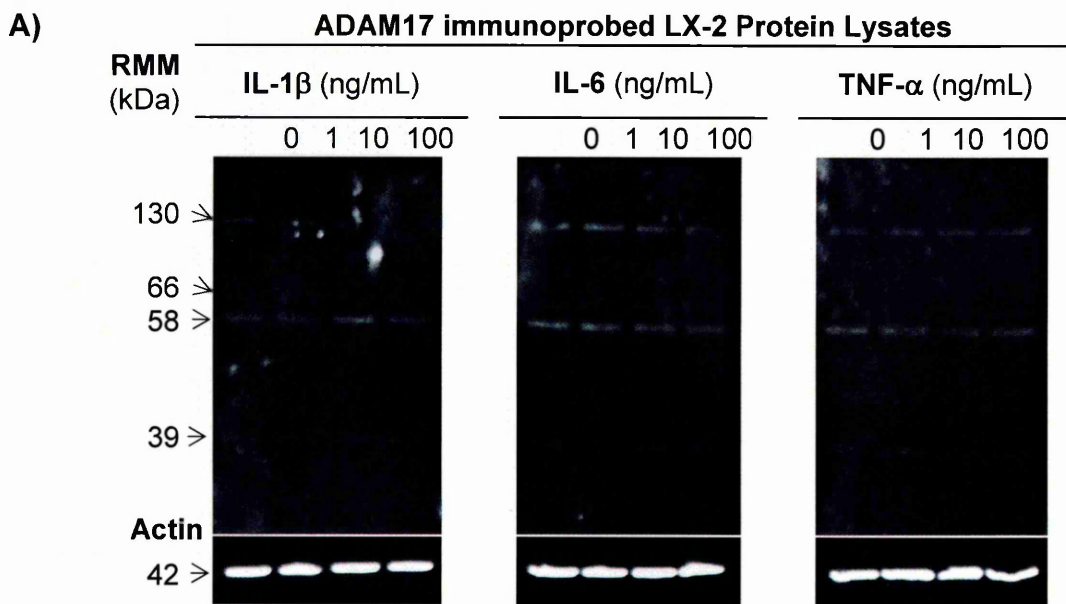


Figure 4.13: ADAM17 immunoprobed western blot of SDS-PAGE fractionated LX-2 protein lysates following 48 hours of treatment with varying concentrations of IL1- β , IL-6 or TNF- α . Equal loading of protein samples (6 μ g) was verified by actin immunoprobing. **B)** Relative quantification of total ADAM17 protein after actin normalisation. (n=1).

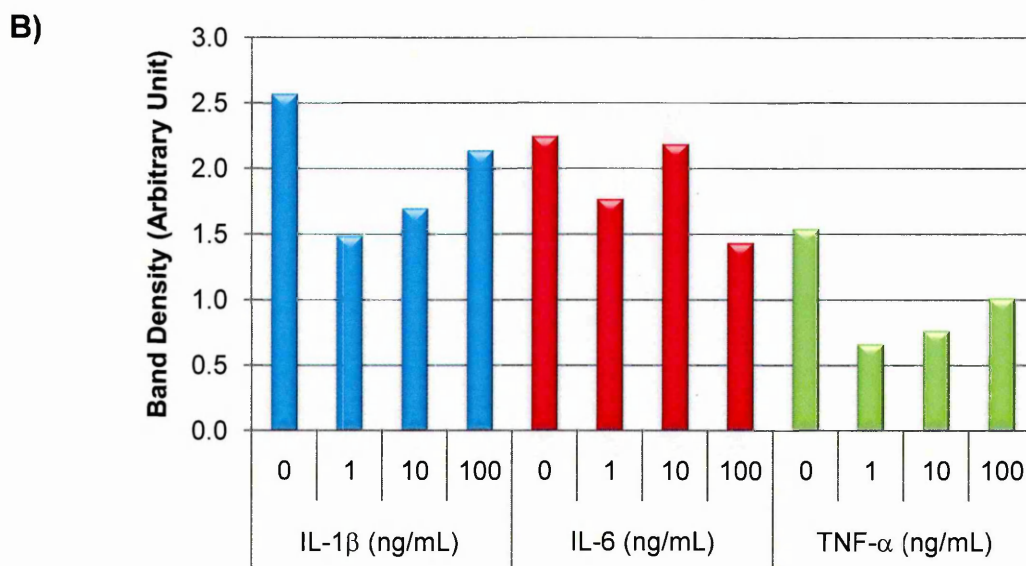
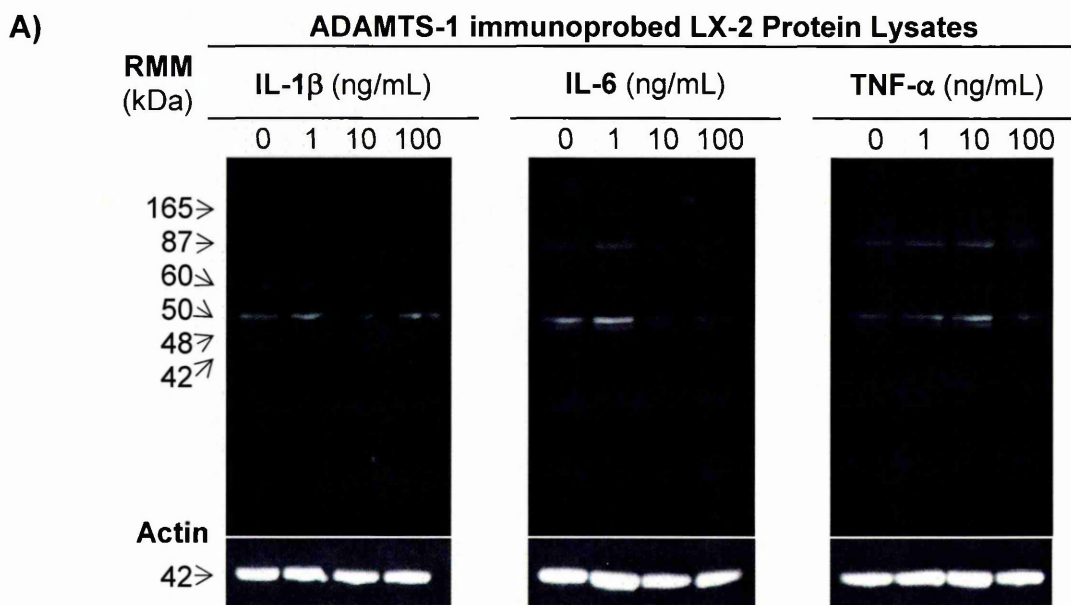


Figure 4.14: ADAMTS-1 immunoprobed western blot of SDS-PAGE fractionated LX-2 protein lysates following 48 hours of treatment with varying concentrations of IL1- β , IL-6 or TNF- α . Equal loading of protein samples (6 μ g) was verified by actin immunoprobing. **B)** Relative quantification of total ADAMTS-1 protein after actin normalisation. (n=1).

Densitometry of ADAMTS-1 protein (Figure 4.14B) showed that this protein was reduced after IL-1 β treatment with the maximal decrease at 1 ng/mL, this was reflected by the active form (87 kDa) (data not shown), as observed through densitometry. The same trend occurred with TNF- α treatments. Variable decreases were observed following IL-6 treatments.

Multiple bands were present on the ADAMTS-4 blot (Figure 4.15A) representing various forms of this protein. The 240 kDa band could indicate a highly glycosylated form of the zymogen, with zymogen present at 110 kDa, active form at 64 kDa, and C-terminally processed isoforms of this active form at 53 and 40 kDa. Other possible forms of ADAMTS-4 were seen at 82, 62, 60 and 49 kDa.

Total ADAMTS-4 protein densitometry (Figure 4.15B) revealed marked increases following 1 and 100 ng/mL of IL-1 β , but 10 ng/mL had no effect, although there was a consistent concentration dependent increase in the active form (64 kDa; data not shown). Minimal modulation occurred with 1 and 100 ng/mL of IL-6 treatment, but a moderate increase was seen after 10 ng/mL. A dose dependent increase in ADAMTS-4 protein was observed after TNF- α treatment, peaking with 10 ng/mL.

The ADAMTS-5 protein immunoblot (Figure 4.16A) showed a predominant band representative of zymogen (120 kDa), with a faint band at 110 kDa. Active ADAMTS-5 protein was evident as a 70 kDa band. A band at 195 kDa may represent a glycosylated form of the zymogen, whilst the 48 kDa band could be a breakdown product of ADAMTS-5 protein.

ADAMTS-5 band density analysis (Figure 4.16B) showed IL-1 β treatment caused minor but comparable decreases at 10 and 100 ng/mL, however active ADAMTS-5 (70 kDa) showed a concentration dependent increase, peaking with 10 ng/mL of IL-1 β (data not shown). A decrease was also observed following 10 ng/mL of IL-6. Minimal modulation of ADAMTS-5 resulted from TNF- α treatment.

TIMP3 protein was evident as a 30 kDa band on the blot (Figure 4.17A). Densitometry (Figure 4.17B) showed an increase in TIMP3 protein after 1 ng/mL of IL-1 β treatment, and a moderate and large decrease respectively following 10 and 100 ng/mL of this treatment. A large concentration dependent increase in TIMP3 protein was observed with IL-6 treatment. TNF- α treatment caused slight increases in TIMP3 protein with 1 and 10 ng/mL, but a decrease in this protein was seen after 100 ng/mL.

4.2.3 Summary of Results

The results presented in this chapter are summarised in Table 4.1.

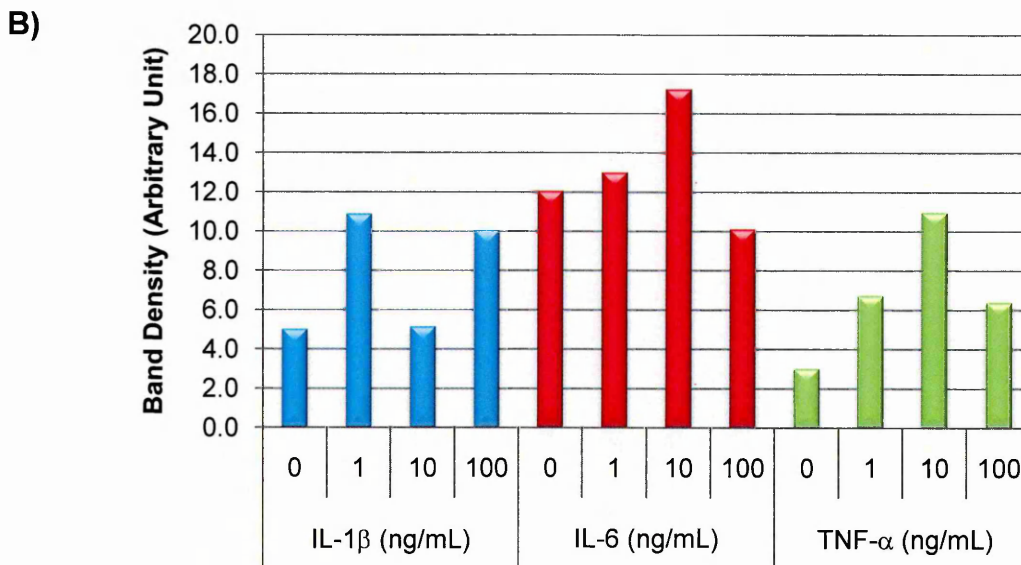
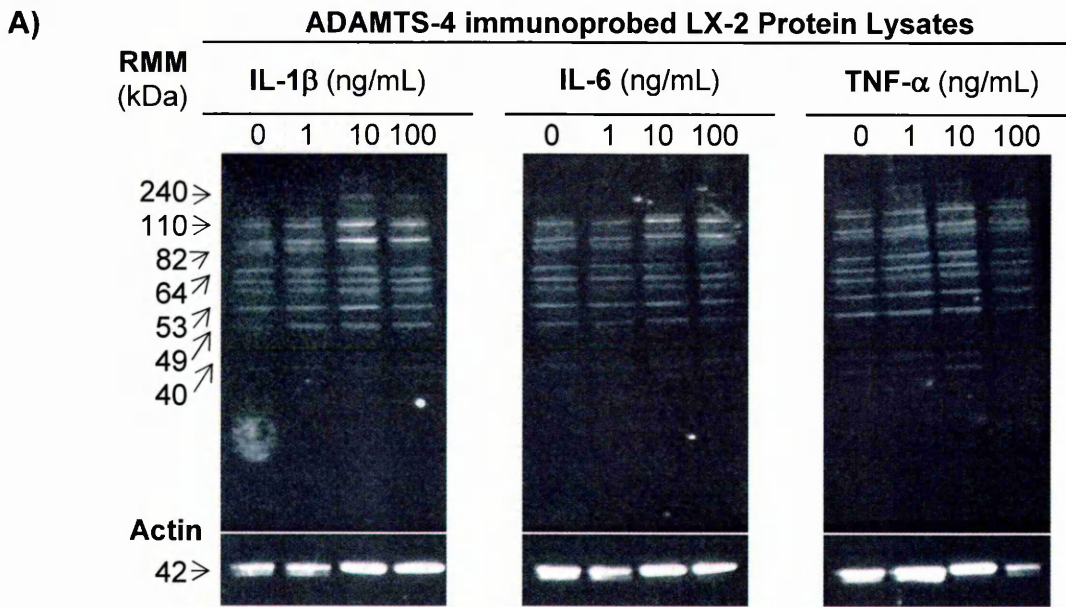


Figure 4.15: ADAMTS-4 immunoprobed western blot of SDS-PAGE fractionated LX-2 protein lysates following 48 hours of treatment with varying concentrations of IL1- β , IL-6 or TNF- α . Equal loading of protein samples (6 μ g) was verified by actin immunoprobing. **B)** Relative quantification of total ADAMTS-4 protein after actin normalisation. (n=1).

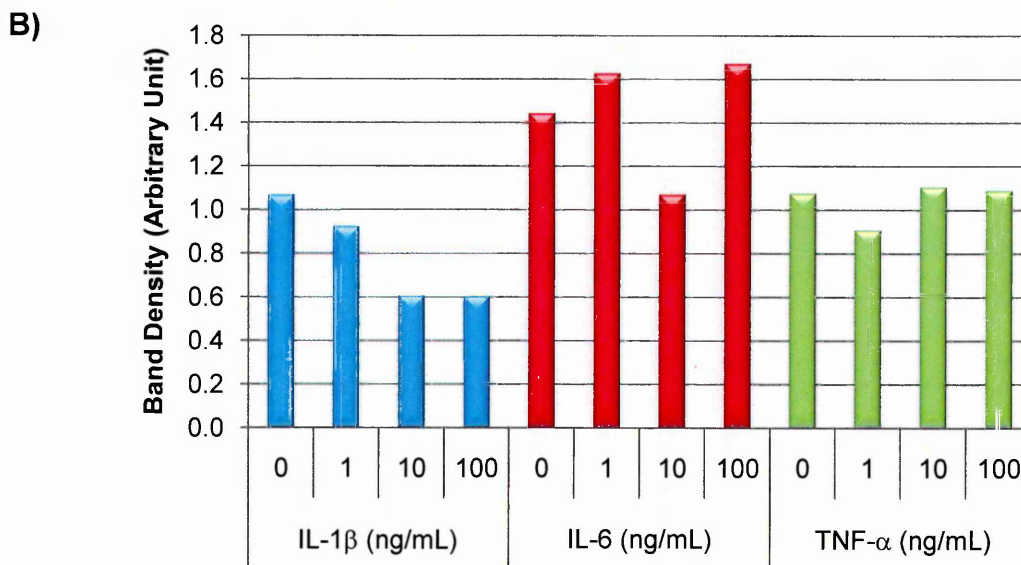
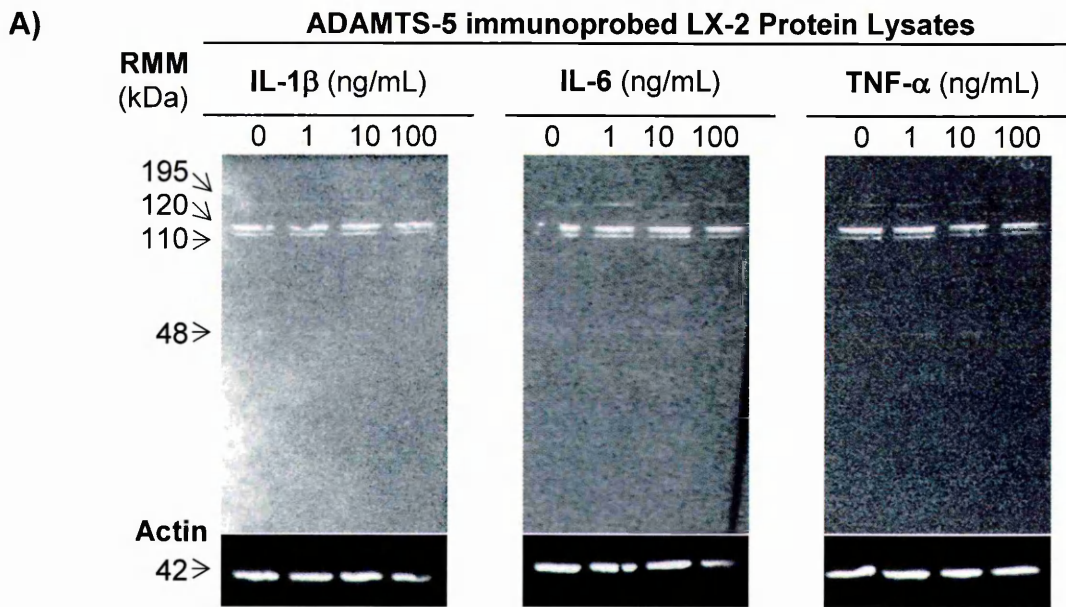


Figure 4.16: ADAMTS-5 immunoprobed western blot of SDS-PAGE fractionated LX-2 protein lysates following 48 hours of treatment with varying concentrations of IL1- β , IL-6 or TNF- α . Equal loading of protein samples (6 μ g) was verified by actin immunoprobing. **B)** Relative quantification of total ADAMTS-5 protein after actin normalisation. (n=1).

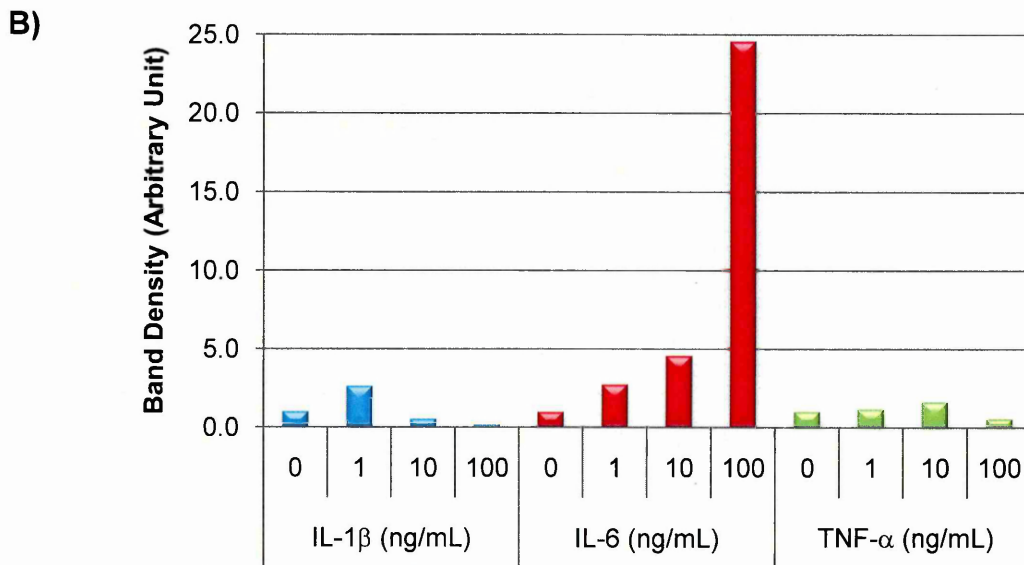
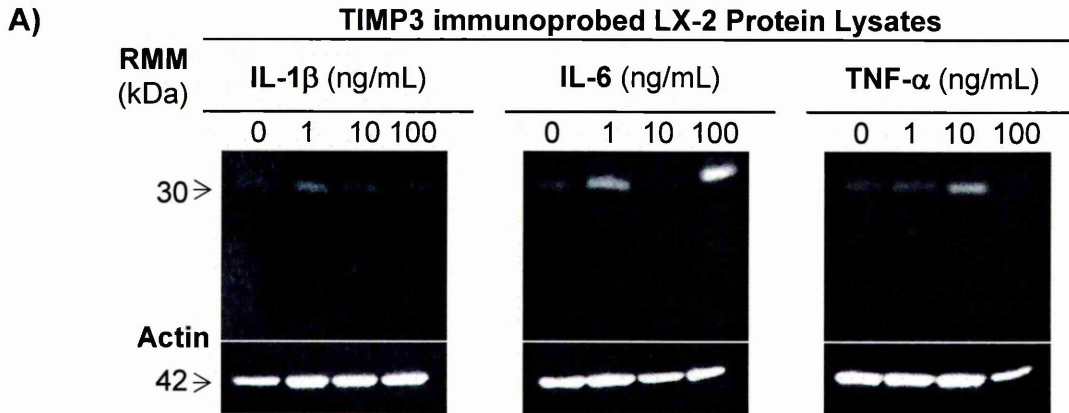


Figure 4.17: TIMP3 immunoprobe western blot of SDS-PAGE fractionated LX-2 protein lysates following 48 hours of treatment with varying concentrations of IL1- β , IL-6 or TNF- α . Equal loading of protein samples (6 μ g) was verified by actin immunoprobe. **B)** Relative quantification of total TIMP3 protein after actin normalisation. (n=1).

Table 4.1: Summary the major species and modulations of ADAM17, ADAMTS-1, -4, -5 and TIMP3 proteins by cytokines as determined by western blotting.

		Cell Lines		
		HepG2	HuH-7	LX-2
ADAM17	Major species	130 & 58 kDa	130, 66 & 58 kDa	130 & 58 kDa; no active
	IL-1 β	Minor \downarrow (1, 10 & 100 ng/mL)	Minor \downarrow (1 & 10 ng/mL)	Minor \uparrow (1 & 10 ng/mL)
	IL6	Moderate \uparrow (1, 10 & 100 ng/mL) Concentration dependent \uparrow of active form	Moderate \downarrow (1 & 10 ng/mL)	Minor \uparrow (1 ng/mL) Moderate \downarrow (10 & 100 ng/mL)
	TNF- α	Minor \uparrow (1 ng/mL) Concentration dependent \uparrow of active form	Moderate \uparrow (100 ng/mL) Concentration dependent \uparrow of active form (peak at 10 ng/mL)	Minor \downarrow (10 ng/mL) Moderate \downarrow (100 ng/mL)
ADAMTS-1	Major species	87, 60 & 48 kDa	87, 50 & 48 kDa	87 & 50 kDa
	IL-1 β	Minor \downarrow (1 & 10 ng/mL)	Moderate \downarrow (10 ng/mL)	Moderate \downarrow (1 & 10 ng/mL) Minor \downarrow (100 ng/mL)
	IL6	Minor \downarrow (1 & 100 ng/mL)	Moderate \downarrow (10 & 100 ng/mL)	Moderate \downarrow (1 & 100 ng/mL)
	TNF- α	Moderate \uparrow (10 ng/mL) Concentration dependent \uparrow of both active forms (peak at 10 ng/mL)	Minor \downarrow (10 ng/mL)	Moderate \downarrow (1 & 10 ng/mL) Minor \downarrow (100 ng/mL)

Table 4.1 (continued): Summary the major species and modulations of ADAM17, ADAMTS-1, -4, -5 and TIMP3 proteins by cytokines as determined by western blotting.

Protein Expression		Cell Lines		
		HepG2	HuH-7	LX-2
ADAMTS-4	Major species	110, 82 & 64 kDa	110 & 64 kDa	110 & 82 kDa
	IL-1 β	Minor \uparrow (100 ng/mL) Concentration dependent \downarrow of active form	Moderate \uparrow (1 ng/mL) Concentration dependent \uparrow of active form (peak at 10 ng/mL)	Moderate \uparrow (1 & 100 ng/mL) Concentration dependent \uparrow of active form
	IL6	Large \uparrow (100 ng/mL)	Minor \uparrow (1 ng/mL) Moderate \downarrow (10 & 100 ng/mL) Concentration dependent \uparrow of active form (peak at 10 ng/mL)	Moderate \uparrow (10 ng/mL)
	TNF- α	Moderate \downarrow (10 & 100 ng/mL)	Minor \uparrow (100 ng/mL)	Moderate to large concentration dependent \uparrow (peak at 10 ng/mL)

Table 4.1 (continued): Summary the major species and modulations of ADAM17, ADAMTS-1, -4, -5 and TIMP3 proteins by cytokines as determined by western blotting.

		Cell Lines		
		HepG2	HuH-7	LX-2
ADAMTS-5	Major species	120 kDa	120 kDa	120 kDa
	IL-1 β	Minor \downarrow (10 & 100 ng/mL)	Cytokines no effect	Minor \downarrow (10 & 100 ng/mL) Concentration dependent \uparrow of active form (peak at 10 ng/mL)
	IL6	Minor \downarrow (10 ng/mL)	Moderate \uparrow (100 ng/mL)	Minor \downarrow (10 ng/mL)
	TNF- α	Concentration dependent \uparrow of active form (peak at 10 ng/mL)	Minor \uparrow (1 ng/mL) Minor \downarrow (10 & 100 ng/mL)	Cytokines no effect
TIMP3	Major species	30 kDa	30 kDa	30 kDa
	IL-1 β	Concentration dependent \downarrow (trough at 10 ng/mL)	Minor \uparrow (1 ng/mL) Moderate \downarrow (100 ng/mL)	Moderate \uparrow (1 ng/mL) Moderate \downarrow (10 ng/mL) Large \downarrow (100 ng/mL)
	IL6	Moderate \uparrow (100 ng/mL)	Minor to moderate \uparrow (1 & 100 ng/mL) Minor \downarrow (10 ng/mL)	Moderate to large concentration dependent \uparrow
	TNF- α	Large \downarrow (1 & 100 ng/mL)	Concentration dependent \uparrow (peak at 10 ng/mL)	Minor \uparrow (1 ng/mL) Large \downarrow (100 ng/mL)

4.3 Discussion

4.3.1 *IL-1 β , IL-6 and TNF- α Differentially Modulate the Protein Expression of ADAM17, ADAMTS-1, -4, -5 and TIMP3 in Liver Cell Lines*

The objectives of these investigations were to determine whether ADAM17 and ADAMTS-1, -4 and -5 proteinases, and their inhibitor TIMP3 are expressed in HepG2, HuH-7 and LX-2 cell lines, and whether their levels are modulated by cytokines IL-1 β , IL-6 and TNF- α .

Following the optimisation and validation of the western blotting procedure, it was shown that all of these proteins were expressed in the studied cell lines albeit at different levels and forms. However, there is a need for caution when interpreting western blot data due to the difficulty in the verification of antibody specificity. This technique only allows the relative quantification of protein bands, and densitometric analysis of each blot demonstrated the generally minor, but differential modulations of each protein of interest by the cytokine treatments.

Previously researchers have documented an increased expression of ADAM17 protein in CRCs (Blanchot-Jossic *et al*, 2005) and metastases resulting from CRCs (Merchant *et al*, 2008), as compared to paired non-cancerous tissue. ADAM17 expression has only been studied at the mRNA level in HCCs (Ding *et al*, 2004), although it is present in some HCC cell lines, including HepG2, HuH-7, HLF, Li-7 and PLC/PRF/5 (Itabashi *et al*, 2008).

These data show that ADAM17 was present in two predominant forms in both HepG2 and LX-2 cells, zymogen (130 kDa) and a processed or degraded form (58 kDa), with an additional predominant 66 kDa band also evident in HuH-7 cells. Active ADAM17 (110 kDa) was present in the hepatoma cell lines, but absent from the hepatic stellate cell line; furthermore HepG2 and HuH-7 cells expressed more total ADAM17 protein than the LX-2 cell line, as determined by band intensity analysis of the blots. This may indicate that active ADAM17 aids liver tumour development, possibly by the promotion of cellular proliferation and/or angiogenesis as demonstrated in other human tumour types including colon carcinomas (Vázquez *et al*, 1999; Blanchot-Jossic *et al*, 2005).

Furthermore, IL-1 β and TNF- α treatments had opposing effects on ADAM17 expression in the hepatoma and LX-2 cell lines, such that IL-1 β caused a decrease in total ADAM17 in the hepatoma cell lines and an increase in LX-2 cells, and TNF- α caused an increase in total ADAM17 protein in the hepatoma cells and a decrease in LX-2 cells. IL-6 treatment resulted in varied modulation of ADAM17 in the cell lines examined with an increase in active and total ADAM17 protein observed in HepG2

cells, a decrease in total ADAM17 protein in HuH-7 cells and variable effects in LX-2 cells dependent upon the concentration of treatment.

The expression of ADAMTS-1, -4 or -5 proteins has not previously been examined in HCC, CRC, or normal liver tissue. So establishing the expression of these classical aggrecanases in three liver cell lines may identify a mechanism by which liver ECM is processed to enable its invasion by tumour cells.

Although ADAMTS-1 zymogen was rarely detected, full length active ADAMTS-1 was present as a predominant 87 kDa band in the liver cell lines examined, with more ADAMTS-1 protein detected in the hepatoma cell lines than the non-cancerous LX-2 cell line, as determined by band intensity analysis. This over-expression of full length ADAMTS-1 may promote tumour angiogenesis and invasion, as shown by other researchers in TA₃ mammary carcinoma, Lewis lung carcinoma (Liu *et al*, 2006b), and CHO cell lines (Kuno *et al*, 2004). Ordinarily though ADAMTS-1 protein inhibits tumour angiogenesis by the sequestration of the tumour angiogenesis mediator, VEGF₁₆₅, and is down-regulated in a number of tumours e.g. mammary and pancreatic tumours, in order to counteract this effect (Porter *et al*, 2004; Masui *et al*, 2001). This indicates that the proteolytic status of ADAMTS-1 protein determines the effect of this protein on cancer development and dissemination.

IL-1 β and IL-6 treatments of the liver cell generally caused decreases in ADAMTS-1 protein, as did TNF- α treatment in LX-2 cells. However, this latter treatment resulted in increases in total ADAMTS-1 protein in the HCC cell lines, with concentration dependent increases in both forms of active protein (87 and 60 kDa) in HepG2 cells. Therefore the finding that IL-1 β and IL-6 treatments of liver cell lines decrease active ADAMTS-1 could provide a mechanism by which liver tumours could facilitate the development of a neovasculature during hepatic injury when circulating levels of these cytokines are elevated.

Total ADAMTS-4 protein was expressed at a higher level and with twice as much active ADAMTS-4 in LX-2 cells than the hepatoma cell lines, as determined by band intensity analysis. A specific role for ADAMTS-4 in cancer has not yet been elucidated, but its up-regulation is thought to contribute to the tumours invasive potential (Held-Feindt *et al*, 2006). Furthermore, various forms of ADAMTS-4 were present in the liver derived cell lines, which may indicate C-terminal processing and altered substrate specificity (Kashiwagi *et al*, 2004).

Generally IL-1 β and IL-6 treatments increased total ADAMTS-4 protein expression in all of the examined cell lines, however in contrast to the total protein level, a concentration dependent decrease in active ADAMTS-4 was seen in HepG2 cells

following IL-1 β treatment, as determined by band intensity analysis. Increased ADAMTS-4 protein was also observed following TNF- α treatment in LX-2 cells, but was decreased in the hepatoma cell lines.

Previously researchers have identified a dual role for ADAMTS-5 in cancer progression. Firstly, its down-regulation could permit tumour angiogenesis by the decreased actions of its anti-angiogenic central TSR (Sharghi-Namini *et al*, 2008). Secondly, elevated ADAMTS-5 protein expression could increase the invasive potential of tumours by accelerating ECM processing (Viapiano *et al*, 2008). ADAMTS-5 protein was observed in the experimental cell lines, although the active form was only detectable in low levels in the hepatoma cell lines and was undetectable in the LX-2 cell line. IL-6 treatment did not modulate ADAMTS-5 protein expression; however IL-1 β increased it in a concentration dependent manner (peak at 10 ng/mL) in HuH-7 and LX-2 cells, with the same trend observed in HepG2 cells following TNF- α treatment.

Zeng *et al* (2001) demonstrated that TIMP3 was consistently decreased in CRCs at the protein level when compared to paired normal colon mucosa; this is in contrast to their findings that TIMP3 mRNA was increased in CRCs. In this study TIMP3 was detected in the glycosylated 30 kDa form in all of the liver cell lines examined, with more of this protein observed in HepG2 cells than the HuH-7 and LX-2 cells. Variable responses were observed following IL-1 β and TNF- α treatments, but IL-6 treatment increased this inhibitor protein in all cell lines, with a clearly observed concentration dependent increase seen in the LX-2 cell line.

These initial observations could suggest that tumour cell invasion of the liver is influenced by the combined effects of increased ADAM17, ADAMTS-4 and -5 protein expressions, and decreased ADAMTS-1 expression. These up-regulations may outweigh the subtle increase observed in their inhibitor, TIMP3. These combined effects could aid liver tumour formation by increasing liver tumour cell proliferation and ECM sculpting, whilst allowing tumour angiogenesis to occur.

4.4 Summary

Preliminary data presented in this chapter demonstrate the differential expression and modulation of ADAM17, ADAMTS-1, -4, -5 and TIMP3 proteins in each of the cell lines investigated. Key findings include the presence of active ADAM17 protein in the hepatoma cell lines, but its absence from the HSC line, and its concentration dependent increase following TNF- α treatment in the hepatoma cell lines. Furthermore, ADAMTS-1 protein was increased in the liver cancer cell lines compared to LX-2 cells.

Chapter 5

Cellular Localisation ADAM17, ADAMTS-1, -4, -5 and TIMP3 in Liver Cell Lines and the effect of IL-1 β , IL-6 and TNF- α on this

5.1 Introduction

This chapter describes an investigation of the cellular localisation of ADAM17, ADAMTS-1, -4, -5 and TIMP3 protein in the three previously characterised liver cell lines, HepG2, HuH-7 and LX-2, and their distribution after treatment with IL-1 β , IL-6 and TNF- α . Qualitative changes in protein expression level were also examined after cytokine treatments.

The proteolytic enzymes under investigation are synthesised as inactive zymogens that require the removal of their prodomain by furin-like proprotein convertases to become proteolytically active (Schlöndorff *et al*, 2000). This activation is accompanied by a change in their cellular location, such that the inactive zymogens are located intracellularly, whilst the active proteinases have a cell membrane (ADAM17), or extracellular location (ADAMTS-1, -4 and -5) (Turner *et al*, 2009). The combined approach of ICC with confocal laser scanning microscopy allowed the *in situ* visualisation of specific proteins in cultured cells, both on the surface of cells and intracellularly.

5.1.1 Confocal Laser Scanning Microscopy (CLSM)

CLSM allows an in-focus image to be obtained from any depth of the specimen, a process known as optical sectioning. The basic principle of this technique (Figure 5.1) involves a laser beam of the correct excitation wavelength being passed through a light source (pinhole) aperture, and focussed by an objective lens onto a single focal point within the specimen, the confocal beam path. Following fluorochrome excitation, the emitted photons together with scattered and reflected light, pass back through the objective lens and are deflected by a dichroic beam splitter through the light detector aperture, which acts to suppress light not originating from the focal point. An emission filter located in front of the light detector eliminates light not of the correct emission wavelength, prior to the detection of the light intensity by the light detector, usually a photomultiplier tube; these data are then converted into a digital format. The number of photons emitted reflects the intensity of the fluorochrome excitation (Wilhelm *et al*, c2006).

By the sequential scanning of the laser across the specimen in the horizontal plane, using oscillating mirrors, a whole image can be generated pixel by pixel. This image represents a specific optical plane within the sample. Adjusting the height of the microscope stage, in-focus images from different optical planes (depths) of the specimen can be obtained allowing three-dimensional reconstructions of the cellular locations of specific fluorescently-labelled proteins. This also allows the cell surface profiling of samples, as well as intracellular imaging.

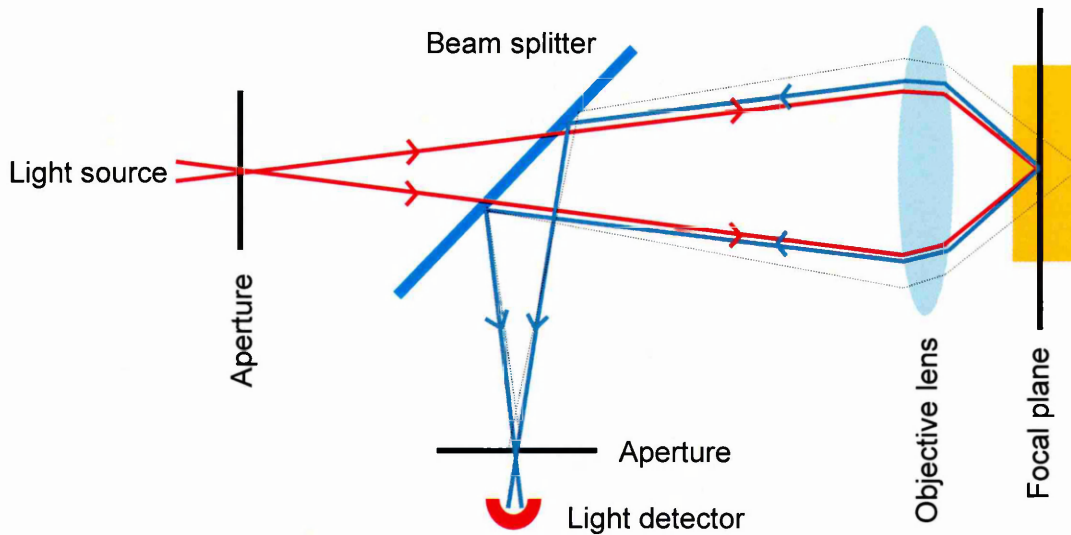


Figure 5.1: Principle of confocal microscopy.

A laser light source (red line) passes through a pinhole aperture, and is focused by an objective lens onto a single point in the focal plane of the sample. Fluorophores in the fluorescently labelled sample become excited by the laser and emit photons (blue line), which together with scattered and reflected light (grey dashed line) pass back through the objective lens and are deflected by a beam splitter towards the light detector. Focused light emitted from the sample passes through a second aperture, and is detected by a light detector. The data are then digitised to form a single pixel of an image. Scanning the sample enables a whole image to be formed.

5.1.2 Specific Objectives

- To optimise the ICC procedure to detect cell surface and intracellular ADAM17, ADAMTS-1, -4, -5 and TIMP3 protein expression.
- To determine the modulating effect of IL-1 β , IL-6 or TNF- α treatments on the cellular location and gross expression levels of ADAM17, ADAMTS-1, -4, -5 and TIMP3 proteins in each of the three cell lines under investigation.

5.2 Results

5.2.1 ICC Optimisation

ICC optimisation is required to ensure the immunodetection of specific antigens in cultured cells. Optimal conditions must be determined for each individual situation, i.e. for each antibody and cell type.

Initially a previously described protocol was used to detect ADAM17 protein in HepG2 cells (personal communication, Dr G. Haddock, Sheffield Hallam University, Sheffield, UK). Briefly, HepG2 cells were seeded at a density of 1×10^5 cells/chamber in 400 μ L complete cell culture medium and allowed to adhere for 24 hours in a cell incubator. Cells were then washed twice by submersion in DPBS for 5 minutes with gentle agitation, and fixed for 10 minutes with 4% PFA, followed by three further DPBS washes. Cells were immunoprobed with 20 μ g/mL or 10 μ g/mL (1 in 50 or 1 in 100 dilutions) of polyclonal ADAM17 antibody (ab2051, Abcam), followed by three DPBS washes, 4 μ g/mL (1:500 dilution) of Alexa Fluor[®] 568 conjugated secondary antibody (A11011, Invitrogen), and three further DPBS washes. DAPI (4', 6-diamidino-2-phenylindole) cell nuclei counter-stain was then applied to the cells.

Actin staining was used as a positive control to assess whether the procedure had worked correctly; two concentrations, 0.236 mg/mL and 0.118 mg/mL (1 in 50 and 1 in 100 dilutions), of polyclonal actin antibody (A5060, Sigma-Aldrich) were tested. Negative controls containing no primary antibody, were performed in duplicate with a secondary antibody concentration of 4.0 μ g/mL (1 in 500 dilution), as recommended by the manufacturer.

Staining was present for both ADAM17 (20 μ g/mL primary antibody) and actin (0.236 mg/mL primary antibody) proteins in HepG2 cells, however very few cells were present on the chamber slides (data not shown). Therefore, the cell washing technique was altered from submersion in DPBS with gentle agitation to the addition of 200 μ L DPBS per well with gentle agitation. The absence of non-specific staining on the negative control slides confirmed that 4.0 μ g/mL of secondary antibody dilution was appropriate.

Acetone (-20°C) fixation of HepG2 cells for 10 minutes was confirmed as a suitable method of cell permeabilisation prior to protein immunodetection as further permeabilisation of cells with 1% Triton-X-100 v/v with DPBS for 10 minutes did not result in any observable differences in staining (data not shown).

Following the optimisation of the conditions, the optimal concentrations of ADAM17, ADAMTS-1, -4, -5 and TIMP3 primary antibodies were determined in each cell line (Table 2.5).

5.2.2 Redistribution of Proteins following IL-1 β , IL-6 and TNF- α Treatment

HepG2, HuH-7 or LX-2 cells were treated with 100 ng/mL of either IL-1 β , IL-6 or TNF- α for 48 hours. ICC analysis was then performed (Section 2.5) to determine the cellular location of these proteins in control samples, and to assess whether they were redistributed due to cytokine treatment. The negative control for each experiment demonstrated only the DAPI stained nuclei of the cells, with no non-specific staining of the secondary antibody (Figure 5.2).

Each experiment was only performed once in each cell line, and therefore should be regarded as preliminary data. IL-1 β and TNF- α treated cells were compared to an untreated control sample, whereas IL-6 treated cells were compared to an acetic acid-containing control sample.

The HepG2 Experimental System

ADAM17 protein was located in a punctate pattern on the cell surface of HepG2 cells (Figure 5.3A & D); its expression was not altered by IL-1 β treatment (Figure 5.3B), however more intense staining was observed following IL-6 and TNF- α treatments (Figure 5.3C & E). In addition, ADAM17 was situated diffusely within the cell cytoplasm, with some perinuclear vesicles present (Figure 5.3F & I). Treatments with IL-1 β and TNF- α did not alter the expression level or intracellular distribution of ADAM17 (Figure 5.3G & H), however, the perinuclear vesicles were not present following IL-6 treatment (Figure 5.3J).

A low level expression of ADAMTS-1 protein was associated with HepG2 cell surfaces (Figure 5.4A & D); this did not change with IL-1 β treatment (Figure 5.4B). ADAMTS-1 surface protein was increased following IL-6 and TNF- α treatments, and the protein was distributed evenly across the membrane (Figure 5.4C & E). Intracellular ADAMTS-1 was present throughout the cytoplasm, with some perinuclear vesicle staining (Figure 5.4F & I). More perinuclear vesicles were present following IL-1 β and IL-6 treatments (Figure 5.4G & J), and completely absent following TNF- α treatment (Figure 5.4H).

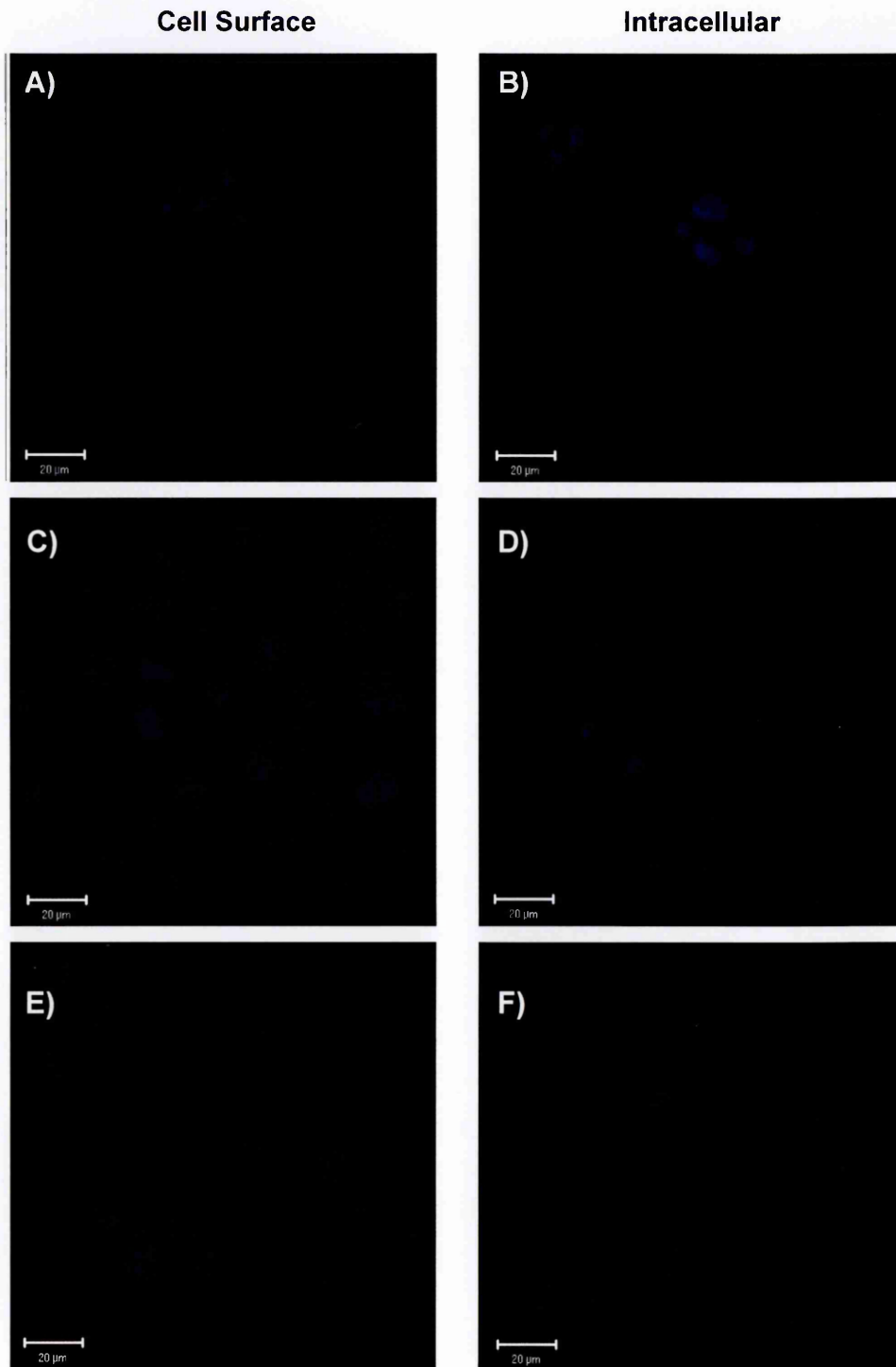


Figure 5.2: Negative controls for the ICC examination of cell surface (4% PFA) and intracellular (-20°C acetone) ADAM17, ADAMTS-1, -4, -5 and TIMP3 proteins in **A & B)** HepG2, **C & D)** HuH-7, **E & F)** LX-2 cells. Nuclei stained with DAPI (blue) in all images. Scale bar is 20 μm.

ADAM17 in HepG2 cells

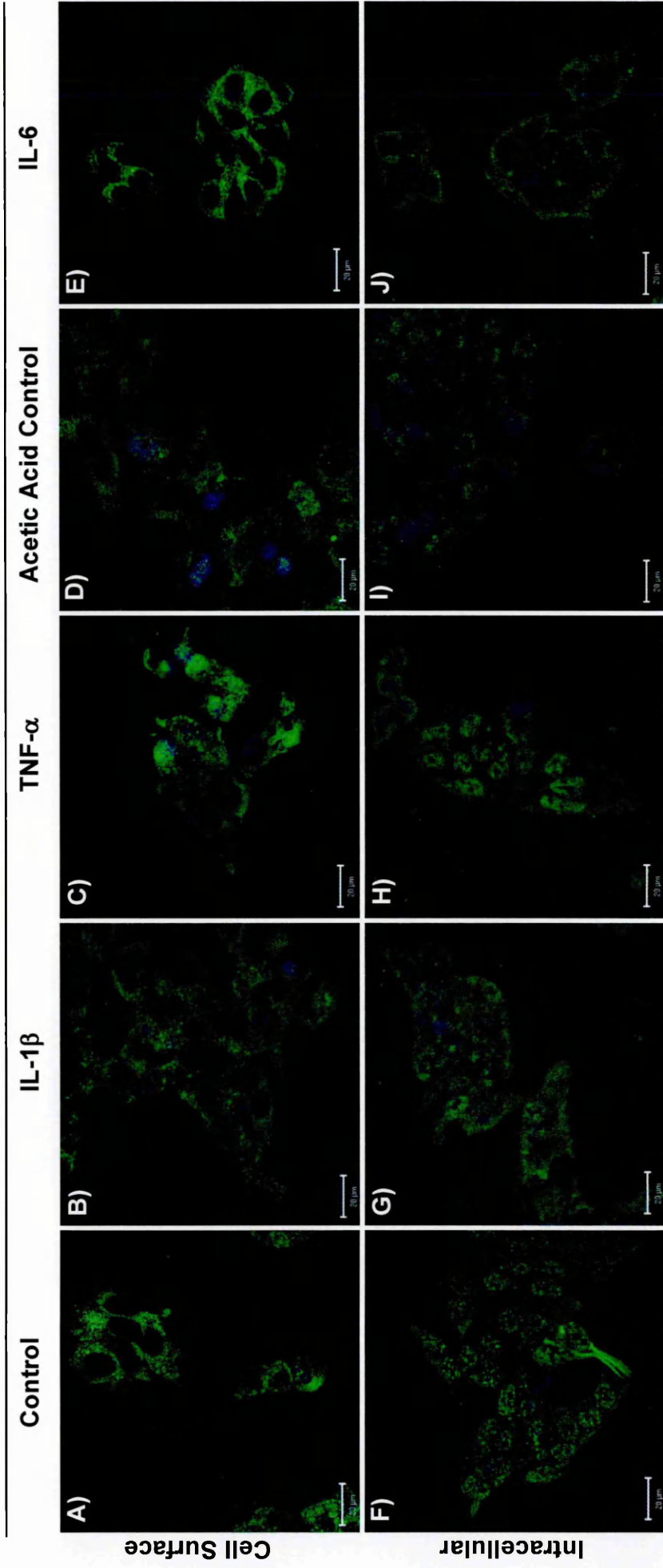


Figure 5.3: ICC examination of cell surface (4% PFA) and intracellular (-20°C acetone) ADAM17 (green) under **A & F** control, **B & G** IL-1 β (100 ng/mL), **C & H** TNF- α (100 ng/mL), **D & I** acetic acid-containing control, and **E & J** IL-6 (100 ng/mL) treatments in HepG2 cells. Nuclei stained with DAPI (blue) in all images. Scale bar is 20 μ m.

ADAMTS-1 in HepG2 cells

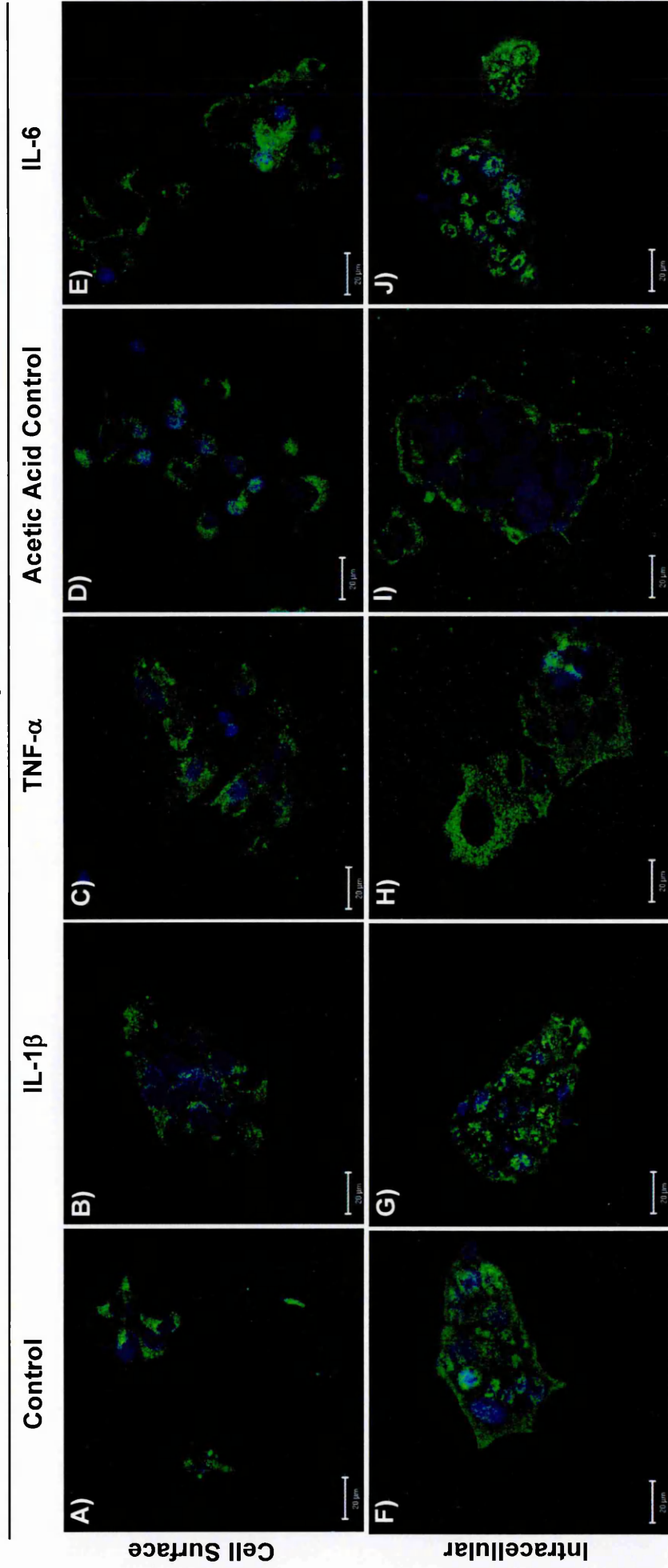


Figure 5.4: ICC examination of cell surface (4% PFA) and intracellular (-20°C acetone) ADAMTS-1 (green) under **A & F** control, **B & G** IL-1 β (100 ng/mL), **C & H** TNF- α (100 ng/mL), **D & I** acetic acid-containing control, and **E & J** IL-6 (100 ng/mL) treatments in HepG2 cells. Nuclei stained with DAPI (blue) in all images. Scale bar is 20 μ m.

Low levels of ADAMTS-4 were associated with the surface of certain HepG2 cells (Figure 5.5A & D). Comparable staining was observed following IL-1 β and IL-6 treatments (Figure 5.5B & E); however ADAMTS-4 was associated with the surface of all HepG2 cells following TNF- α treatment (Figure 5.5C). Permeabilisation of cells revealed intense cytoplasmic staining of ADAMTS-4 (Figure 5.5F & I); this was not altered by cytokine treatment (Figure 5.5G, H & J).

Low levels of ADAMTS-5 protein were associated with the surface of cells with a punctate distribution (Figure 5.6A & D), and little effect was observed following IL-1 β and IL-6 treatments (Figure 5.6B & E). In contrast TNF- α treatment increased the cell surface association of ADAMTS-5 protein (Figure 5.6C). Intense granular perimembrane ADAMTS-5 was observed following permeabilisation of HepG2 cells (Figure 5.6F), although the intracellular localisation in the acetic-acid containing control displayed a diffuse cytoplasmic pattern of this protein (Figure 5.6I). Each of the cytokine treatments also altered the distribution pattern of ADAMTS-5, such that intense perinuclear vesicles were present with minimal cytoplasmic presence (Figure 5.6G, H & J).

Minimal, but evenly dispersed TIMP3 was detected on the cell surface of HepG2 cells (Figure 5.7A & D). It was present with increasing intensity following IL-1 β , IL-6 and TNF- α treatments, with a distinct speckled pattern (Figure 5.7B, C & E). Intracellular TIMP3 had a diffuse cytoplasmic location with increased intensity at the perimembrane (Figure 5.7F & I); this was unaltered by cytokine treatment (Figure 5.7G, H & J).

The HuH-7 Experimental System

ADAM17 protein was located in a punctate pattern on the cell surface of HuH-7 cells (Figure 5.8A & D); its expression was not altered by cytokine treatment (Figure 5.8B, C & E). Intracellular ADAM17 had a granular appearance throughout the cell cytoplasm (Figure 5.8F & I), treatment with IL-1 β decreased intracellular ADAM17 protein levels (Figure 5.8G), but with IL-6 and TNF- α treatments the protein level appeared to be unaltered (Figure 5.8H and J).

ADAMTS-1 protein was associated with the surface of HuH-7 cells with a speckled distribution (Figure 5.9A & D); the distribution of this protein was unaltered by cytokine treatments (Figure 5.9B, C & E). However, following IL-1 β and more noticeably IL-6 treatments, ADAMTS-1 was absent from some cells (Figure 5.9B & E). Intracellular ADAMTS-1 was distributed uniformly throughout the cytoplasm, with some speckled perinuclear staining (Figure 5.9F & I). Increased cytoplasmic and perinuclear ADAMTS-1 protein levels were evident following IL-1 β and IL-6 treatments (Figure 5.9G & J), but remained unaltered following TNF- α treatment (Figure 5.9H).

ADAMTS-4 in HepG2 cells

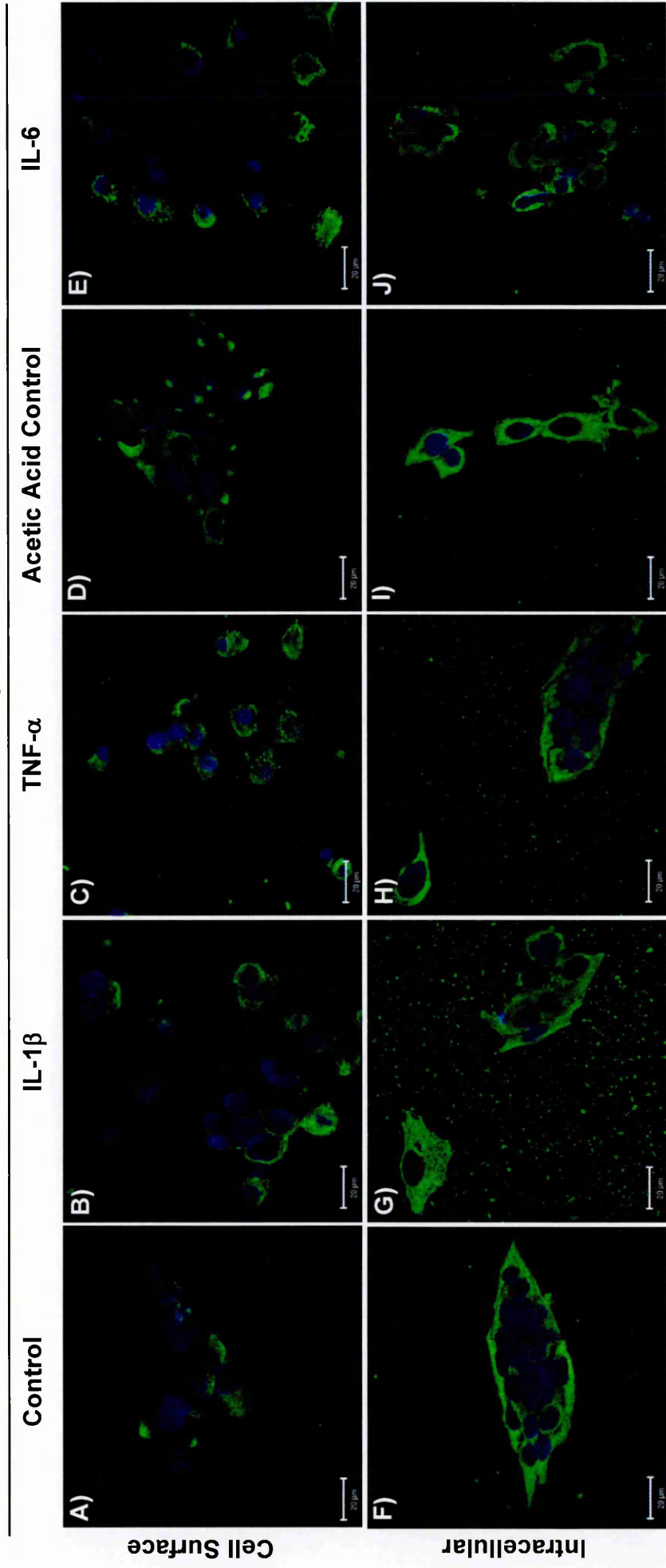


Figure 5.5: ICC examination of cell surface (4% PFA) and intracellular (-20°C acetone) ADAMTS-4 (green) under **A & F** control, **B & G** IL-1 β (100 ng/mL), **C & H** TNF- α (100 ng/mL), **D & I** acetic acid-containing control, and **E & J** IL-6 (100 ng/mL) treatments in HepG2 cells. Nuclei stained with DAPI (blue) in all images. Scale bar is 20 μ m.

ADAMTS-5 in HepG2 cells

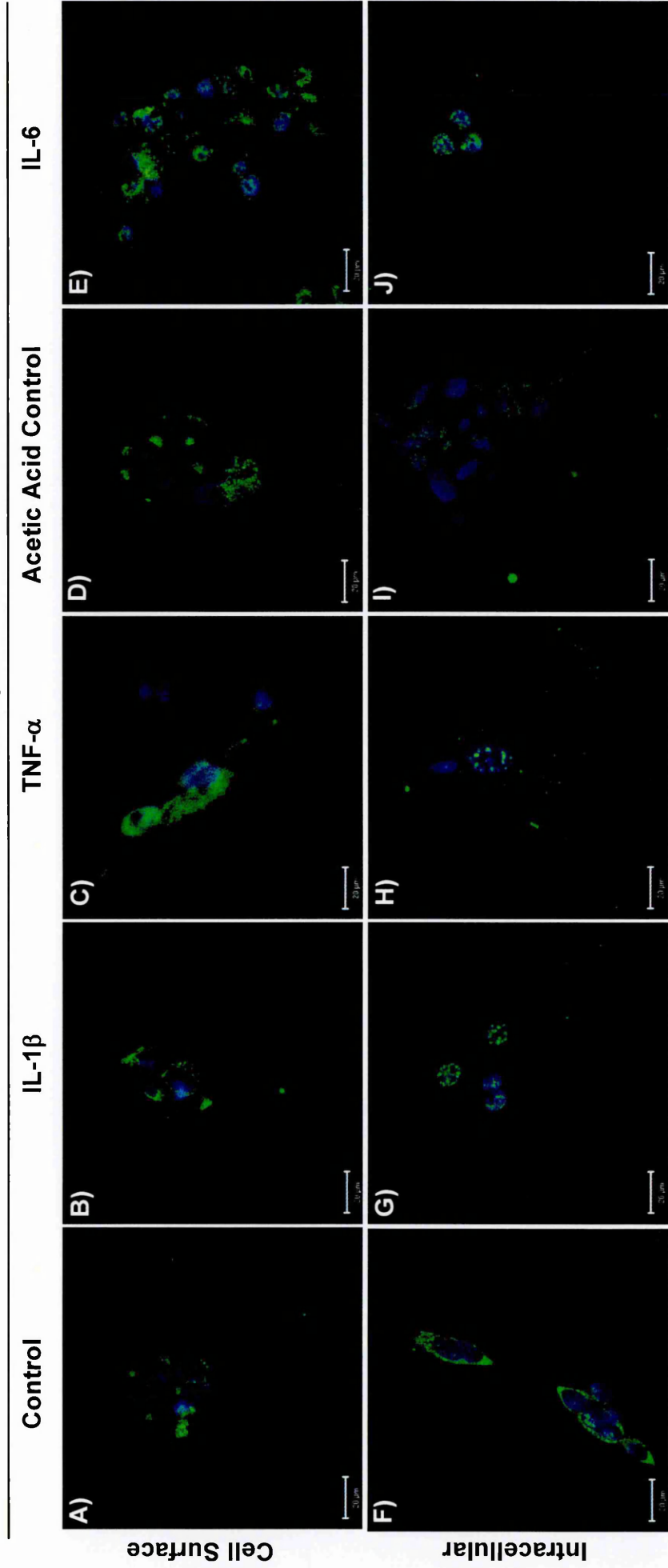


Figure 5.6: ICC examination of cell surface (4% PFA) and intracellular (-20°C acetone) ADAMTS-5 (green) under **A & F** control, **B & G** IL-1 β (100 ng/mL), **C & H** TNF- α (100 ng/mL), **D & I** acetic acid-containing control, and **E & J** IL-6 (100 ng/mL) treatments in HepG2 cells. Nuclei stained with DAPI (blue) in all images. Scale bar is 20 μ m.

TIMP3 in HepG2 cells

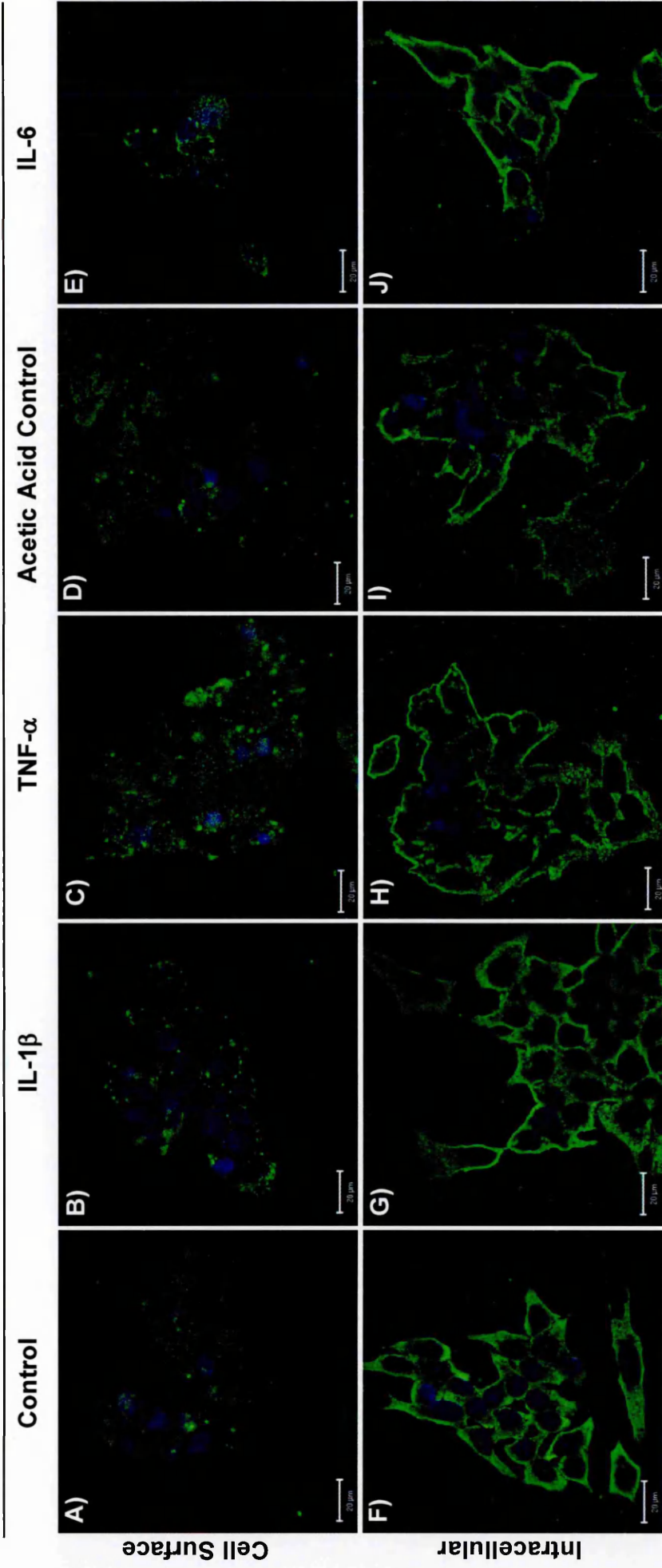


Figure 5.7: ICC examination of cell surface (4% PFA) and intracellular (-20°C acetone) TIMP3 (green) under **A & F** control, **B & G** IL-1 β (100 ng/mL), **C & H** TNF- α (100 ng/mL), **D & I** acetic acid-containing control, and **E & J** IL-6 (100 ng/mL) treatments in HepG2 cells. Nuclei stained with DAPI (blue) in all images. Scale bar is 20 μ m.

ADAM17 in HuH-7 cells

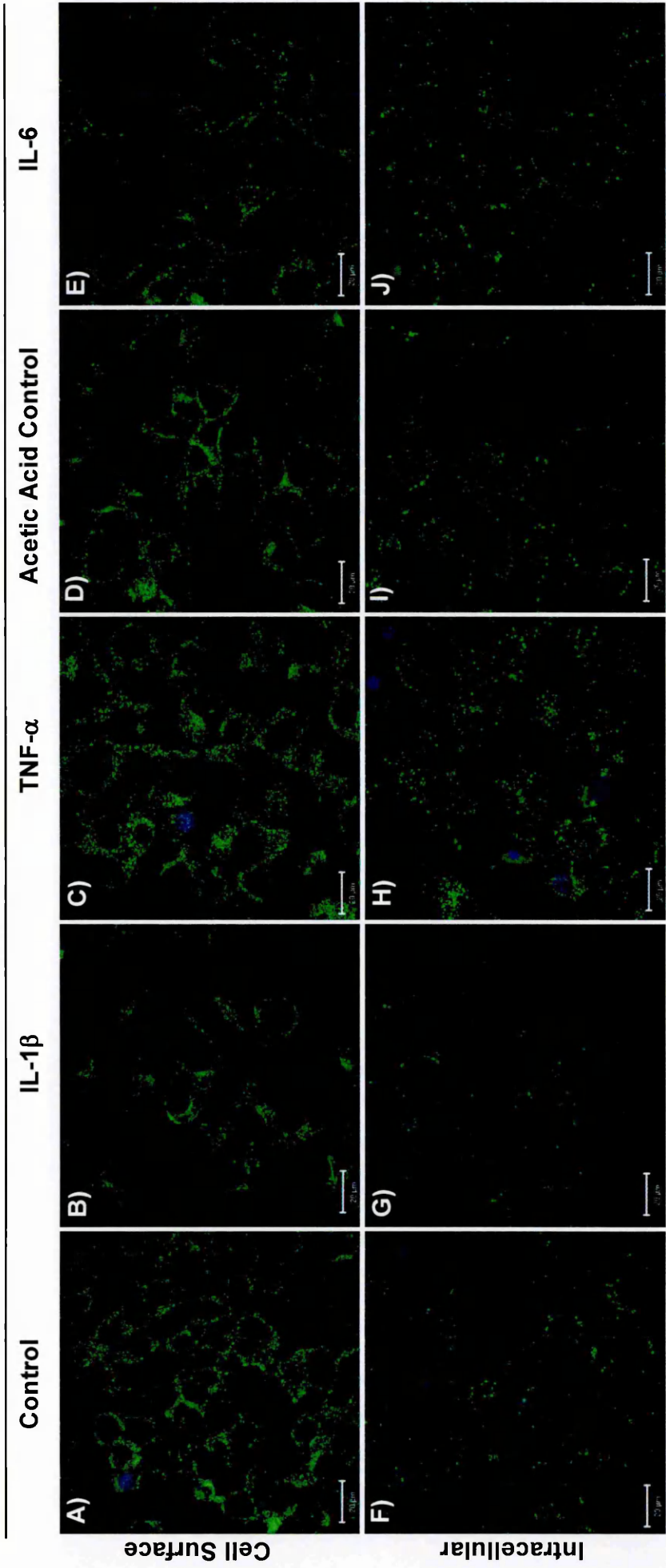


Figure 5.8: ICC examination of cell surface (4% PFA) and intracellular (-20°C acetone) ADAM17 (green) under **A & F** control, **B & G** IL-1 β (100 ng/mL), **C & H** TNF- α (100 ng/mL), **D & I** acetic acid-containing control, and **E & J** IL-6 (100 ng/mL) treatments in HuH-7 cells. Nuclei stained with DAPI (blue) in all images. Scale bar is 20 μ m.

ADAMTS-1 in HuH-7 cells

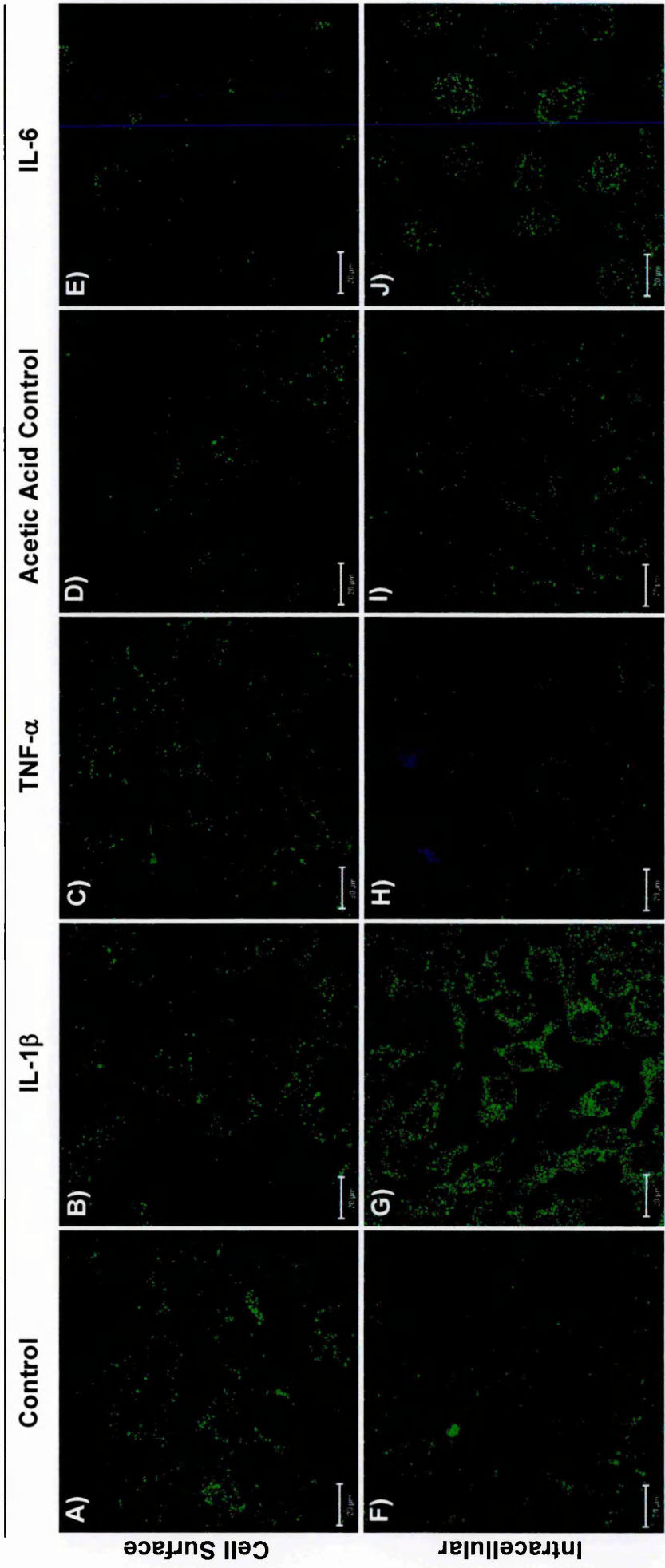


Figure 5.9: ICC examination of cell surface (4% PFA) and intracellular (-20°C acetone) ADAMTS-1 (green) under **A & F** control, **B & G** IL-1 β (100 ng/mL), **C & H** TNF- α (100 ng/mL), **D & I** acetic acid-containing control, and **E & J** IL-6 (100 ng/mL) treatments in HuH-7 cells. Nuclei stained with DAPI (blue) in all images. Scale bar is 20 μ m.

Some ADAMTS-4 was associated with the surface of some HuH-7 cells (Figure 5.10A & D), with comparable staining following cytokine treatments (Figure 5.10B, C & E). Permeabilisation of these cells revealed intense perimembrane staining of ADAMTS-4 (Figure 5.10F & I), with each cytokine treatment altering this to a diffuse cytoplasmic location (Figure 5.10G, H & J). Intracellular ADAMTS-4 was increased in some cells and decreased in others after IL-1 β and IL-6 treatments, whereas TNF- α treatment consistently increased intracellular ADAMTS-4 levels (Figure 5.10J).

Low levels of ADAMTS-5 were associated with the surface of this cell type with a punctate distribution (Figure 5.11A & D); this was unaltered by IL-6 and TNF- α treatments (Figure 5.11C & E). In contrast, ADAMTS-5 was associated with the surface of fewer HuH-7 cells following IL-1 β treatment (Figure 5.11B). Intracellular ADAMTS-5 had a diffuse cytoplasmic location (Figure 5.11F & I). IL-1 β treatment decreased the level of cytoplasmic ADAMTS-5 protein (Figure 5.11G), the opposite was true of IL-6 treatment (Figure 5.11J). TNF- α treatment of HuH-7 cells altered the distribution pattern of ADAMTS-5 such that intense perinuclear vesicles were evident (Figure 5.11H).

Minimal levels of TIMP3 with a distinct speckled pattern were associated with the cell surface of HuH-7 cells (Figure 5.12A); more TIMP3 protein was detected in the acetic acid-containing control compared to the untreated control (Figure 5.12D), with comparable levels seen in the cytokine treated samples (Figure 5.12B, C & E). Intracellular TIMP3 had a diffuse cytoplasmic location with intense granular perinuclear staining (Figure 5.12F). This perinuclear localisation is absent from the acetic acid-containing control (Figure 5.12I), and decreased following cytokine treatments (Figure 5.12G, H & J).

The LX-2 Experimental System

ADAM17 protein was located in a punctate pattern on the cell surface of LX-2 cells (Figure 5.13A & D); its expression was not altered by cytokine treatment (Figure 5.13B, C & E). Intracellular ADAM17 had a granular appearance throughout the cell cytoplasm, with possible perinuclear vesicles present (Figure 5.13F & I). Treatment with IL-1 β decreased cytoplasmic ADAM17 protein levels, but increased the intensity of the nuclear vesicles (Figure 5.13G). Conversely, IL-6 and TNF- α treatments increased the cytoplasmic level of ADAM17 (Figure 5.13H and J).

Low levels of ADAMTS-1 protein were associated with the surface of LX-2 cells with a punctate distribution (Figure 5.14A & D); cytokine treatments did not appear to alter the distribution of this protein (Figure 5.14B, C & E). Intracellular ADAMTS-1 was evident

ADAMTS-4 in HuH-7 cells

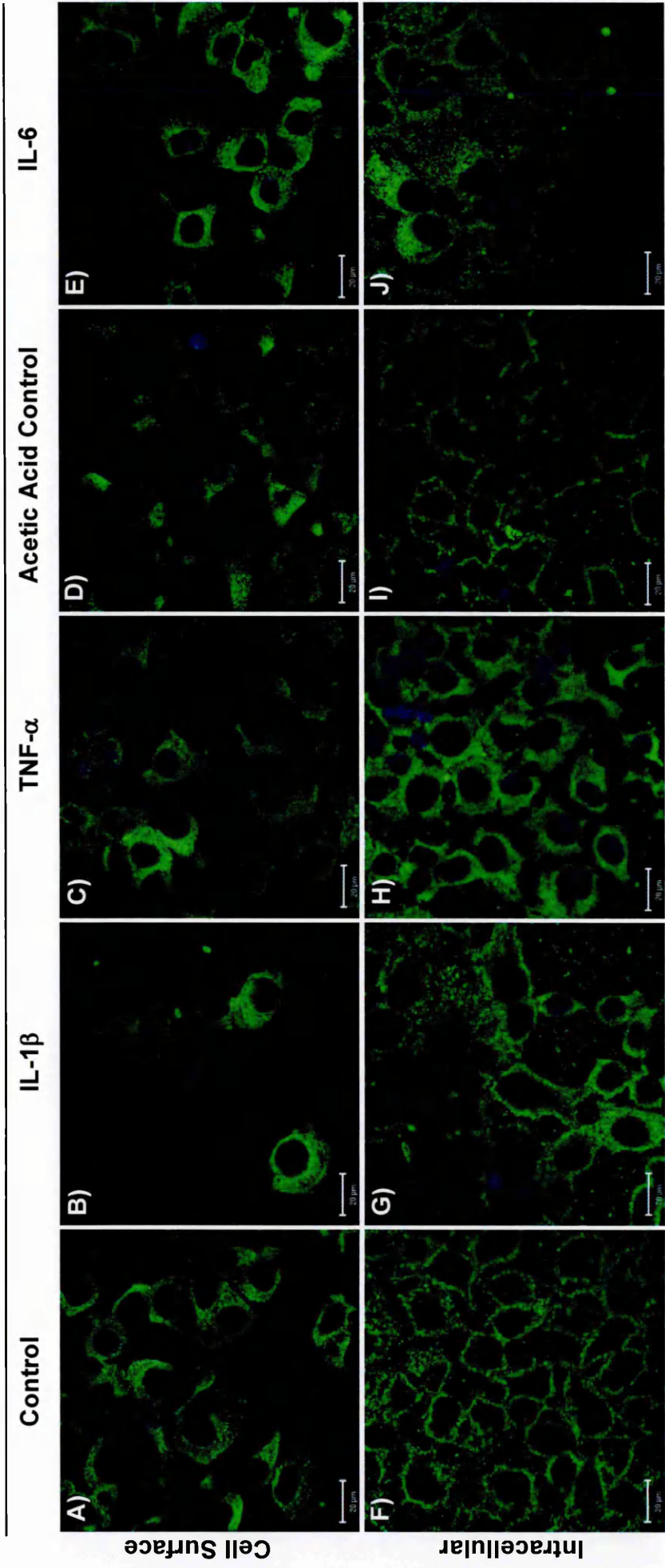


Figure 5.10: ICC examination of cell surface (4% PFA) and intracellular (-20°C acetone) ADAMTS-4 (green) under **A & F** control, **B & G** IL-1 β (100 ng/mL), **C & H** TNF- α (100 ng/mL), **D & I** acetic acid-containing control, and **E & J** IL-6 (100 ng/mL) treatments in HuH-7 cells. Nuclei stained with DAPI (blue) in all images. Scale bar is 20 μ m.

ADAMTS-5 in HuH-7 cells

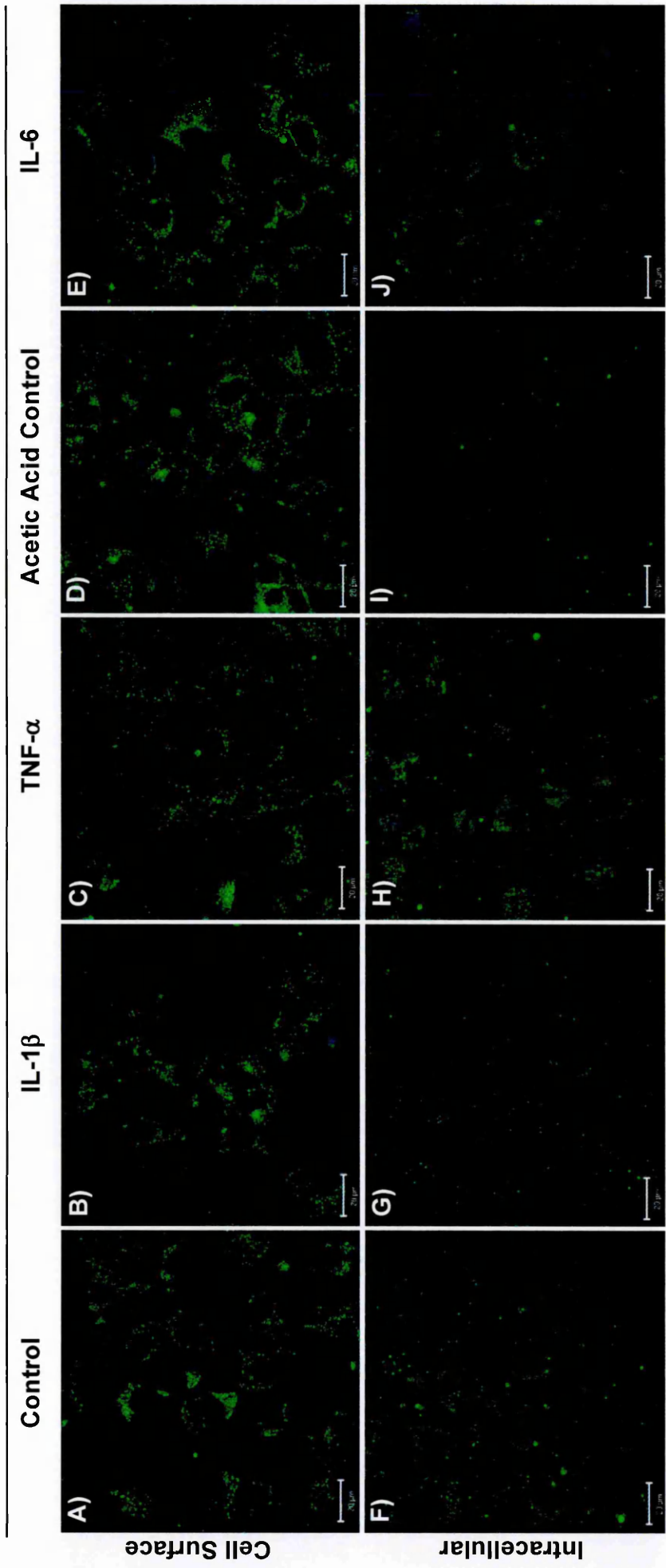


Figure 5.11: ICC examination of cell surface (4% PFA) and intracellular (-20°C acetone) ADAMTS-5 (green) under **A & F** control, **B & G** IL-1 β (100 ng/mL), **C & H** TNF- α (100 ng/mL), **D & I** acetic acid-containing control, and **E & J** IL-6 (100 ng/mL) treatments in HuH-7 cells. Nuclei stained with DAPI (blue) in all images. Scale bar is 20 μ m.

TIMP3 in HuH-7 cells

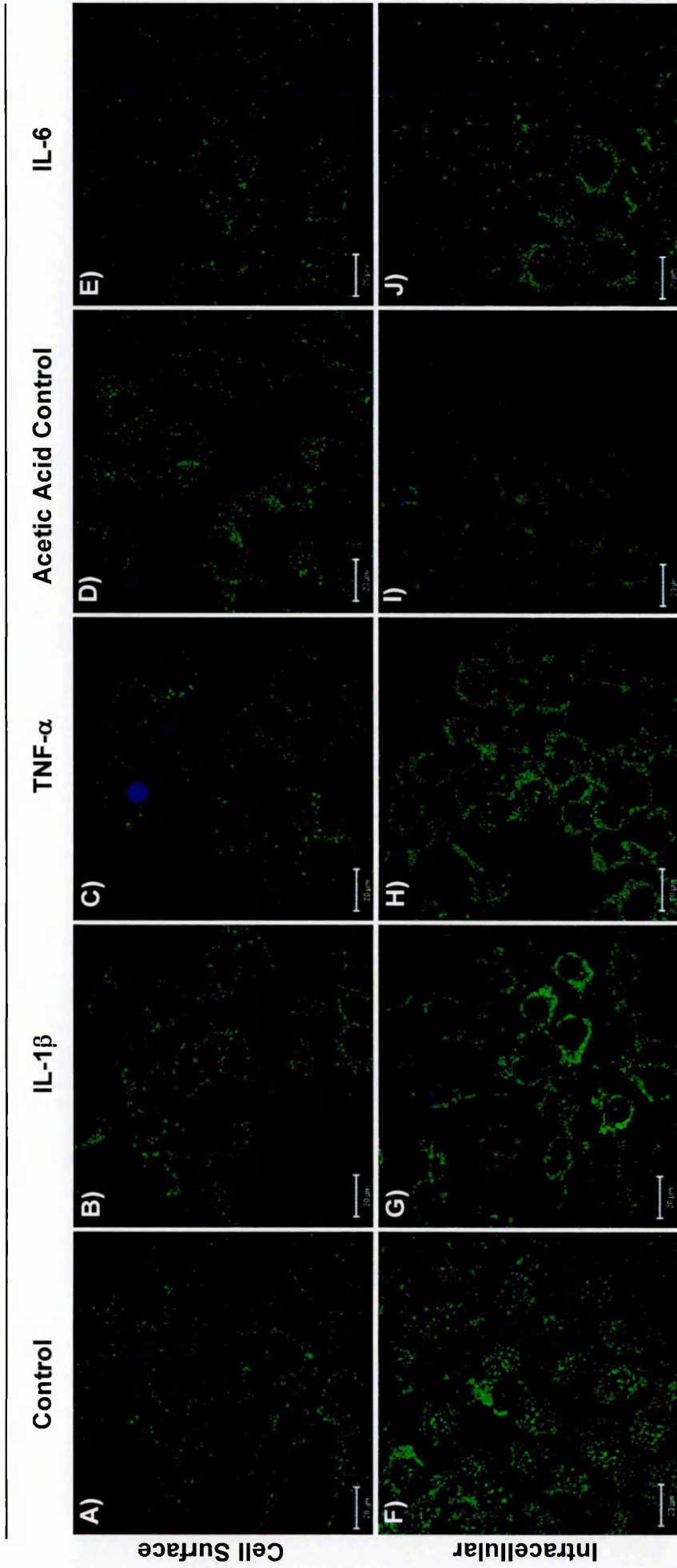


Figure 5.12: ICC examination of cell surface (4% PFA) and intracellular (-20°C acetone) TIMP3 (green) under **A & F** control, **B & G** IL-1 β (100 ng/mL), **C & H** TNF- α (100 ng/mL), **D & I** acetic acid-containing control, and **E & J** IL-6 (100 ng/mL) treatments in HuH-7 cells. Nuclei stained with DAPI (blue) in all images. Scale bar is 20 μ m.

ADAM17 in LX-2 cells

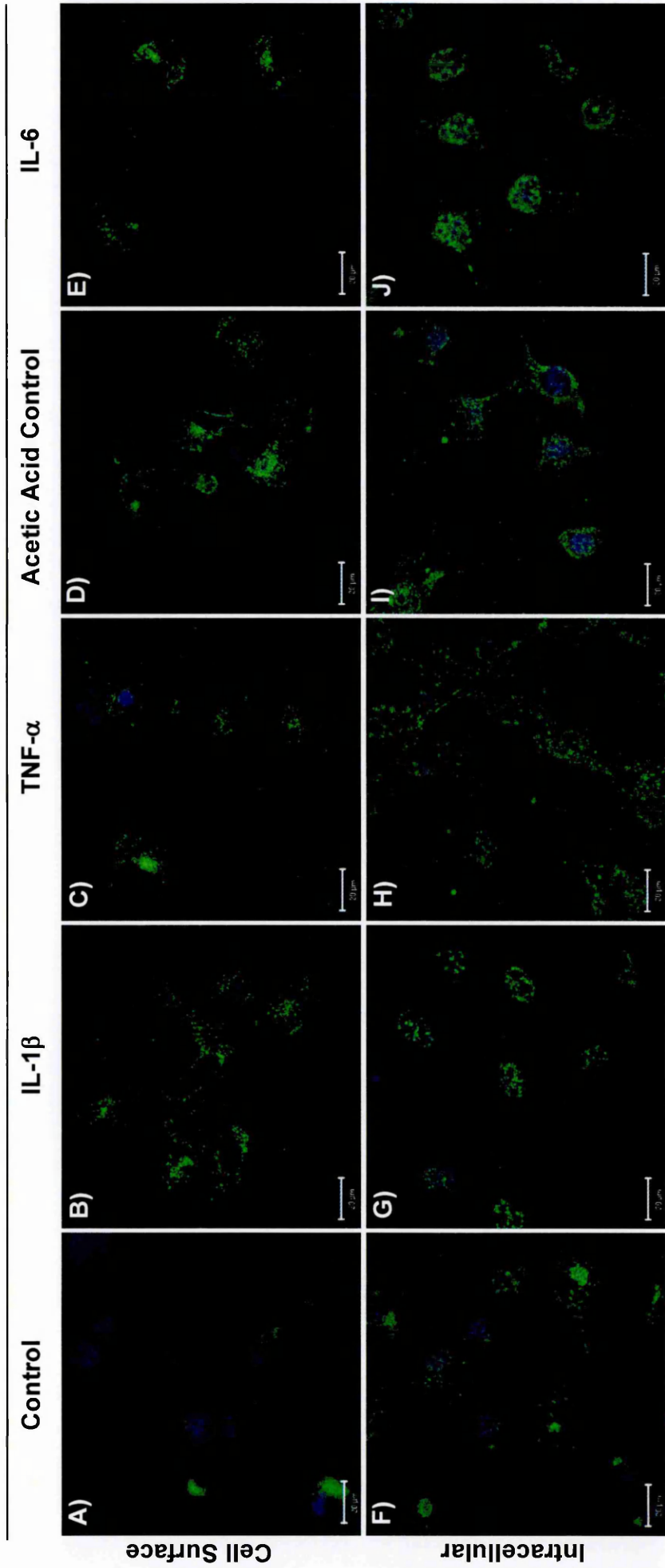


Figure 5.13: ICC examination of cell surface (4% PFA) and intracellular (-20°C acetone) ADAM17 (green) under **A & F** control, **B & G** IL-1 β (100 ng/mL), **C & H** TNF- α (100 ng/mL), **D & I** acetic acid-containing control, and **E & J** IL-6 (100 ng/mL) treatments in LX-2 cells. Nuclei stained with DAPI (blue) in all images. Scale bar is 20 μ m.

ADAMTS-1 in LX-2 cells

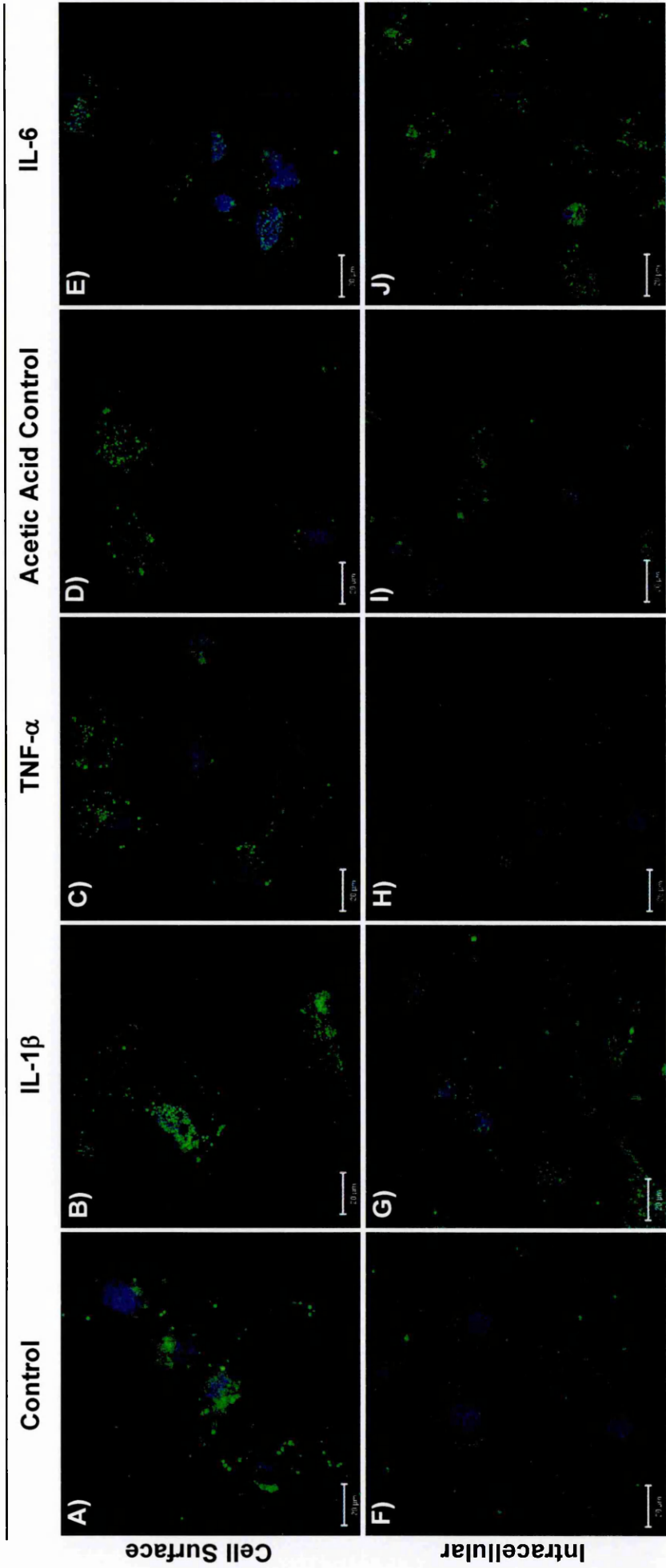


Figure 5.14: ICC examination of cell surface (4% PFA) and intracellular (-20°C acetone) ADAMTS-1 (green) under **A & F** control, **B & G** IL-1 β (100 ng/mL), **C & H** TNF- α (100 ng/mL), **D & I** acetic acid-containing control, and **E & J** IL-6 (100 ng/mL) treatments in LX-2 cells. Nuclei stained with DAPI (blue) in all images. Scale bar is 20 μ m.

uniformly throughout the cytoplasm, with some perinuclear vesicles (Figure 5.14F & I). Cytoplasmic staining was unaltered by cytokine treatments (Figure 5.14G, H & J). However increased vesicular ADAMTS-1 protein levels were evident following IL-1 β and IL-6 treatments (Figure 5.14G & J).

ADAMTS-4 protein was associated with the surface of LX-2 cells in a filamentous-like form (Figure 5.15A & D), with comparable staining after cytokine treatments (Figure 5.15B, C & E). Intracellular ADAMTS-4 protein had a diffuse cytoplasmic location (Figure 5.15F & I), which was unaltered by TNF- α and IL-6 treatments (Figure 5.15H & J) and slightly decreased after IL-1 β treatment (Figure 5.15G).

ADAMTS-5 protein had a punctate distribution across the surface of LX-2 cells (Figure 5.16A & D); this was unaltered by cytokine treatments (Figure 5.16B, C & E). ADAMTS-5 had a granular cytoplasmic location, with some speckled perinuclear staining (Figure 5.16F & I). IL-1 β treatment decreased ADAMTS-5 protein levels without altering its intracellular distribution pattern (Figure 5.16G), however TNF- α and IL-6 treated cells had increased cytoplasmic ADAMTS-5 protein (Figure 5.16H & J), with higher levels of perinuclear protein present following IL-6 treatment (Figure 5.16J).

Minimal TIMP3 protein, with a distinct speckled pattern was observed associated with the cell surface of LX-2 cells (Figure 5.17A & D); this was unaltered by the cytokine treatments (Figure 5.17B, C & E). Higher levels of intracellular TIMP3 protein were detected with a granular cytoplasmic location (Figure 5.17F & I); again it was not affected by cytokine treatments (Figure 5.17G, H & J).

5.2.3 Summary of Results

The results presented in this chapter are summarised in Table 5.1.

ADAMTS-4 in LX-2 cells

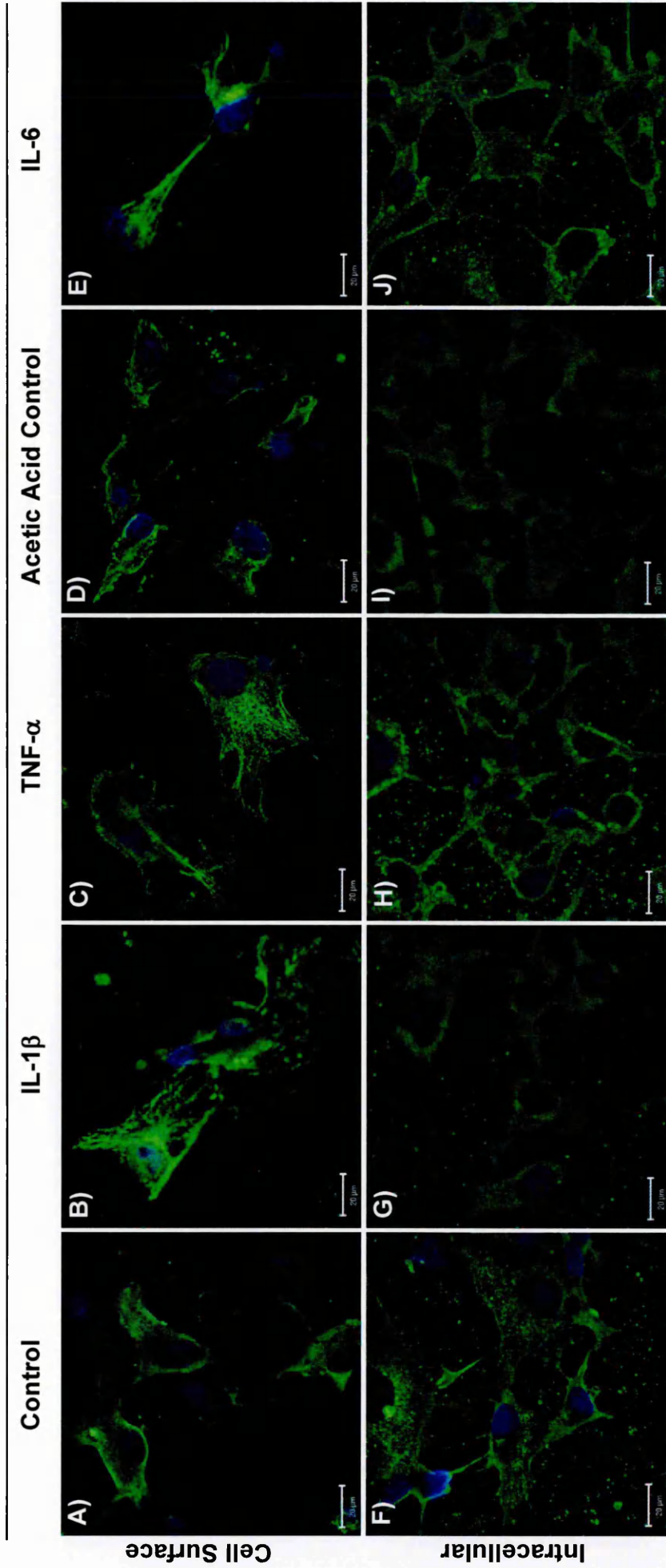


Figure 5.15: ICC examination of cell surface (4% PFA) and intracellular (-20°C acetone) ADAMTS-4 (green) under **A & F** control, **B & G** IL-1 β (100 ng/mL), **C & H** TNF- α (100 ng/mL), **D & I** acetic acid-containing control, and **E & J** IL-6 (100 ng/mL) treatments in LX-2 cells. Nuclei stained with DAPI (blue) in all images. Scale bar is 20 μ m.

ADAMTS-5 in LX-2 cells

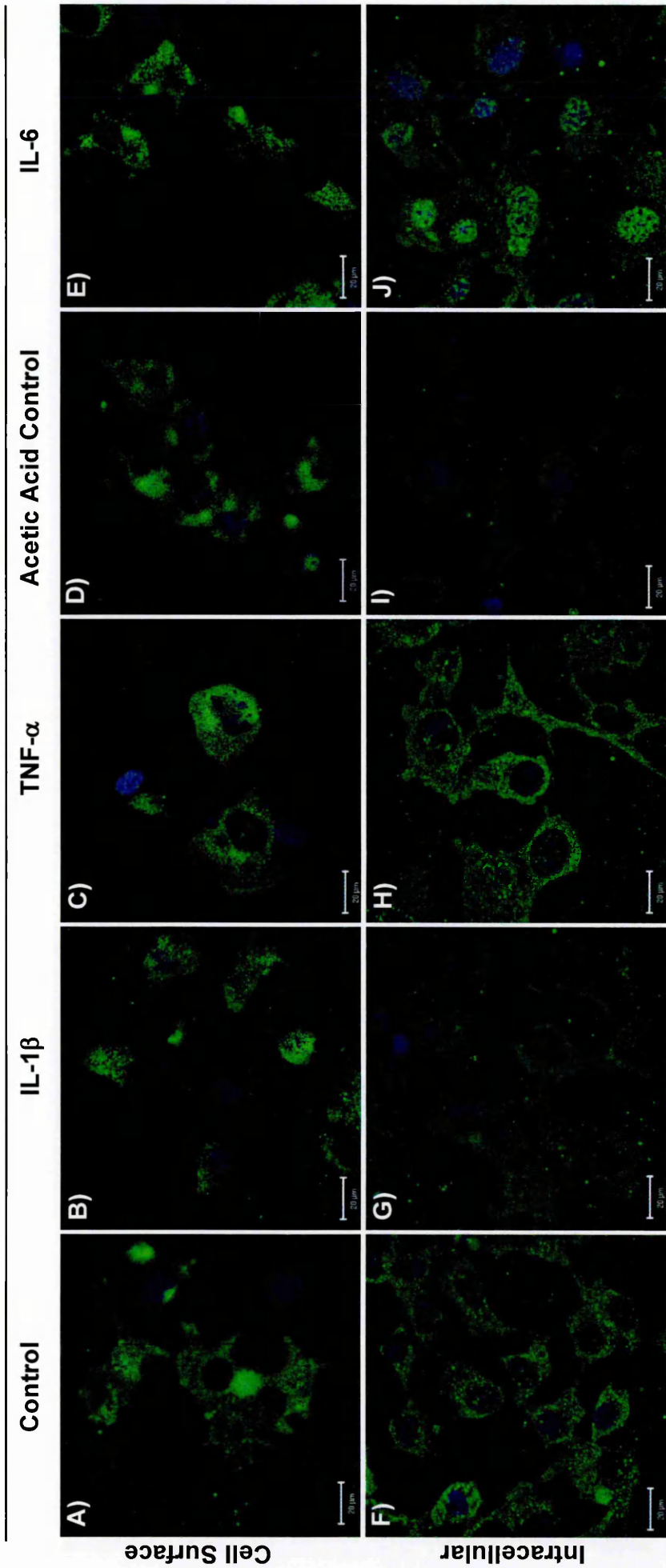


Figure 5.16: ICC examination of cell surface (4% PFA) and intracellular (-20°C acetone) ADAMTS-5 (green) under **A & F** control, **B & G** IL-1 β (100 ng/mL), **C & H** TNF- α (100 ng/mL), **D & I** acetic acid-containing control, and **E & J** IL-6 (100 ng/mL) treatments in LX-2 cells. Nuclei stained with DAPI (blue) in all images. Scale bar is 20 μ m.

TIMP3 in LX-2 cells

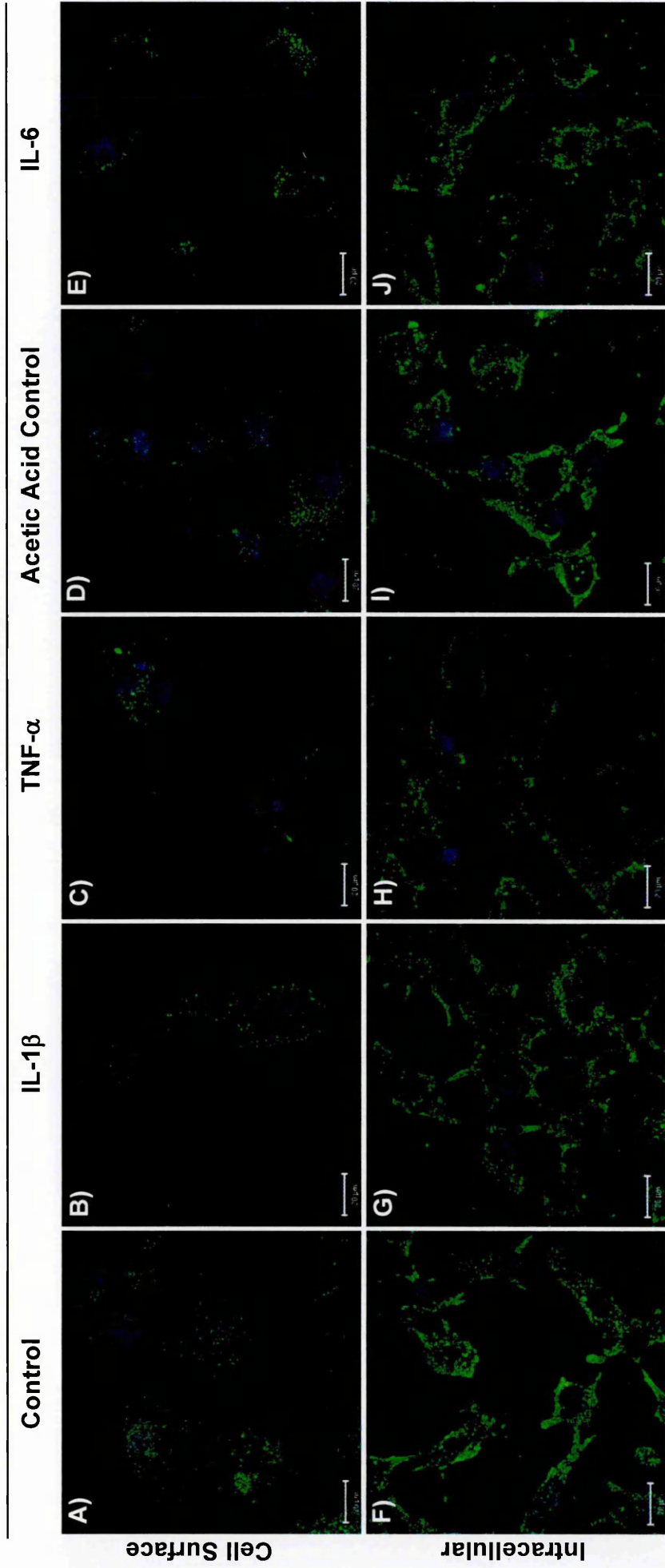


Figure 5.17: ICC examination of cell surface (4% PFA) and intracellular (-20°C acetone) TIMP3 (green) under **A & F** control, **B & G** IL-1 β (100 ng/mL), **C & H** TNF- α (100 ng/mL), **D & I** acetic acid-containing control, and **E & J** IL-6 (100 ng/mL) treatments in LX-2 cells. Nuclei stained with DAPI (blue) in all images. Scale bar is 20 μ m.

Table 5.1: Summary of protein location and modulation by cytokines as determined by ICC.

Cell Surface		Cell Lines		
		HepG2	HuH-7	LX-2
ADAM17		Punctate; ↑ by IL-6 & TNF- α	Punctate; cytokines no effect	Punctate; cytokines no effect
ADAMTS-1		Minimal punctate; ↑ by IL-6 & TNF- α	Punctate; absent from some cells after IL-6 & TNF- α	Minimal punctate; cytokines no effect
ADAMTS-4		Minimal dispersed on some cells; present on all cells after TNF- α	Minimal dispersed on some cells; cytokines no effect	Filamentous-like form; cytokines no effect
ADAMTS-5		Minimal punctate; ↑ by TNF- α	Minimal punctate; absent from some cells after IL-1 β	Punctate; cytokines no effect
TIMP3		Minimal dispersed; punctate & ↑ by IL-1 β , IL-6 & TNF- α	Minimal punctate; ↑ by IL-1 β , IL-6 & TNF- α	Minimal punctate; cytokines no effect

Table 5.1 (continued): Summary of protein location and modulation by cytokines as determined by ICC.

		Cell Lines	
		HepG2	HuH-7
Intracellular	ADAM17	Diffuse cytoplasmic with perinuclear vesicles; vesicles absent after IL-6	Granular cytoplasmic; ↓ by IL-1β
	ADAMTS-1	Diffuse cytoplasmic with perinuclear vesicles; vesicles ↑ after IL-1β, & IL-6, & absent TNF-α	Diffuse cytoplasmic with some perinuclear vesicles; ↑ by IL-1β & IL-6
	ADAMTS-4	Intense cytoplasmic; cytokines no effect	Perimembrane; diffuse cytoplasmic and ↑↓ by IL-1β & IL-6 & ↑ by TNF-α
	ADAMTS-5	Granular perimembrane; perinuclear vesicles after IL-1β, & IL-6, & TNF-α	Diffuse cytoplasmic; ↓ by IL-1β, ↑ by IL-6, perinuclear vesicles after TNF-α
	TIMP3	Diffuse cytoplasmic with ↑ at perimembrane; cytokines no effect	Diffuse cytoplasmic, perimembrane vesicles; vesicles ↓ by IL-1β, IL-6 & TNF-α
			Granular cytoplasmic with perinuclear vesicles; ↓ by IL-1β, ↑ by IL-6 & TNF-α
			Diffuse cytoplasmic with some perinuclear vesicles; vesicles ↑ by IL-1β & IL-6
			Diffuse cytoplasmic; ↓ by IL-1β
			Granular cytoplasmic; ↓ by IL-1β & ↑ by IL-6 & TNF-α
			Granular cytoplasmic; cytokines no effect

5.3 Discussion

5.3.1 *IL-1 β , IL-6 and TNF- α Differentially Modulate the Cellular Location of ADAM17, ADAMTS-1, -4, -5 and TIMP3 Proteins in Liver Cell Lines*

The objective of investigations described in this chapter was to determine whether the cellular locations of ADAM17 and ADAMTS-1, -4, -5 and TIMP3 proteins in HepG2, HuH-7 and LX-2 cells are modulated by the cytokines IL-1 β , IL-6 and TNF- α , and to determine gross qualitative changes in their level of expression as a result of exposure to these cytokines.

Following the optimisation of the ICC procedure for the detection of cell surface and intracellular ADAM17, ADAMTS-1, -4, -5 and TIMP3 proteins, it was determined that each of these proteins were expressed in HepG2, HuH-7 and LX-2 cells, and present at different levels on the cell surface and intracellularly. Furthermore their expression levels and cellular locations could be modulated by cytokine treatments.

Blanchot-Jossic, *et al* (2005) demonstrated by immunohistochemistry that ADAM17 was strongly expressed by neoplastic colon carcinomas as compared to paired normal colonic mucosa, with expression on the basolateral plasma membrane and a diffuse intracellular staining pattern. They also determined that ADAM17 was co-expressed with the active phosphorylated form of EGFR in the colon cancer cells and ECs of the stromal reaction of the tumour, suggesting a role for ADAM17 protein in tumour angiogenesis via the activation of endothelial EGFR signalling pathway.

These data show that ADAM17 protein was present on the surface of the hepatoma cell lines and to a lesser extent on LX-2 cells, with a punctate distribution observed for all cell lines; ADAM17 was increased in this location following IL-6 and TNF- α treatments in HepG2 cells. Intracellular ADAM17 was present throughout the cytoplasm of the observed liver cell lines, with vesicle-like staining evident over the nuclei of HepG2 and LX-2 cells. IL-1 β treatment decreased the abundance of cytoplasmic ADAM17 in HuH-7 and LX-2 cells; this was accompanied by an increase in the vesicular-like staining in LX-2 cells. In contrast, IL-6 treatment resulted in the elimination of vesicular ADAM17 in HepG2 cells. This may indicate that ADAM17 is packaged and stored as intracellular secretory vesicles after processing in the trans-Golgi network until an appropriate signal is received, upon which it migrates to and fuses with the cell membrane. This would effectively increase the amount of active ADAM17 present on the cell surface, and promote angiogenesis possibly by EGFR pathway activation (Blanchot-Jossic *et al*, 2005).

The cellular localisation of ADAMTS-1, -4 or -5 proteins in HCC, CRC, or normal liver tissue has not previously been examined.

ADAMTS-1 protein was associated with the cell membrane of HuH-7 and LX-2 cells with a punctate distribution; less of this protein was associated with HepG2 cells. Opposing effects of IL-1 β and IL-6 on the hepatoma cell lines were observed, such that cell surface associated ADAMTS-1 was increased on HepG2 cells and absent from some HuH-7 cells. This protein was located diffusely within the cytoplasm of all cells with some perinuclear vesicle-like staining present. In all cases IL-1 β and IL-6 increased the vesicular ADAMTS-1 protein levels; however this was not seen following TNF- α treatment of HepG2 cells. These vesicles could be secretory vesicles as observed in cells isolated from ovulating ovaries of mice (Russell *et al*, 2003).

These data could indicate that IL-1 β and IL-6 act as a signal to liver cells to form active ADAMTS-1 protein-containing secretory vesicles that could be released when an appropriate signal is received. This could act as a protective mechanism against tumour formation by increasing the amount of extracellular anti-angiogenic ADAMTS-1 protein. However, over-expression of ADAMTS-1 has been observed in some cancers, e.g. mammary and Lewis lung carcinomas, where it has an angiogenic and invasive effect, which would promote tumour growth and dissemination (Kuno *et al*, 2004; Liu *et al*, 2006b). These effects could be mediated by the promotion of heparin-binding EGF (HB-EGF) and amphiregulin shedding, and the consequent increased activation of EGFR as observed when ADAMTS-1 is over-expressed in TA₃ mammary carcinoma cells (Liu *et al*, 2006b); these events are more often associated with ADAM17 activity.

Low levels of cell surface associated ADAMTS-4 with a diffuse distribution were observed in the hepatoma cell lines, with some HepG2 cells devoid of ADAMTS-4. TNF- α treatment of HepG2 cells resulted in all cells having cell surface ADAMTS-4. In contrast, a very distinctive filamentous-like arrangement of ADAMTS-4 protein was evident on the surface of LX-2 cells, which was decreased by IL-1 β treatment. This could indicate the slight permeabilisation of these cells by PFA (4%), revealing part of the intracellular cytoskeleton.

Furthermore, intracellular ADAMTS-4 staining showed that HuH-7 cells had intense perimembrane ADAMTS-4, which was modulated by cytokine treatments to a diffuse cytoplasmic location, as seen in HepG2 and LX-2 cells. Intracellular ADAMTS-4 levels were decreased in LX-2 cells after IL-1 β cells, whereas this treatment had variable effects in HuH-7 cells, decreasing expression in some cells and increasing expression in others. This effect was also observed in HuH-7 cells after IL-6 treatment. Conversely, TNF- α treatments of HuH-7 cells consistently increased intracellular ADAMTS-4 levels.

Low levels of ADAMTS-5 were associated with the extracellular surfaces of the hepatoma cell lines, with more evident on LX-2 cells. In all cases it had a punctate

distribution. TNF- α treatment increased cell surface associated ADAMTS-5 in HepG2 cells, whilst IL-1 β decreased the number of HuH-7 cells with extracellular ADAMTS-5 associations. This down-regulation in anti-angiogenic ADAMTS-5 protein could provide a growth advantage to liver tumours, by permitting the development of neovasculature within the tumour (Sharghi-Namini *et al*, 2008).

Differential ADAMTS-5 staining patterns were observed intracellularly in the three cell lines. HepG2 cells had minimal cytoplasmic staining with intense vesicular and perimembrane staining, whereas HuH-7 cells had a diffuse cytoplasmic stain that was decreased with IL-1 β , increased with IL-6 and had vesicle formation following TNF- α treatment. Granular cytoplasmic staining was observed in LX-2 cells with some vesicles evident. TNF- α and IL-6 increased LX-2 cytoplasmic ADAMTS-5, with increased vesicle formation following IL-6 treatment.

There is increasing evidence that TIMP3 has a protective role against tumour development by the suppression of tumour growth, metastasis and angiogenesis, and the induction of tumour cell apoptosis (Darnton *et al*, 2005). In a number of human cancers, including salivary gland, renal, pancreatic endocrine tumours, uveal melanomas, oesophageal adenocarcinomas (Darnton *et al*, 2005) and oesophageal squamous cell carcinomas (Miyazaki *et al*, 2004), TIMP3 has a largely cytoplasmic location. Further to this, a reduction in TIMP3 expression has been reported in a wide range of human cancers, which has been attributed to the hyper methylation of its promoter. This hyper methylation was not seen in their corresponding normal tissue samples (Miyazaki *et al*, 2004).

Minimal TIMP3 protein was evident on the surface of the liver cell lines, but it was notably increased following each cytokine treatment in the hepatoma cell lines. Intracellular TIMP3 had a diffuse cytoplasmic location, which increased in abundance towards the perimembrane in HepG2 cells; HuH-7 cells had intense vesicular staining that was increased by cytokine treatment.

If future investigations confirm these preliminary findings, these data could suggest that liver tumour development is encouraged by increased ADAM17 protein expression, and decreased ADAMTS-1, -4, -5 and TIMP3 proteins in cellular locations associated with their active forms. These combined effects could promote tumour angiogenesis, and tumour cell invasiveness.

5.4 Summary

Preliminary data presented in this chapter demonstrate the different expression and cellular locations of ADAM17, ADAMTS-1, -4, -5 and TIMP3 in the cell lines investigated. Effects of IL-1 β , IL-6 and TNF- α on these characteristics are also described. Key findings include the increased presence of cell surface ADAM17 protein following IL-6 treatment, which may correlate with the induced absence of ADAM17-containing secretory vesicles. Furthermore, TIMP3 protein is largely absent from the surface of all the liver cell lines investigated, which could be due to its sequestration into the ECM.

Chapter 6

Assessment of ADAM17 Activity in HepG2 Cells

6.1 Introduction

This chapter describes an investigation into the *in vitro* effects of IL-1 β , IL-6 and TNF- α on the shedding of fractalkine as an indicator of ADAM17 proteolytic activity in HepG2 cells, together with a quantitative assessment of ADAM17 cellular redistribution in response to these cytokines by use of flow cytometry. Furthermore, the effect of down-regulation of ADAM17 gene expression by siRNA on fractalkine shedding was assessed.

Increased ADAM17 activity is often associated with cancer-related angiogenesis and enhanced cellular proliferation, for example by the shedding of EGFR ligands (Sahin *et al*, 2004; Itabashi *et al*, 2008). However, elevated ADAM17 levels may not correlate with increased activity if for example the protein is inactive; therefore it is important to perform activity assays. The examination of ADAM17 activity is notoriously difficult, with many commercially available assays yielding inconsistent data (personal communication, Dr. L.A. Hurst, Sheffield Hallam University, Sheffield, UK). Therefore, as fractalkine is a substrate of ADAM17 (Umehara *et al*, 2004), the assessment of its shedding from HepG2 cells (by use of a fractalkine-directed ELISA) was selected as an appropriate alternative to commercial ADAM17 activity assays. Elevated levels of this substrate have also been associated with cancer progression (Section 6.1.1), so it was of particular interest.

6.1.1 Fractalkine

Chemokines are a family of over 50 members of soluble chemotactic cytokines, divided into four classes dependent upon the number of conserved N-terminal cysteine residues: C, CC, CxC, and Cx₃C (Bazen *et al*, 1997; Efsen *et al*, 2002). Fractalkine, also known as Cx₃CL1, is the only member of the Cx₃C group of chemokines, and one of only two chemokines, the other is CxCL16, known to exist in two forms, soluble and membrane-bound (Hyakudomi *et al*, 2008). Its receptor, Cx₃CR1, is expressed on leucocytes, including monocytes, NK cells, cytotoxic T-cells (CTLs; CD8⁺ T-cells), and to a lesser extent CD4⁺ T-cells (Efsen *et al*, 2002).

Soluble fractalkine, shed from the surface of cells by ADAM17, ADAM10, MMP-2 and cathepsin S, induces the chemotactic migration of leucocytes in the same manner as conventional chemokines (Umehara *et al*, 2004; Hyakudomi *et al*, 2008; Dean & Overall, 2007; Clark *et al*, 2007). Whereas, membrane-bound fractalkine acts as an adhesion molecule, independent of integrin and selectin, facilitating the adhesion of fractalkine expressing cells and Cx₃CR1 expressing leucocytes (Umehara *et al*, 2004).

Fractalkine is an important inflammatory mediator, and is linked to a number of inflammatory diseases, including rheumatoid arthritis (Volin *et al*, 2001),

atherosclerosis (Lee *et al*, 2006) acute hepatitis (Efsen *et al*, 2002) and cancer (Hyakudomi *et al*, 2008; Ohta *et al*, 2005), with both protective and disease promoting effects.

When fractalkine is up-regulated in certain cancers, e.g. CRC and gastric adenocarcinomas, it can invoke anti-tumour responses by the recruitment of tumour infiltrating lymphocytes (TILs), comprising mainly NK cells and cytotoxic T-cells (Hyakudomi *et al*, 2008; Ohta *et al*, 2005). These cytotoxic effector cells induce target HCC cell line (HLE, HLF, HuH-7, SK-Hep1, Chang Liver & Hep3B) apoptosis via the secretion of perforin, which forms a pore in the target cell membrane through which granzyme B enters the target cell, and activates caspase 3 to initiate target cell apoptosis (Hayashida *et al*, 2000).

Generally CRC patients have impaired local and systemic immune responses, with few TILs. However, fractalkine is up-regulated by some CRCs with these tumours containing a large fraction of TILs, which correlates with a better prognosis of disease-free survival (Ohta *et al*, 2005). Similarly, fractalkine is up-regulated in gastric adenocarcinomas compared to normal gastric mucosa, which again correlates with an increased level of TILs and a better prognosis of disease-free survival than for patients with lower fractalkine expression levels (Hyakudomi *et al*, 2008).

Conversely, fractalkine can act as a mediator of pathogenic angiogenesis. For example, fractalkine present in the synovial fluid of rheumatoid arthritis patients promotes angiogenesis *in vitro* (Volin *et al*, 2001), by increasing EC proliferation, migration and tube formation in a manner similar to VEGF (Lee *et al*, 2006). Similarly, fractalkine can facilitate inflammation related angiogenesis via the activation of the G-protein coupled receptor mediated Raf-1/MEK/ERK and PI3-K/Akt/endothelial nitric oxide synthase pathways *in vivo* (Lee *et al*, 2006). This could mean that fractalkine-dependent angiogenesis is also possible in inflammation related cancers, e.g. HCC.

6.1.2 Flow Cytometry

Flow cytometry is a high-throughput technique used to analyse and quantify the physical and/or chemical properties of individual cells (Figure 6.1). It can also be used to sort cells according to these characteristics to allow further biological analysis.

Typically, a specific antigen of interest, e.g. a cell surface or intracellular protein, is targeted by a fluorochrome-conjugated antibody prior to the introduction of a cell suspension into the flow cytometer. To allow access of the labelling antibody to intracellular antigens, cells must first be fixed and permeabilised. The labelled sample is subjected to hydrodynamic focussing, where the randomly distributed cell suspension is ordered by a fluidics system into a single stream. This system consists of

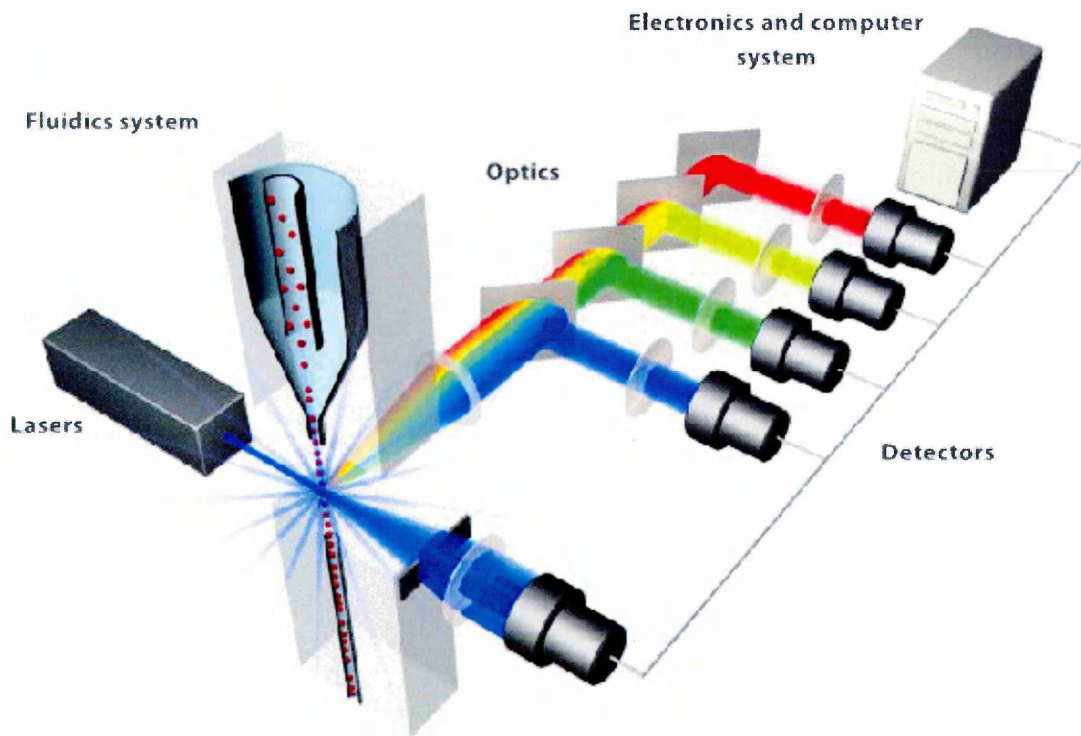


Figure 6.1: Principle of flow cytometry (Invitrogen tutorial).

The fluidic system sorts the fluorescently-labelled sample into a column of single cells (red spheres), which are passed through a laser beam (narrow blue). Light scattered in the forward direction (FSC; widest blue) is detected and converted into a voltage proportional to its intensity. Side scattered light (SSC; mid-width blue) and fluorescent light (red, yellow, green) emitted from the excited sample pass through a number of filters that function to direct light of the correct wavelength to its appropriate detector where it is also converted into voltage. These data are processed by a computer to allow the analysis and quantification of the collected data. FSC indicates cell size; SSC indicates cell granularity; fluorescence indicates abundance of a specifically labelled antigen.

a central core through which the sample is injected and an outer sheath of fast flowing fluid, which draws the sample through the narrowing central cavity creating a single column of cells or particles (Rahman *et al*, 2005).

Particles then pass through a beam from a light source, usually a laser beam, resulting in light being scattered off the particle; this scatter pattern is characteristic to each individual particle. Light scattered in the forward direction, i.e. light scattered less than 20° from the direction of the light source, also known as forward scatter channel (FSC), can be used as a measure of particle size, with a higher intensity indicative of a larger particle. FSC can therefore be used to distinguish between cellular debris, intact cells and clumps of cells. Side scatter on the other hand, i.e. light scattered at a 90° angle from the light source, also known as side scatter channel (SSC), provides information concerning the intracellular granular and structural complexity of the cell. The combination of FSC and SSC are used to differentiate between cell types in a heterogeneous sample; during data analysis specific regions on the SSC versus FSC plot can be gated to allow the selective analysis of particular cell types (Rahman *et al*, 2005).

The laser also acts to excite fluorophores on the labelled cells. Any emitted fluorescent light is channelled down the same path as side scattered light, where it is further directed through a series of filters positioned at 45° angles to ensure the correct wavelength of light is delivered to the appropriate detector, whilst other light is deflected. These filters are described as “long pass”, “short pass”, or “band pass”, and allow light >500 nm, <560 nm, or of a specified narrow range of wavelengths to pass through respectively. Histogram plots of the fluorescent data can then be used to display the number of immunopositive cells within the sample (Rahman *et al*, 2005).

In all incidences the detectors convert detected light into voltage proportional to the intensity of the detected light. The voltage is then converted into a numerical value used for data quantification.

Suitable control samples must be used in this technique to distinguish between non-specific background fluorescence and specific primary antibody fluorescence. Typically an isotype control antibody, i.e. an antibody that is species and isotype matched to the primary antibody, is used for this purpose in flow cytometry.

6.1.3 RNA interference (RNAi)

RNAi is an evolutionally conserved phenomenon in eukaryotes, which represents a unique form of post-transcriptional gene silencing. Exploitation of this naturally occurring process has allowed researchers to more clearly understand the roles of individual proteins.

The RNAi pathway (Figure 6.2) is triggered by dsRNA molecules which are processed by an RNase-III like enzyme (Dicer), to generate short interfering RNA duplexes. Alternatively chemically synthesised siRNA can be used to trigger the pathway. siRNA is incorporated into an RNA-induced silencing complex (RISC), which then probes the target mRNA for complementary sequences. When it finds this, RISC mediates mRNA cleavage, and consequently silencing of gene expression (Boese, 2004).

To ensure accurate interpretation of experimental data it is crucial to employ several critical controls. Without these, non-specific effects of the transfection procedure itself or siRNA-indirect gene knockdown may lead to data misinterpretation. Firstly, a baseline reference of untreated controls must be used to allow the comparison and normalisation of all other samples.

Secondly, a positive silencing control should be used to check RNAi functionality in a particular experimental system. Typically a validated siRNA targeting an endogenous housekeeping gene, such as GAPDH or cyclophilin B, is used. GAPDH was selected for the HepG2 experimental system, as this siRNA typically reduces GAPDH gene expression by 91% when measured at the mRNA level 24 hours after transfection under optimal conditions (Boese, 2004).

Finally, a negative silencing control should be used to highlight off-target effects caused by the activation of the RNAi pathway. Mock transfections where lipid transfection reagent is applied to cells in the absence of siRNA could be performed to ensure cellular function is not disrupted by the lipid transfection reagent. However, a more biologically relevant control is transfection with either functional, non-targeting siRNA or non-functional, non-targeting siRNA together with lipid transfection reagent.

6.1.4 Specific Objectives

- To determine the effect of IL-1 β , IL-6 and TNF- α treatments on the shedding of fractalkine from the surface of HepG2 cells.
- To optimise the method of HepG2 cell detachment for the analysis of ADAM17 by flow cytometry.
- To establish whether IL-1 β , IL-6 and TNF- α treatments alter the cellular location of ADAM17 in HepG2 cells.
- To optimise the method of ADAM17 gene silencing by siRNA, and determine siRNA transfection efficiency.
- To demonstrate effective ADAM17 gene and protein silencing in HepG2 cells.
- To determine the effect of ADAM17 silencing on HepG2 cell proliferation.
- To determine the effect of ADAM17 silencing on the shedding of fractalkine from the surface of HepG2 cells.

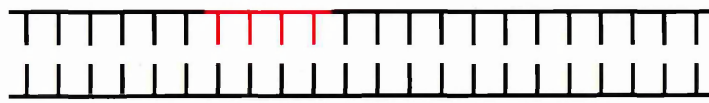
Figure 6.2: The RNAi pathway (Adapted from Boese, 2004).

The RNAi pathway is initiated in the cytoplasm of host cells by long dsRNA molecules or small hairpin RNA (shRNA) molecules that have sequence-specific homology for a “target” mRNA. Similarly, non-coding microRNAs (miRNAs) synthesised in the nucleus can be processed by Drosha into pre-miRNAs (~70mers) and exported into the cytoplasm where they too can trigger RNAi.

These RNA molecules are processed in the cytoplasm by the ATP-dependent RNase-III-like enzyme Dicer, to generate short interfering RNA (siRNA) duplexes, the mediators of RNAi. Alternatively, chemically synthesised siRNAs can be used to trigger RNAi. siRNA is incorporated into an RNA-induced silencing complex (RISC), which activates the ATP-dependent helicase activity of RISC to unwind the siRNA duplex.

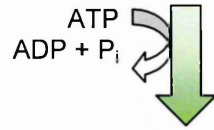
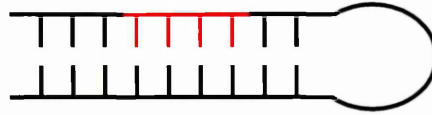
The siRNA-RISC then probes the target mRNA for complementary sequences, and when high sequence complementarity is found, RISC mediates site-specific mRNA cleavage, and consequently gene silencing. The siRNA-RISC is released and recycled following mRNA cleavage to further deplete the target mRNA pool. However, when sequence complementarity is lower, gene silencing occurs by translation repression, where the siRNA-RISC does not cleave the target mRNA, but remains bound to it; this halts the progression of mRNA translation to protein. The siRNA-RISC is not available for further target probing when gene silencing occurs by this method.

Long dsRNA
(>30-50 bp)



OR

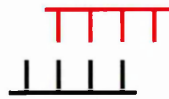
miRNA or
shRNA



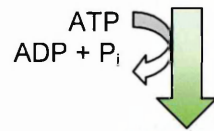
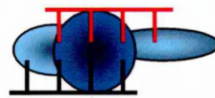
RNA processing by
Dicer



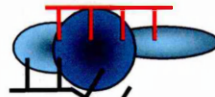
21-23 nt siRNAs



siRNA - RISC
complex formation



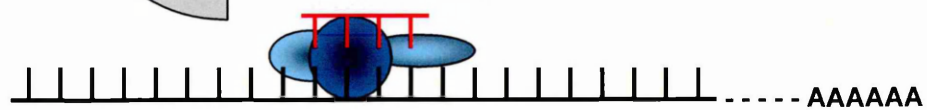
RISC activation



RISC siRNA
recycling



mRNA recognition



mRNA cleavage



6.2 Results

6.2.1 Fractalkine Shedding from HepG2 Cells

To determine the effect of cytokine treatment on the shedding of fractalkine from the surface of HepG2 cells, 1, 10 or 100 ng/mL of IL-1 β , IL-6 or TNF- α was applied to the cells for 24 or 48 hours. The supernatant was collected and an ELISA directed against fractalkine was used to quantify the amount of shed fractalkine (Section 2.6). No optimisation of this technique was required. These treatments are known to influence the proliferative capacity of HepG2 cells (Figure 3.2); therefore the amount of soluble fractalkine was expressed per mg of protein. Supernatants from IL-1 β and TNF- α treated cells were compared to supernatants from untreated control samples, whereas supernatants from IL-6 treated cells were compared to supernatants from acetic acid-containing control samples.

At the 24 hour time point approximately 35.6 ng fractalkine/mg protein was shed from untreated HepG2 cells (Figure 6.3A). IL-1 β treatment significantly increased the amount of fractalkine shed from HepG2 cells following 10 and 100 ng/mL of treatment (145.9 & 142.9 ng fractalkine/mg protein respectively; both $P=0.0001$). A concentration dependent increase in shed fractalkine was also seen after TNF- α treatment, reaching significance with 10 and 100 ng/mL (82.4 & 113.4 ng fractalkine/mg protein; $P=0.001$ & 0.0001 respectively). IL-6 treatment did not affect fractalkine shedding relative to its acetic acid-containing control. However, fractalkine was shed at a higher level in the acetic acid-containing control compared to the untreated control (99.3 ng fractalkine/mg protein; $P=0.001$).

These trends in shed fractalkine levels were paralleled after 48 hours of treatment (Figure 6.3B), albeit with higher levels of fractalkine shed. HepG2 cells shed 90.9 ng fractalkine/mg protein under control conditions; this was significantly increased following 1, 10 and 100 ng/mL of IL-1 β (171.8, 203.6 & 212.7 ng fractalkine/mg protein; $P=0.005$, 0.001 & 0.0001 respectively). Similarly, TNF- α treatment caused significant increases in the amount of fractalkine shed from HepG2 cells with 1, 10 and 100 ng/mL (124.8, 172.8 & 205.6 ng fractalkine/mg protein; $P=0.046$, 0.005 & 0.001 respectively). No significant changes were observed following 48 hours of IL-6 treatment, and fractalkine shedding in the untreated and acetic acid-containing controls were comparable.

ICC analysis (Section 2.5) was then performed on HepG2 cells after 24 hours of treatment with 100 ng/mL of IL-1 β , IL-6 or TNF- α to determine whether the cellular location of fractalkine was redistributed in response to cytokine treatment as compared

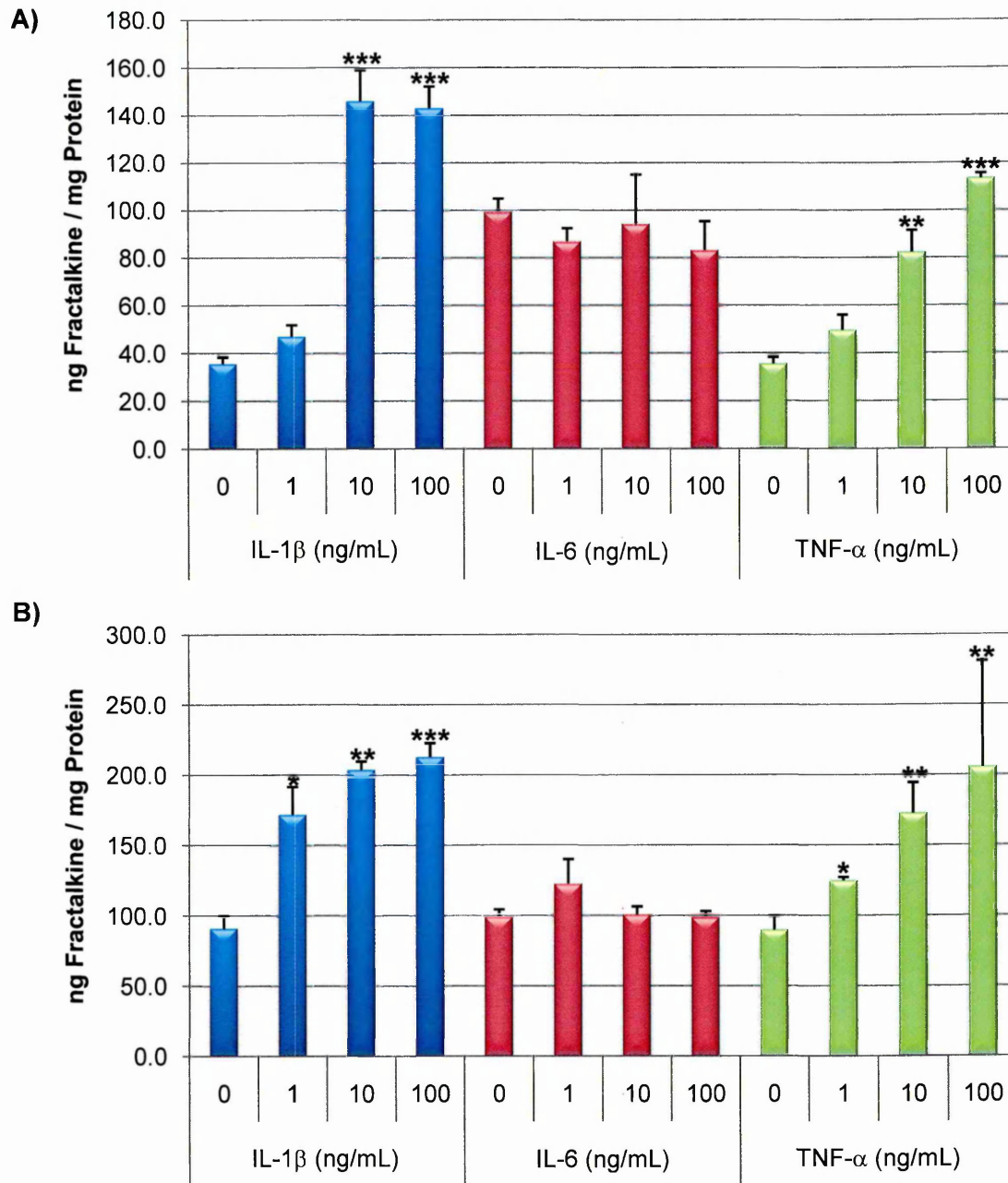


Figure 6.3: Amount of fractalkine (ng) per mg of protein shed from the surface of HepG2 cells into the supernatant following cytokine treatment for **A)** 24 hours and **B)** 48 hours with varying concentrations of IL-1 β , IL-6 or TNF- α . Data presented as mean \pm SEM. Significant difference from control, * P<0.05, ** P<0.01, ***P<0.001 (ANOVA with Dunnett's test; n=3).

to an appropriate control (Figure 6.4). This cytokine concentration was selected as it caused the most extreme alterations in fractalkine shedding in this cell line.

Each cytokine treatment was only performed once, and should therefore be regarded as preliminary data. IL-1 β and TNF- α treated cells were compared to an untreated control sample, whereas IL-6 treated cells were compared to an acetic acid-containing control sample. Details of the optimisation of the ICC technique are in Section 5.2.1.

Fractalkine protein was distributed evenly across the cell surface of HepG2 cells (Figure 6.4A); its expression was increased in the acetic acid-containing control (Figure 6.4D), and to a comparable level following each cytokine treatment (Figure 6.4B, C & E). In addition, fractalkine was situated diffusely within the cell cytoplasm (Figure 6.4F & I), cytokine treatments did not alter intracellular levels or distribution of fractalkine (Figure 6.4G, H & J). The negative control for each experiment demonstrated only the DAPI stained nuclei of the cells, with no non-specific staining caused by the secondary antibody (Figure 6.4K & L).

6.2.2 Flow Cytometry Optimisation

Optimisation of the sample preparation procedure prior to flow cytometric analysis is essential in obtaining accurately quantified data. A previously described flow cytometry sample preparation protocol (personal communication, Dr. S.L. Haywood-Small, Sheffield Hallam University, Sheffield, UK) was adapted to incorporate the optimum conditions for ADAM17 fluorescein-conjugate staining of HepG2 cells determined by the manufacturer (Section 2.7).

Three methods of HepG2 cell dissociation were tested for their suitability in cell surface ADAM17 detection; these were 0.02% EDTA solution (E8008, Sigma-Aldrich), non-enzymatic cell dissociation solution (C5914, Sigma-Aldrich), and manual cell scraping plus DPBS. A 0.05% trypsin-EDTA solution was not tested as it can cleave proteins and may therefore influence the results. Each method yielded a single cell suspension suitable for flow cytometry analysis. Appropriate light detectors were set to voltages capable of detecting forward and side scattered light and emitted fluorescence from fluorescein and propidium iodide.

Test samples (isotype control and ADAM17 antibody labelled samples, dual labelled with propidium iodide) were analysed and their fluorescence indices (FI) calculated (Figure 6.5A). The largest shift in fluorescence (FI=2) was observed in cells lifted from the substratum using non-enzymatic cell dissociation solution, hence this dissociation method was selected for cell surface antigen detection. Cell dissociation by 0.02% EDTA solution gave the lowest FI (1.4).

Fractalkine in HepG2 cells

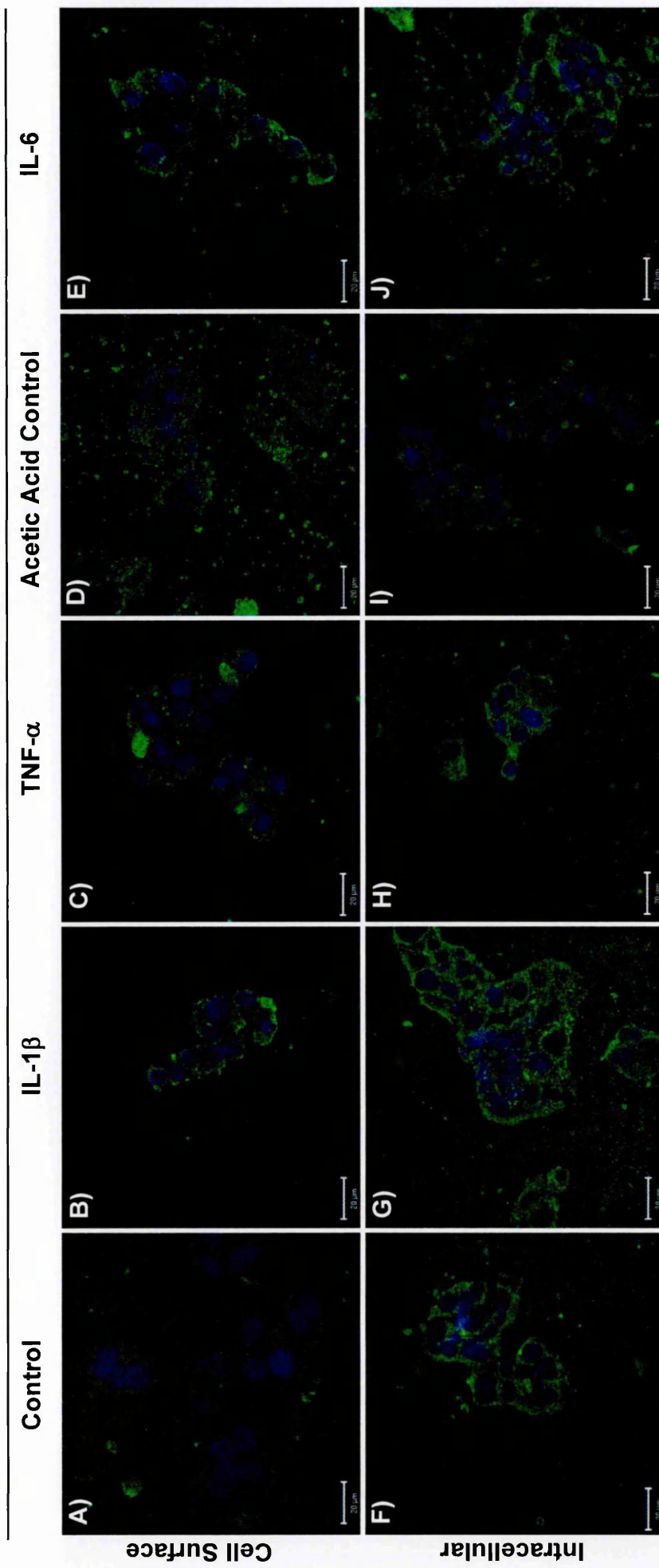


Figure 6.4: ICC examination of cell surface (4% PFA) and intracellular (-20°C acetone) fractalkine (green) under **A & F** control, **B & G** IL-1 β (100 ng/mL), **C & H** TNF- α (100 ng/mL), **D & I** acetic acid-containing control, and **E & J** IL-6 (100 ng/mL) treatments in HepG2 cells. Nuclei stained with DAPI (blue) in all images. Scale bar is 20 μ m.

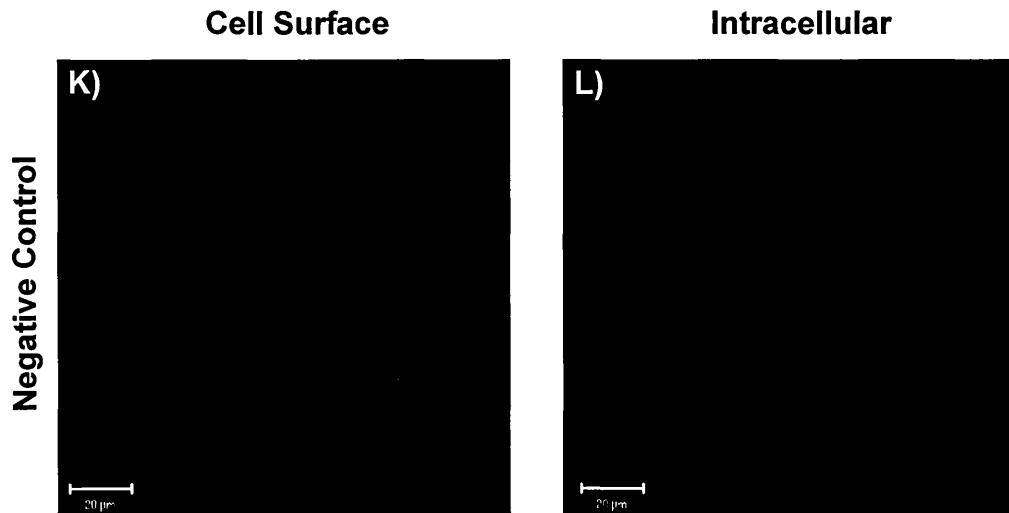


Figure 6.4 (continued): K) Cell surface (4% PFA) and L) intracellular (-20°C acetone) negative controls for the ICC examination of cell surface and intracellular fractalkine in HepG2 cells. Nuclei stained with DAPI (blue) in all images. Scale bar is 20 μm.

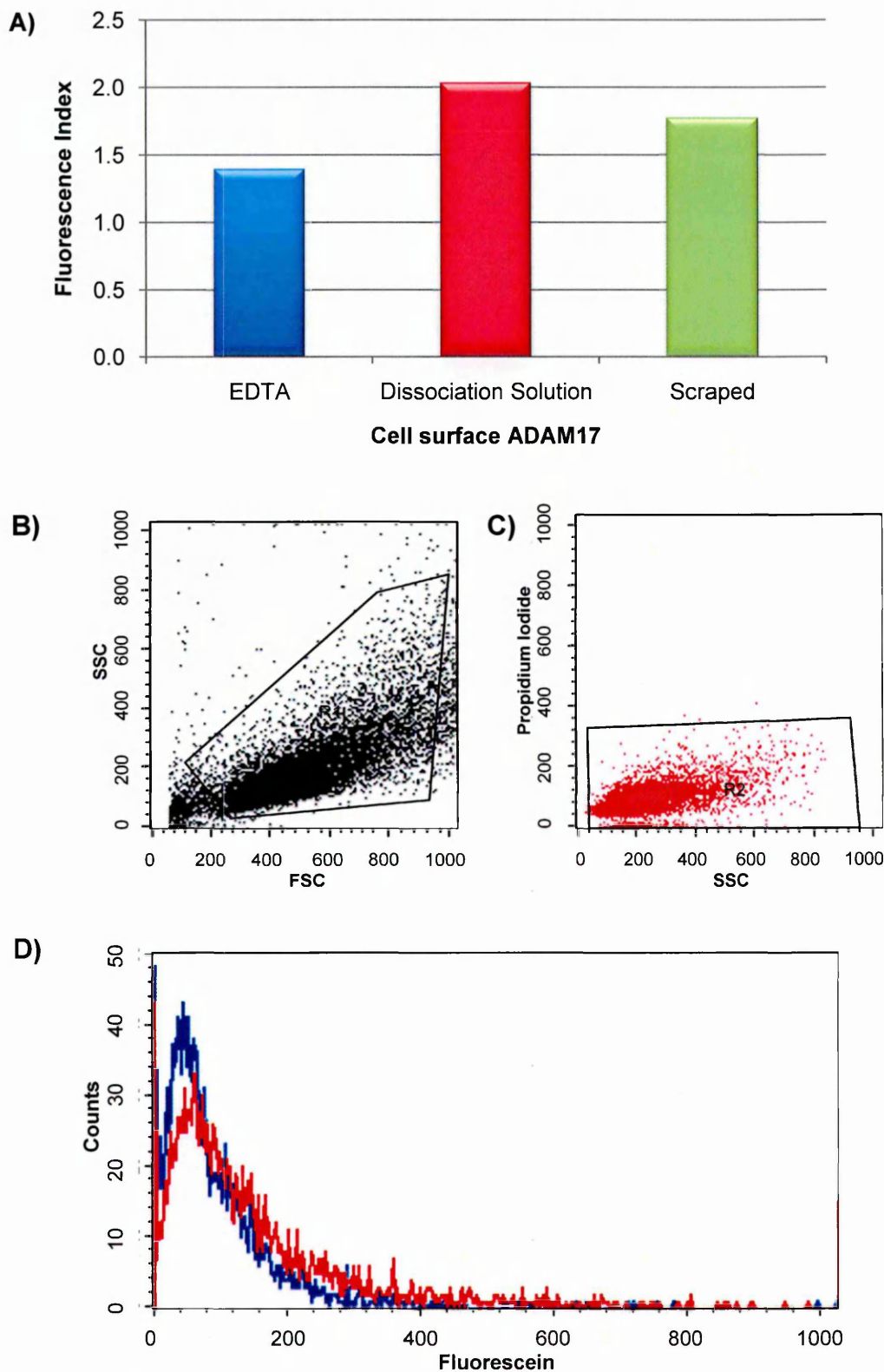


Figure 6.5: **A)** Fluorescence indices from different HepG2 cell dissociation methods for the detection of cell surface ADAM17 by flow cytometry (n=1). Representative plots of **B)** gated intact and **C)** gated viable HepG2 cells, and **D)** the fluorescence shift from isotype control labelled cells (blue) to ADAM17 labelled cells (red) prepared for cell surface antigen detection (linear fluorescence scale).

During the analysis of the flow cytometry data, intact cells were gated on the FSC versus SSC plot (Figure 6.5B) to ensure fluorescence data was only analysed from these intact cells and not cellular debris (lower left hand corner of plot) or cell clumps (far right hand side of plot). Similarly, viable cells, indicated by propidium iodide, were gated to ensure only data collected on viable cells was analysed (Figure 6.5C).

Four cell dissociation methods were tested for their suitability in intracellular ADAM17 detection; these were 0.02% EDTA solution, non-enzymatic cell dissociation solution, manual cell scraping plus DPBS, and 1% PFA fixation followed by manual cell scraping. Following cell dissociation, cells were fixed and permeabilised using the IntraSure kit according to the manufacturers' protocol, prior to antigen labelling. A final fixation step preceded flow cytometric analysis. Again the light detector voltage settings were adjusted to detect forward and side scattered light and emitted fluorescein fluorescence using a combination of unlabelled and isotype control labelled samples; due to the fixation steps during sample preparation, cells were not viable and so propidium iodide was not used.

Test samples (isotype control and ADAM17 antibody labelled samples) were analysed and their FIs calculated (Figure 6.6A). As for cell surface ADAM17 detection, non-enzymatic cell dissociation solution had the highest shift in fluorescence (FI=1.49), so this method was selected for intracellular antigen detection. Cell dissociation by 0.02% EDTA solution had a negative shift in fluorescence (FI=0.9), indicating a high level of background staining with the isotype control and no positive signal from the ADAM17 antibody. Intact cells were gated on the FSC versus SSC plot (Figure 6.6B) to ensure only fluorescence data from these cells was analysed.

6.2.3 Modulation of ADAM17 Cellular Location by IL-1 β , IL-6 and TNF- α in HepG2 Cells

Cells were treated with 100 ng/mL of IL-1 β , IL-6 or TNF- α for 24 hours, after which flow cytometry was performed to quantify the influence of these treatments on the cellular location of ADAM17 (Section 2.7). Three independent experiments were performed to confirm the trends found. IL-1 β and TNF- α treated cells were compared to an untreated control, whereas IL-6 treated samples were compared to an acetic acid-containing control sample.

These data indicate that more ADAM17 protein is expressed intracellularly than on the surface of HepG2 cells, evident by the higher FIs obtained following intracellular antigen detection (Figure 6.7). This correlates with ICC data for this protein (Figure 5.3).

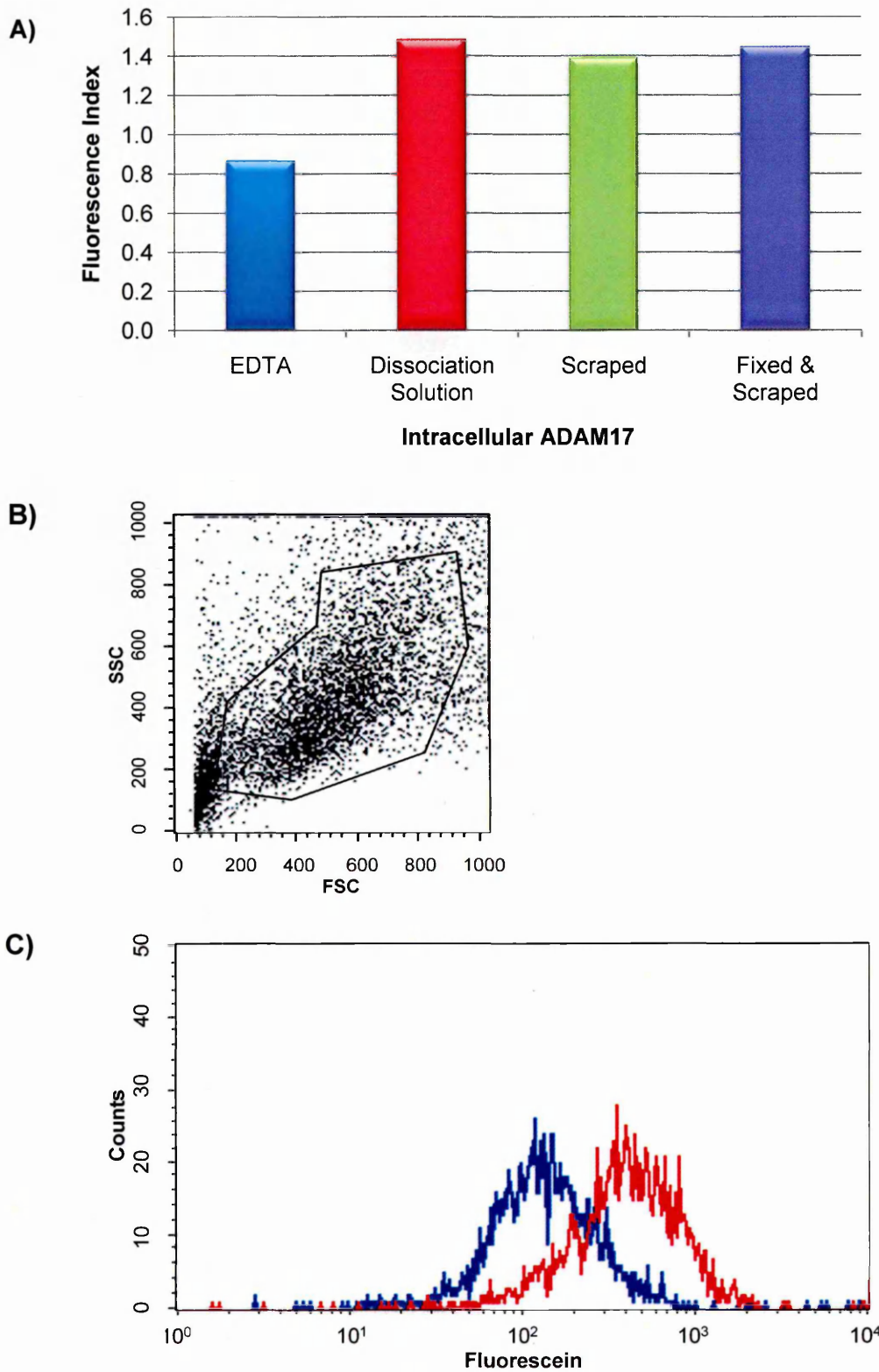


Figure 6.6: **A)** Fluorescence indices from different HepG2 cell dissociation methods for the detection of intracellular ADAM17 by flow cytometry (n=1). Representative plots of **B)** gated intact HepG2 cells, and **C)** the fluorescence shift from isotype control labelled cells (blue) to ADAM17 labelled cells (red) prepared for intracellular antigen detection (logarithmic fluorescence scale).

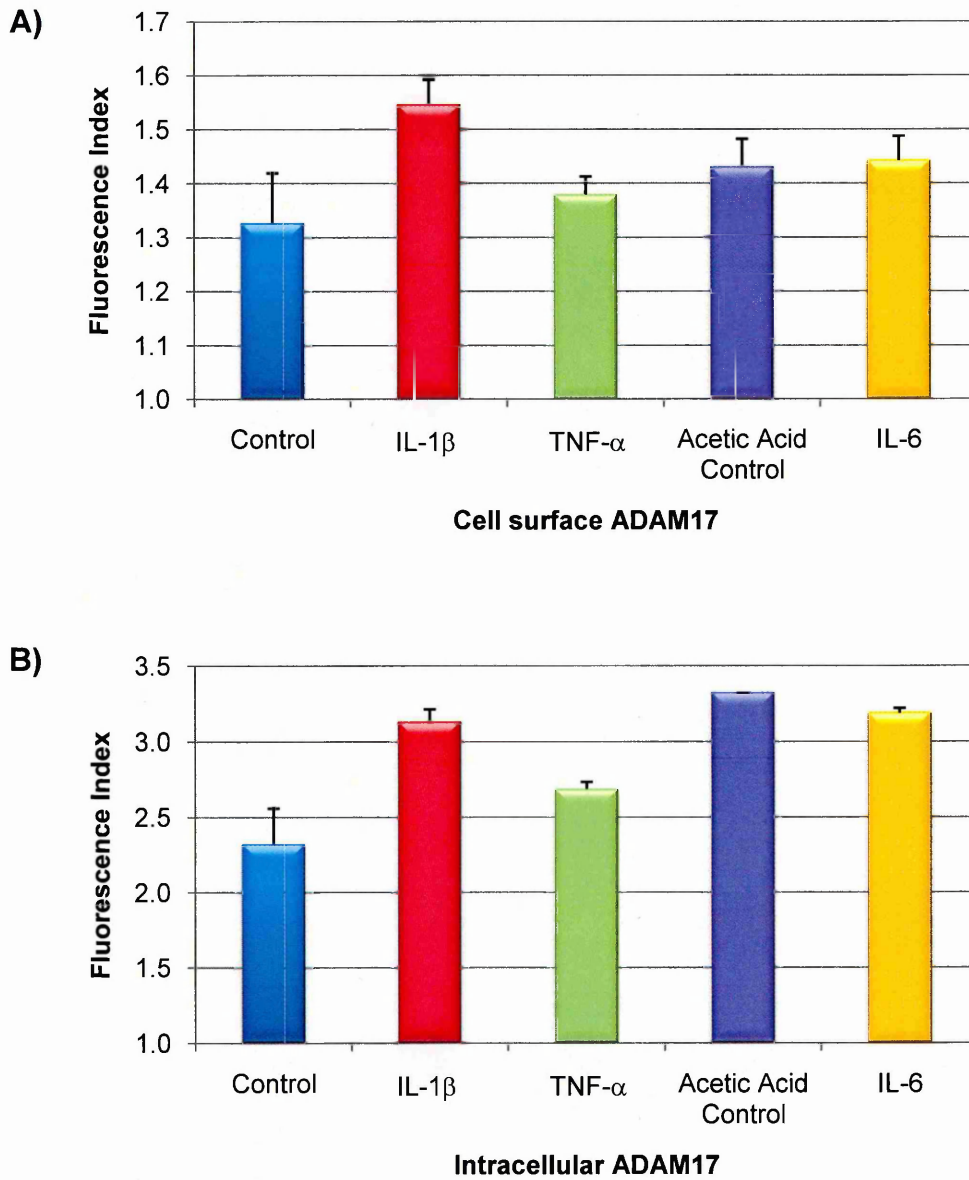


Figure 6.7: Fluorescence indices for A) cell surface and B) intracellular ADAM17 in HepG2 cells following 24 hours of treatment with 100 ng/mL of IL-1 β , IL-6 or TNF- α . There were no significant differences in the data (Kruskal-Wallis test; n=3).

Furthermore, cell surface (Figure 6.7A) and intracellular (Figure 6.7B) ADAM17 proteins were not significantly altered by cytokine treatment when compared to their appropriate controls. However, IL-1 β treatment did increase both cell surface and intracellular ADAM17 expression (FI=1.55 & FI=3.13 respectively) to a level higher than the untreated control (FI=1.33 & FI=2.32 respectively); TNF- α treatment also increased cell surface and intracellular ADAM17 expression, but to a lesser extent than IL-1 β treatment (FI=1.38 & FI=2.69 respectively).

Furthermore, ADAM17 was expressed at an elevated level both on the cell surface and intracellularly in the acetic acid-containing control (FI=1.43 & FI=3.32 respectively) compared to the untreated control. IL-6 treated cells expressed levels of ADAM17 (FI=1.44 & FI=3.19 respectively) comparable to its control, indicating that acetic acid influences ADAM17 expression, and not IL-6.

These data combined with the data regarding fractalkine shedding may suggest that 100 ng/mL of IL-1 β and TNF- α , and 5 μ M/mL of acetic acid increase the shedding of fractalkine from the surface of HepG2 cells by increasing ADAM17 expression.

6.2.4 siRNA Optimisation

The optimisation of siRNA lipid-mediated transfection conditions combined with the use of appropriate control samples was essential in obtaining effective target gene silencing with accurate data interpretation.

Three control samples were used to assess the effectiveness of target gene silencing (Section 6.1.3). An untreated control was employed as a baseline reference, GAPDH gene silencing with a GAPDH targeted siRNA was used as a positive control and a mock transfection with a non-targeting siRNA was used as a biologically relevant negative control.

The manufacturers' recommended transfection conditions for HepG2 cells were verified by use of a fluorescent transfection indicator (siGLO), i.e. for a 96-well plate format, 1×10^4 cells/well, 0.4 μ L/well DharmaFECT reagent 4, and 100 mM/well appropriate siRNA. Three independent ICC experiments were performed after 24 hours of transfection with siGLO alone (100 mM/well; Figure 6.8A) or siGLO plus GAPDH siRNA, non-targeting siRNA or ADAM17 siRNA (50 mM/well + 50 mM/well); untreated HepG2 cells were used as negative controls (Figure 6.8B). Cells were fixed with 4% PFA, as acetone can affect the fluorescence of siGLO. Three frames from each of these samples were viewed by confocal microscopy, and the transfection efficiency calculated to be >90% (Table 6.1), i.e. the mean percentage of cells with nuclear and perinuclear siGLO fluorescence was more than 90%.

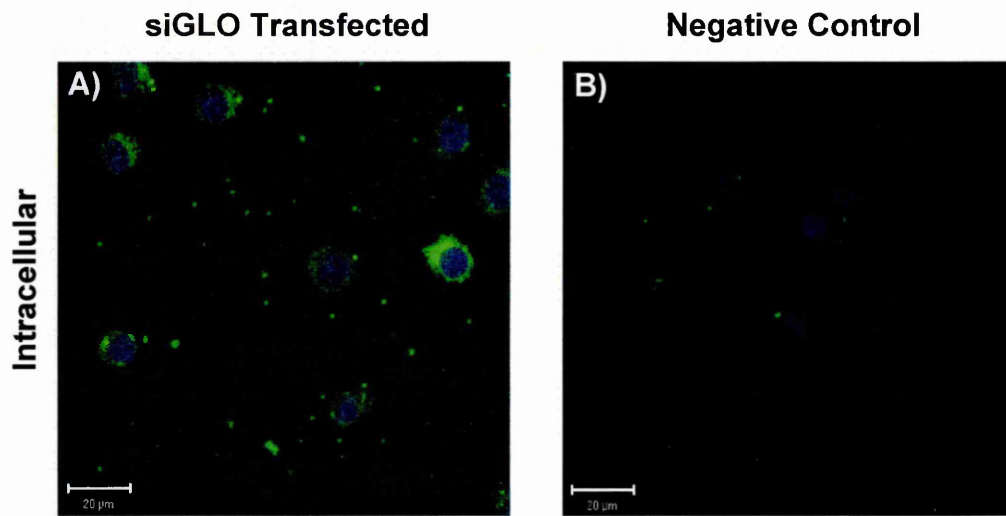


Figure 6.8: ICC examination of **A)** siGLO transfected HepG2 cells (green), and **B)** its negative control. Nuclei stained with DAPI (blue) in all images. Scale bar is 20 µm. Images representative of three independent experiments.

Table 6.1: siRNA transfection efficiencies for HepG2 cells.

Sample	Transfection Efficiency
siGLO alone	93.24%
siGLO + GAPDH	91.81%
siGLO + Non-Targeting	93.18%
siGLO + ADAM17	91.51%

The down-regulation of ADAM17 and GAPDH mRNA and protein in HepG2 cells was assessed by qRT-PCR and western blotting. Optimisation details are in Sections 3.2.4 and 4.2.1 respectively.

It was determined by geNorm analysis that HPRT1 was the single most stable reference transcript tested in the siRNA transfected HepG2 experimental system (M-value = 1.072). The primer pair efficiency for GAPDH detection was shown to be 99.6% by use of the standard curve method (Figure 6.9A). Analysis of the amplification and melt curve data (Figure 6.9B) together with agarose gel electrophoresis of the resultant qRT-PCR products obtained (Figure 6.9C) confirmed the correct product amplification; no amplification was seen in the NTC. The verification of HPRT1 and ADAM17 detection by qRT-PCR were previously described in Sections 3.2.6 and 3.2.7.

Optimisation details of ADAM17 and actin protein detection by western blot are described in Section 4.2.1. GAPDH immuno-detection was previously optimised (personal communication, Dr. G.A. Frentzou, Sheffield Hallam University, Sheffield, UK). Blots were first probed for ADAM17, stripped and re-probed for actin, and finally stripped and re-probed for GAPDH. This order of probing proved to be the most effective, as GAPDH antibody could not be effectively stripped from the membrane due to its very high binding avidity.

6.2.5 Down-Regulation of ADAM17 expression

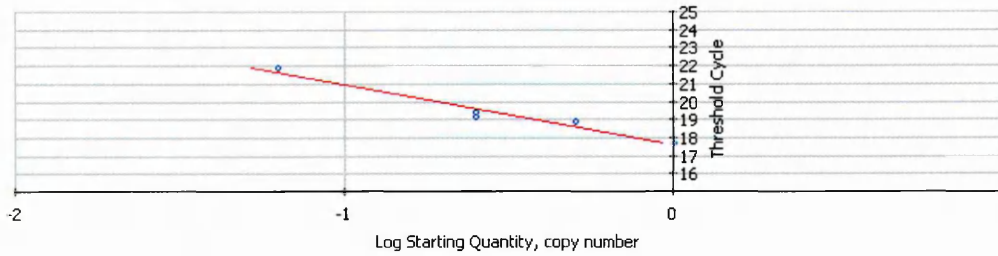
Following the optimisation of siRNA transfection conditions in HepG2 cells, qRT-PCR was performed to assess the level of ADAM17 gene down-regulation after 24 and 48 hours of transfection with an ADAM17 targeted siRNA (Sections 2.2.5 & 2.3.6). GAPDH gene down-regulation using a GAPDH targeted siRNA was used as a positive control for the technique, and non-targeting siRNA acted as a negative control to assess the off-target effects caused by activation of the RNAi pathway. qRT-PCR data were normalised against HPRT1, to ensure accurate data quantification. See Section 3.2.9 for sample preparation details.

GAPDH expression was reduced in the non-targeting siRNA transfected samples (62.2% reduction; $P=0.032$) and ADAM17 siRNA transfected samples (51% reduction; insignificant) after 24 hours; highlighting the off-target effects of RNAi pathway activation at this time point. Small comparable decreases in GAPDH expression were observed in the non-targeting and ADAM17 siRNA transfected samples after 48 hours (26.3% & 35.1% gene silencing respectively; insignificant), demonstrating GAPDH expression recovery.

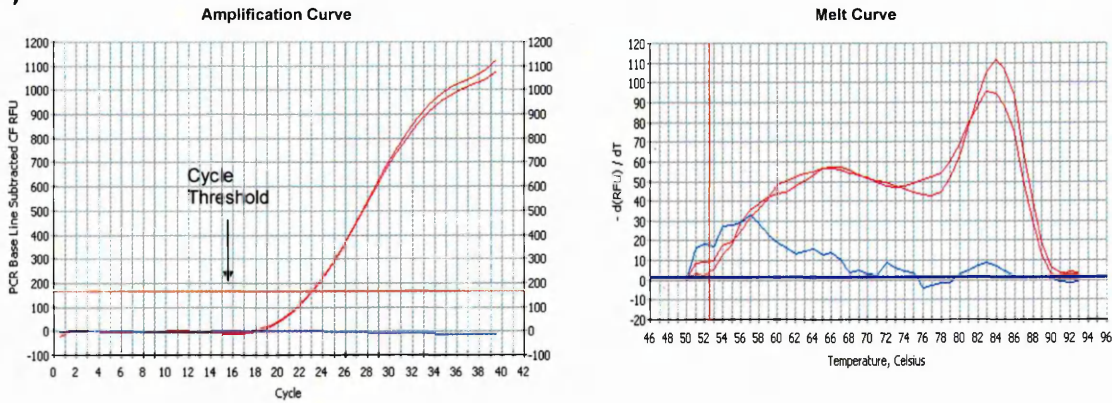
ADAM17 gene expression (Figure 6.10B) was not significantly reduced after 24 hours of transfection with ADAM17 siRNA transfected samples (55.8% gene silencing).

A)

Correlation Coefficient: 0.977 Slope: -3.332 Intercept: 17.646 $Y = -3.332 X + 17.646$
PCR Efficiency: 99.6 %



B)



C)

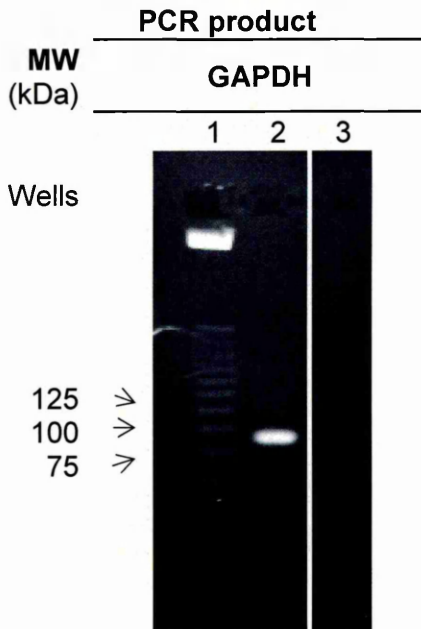
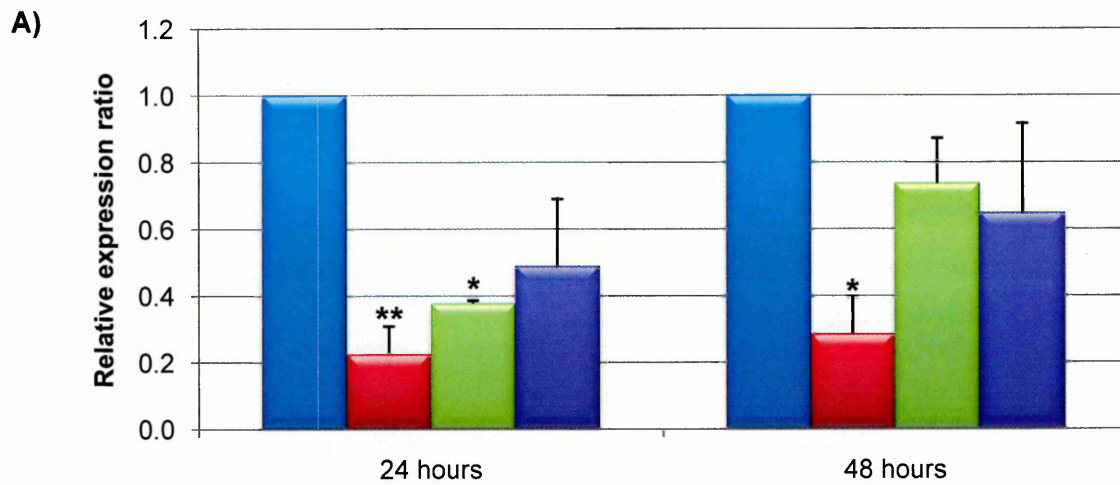
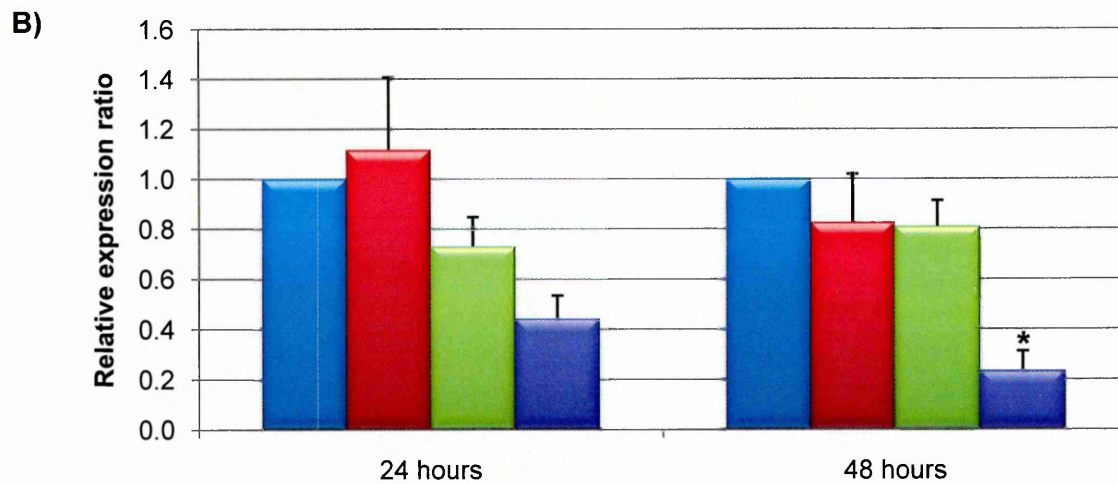


Figure 6.9: A) Standard curve plot generated from qRT-PCR data showing the PCR primer pair efficiency for GAPDH. B) Amplification and melt curves generated from qRT-PCR data for GAPDH. C) Agarose gel electrophoresis of the qRT-PCR products generated for GAPDH (87 bp), where 1 represents 25 bp marker, 2, signifies specific amplified product, and 3 denotes the NTC.

GAPDH mRNA levels (Figure 6.10A) were significantly lower after 24 and 48 hours of transfection, by 77.3% ($P=0.005$) and 71.3% ($P=0.033$) respectively. In addition,



GAPDH mRNA expression after siRNA treatment



ADAM17 mRNA expression after siRNA treatment

■ Control ■ GAPDH siRNA ■ Non-Targeting siRNA ■ ADAM17 siRNA

Figure 6.10: A) GAPDH mRNA expression in HepG2 cells following siRNA transfection for 24 and 48 hours. **B)** ADAM17 mRNA expression in HepG2 cells following siRNA transfection for 24 and 48 hours. Data presented as mean \pm SEM. Significant difference from control, * $P < 0.05$, ** $P < 0.01$ (ANOVA with Dunnett's test; $n=3$).

ADAM17 expression was slightly increased in the GAPDH siRNA transfected samples after 24 hours (11.8% gene up-regulation), whilst it was decreased in the non-targeting siRNA transfected samples (27% gene silencing); significance was not reached. However, ADAM17 gene expression was significantly down-regulated after 48 hours of transfection with ADAM17 targeted siRNA (78.3% gene silencing; $P=0.031$). Small comparable decreases in ADAM17 expression also were observed after 48 hours of transfection with GAPDH and non-targeting siRNAs (17.2% & 19.1% gene silencing respectively; statistically insignificant).

To confirm whether these findings translated from the mRNA to the protein level, western blot analysis was performed after 48, 72 and 96 hours of siRNA transfection (Section 2.4). The obtained data were quantified using IOD analysis, with normalisation against the internal control protein actin. Each band was examined individually and where appropriate the combined band densities (total protein data) displayed on the relative quantification plots.

ADAM17 was present on the blots as two predominant bands representing processed forms (66 and 58 kDa) in the control and GAPDH siRNA transfected samples (Figure 6.11A). The 66 kDa band was reduced or absent from the non-targeting and ADAM17 siRNAs transfected samples. Total band intensity analysis of ADAM17 (Figure 6.11B) showed that after 48 hours of transfection ADAM17 protein was slightly decreased in the ADAM17 siRNA transfected sample. Larger decreases in ADAM17 were also observed in the ADAM17 siRNA transfected samples after 72 and 96 hours, although significance was not reached. At these later time points the non-targeting and GAPDH siRNAs transfected samples also had decreased ADAM17 expression.

GAPDH protein was present in all samples as a 37 kDa band (Figure 6.11A), and it was evident that the GAPDH siRNA transfected samples at the 72 and 96 hour time points contained less GAPDH protein compared to all other samples. This was confirmed by densitometry (Figure 6.11B); GAPDH was also expressed at a slightly lower level after 48 hours of transfection. Small decreases in GAPDH expression were also evident in non-targeting and ADAM17 siRNAs transfected samples after 72 and 96 hours.

ICC analysis of ADAM17 was performed after siRNA transfection for 72 hours to confirm the western blot results, and determine whether cell surface and/or intracellular ADAM17 protein was reduced (Section 2.5). Experiments were performed three times to confirm any observed trends. The negative control for each experiment demonstrated only DAPI stained nuclei, with no non-specific staining of the secondary antibody (Figure 6.12E and J).

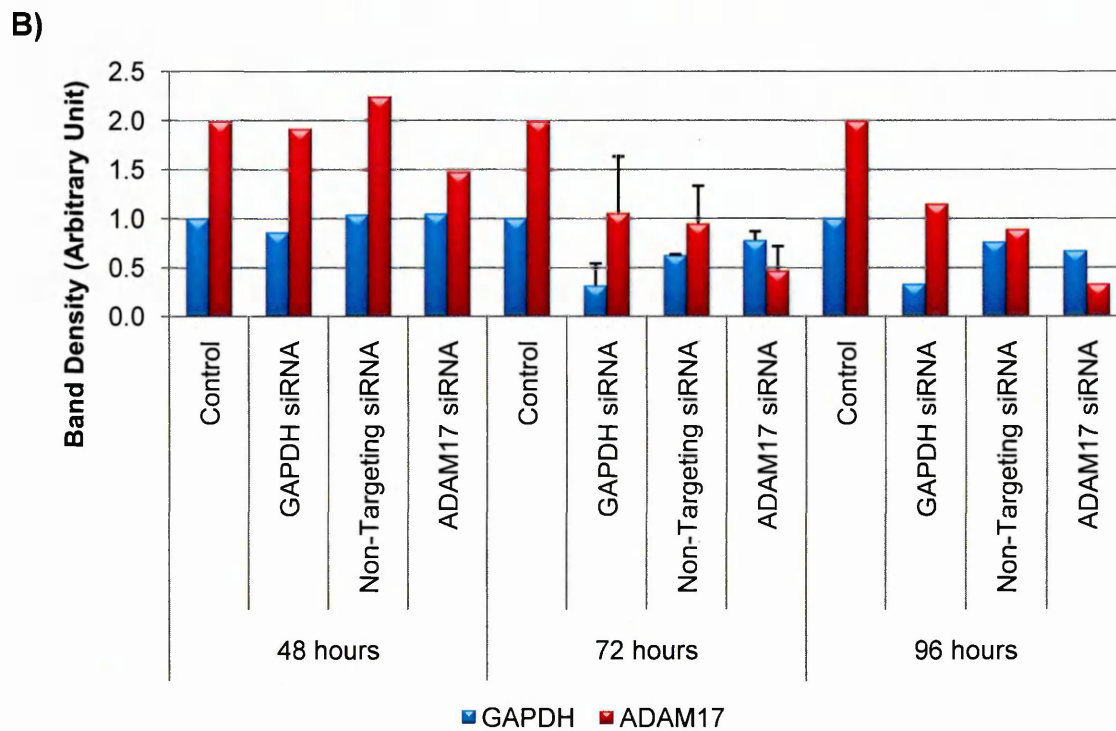
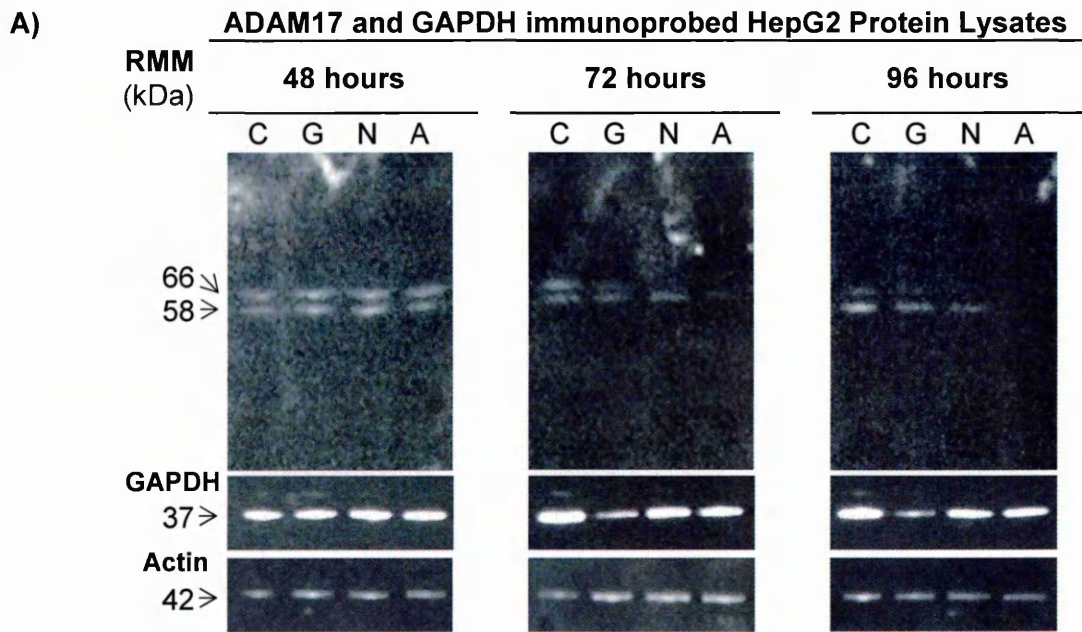


Figure 6.11: A) ADAM17 and GAPDH immunoprobed western blots of SDS-PAGE fractionated HepG2 protein lysates following 48, 72 and 96 hours of transfection with GAPDH (G), non-targeting (N) or ADAM17 (A) siRNAs, and an untreated control (C). Equal loading of protein samples (6 μ g) was verified by actin immunoprobe. **B)** Relative quantification of total ADAM17 and GAPDH proteins after actin normalisation. There were no significant differences in the 72 hour data (ANOVA with Dunnett's test; n=3). Statistics not performed on 48 and 96 hour data (n=1).

ADAM17 in HepG2 cells 72 hours post siRNA transfection

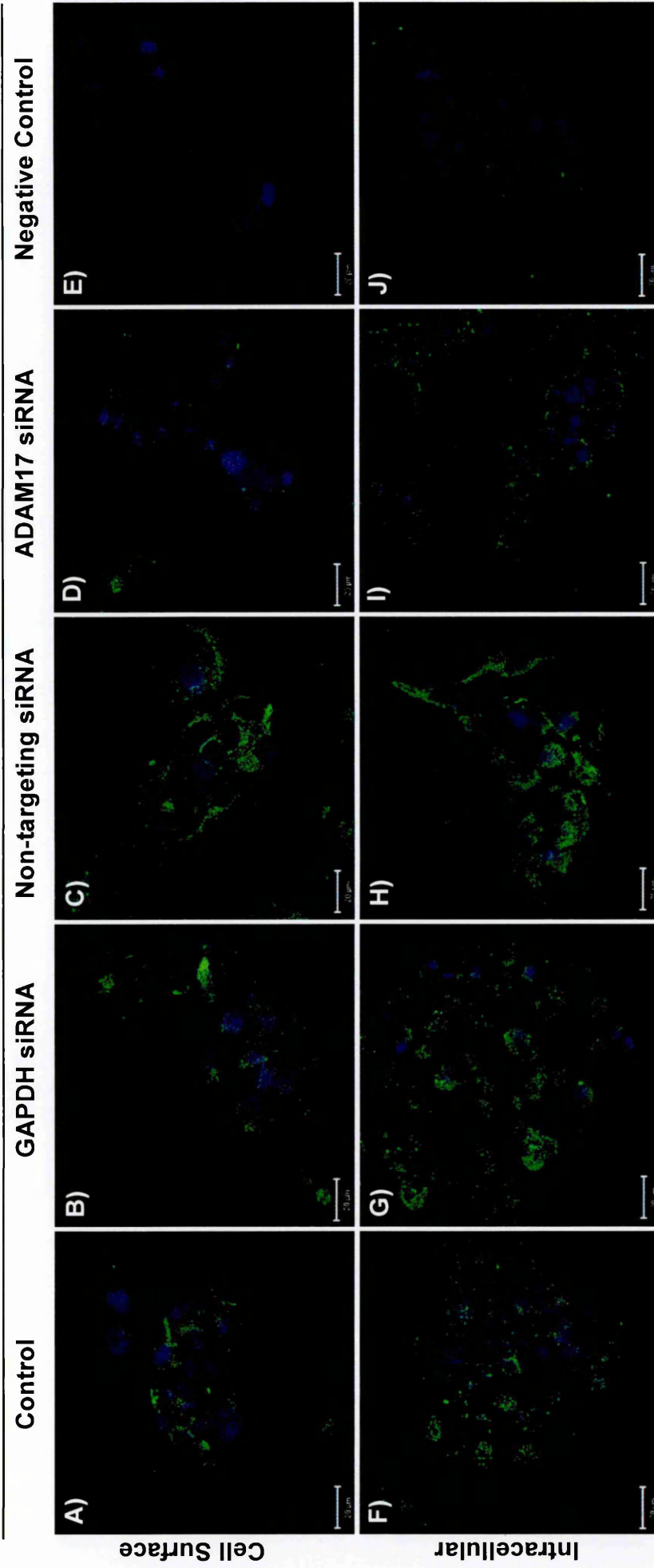


Figure 6.12: ICC examination of cell surface (4% PFA) and intracellular (-20°C) ADAM17 (green) in **A & F**) untreated and **E & J**) negative controls, and following **B & G**) GAPDH siRNA, **C & H**) non-targeting siRNA, **D & I**) ADAM17 siRNA transfections in HepG2 cells. Nuclei stained with DAPI (blue) in all images. Scale bar is 20 μm. Images representative of three independent experiments.

ADAM17 protein was located in a punctate pattern on the cell surface of HepG2 cells (Figure 6.12A), its expression pattern and staining intensity were comparable in GAPDH and non-targeting siRNAs transfected samples (Figure 6.12B & C). However, less ADAM17 was present on the surface of ADAM17 siRNA transfected cells (Figure 6.12D). Additionally, ADAM17 was situated diffusely within the cytoplasm, with possible perinuclear secretory vesicles (Figure 6.12F), GAPDH and non-targeting siRNAs did not alter the expression level or intracellular location of ADAM17 (Figure 6.12G & H). The secretory vesicles were absent from the ADAM17 siRNA transfected cells, and the cytoplasmic staining was less intense (Figure 6.12I). These data support the western blot data in the finding that ADAM17 protein is down-regulated following the transfection of HepG2 cells with ADAM17 siRNA for 72 hours.

6.2.6 Proliferative Responses of HepG2 Cells after ADAM17 Down-Regulation

To determine whether ADAM17 down-regulation altered the growth rate of HepG2 cells, cells were transfected with GAPDH, non-targeting or ADAM17 siRNAs for 24, 48, 72 or 96 hours, prior to the number of cells in each cell population being determined by the MTT assay (Section 2.2.6). A standard curve of actual cell numbers was used to convert the absorbance reading of metabolic activity to a cell number. Four independent experiments were performed to allow statistical analysis of the data obtained.

Figure 6.13 illustrates that siRNA transfection of HepG2 cells did not significantly alter the number of viable cells at any time point when compared to an untreated control. However, cell numbers were moderately increased following 24 hours of GAPDH, non-targeting and ADAM17 siRNA transfection, although statistical significance was not reached.

6.2.7 Fractalkine Shedding from HepG2 Cells after ADAM17 Down-Regulation

To determine whether the down-regulation of ADAM17 altered fractalkine shedding from the surface of HepG2 cells, cells were transfected with GAPDH, non-targeting or ADAM17 siRNAs for 24, 48, 72 or 96 hours, prior to supernatant collection and fractalkine ELISA analysis (Sections 2.2.5 & 2.6). Transfection of HepG2 cells with the test siRNAs did not statistically alter the proliferative capacity of HepG2 cells (Figure 6.13), so the amount of soluble fractalkine was expressed as ng/mL.

siRNA transfection did not significantly alter the amount of fractalkine shed from HepG2 cells at any time point examined (Figure 6.14). However, marginally less fractalkine was shed from ADAM17 silenced cells after 48 hours (5.4 ng/mL fractalkine) compared to the untreated control, GAPDH and non-targeting siRNA transfected samples (9.7, 7.8 & 6.8 ng/mL fractalkine respectively; Figure 6.14B). Furthermore, comparable

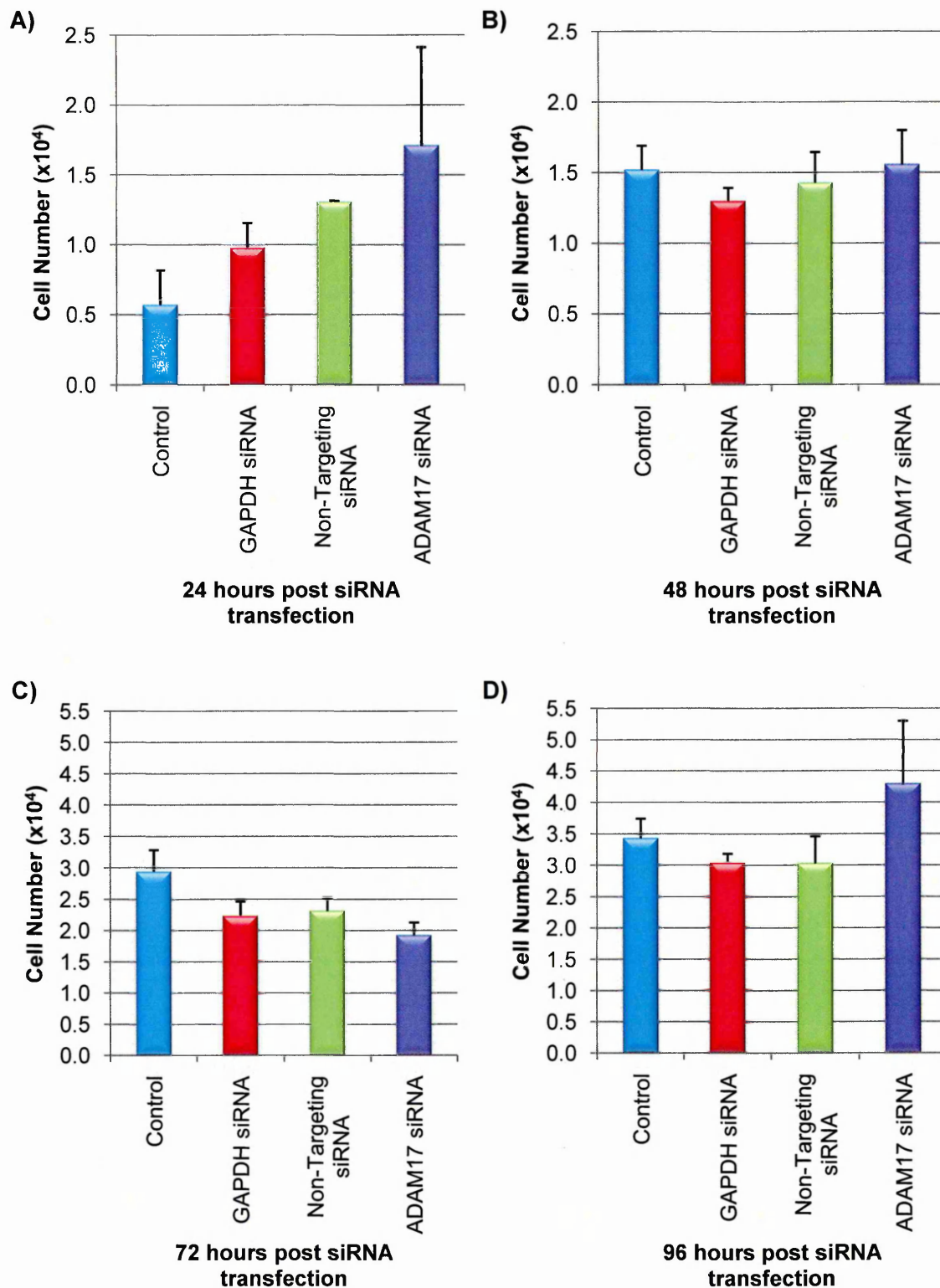


Figure 6.13: Viable HepG2 cell numbers following transfection with siRNA for **A)** 24 hours, **B)** 48 hours, **C)** 72 hours, and **D)** 96 hours. Data presented as mean \pm SEM. There were no significant differences in the data (ANOVA with Dunnett's test; $n=4$).

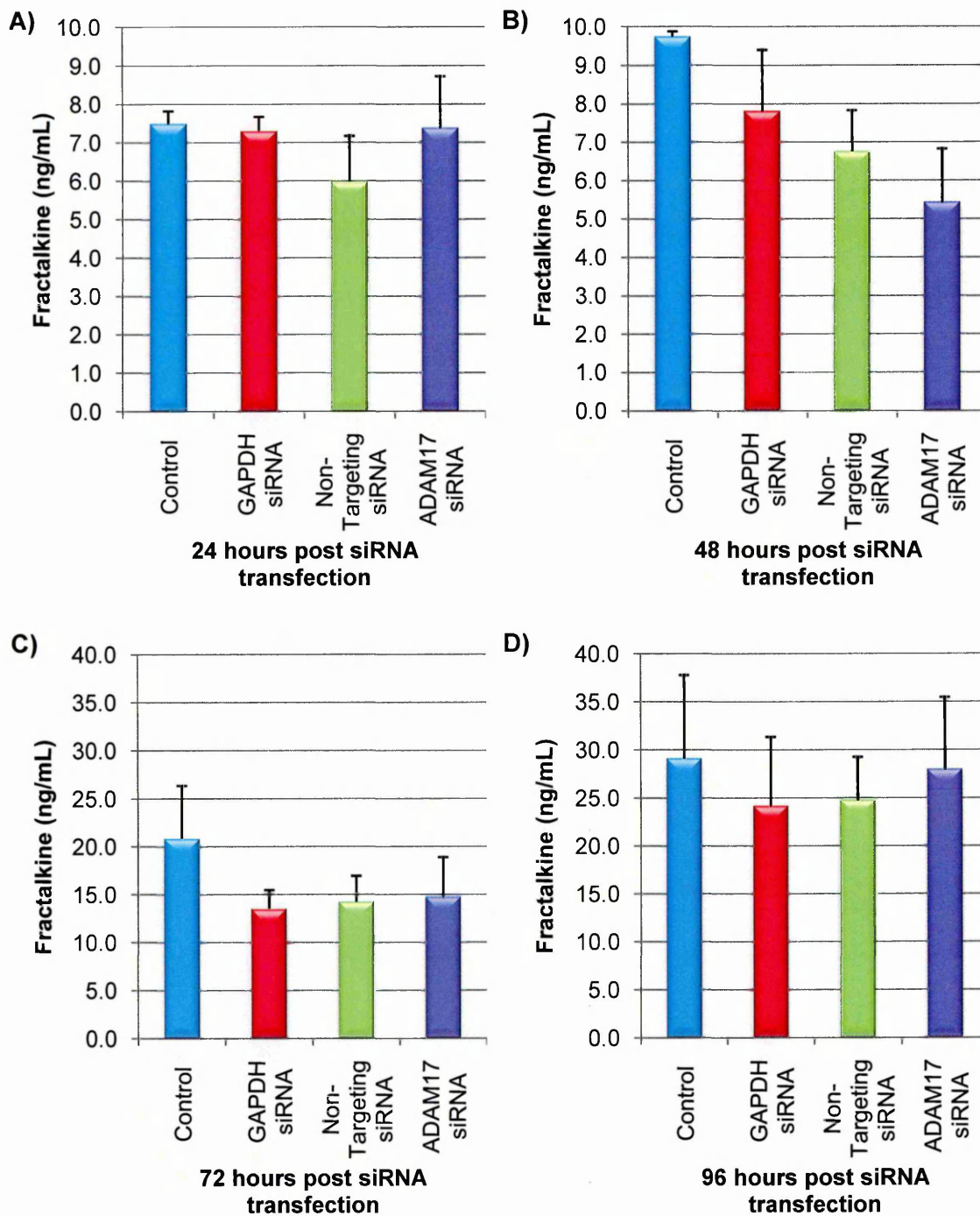


Figure 6.14: Amount of fractalkine (ng/mL) shed from the surface of HepG2 cells into the supernatant following transfection with siRNA for **A)** 24 hours (n=3), **B)** 48 hours (n=4), **C)** 72 hours (n=5), and **D)** 96 hours (n=4). Data presented as mean \pm SEM. There were no significant differences in the data (ANOVA with Dunnett's test).

levels of fractalkine were shed from siRNA transfected samples at the 72 time point (~14.2 ng/mL fractalkine), at a lower level than the control (20.8 ng/mL fractalkine). Similar results were obtained at the 96 hour time point.

6.2.7 Summary of Results

The results presented in this chapter are summarised in Table 6.2.

Table 6.2: Summary of the results presented in Chapter 6.

		Observation
Fractalkine	Soluble	↑ by IL-1 β , TNF- α and acetic acid (24 hours) ↑ by IL-1 β and TNF- α (48 hours)
	Membrane-bound	Evenly distributed; ↑ by IL-1 β , TNF- α and acetic acid (24 hours)
	Intracellular	Diffuse cytoplasmic; cytokines no effect
ADAM17	Membrane-bound	Minor ↑ by IL-1 β , TNF- α and acetic acid (24 hours)
	Intracellular	Minor ↑ by IL-1 β , TNF- α and acetic acid (24 hours)
ADAM17 down-regulation	mRNA	78.3% down-regulated; P=0.031 (48 hours)
	Total protein	76.7% down-regulated; P=0.138 (72 hours)
	Membrane-bound	↓ (72 hours)
	Intracellular	↓ (72 hours)
	Cellular proliferation	Down-regulation no effect
	Soluble fractalkine	Down-regulation no effect

6.3 Discussion

The aim of investigations described in this chapter was to determine whether IL-1 β , IL-6 and TNF- α modulated the shedding of fractalkine from the surface of the hepatoma cell line HepG2, and whether these modulations were due to alterations in ADAM17 activity.

6.3.1 Fractalkine Shedding from HepG2 Cells as an Indicator of ADAM17 Activity

Fractalkine is expressed at the gene and protein level in HepG2 cells (Efsen *et al*, 2002) and in agreement with Efsen *et al* (2002) it was determined that soluble fractalkine was present in HepG2 media, indicating its cleavage from the surface of these cells. Further to this, fractalkine shedding was significantly increased after 24 hours of treatment with 10 and 100 ng/mL IL-1 β (comparable levels) and 10 and 100 ng/mL TNF- α (concentration dependent increase). IL-6 treatment did not alter fractalkine shedding compared to its control, although increased shedding did occur in the acetic acid-containing control to a level comparable with that seen after 10 ng/mL of TNF- α treatment.

These findings were paralleled at the 48 hour time point with respect of IL-1 β and TNF- α , with significant increases in soluble fractalkine observed at all concentrations tested. Other researchers have also noted similar increases in soluble fractalkine in response to IL-1 β in the intestinal epithelial cell line T-84 (Muehlhoefer *et al*, 2000) and in response to TNF- α in the endothelial cell line hCMEC/D3 (Hurst *et al*, 2009).

These data may indicate that liver tumours, in particular well-differentiated liver tumours, up-regulate soluble fractalkine in response to pro-inflammatory cytokines that are elevated during times of hepatic injury and hepatic tumour development (Whitworth *et al*, 2006; Kuninaka *et al*, 2000). Furthermore, HepG2-conditioned medium is chemotactic for cells over-expressing Cx₃CR1 (Efsen *et al*, 2002), suggesting that soluble fractalkine recruits Cx₃CR1 expressing inflammatory cells and activated HSCs (Wasmuth *et al*, 2008) to the tumour site. The combination of these recruited lymphocytes, which are important in the inflammatory phase of the fibrogenic response, and activated HSCs, which are important in the later stages of liver fibrogenesis, may facilitate the formation of the fibrotic capsule (desmoplastic reaction) surrounding well-differentiated primary and metastatic CRC liver tumours.

Additionally, soluble fractalkine is an angiogenic mediator, inducing the chemotaxis and chemokinesis of ECs both *in vitro* and *in vivo* by the binding of fractalkine to its receptor on the surface of ECs (Volin *et al*, 2001). This same study also demonstrated that soluble fractalkine can induce ECs to form tubes *in vitro* and functional blood vessels *in vivo*, establishing its angiogenic properties. As fractalkine is elevated by cytokines

present during the initial stages of liver tumour formation, it is possible that soluble fractalkine could attract ECs to the tumour and induce the formation of a neovasculature capable of supplying blood to the developing tumour.

Flow cytometry demonstrated minor increases in cell surface and intracellular ADAM17 in response to IL-1 β , and TNF- α (significance was not reached). And as observed for fractalkine shedding, ADAM17 was increased in the acetic acid-containing control compared to the untreated control, without further increases following IL-6 treatment. This suggests that minor modulations of the proteolytically active membrane-bound form of ADAM17 can potentially control the amount of fractalkine cleaved from the surface of HepG2 cells, although it must be remembered that other enzymes could also be involved (see below).

To determine whether fractalkine shedding was solely facilitated by ADAM17 in the HepG2 system, ADAM17 was post-transcriptionally silenced and the amount of soluble fractalkine in their supernatants assessed after 72 hours of siRNA transfection when ADAM17 protein was effectively silenced (as shown by western blotting and ICC). Fractalkine shedding was not significantly altered by ADAM17 silencing, indicating that perhaps other proteases, e.g. ADAM10, MMP-2 or cathepsin S, are involved in fractalkine cleavage in this system.

ICC analysis of fractalkine in HepG2 cells demonstrated that intracellular fractalkine expression was unaffected by the cytokine treatments investigated, whereas its membrane-bound expression was slightly increased following IL-1 β and TNF- α treatment for 24 hours. A comparable increase in cell surface fractalkine was also observed in the acetic acid-containing control, without further increases following IL-6 treatment. This parallels the trends of soluble fractalkine under the same treatments in HepG2 cells, and is also in agreement with the finding that the expression of membrane-bound fractalkine can be greatly induced on ECs by certain pro-inflammatory cytokines, including IL-1 β , TNF- α and IFN- γ (Umehara *et al*, 2004; Hurst *et al*, 2009).

Membrane-bound fractalkine mediates the firm adhesion of cells carrying Cx₃CR1, independent of integrins, calcium, or an opposing cell membrane (Schäfer *et al*, 2004). This could explain the dense lymphocytic infiltrate and activated HSCs present in the desmoplastic reaction of well-differentiated liver tumours (Vermeulen *et al*, 2001; Wasmuth *et al*, 2008).

6.4 Summary

The data presented in this chapter demonstrate that fractalkine is shed from the surface of HepG2 cells, and that it is also present in its membrane-bound form in this cell type. Furthermore, IL-1 β and TNF- α treatment of cells significantly increased the soluble form of fractalkine, and marginally increased cell surface ADAM17 (significance was not reached), indicating that ADAM17 may be involved in the regulation of fractalkine shedding in this system. However, post-transcriptional silencing of ADAM17 did not alter fractalkine shedding, indicating that other proteases may compensate for ADAM17 down-regulation.

Chapter 7

General Discussion

The overall aim of this project was to determine whether ADAM17 and ADAMTS-1, -4 and -5 are potential mediators of tumour cell invasion and metastasis in the liver. A review of the literature revealed that the dysregulated expression of these proteolytic enzymes is associated with the development and dissemination of many human tumours, but their role in liver tumours, primary or metastatic, has not been extensively investigated.

The current study has described the expression of these enzymes, and their endogenous inhibitor TIMP3, in human adult and foetal liver total RNA samples, and in two HCC cell lines (HepG2 & HuH-7) and an activated HSC line (LX-2). The modulation of ADAM17, ADAMTS-1, -4, -5 and TIMP3 expression by specific pro-inflammatory cytokines was also examined in the cell lines, as was the effect of these cytokines on cell proliferation. Furthermore, the cleavage of fractalkine from HepG2 cells in combination with the analysis of cell surface ADAM17 levels was used as a potential indicator of ADAM17's sheddase activity.

7.1 *In Vitro* Model of Liver Cancer

Primary HCC and CRC liver metastases (the most common metastatic liver tumour) are distinct malignancies, but share many morphological characteristics (Vermeulen *et al*, 2001; Nakashima *et al*, 1983), in fact more than CRC liver metastases share with their primary colorectal tumour (Rajaganeshan *et al*, 2007). This suggests that the host tissue microenvironment sculpts the development of the tumour.

There are many established HCC cell lines available for the *in vitro* study of primary liver tumours, e.g. HLE, HLF, HuH-7, SK-Hep1, HepG2 & Hep3B cells. Two cell lines derived from well-differentiated HCCs, HepG2 and HuH-7, were selected for use in this study, as the majority of these tumours are surrounded by a fibrous capsule (desmoplastic reaction) (Nakashima *et al*, 1983) and require the secretion of proteolytic enzymes in order to breakdown liver ECM enabling their growth and expansion (Illemann *et al*, 2009). An activated HSC line, LX-2, derived from a healthy human liver, was also studied as this cell type is responsible for the secretion of proteolytic enzymes and the production of neomatrix in response to liver damage.

Currently there are no commercially available cell lines derived from CRC liver metastases, although one such cell line, CLY, has recently been developed from a poorly differentiated CRC liver metastasis (Li *et al*, 2007). Numerous primary CRC cell lines are, however, available, e.g. Caco-2, HT29 and HCA-24, but these were deemed unsuitable for use in this study as CRC liver metastases exhibit growth characteristics more closely associated with primary HCCs than primary CRCs. Therefore in the absence of specific CRC liver metastases cell lines, the selected HCC cell lines were

used as an appropriate substitute model for the *in vitro* assessment of well-differentiated CRC liver metastases.

HCC can be described as an inflammation-associated cancer developing predominantly in patients with chronic hepatitis and cirrhosis (Parkin *et al*, 2005; Ryder, 2003), conditions characterised by persistent liver injury, inflammation and hepatocellular proliferation (Berasain *et al*, 2007). Therefore the elevated presence of three pro-inflammatory cytokines, IL-1 β , IL-6 and TNF- α , within the liver during times of injury is unsurprising (Zimmers *et al*, 2003). Serum and peritoneal concentrations of these cytokines are also elevated in many patients with CRC (Simpson *et al*, 1997; Whitworth *et al*, 2006). Consequently these cytokines may be important in liver cancer progression, as they are with other tumour types, e.g. prostate and breast cancers (Dunlop & Campbell, 2000; Reed *et al*, 2009; Chung & Chang, 2003; Balkwill & Mantovani, 2001), but their specific functions remain to be determined.

Following the verification of the parental origin of HepG2, HuH-7 and LX-2 cells (Section 3.2.1), the proliferative effects of IL-1 β , IL-6 and TNF- α were examined on these cell lines (Section 3.2.3). The cytokines studied had no proliferative effect on the normal liver cell line LX-2, however differential increases in cell numbers were observed in the hepatoma cell lines, HepG2 and HuH-7, highlighting genetic variances in these cell lines.

Specifically, IL-1 β induced a rapid proliferative response in both hepatoma cell lines, which was prolonged in HepG2 cells and short-lived in HuH-7 cells. IL-6 also induced a short term increase in HepG2 cell proliferation, an effect also observed in primary hepatocytes (Gao, 2005), but not HuH-7 cells. Furthermore, TNF- α induced a delayed, but prolonged increase in the cellular proliferation of both hepatoma lines.

Combined, these findings could suggest that pro-inflammatory cytokines elevated in the liver when tumour formation is initiated could act sequentially to induce the sustained proliferation of liver tumour cells, and consequently aid tumour development.

7.2 ADAM17, ADAMTS-1, -4, -5 and TIMP3 Expression in Liver Cell Lines

7.2.1 ADAM17

ADAM17 was first identified as the major sheddase of TNF- α (Black *et al*, 1997), but many substrates have since been identified (Table 1.3). ADAM17 is now acknowledged as the principle EGFR (ErbB1) ligand sheddase (Blobel *et al*, 2009), and as such has a well established function in the EGFR signalling pathway, which is critical in both normal development (Sahin *et al*, 2004) and the development and progression of an

increasing number of cancers, including HCC (Fischer *et al*, 2003; Borrel-Pagès *et al*, 2003; Ding *et al*, 2004).

Although the role of ADAM17 in liver cancer has not been extensively studied, Ding *et al* (2004) initially documented the up-regulation of ADAM17 mRNA in primary HCC, before determining that poorly differentiated HCCs have a significantly higher level of ADAM17 mRNA than well and moderately differentiated HCCs. ADAM17 has since been found to be over-expressed at the protein level in both primary and metastatic CRC, including liver metastases, when compared to normal colonic mucosa (Blanchot-Jossic *et al*, 2005; Merchant *et al*, 2008).

This study demonstrated that ADAM17 was expressed at a higher level in hepatoma cells than activated HSCs, and that the level of ADAM17 mRNA expression correlated with the level of ADAM17 protein expression in the liver cell lines examined. The western blot data also indicated that active ADAM17 (110 kDa) was present in both hepatoma cell lines, but was not present at a detectable level in LX-2 cells.

Furthermore, Caja *et al* (2007) demonstrated in a rat model (male Wistar rats) that adult hepatocytes had very low ADAM17 mRNA expression, with increased expression observed in hepatoma cells (FaO cells). It was also determined that ADAM17 mRNA status correlated with the ability to transactivate EGFR pathway signalling, such that this pathway was not activated in adult hepatocytes, but was in hepatoma cells (Caja *et al*, 2007). Together these data may indicate that active ADAM17 is up-regulated in liver tumour cells compared to normal liver cells, where it may promote tumour progression via the transactivation of the EGFR signalling pathway. This pathway can lead to the acquisition of cellular properties associated with cancer progression, including growth, proliferation, survival (Oda *et al*, 2005), and angiogenesis (Blanchot-Jossic *et al*, 2005).

This study also demonstrated that ADAM17 expression was not significantly modulated by the cytokines investigated at the mRNA or protein level in any of the cell lines examined, although minor to moderate differential alterations were observed. Modulations at the mRNA level did not correlate with modulations at the protein level, indicating ADAM17 may have other methods of regulatory control, for example post-translational modifications of the protein including protein activation or modulation of its inhibitor TIMP3. These data may also indicate that ADAM17 activity is more important than the level at which it is expressed.

The presence of ADAM17 does not necessarily equate to its functionality. Therefore, to determine whether ADAM17 was present as a functional proteinase, fractalkine shedding from HepG2 cells was examined before and after ADAM17 down-regulation. Fractalkine was of interest not only as a substrate for ADAM17 (Umehara *et al*, 2004), but also as it is a mediator of pathogenic angiogenesis (Volin *et al*, 2001). Although it

must be remembered that other proteases may also be involved in the shedding of fractalkine, including ADAM10, cathepsin S and MMP-2 (Umehara *et al*, 2004; Hyakudomi *et al*, 2008; Dean & Overall, 2007; Clark *et al*, 2007). Soluble fractalkine, which acts as a conventional chemokine (Umehara *et al*, 2004; Efsen *et al*, 2002), was significantly increased following IL-1 β and TNF- α treatments. Interestingly, some increases albeit minor in cell surface and intracellular ADAM17 protein were also observed in the same conditions.

So it would be possible to postulate that minor alterations in ADAM17 can greatly increase its functionality. However, the post-transcriptional silencing of ADAM17 did not significantly reduce fractalkine shedding as would be expected if this hypothesis were true, indicating that other proteases are involved in the cleavage of membrane-bound fractalkine in this system, and that these proteases could compensate for the loss/reduction of functional ADAM17. A similar conclusion was also reached by Hurst *et al* (2009) in relation to fractalkine shedding from the endothelial cell line hCMEC/D3.

7.2.2 ADAMTS-1, -4 and -5

ADAMTS-1, -4 and -5 are primarily known for their ability to cleave aggrecan (Jones & Riley, 2005), the major structural component of cartilage. However, they can also influence cancer progression, as the central TSRs of ADAMTS-1 and -5 convey anti-angiogenic properties (Vázquez *et al*, 1999; Sharghi-Namini *et al*, 2008), whilst the over-expression of full-length ADAMTS-1 has the opposite effect by promoting angiogenesis (Kuno *et al*, 2004; Liu *et al*, 2006b). A distinct role for ADAMTS-4 in cancer is yet to be elucidated; however its altered expression has been associated with cancer progression (Held-Feindt *et al*, 2006).

This study demonstrated that ADAMTS-1 mRNA was expressed at a moderate level in HuH-7 cells, which was translated to the protein level. However, very low levels of ADAMTS-1 mRNA generated a moderate level of protein in HepG2 cells, and an inverse relationship was observed in LX-2 cells where a moderate level of mRNA produced a low level of protein. This demonstrates that higher levels ADAMTS-1 protein in hepatoma cells may induce angiogenic responses within the tumour, aiding its growth past the critical 2mm sphere of an avascular tumour (Lodish *et al*, 2000), and/or providing a route for the dissemination of tumour cells throughout the body (Handsley & Edwards, 2005).

Interestingly though, this study also showed that the cellular distribution of ADAMTS-1 varied between the hepatoma cell lines, with higher levels of cell surface-associated ADAMTS-1 on HuH-7 cells than HepG2 cells. ADAMTS-1 in this location is thought to be in its full-length active conformation (Seals & Courtneidge, 2003) where over-

expression can promote angiogenesis by the promotion of HB-EGF and amphiregulin shedding and the subsequent increase in EGFR transactivation (Liu *et al*, 2006b).

Conversely, HepG2 cells contained more intracellular ADAMTS-1-containing vesicles, thought to be secretory vesicles, indicating an extra level of regulatory control over ADAMTS-1 in HepG2 cells. These data could suggest that anti-angiogenic ADAMTS-1 is initially down-regulated in HepG2 cells allowing the initiation of angiogenesis, possibly by VEGF signalling, and then following an appropriate signal and the subsequent release of ADAMTS-1-containing secretory vesicles, the over-expression of ADAMTS-1 could elicit its angiogenic and invasive effect (Kuno *et al*, 2004; Liu *et al*, 2006b) to further promote tumour growth and dissemination.

A specific role for ADAMTS-4 in cancer progression is yet to be determined; however this study suggests that active ADAMTS-4 is present at lower levels in hepatoma cells than LX-2 cells. ADAMTS-4 mRNA was only detected at low levels in HepG2 and LX-2 cells, and very low levels in HuH-7 cells. This translated to low protein expression in HepG2 cells, moderate levels in HuH-7 cells and moderate to high levels in LX-2 cells, with double the amount of active ADAMTS-4 detected in LX-2 cells compared to the hepatoma cell lines (determined by band intensity analysis). Furthermore, minimal cell surface-associated ADAMTS-4 was observed on some, but not all hepatoma cells; ADAMTS-4 in this location is in its full-length active conformation (Seals & Courtneidge, 2003).

This could indicate that less ADAMTS-4 in liver tumours mediates a growth advantage to the tumour. A contrasting conclusion was reached by Held-Feindt *et al* (2006) who suggested that the over-expression of ADAMTS-4 increased the growth and invasive capacity of glioblastoma cells via the cleavage of brevican, which can lead to EGFR transactivation (Hu *et al*, 2008). This protein can also undergo C-terminal processing, which can effect its substrate specificity (Kashiwagi *et al*, 2004), and may therefore influence ECM sculpting.

This study also determined that ADAMTS-5 mRNA was expressed at a higher level in LX-2 cells than in the hepatoma cell lines, where it was not detected in HepG2 cells and only present at very low levels in HuH-7 cells. This correlated with low levels of mature ADAMTS-5 protein associated with the extracellular surfaces of the hepatoma cell lines, with more evident on LX-2 cells; again ADAMTS-5 is in its active conformation in this location (Seals & Courtneidge, 2003). However, comparable levels of total ADAMTS-5 protein were present in each of the liver cell lines. Combined, these data may suggest that the active form of ADAMTS-5, which purveys anti-angiogenic effects, is lower in liver cancer cells than in activated HSCs.

This study further demonstrated that ADAMTS-1 and -4 mRNA expressions were significantly increased by IL-1 β in HepG2 and LX-2 cells; ADAMTS-1 expression was also increased significantly by IL-6 in HepG2 cells. The cytokine treatment of cells also resulted in modulations at the protein level, although these modulations were generally minor and differed between the cell lines.

The obvious next step in this investigation would be to examine the functionality of each of these proteinases, although this is complicated by their overlapping substrates. The identification of novel substrates would be beneficial to this purpose, particularly as substrate specificity changes with C-terminal processing of these enzymes (Kashiwagi *et al*, 2004). A number of substrates have already been identified for these enzymes e.g. ECM PGs, but it remains to be determined whether these are biologically relevant in the liver.

7.2.3 TIMP3

TIMP3 is an endogenous inhibitor of all of the proteinases investigated in this study (Nagase *et al*, 2006), with ADAM17 being one of its major targets *in vivo* (Mohammed *et al*, 2004). TIMP3 also effectively regulates the proteolytic actions of ADAMTS-4 and -5 (Hashimoto *et al*, 2001; Kashiwagi *et al*, 2001), and can partially inhibit ADAMTS-1 activity (Rodriguez-Manzaneque *et al*, 2002). Under normal physiological conditions TIMP3 acts to tightly regulate the activity of these enzymes preventing them from having pathological effects.

However, the dysregulated expression of TIMPs can occur at various stages of cancer progression, with their down-regulation being associated with increased tumour cell invasiveness and their over-expression providing a protective effect by reducing tumour growth, metastasis formation and angiogenesis, and inducing tumour cell apoptosis (Lambert *et al*, 2004; Darnton *et al*, 2005). Furthermore, TIMP3 expression has been shown to be inhibited in brain ECs by the simultaneous application of IL-1 β and TNF- α (Bugno *et al*, 1999), two of the pro-inflammatory cytokines associated with liver tumour formation.

The expression of TIMP3 has previously been examined in CRC by Zeng *et al* (2001), where it was found to be consistently down-regulated at the protein level compared with paired normal colon mucosa; this is in contrast to its increased mRNA expression in CRC. TIMP3 expression in HCC and CRC liver metastases has not been examined. Therefore, this study demonstrates for the first time that TIMP3 mRNA expression was higher than that of the proteolytic enzymes it acts upon in all of the systems examined, liver cell lines and adult/foetal liver samples, with comparable levels in all samples. In

addition, TIMP3 mRNA expression was significantly down-regulated by TNF- α treatment in HuH-7 and LX-2 cells.

Although TIMP3 is usually found associated with sulphated GAGs present in the ECM (Lambert *et al*, 2004; Hashimoto *et al*, 2004), it can also be associated with the cell membrane (Hashimoto *et al*, 2004). This study demonstrated that minimal amounts of TIMP3 were associated with the surface of each liver cell line examined, with the majority of the protein present in the cytoplasm. This is in agreement with Miyazaki *et al* (2004) and Darnton *et al* (2005) who found that TIMP3 is largely cytoplasmic in many human tumours including renal carcinomas, pancreatic endocrine tumours, uveal melanomas and oesophageal adenocarcinomas.

Due to the findings above, it is probable that the western blot data presented in this study largely reflects intracellular TIMP3 levels, with more of this protein observed in HepG2 cells compared to the HuH-7 and LX-2 cells. The down-regulation of TIMP3 mRNA by TNF- α in LX-2 cells translated to the down-regulation of TIMP3 protein; this was not true for HuH-7 cells, although TIMP3 was decreased in HepG2 cells. Furthermore, IL-1 β treatment of each cell line resulted in a general decrease in TIMP3, whilst IL-6 treatment resulted in the over-expression of this inhibitor.

This data could suggest that TIMP3 expression can be differentially modulated by cytokines in normal and cancerous liver cells and this may yield tumour promoting or tumour suppressive effects depending upon its expression status.

7.3 Conclusions

Due to the absence of clinical symptoms, HCC and CRC liver metastases are often diagnosed at an advanced stage when curative therapies are limited to surgical resection (Burke & Allen-Mersh, 1996; Harris *et al*, 2003). As this treatment option is only feasible in a minority of HCC patients (Ryder, 2003), and only 20% of all CRC liver metastases patients (Burke & Allen-Mersh, 1996) it is of paramount importance that an effective, widely available treatment is developed.

This preliminary investigation showed higher expression levels of ADAM17 and ADAMTS-1 and lower expression levels of ADAMTS-4 and -5 in the hepatoma cell lines HepG2 and HuH-7 than in the LX-2 cell line. The expression of ADAM17, ADAMTS-1, -4, -5 and TIMP3 can be modulated by pro-inflammatory cytokines present during liver tumour development, namely IL-1 β , IL-6 and TNF- α , in all of the experimental cell lines investigated; however these modulations were generally minor and differed between the cell lines. In addition, cellular proliferation was increased in hepatoma cells, but not in LX-2 cells by these cytokine treatments.

Furthermore, fractalkine shedding, used as an indicator of ADAM17 activity, determined that although IL-1 β and TNF- α significantly increased fractalkine shedding from HepG2 cells, this did not correlate with the minor up-regulation of ADAM17 protein following these same treatments. Also, the down-regulation of ADAM17 by siRNA did not influence fractalkine shedding, indicating the involvement of other proteases in this process, e.g. ADAM10,

Collectively this data may suggest that the dysregulated expressions of ADAM17, ADAMTS-1, -4 -5 and TIMP3, and their modulation by pro-inflammatory cytokines act synergistically to promote the formation of liver tumours. Further studies into this research area may establish specific roles for these proteins in this process, enabling the development of novel liver tumour treatments.

Some of the experimental results and findings included in this thesis have been presented at a number of conferences and departmental events; details of which are included in Appendix A.

7.4 Future Work

Previous research into adamalysins in liver cancer is very limited, although ADAM17 and ADAMTS-1, -4 and -5 have been identified as mediators of tumorigenesis in other tumour types. The current study has provided evidence that the expression of these enzymes and their inhibitor TIMP3 is dysregulated in liver cancer cell lines, which if paralleled *in vivo* could facilitate liver tumour development. The current knowledge could be enhanced by additional work including the following:

- Substantiation of the preliminary protein data concerning the modulation of ADAM17, ADAMTS-1, -4, -5 and TIMP3 expression and cellular location *in vitro* by IL-1 β , IL-6 and TNF- α .
- The continued investigation of ADAM17 activity, and examination of ADAMTS-1, -4 and -5 activity in HCC cell lines, to determine whether these proteins are functional, and an investigation of their substrates in the liver.
- Investigations into the role of ADAM17 or other proteases in the shedding of fractalkine and other substrates relevant to tumour invasion/metastasis.
- Investigations of ADAM17, ADAMTS-1, -4, -5 and TIMP3 expression in CRC liver metastases cell lines, e.g. CLY, to allow comparisons to HCC cell lines.
- Investigations of ADAM17, ADAMTS-1, -4, -5 and TIMP3 expression in primary and metastatic liver tumours compared to paired normal liver tissue, with the aim of establishing a definite role for these proteinases in liver cancer progression.

Chapter 8

References

Introduction to flow cytometry (Unknown). Online at:

http://probes.invitrogen.com/resources/education/tutorials/4Intro_Flow/player.html.

UK liver cancer statistics (2009). Online at:

<http://info.cancerresearchuk.org/cancerstats/types/liver/?a=5441>.

Abbaszade, I., Liu, R., Yang, F., Rosenfeld, S.A., Ross, O.H., Link, J.R., Ellis, D.M., Tortorella, M.D., Pratta, M., Hollis, J.M., Wynn, R., Duke, J.L., George, H.J., Hillman, M.C., Murphy, K., Wiswall, B.H., Copeland, R.A., Decicco, C.P., Bruckner, R., Nagase, H., Itoh, Y., Newton, R.C., Magolda, R.L., Trzaskos, J.M., Hollis, G.F., Arner, E.C. & Burn, T.C. (1999). Cloning and characterization of *ADAMTS11*, an aggrecanase from the ADAMTS family. *The Journal of Biological Chemistry*, **274** 23443-23450.

Adams, D.H. & Eksteen, B. (2006). Aberrant homing of mucosal T cells and extra-intestinal manifestations of inflammatory bowel disease. *Nature Reviews Immunology*, **6** 244-251.

Adams, D.H. & Eksteen, B. (1979). Controlled synthesis of HBsAg in a differentiated human liver carcinoma-derived cell line. *Nature*, **282** 615-616.

Aimes, R.T. & Quigley, J.P. (1995). Matrix metallo-proteinase-2 is an interstitial collagenase. Inhibitor-free enzyme catalyses the cleavage of collagen fibrils and soluble native type I collagen generating the specific 3/4-and 1/4-length fragments. *The Journal of Biological Chemistry*, **270** 5872-5876.

Alberts, B., Johnson, A., Walter, P., Lewis, J., Raff, M. & Roberts, K. (2008). *Molecular Biology of the Cell*. Fifth ed., USA, Garland Publishing.

Anders, A., Gilbert, S., Garten, W., Postina, R. & Fahrenholz, F. (2001). Regulation of the α -secretase ADAM10 by its prodomain and proprotein convertases. *The Federation of American Societies for Experimental Biology Journal*, **15** 1837-1839.

Arribas, J. & Bech-Serra, J.J. (2006). ADAMs, cell migration and cancer. *Cancer Metastasis Reviews*, **25** 57-68.

Asai, M., Hattori, C., Szabo, B., Sasagawa, N., Maruyama, K., Tanuma, S.I. & Ishiura, S. (2003). Putative function of ADAM9, ADAM10, and ADAM17 as APP α -secretase. *Biochemical and Biophysical Research Communications*, **301** 231-235.

Atreya, R. & Neurath, M.F. (2005). Involvement of IL-6 in the pathogenesis of inflammatory bowel disease and colon cancer. *Clinical Reviews in Allergy & Immunology*, **28** 187-196.

Balkwill, F. & Mantovani, A. (2001). Inflammation and cancer: Back to Virchow? *The Lancet*, **357** 539-545.

Bandtlow, C.E. & Zimmermann, D.R. (2000). Proteoglycans in the developing brain: New conceptual insights for old proteins. *Physiological Reviews*, **80** 1267-1290.

- Bazen, J.F., Bacon, K.B., Hardiman, G., Wang, W., Soo, K., Rossi, D., Greaves, D.R., Zlotnik, A. & Schall, T.J. (1997). A new class of membrane-bound chemokine with a CX₃C motif. *Nature*, **385** 640-644.
- Becker, C., Fantini, M.C., Schramm, C., Lehr, H.A., Wirtz, S., Nikolaev, A., Burg, J., Strand, S., Kiesslich, R., Huber, S., Ito, H., Nishimoto, N., Yoshizaki, K., Kishimoto, T., Galle, P.R., Blessing, T., Rose-John, S. & Neurath, M.F. (2004). TGF- β suppresses tumor progression in colon cancer by inhibition of IL-6 *trans*-signaling. *Immunity*, **21** 491-501.
- Bedossa, P. & Paradis, V. (2003). Review article: Liver extracellular matrix in health and disease. *Journal of Pathology*, **200** 504-515.
- Begg, A.C. & Steel, G.G. (2002). Cell proliferation and growth rate of tumours. In: Steel, G.G. (ed.). *Basic Clinical Radiobiology*. Third ed., UK, Hodder Arnold, 8-22.
- Benyon, R.C. & Iredale, J.P. (2000). Is liver fibrosis reversible? *Gut*, **46** 443-446.
- Berasain, C., Castillo, J., Prieto, J. & Avila, M.A. (2007). New molecular targets for hepatocellular carcinoma: The ErbB1 signaling system. *Liver International*, **153** 174-185.
- Bird, N.C., Mangnall, D. & Majeed, A.W. (2006). Biology of colorectal liver metastases: A review. *Journal of Surgical Oncology*, 1-13.
- Black, R.A., Rauch, C.T., Kozlosky, C.J., Peschon, J.J., Slack, J.L., Wolfson, M.F., Castner, B.J., Stocking, K.L., Reddy, P., Srinivasan, S., Nelson, N., Boiani, N., Schooley, K.A., Gerhart, M., Davis, R., Fitzner, J.N., Johnson, R.S., Paxton, R.J., March, C.J. & Cerretti, D.P. (1997). A metalloproteinase disintegrin that releases tumour-necrosis factor α from cells. *Nature*, **385** 729-733.
- Blanchot-Jossic, F., Jarry, A., Masson, D., Bach-Ngohou, K., Paineua, J., Denis, M.G., Laboissee, C.L. & Mosnier, J.F. (2005). Up-regulated expression of ADAM17 in human colon carcinoma: Co-expression with EGFR in neoplastic and endothelial cells. *Journal of Pathology*, **207** 156-163.
- Blobel, C.P., Carpenter, G. & Freeman, M. (2009). The role of protease activity in ErbB biology. *Experimental Cell Research*, **315** 671-682.
- Boese, Q. (ed.) (2004). *RNA Interference: Technical Reference and Application Guide*. UK, Dharmacon RNA Technologies.
- Borrel-Pagès, M., Rojo, F., Albanell, J., Baselga, J. & Arribas, J. (2003). TACE is required for the activation of the EGFR by TGF- α in tumors. *The European Molecular Biology Organization Journal*, **22** 1114-1124.
- Bosch, F.X., Ribes, J., Díaz, M. & Cléries, R. (2004). Primary liver cancer: Worldwide incidence and trends. *Gastroenterology*, **127** S5-S16.
- Bowen, R. (2003). *Hepatic histology: Sinusoids*. Online at: http://www.vivo.colostate.edu/hbooks/pathphys/digestion/liver/histo_sinusoids.html.

- Bowen, R. (1998). *Hepatic histology: Hepatocytes*. Online at:
http://www.vivo.colostate.edu/hbooks/pathphys/digestion/liver/histo_hcytes.html.
- Bugno, M., Witek, B., Bereta, J., Bereta, M., Edwards, D.R. & Kordula, T. (1999). Reprogramming of TIMP-1 and TIMP-3 expression profiles in brain microvascular endothelial cells and astrocytes in response to proinflammatory cytokines. *Federation of European Biochemical Societies Letters*, **448** 9-14.
- Burke, D. & Allen-Mersh, T.G. (1996). Colorectal liver metastases. *Postgraduate Medical Journal*, **72** 464-469.
- Bustin, S.A. & Mueller, R. (2005). Real-time reverse transcription PCR (qRT-PCR) and its potential use in clinical diagnosis. *Clinical Science*, **109** 365-379.
- Caja, L., Ortiz, C., Bertran, E., Murillo, M.M., Miró-Obradors, M.J., Palacios, E. & Fabregat, I. (2007). Differential intracellular signalling induced by TGF- β in rat adult hepatocytes and hepatoma cells: Implications in liver carcinogenesis. *Cellular Signalling*, **19** 683-694.
- Cal, S., Freije, J.M.P., Lopez, J.M., Takada, Y. & Lopez-Otin, C. (2000). ADAM 23/MDC3, a human disintegrin that promotes cell adhesion via interaction with the $\alpha V\beta 3$ integrin through an RGD-independent mechanism. *Molecular Biology of the Cell*, **11** 1457-1469.
- Cal, S., Obaya, A.J., Llamazares, M., Garabaya, C., Quesada, V. & López-Otín, C. (2002). Cloning, expression analysis, and structural characterization of seven novel human ADAMTSs, a family of metalloproteinases with disintegrin and thrombospondin-1 domains. *Gene*, **283** 49-62.
- Carl-McGrath, S., Lendeckel, U., Ebert, M., Roessner, A. & Rocken, C. (2005). The disintegrin-metalloproteinases ADAM9, ADAM12, and ADAM15 are upregulated in gastric cancer. *International Journal of Oncology*, **26** 17-24.
- Carmeliet, P. & Jain, R.K. (2000). Angiogenesis in cancer and other diseases. *Nature*, **407** 249-257.
- Chang, C. & Werb, Z. (2001). The many faces of metalloproteases: Cell growth, invasion, angiogenesis and metastasis. *Trends in Cell Biology*, **11** S37-S43.
- Chung, Y-C. & Chang, Y-F. (2003). Serum interleukin-6 levels reflect the disease status of colorectal cancer. *Journal of Surgical Oncology*, **83** 222-226.
- Clark, A.K., Yip, K.P., Grist, J., Gentry, C., Staniland, A.A., Marchand, F., Dehvari, M., Wotherspoon, G., Winter, J., Ullah, J., Bevan, S. & Malcangio, M. (2007). Inhibition of spinal microglial cathepsin S for the reversal of neuropathic pain. *Proceedings of the National Academy of Science USA*, **104** 10655-10660.

- Condon, T.P., Flournoy, S., Sawyer, G.J., Baker, B.F., Kishimoto, T.K. & Bennett, C.F. (2001). ADAM17 but not ADAM10 mediates tumor necrosis factor- α and L-selectin shedding from leukocyte membranes. *Antisense & Nucleic Acid Drug Development*, **11** 107-116.
- Conti, J.A., Kendall, T.J., Bateman, A., Armstrong, T.A., Papa-Adams, A., Xu, Q., Packman, G., Primrose, J.N., Benyon, R.C. & Iredale, J.P. (2008). The desmoplastic reaction surrounding hepatic colorectal adenocarcinoma metastases aids tumour growth and survival via α 5 β 1 integrin ligation. *Clinical Cancer Research*, **15** 6405-6413.
- Cosgrove, B.D., Cheng, C., Pritchard, J.R., Stolz, D.B.L., D.A. & Griffith, L.G. (2008). An inducible autocrine cascade regulates rat hepatocyte proliferation and apoptosis responses to tumor necrosis factor- α . *Hepatology*, **48** 276-288.
- Costa, F.F., Verbisck, N.V., Salim, A.C.M., Ierardi, D.F., Pires, L.C., Sasahara, R.M., Sogayar, M.C., Zanata, S.M., Mackay, A., O'Hare, M., Soares, F., Simpson, A.J.G. & Camargo, A.A. (2004). Epigenetic silencing of the adhesion molecule ADAM23 is highly frequent in breast tumors. *Oncogene*, **23** 1481-1488.
- Coussens, L.M. & Werb, Z. (2001). Inflammatory cells and cancer: Think different! *The Journal of Experimental Medicine*, **193** F23-F26.
- Crawford, A.R., Lin, X.Z. & Crawford, J.M. (1998). The normal adult human liver biopsy: A quantitative reference standard. *Hepatology*, **28** 323-331.
- Creighton, T.E. (1993). *Proteins: Structures & molecular properties*. 2nd ed., New York, U.S.A, W.H. Freeman.
- Curran, S. & Murray, G.I. (1999). Matrix metalloproteinases in tumour invasion and metastasis. *Journal of Pathology*, **189** 300-308.
- Darnton, S.J., Hardie, L.J., Muc, R.S., Wild, C.P. & Casson, A.G. (2005). Tissue inhibitor of metalloproteinase-3 (*TIMP-3*) gene is methylated in the development of esophageal adenocarcinoma: Loss of expression correlates with poor prognosis. *International Journal of Cancer*, **115** 351-358.
- Dean, R.A. & Overall, C.M. (2007). Proteomics discovery of metalloproteinase substrates in the cellular context by iTRAQTM labeling reveals a diverse MMP-2 substrate degradome. *Molecular and Cellular Proteomics*, **6** 611-623.
- Deuss, M., Reiss, K. & Hartmann, D. (2008). Part-time α -secretases: The functional biology of ADAM9, 10 and 17. *Current Alzheimer Research*, **5** 187-201.
- Ding, X., Yang, L.Y., Huang, G.W., Wang, W. & Lu, W.Q. (2004). ADAM17 mRNA expression and pathological features of hepatocellular carcinoma. *World Journal of Gastroenterology*, **10** 2735-2739.
- Doerr, R., Zvibel, I., Chiuten, D., D'Olimpio, J. & Reid, L.M. (1989). Clonal growth of tumors on tissue-specific biomatrices and correlation with organ-site specificity of metastases. *Cancer Research*, **49** 384-392.

- Dranoff, G. (2004). Cytokines in cancer pathogenesis and cancer therapy. *Nature Reviews Cancer*, **4** 11-22.
- Duffy, M.J. (1992). The role of proteolytic enzymes in cancer invasion and metastasis. *Clinical and Experimental Metastasis*, **10** 145-155.
- Duffy, M.J., Maguire, T.M., Hill, A., McDermott, E. & O'Higgins, N. (2000). Review: Metalloproteinases: Role in breast carcinogenesis, invasion and metastasis. *Breast Cancer Research*, **2** 252-257.
- Dunlop, R.J. & Campbell, C.W. (2000). Cytokines and advanced cancer. *Journal of Pain and Symptom Management*, **20** 214-232.
- Dunn, J.R., Panutsopoulos, D., Shaw, M.W., Heighway, J., Dormer, R., Salmo, E.N., Watson, S.G., Field, J.K.L. & Liloglou, T. (2004). METH-2 silencing and promoter hypermethylation in NSCLC. *British Journal of Cancer*, **91** 1149-1154.
- Dunn, J.R., Reed, J.E., du Plessis, D.G., Shaw, E.J., Reeves, P., Gee, A.L., Warnke, P. & Walker, C. (2006). Expression of ADAMTS-8, a secreted protease with antiangiogenic properties, is downregulated in brain tumours. *British Journal of Cancer*, **94** 1186-1193.
- Edwards, D.R., Handsley, M.M. & Pennington, C.J. (2008). The ADAM metalloproteinases. *Molecular Aspects of Medicine*, **29** 258-289.
- Efsen, E., Grappone, C., DeFranco, R.M.S., Milani, S., Romanelli, R.G., Bonacchi, A., Caligiuri, A., Failli, P., Annunziato, F., Pagliai, G., Pinzani, M., Laffi, G., Gentilini, P. & Marra, F. (2002). Up-regulated expression of fractalkine and its receptor CX3CR1 during liver injury in humans. *Journal of Hepatology*, **37** 39-47.
- Emonard, H., Guillouzo, A., Lapiere, C.M. & Grimaud, J.A. (1990). Human liver fibroblast capacity for synthesizing interstitial collagenase *in vitro*. *Cell and Molecular Biology*, **36** 461-467.
- Eto, K., Huet, C., Tarui, T., Kupriyanov, S., Liu, H.Z., Puzon-MaLaughlin, W., Zhang, X.P., Sheppard, D., Engvall, E. & Takada, Y. (2002). Functional classification of ADAMs based on a conserved motif for binding to integrin $\alpha 9\beta 1$: Implications for sperm-egg binding and other cell interactions. *The Journal of Biological Chemistry*, **277** 17804-17810.
- Fearon, K.C.H., McMillan, D.C., Preston, T., Winstanley, P., Cruickshank, A.M. & Shenkin, A. (1991). Elevated circulating interleukin-6 is associated with an acute-phase response but reduced fixed hepatic protein synthesis in patients with cancer. *Annals of Surgery*, **213** 26-31.
- Fischer, O.M., Hart, S., Gschwind, A. & Ullrich, A. (2003). EGFR signal transactivation in cancer cells. *Biochemical society transactions*, **31** 1203-1208.
- Flannery, C.R. (2006). MMPs and ADAMTSs: Functional studies. *Frontiers in Bioscience*, **11** 544-569.

- Foda, H.D. & Zucker, S. (2001). Matrix metalloproteinases in cancer invasion, metastasis and angiogenesis. *Drug Discovery Today*, **6** 478-482.
- Fogel, M., Gutwein, P., Mechtersheimer, S., Riedle, S., Stoeck, A., Smirnov, A., Edler, L., Ben-Arie, A., Huszar, M. & Altevogt, P. (2003). L1 expression as a predictor of progression and survival in patients with uterine and ovarian carcinomas. *The Lancet*, **362** 869-875.
- Fox, J.W. & Bjarnason, J.B. (1996). Reprolysins: Snake venom and mammalian reproductive metalloproteinases. In: Hooper, N.M. (ed.). *Zinc Metalloproteinases in Health and Disease*. UK, Taylor and Francis, 47-81.
- Friedman, S.L. (1993). The cellular basis of hepatic fibrosis: Mechanisms and treatment strategies. *The New England Journal of Medicine*, **328** 1828-1835.
- Fritzsche, F.R., Jung, M., Xu, C., Rabien, A., Schick Tanz, H., Stephan, C., Dietel, M., Jung, K. & Kristiansen, G. (2006). ADAM8 expression in prostate cancer is associated with parameters of unfavorable prognosis. *Virchows Archiv*, **449** 628-636.
- Fritzsche, F.R., Wassermann, K., Jung, M., Tolle, A., Kristiansen, I., Lein, M., Johannsen, M., Dietel, M., Jung, K. & Kristiansen, G. (2008). ADAM9 is highly expressed in renal cell cancer and is associated with tumour progression. *BioMed Central Cancer*, **8** 179-187.
- Fröhlich, C., Albrechtsen, R., Dyrskjot, L., Rudkjaer, L., Orntoft, T.F. & Wewer, U. (2006). Molecular profiling of ADAM12 in human bladder cancer. *Clinical Cancer Research*, **12** 7359-7368.
- Gao, B. (2005). Cytokines, STATs and liver disease. *Cellular and Molecular Immunology*, **2** 92-100.
- Gaur, U. & Aggarwal, B.B. (2003). Regulation of proliferation, survival and apoptosis by members of the TNF superfamily. *Biochemical Pharmacology*, **66** 1403-1408.
- Gavert, N., Sheffer, M., Raveh, S., Spaderna, S., Shtutman, M., Brabletz, T., Barany, F., Paty, P., Notterman, D., Domany, E. & Ben-Ze'ev, A. (2007). Expression of L1-CAM and ADAM10 in human colon cancer cells induces metastasis. *Cancer Research*, **67** 7703-7712.
- Grützmann, R., Luttges, J., Sipos, B., Ammerpohl, O., Dobrowolski, F., Aldinger, I., Kersting, S., Ockert, D., Koch, R., Kalthoff, H., Schackert, H.D., Kloppel, G. & Pilarsky, C. (2004). ADAM9 expression in pancreatic cancer is associated with tumour type and is a prognostic factor in ductal adenocarcinoma. *British Journal of Cancer*, **90** 1053-1058.
- Guo, W. & Giancotti, F.G. (2004). Integrin signalling during tumour progression. *Nature Reviews Molecular Cell Biology*, **5** 816-826.
- Gutman, M. & Fidler, I.J. (1995). Biology of human colon cancer metastasis. *World Journal of Surgery*, **19** 226-234.

- Haddock, G., Cross, A.K., Plumb, J., Surr, J., Buttle, D.J., Bunning, R.A.D. & Woodroffe, M.N. (2006). Expression of ADAMTS-1, -4, -5 and TIMP-3 in normal and multiple sclerosis CNS white matter. *Multiple Sclerosis*, **12** 386-396.
- Hanahan, D. & Weinberg, R.A. (2000). The hallmarks of cancer. *Cell*, **100** 57-70.
- Handsley, M.M. & Edwards, D.R. (2005). Metalloproteinases and their inhibitors in tumor angiogenesis. *International Journal of Cancer*, **115** 849-860.
- Harris, J.N., Robinson, P., Lawrance, J., Carrington, B.M., Hopwood, P. & Makin, W. (2003). Symptoms of colorectal liver metastases: Correlation with CT findings. *Clinical Oncology*, **15** 78-82.
- Hashimoto, G., Aoki, T., Nakamura, H., Tanzawa, K. & Okada, Y. (2001). Inhibition of ADAMTS4 (aggrecanase-1) by tissue inhibitors of metalloproteinases (TIMP-1, 2, 3 and 4). *Federation of European Biochemical Societies Letters*, **494** 192-195.
- Hashimoto, G., Shimoda, M. & Okada, Y. (2004). ADAMTS-4 (aggrecanase-1) interaction with the C-terminal domain of fibronectin inhibits proteolysis of aggrecan. *The Journal of Biological Chemistry*, **279** 32483-32491.
- Haubrich, W.S. (2004). Kupffer of Kupffer cells. *Gastroenterology*, **127** 16.
- Hayashida, M., Kawano, H., Nakano, T., Shiraki, K. & Suzuki, A. (2000). Cell death induction by CTL: Perforin/granzyme B system dominantly acts for cell death induction in human hepatocellular carcinoma cells. *Proceedings of the National Academy of Science USA*, **225** 143-150.
- Heinrich, P.C., Behrmann, I., Haan, S., Hermanns, H.M., Müller-Newen, G. & Schaper, F. (2003). Principles of interleukin (IL)-6-type cytokine signalling and its regulation. *The Biochemical Journal*, **374** 1-20.
- Held-Feindt, J., Paredes, E.B., Blomer, U., Seidenbecher, C., Stark, A.M., Mehdorn, H.M. & Mentlein, R. (2006). Matrix-degrading proteases ADAMTS4 and ADAMTS5 (disintegrins and metalloproteinases with thrombospondin motifs 4 and 5) are expressed in human glioblastomas. *International Journal of Cancer*, **118** 55-61.
- Hoffmann, J., Twisselmann, C., Kummer, M.P., Romagnoli, P. & Herzog, V. (2000). A possible role for the Alzheimer amyloid precursor protein in the regulation of epidermal basal cell proliferation. *European Journal of Cell Biology*, **79** 905-914.
- Howard, L., Maciewicz, R.A. & Blobel, C.P. (2000). Cloning and characterization of ADAM28: Evidence for autocatalytic pro-domain removal and for cell surface localization of mature ADAM28. *Biochemical Journal*, **348** 21-27.
- Hu, B., Kong, L.L., Matthews, R.T. & Viapiano, M.S. (2008). The proteoglycan brevican binds to fibronectin after proteolytic cleavage and promotes glioma cell motility. *The Journal of Biological Chemistry*, **283** 24848-24859.

- Huang, J., Bridges, L.C. & White, J.M. (2005). Selective modulation of integrin-mediated cell migration by distinct ADAM family members. *Molecular Biology of the Cell*, **16** 4982-4991.
- Huovila, A.P.J., Almeida, E.A.C. & White, J.M. (1996). ADAMs and cell fusion. *Current Opinion in Cell Biology*, **8** 692-699.
- Huovila, A.P.J., Turner, A.J., Pelto-Huikko, M., Kerkkeinen, I. & Ortiz, R.M. (2005). Shedding light on ADAM metalloproteinases. *Trends in Biochemical Sciences*, **30** 413-422.
- Hurst, L.A., Bunning, R.A.D., Couraund, P., Romero, I.A., Weksler, B.B., Sharrack, B. & Woodroffe, M.N. (2009). Expression of ADAM-17, TIMP3 and fractalkine in the human adult brain endothelial cell line, hCMEC/D3, following pro-inflammatory cytokine treatment. *Journal of Neuroimmunology*, **210** 108-112.
- Hyakudomi, M., Matsubara, T., Hyakudomi, R., Yamamoto, T., Kinugasa, S., Yamanoi, A., Maruyama, R. & Tanaka, T. (2008). Increased expression of fractalkine is correlated with better prognosis and an increased number of both CD8⁺ T cells and natural killer cells in gastric adenocarcinoma. *Annals of Surgical Oncology*, **15** 1775-1782.
- Iba, K., Albrechtsen, R., Gilpin, B.J., Frohlich, C., Loechel, F., Zolkiewska, A., Ishiguro, K., Kojima, T., Liu, W., Langford, J.K., Sanderson, R.D., Brakebusch, C., Fassler, R. & Wewer, U.M. (2000). The cysteine-rich domain of human ADAM12 supports cell adhesion through syndecans and triggers signaling events that lead to β 1 integrin-dependent cell spreading. *The Journal of Cell Biology*, **149** 1143-1155.
- Iba, K., Albrechtsen, R., Gilpin, B.J., Loechel, F. & Wewer, U.M. (1999). Cysteine-rich domain of human ADAM 12 (meltrin- α) supports tumor cell adhesion. *American Journal of Pathology*, **154** 1489-1501.
- Illemann, M., Bird, N.C., Majeed, A., Lærum, O.D., Lund, L.R., Danø, K. & Nielsen, B. (2009). Two distinct expression patterns of urokinase, urokinase receptor and plasminogen activator inhibitor-1 in colon cancer liver metastases. *International Journal of Cancer*, **124** 1860-1870.
- Iredale, J.P. (2001). Hepatic stellate cell behavior during resolution of liver injury. *Seminars in Liver Disease*, **21** 427-436.
- Iruela-Arispe, M.L., Carpizo, D.R. & Luque, A. (2003). ADAMTS-1: A matrix metalloprotease with angioinhibitory properties. *Annals of the New York Academy of Sciences*, **995** 183-190.
- Ishikawa, N., Daigo, Y., Yasui, W., Inai, K., Nishimura, H., Tsuchiya, E., Kohno, N. & Nakamura, Y. (2004). ADAM8 as a novel serological and histochemical marker for lung cancer. *Clinical Cancer Research*, **10** 8363-8370.

- Itabashi, H., Maesawa, C., Oikawa, H., Kotani, K., Sakurai, E., Kato, K., Nitta, H., Kawamura, H., Wakabayashi, G. & Masuda, T. (2008). Angiotensin II and epidermal growth factor receptor cross-talk mediated by a disintegrin and metalloprotease accelerates tumor cell proliferation of hepatocellular carcinoma cell lines. *Hepatology Research*, **38** 601-613.
- Ito, H. & Miki, C. (1999). Profile of circulating levels of interleukin-1 receptor antagonist and interleukin-6 in colorectal cancer patients. *Scandinavian Journal of Gastroenterology*, **34** 1139-1143.
- Jamil, A.M. & Iredale, J.P. (2006). Matrix metalloproteinases, tissue inhibitors of metalloproteinase and matrix turnover and the fate of hepatic stellate cells. *Landes Bioscience and Springer*, **141**.
- Janeway, C.A., Travers, P., Walport, M. & Shlomchik, M.J. (2005). *Immunobiology. The Immune System in Health and Disease*. Sixth ed., New York & London, Garland Science Publishing & Churchill Livingstone.
- Jin, H., Wang, X., Ying, J., Wong, A.H.Y., Li, H., Lee, K.Y., Srivastava, G., Chan, A.T.C., Yeo, W., Ma, B.B.Y., Putti, T.C., Lung, M.L., Shen, Z., Xu, L., Langford, C. & Tao, Q. (2007). Epigenetic identification of ADAMTS-8 as a novel 16q23.1 tumor suppressor frequently silenced in esophageal, nasopharyngeal and multiple other carcinomas. *Oncogene*, **26** 7490-7498.
- Jones, G.C. & Riley, G.P. (2005). ADAMTS proteinases: A multi-domain, multi-functional family with roles in extracellular matrix turnover and arthritis. *Arthritis Research & Therapy*, **7** 160-169.
- Jones, L.L., Margolis, R.U. & Tuszynski, M.H. (2003). The chondroitin sulfate proteoglycans neurocan, brevican, phosphacan, and versican are differentially regulated following spinal cord injury. *Experimental Neurology*, **182** 399-411.
- Jönsson-Rylander, A., Nilsson, T., Fritsche-Danielson, R., Hammarström, A., Behrendt, M., Andersson, J., Lindgren, K., Andersson, A., Wallbrandt, P., Rosengren, B., Brodin, P., Thelin, A., Westin, A., Hurt-Camejo, E. & Lee-Søgaard, C. (2005). Role of ADAMTS-1 in atherosclerosis: Remodeling of carotid artery, immunohistochemistry, and proteolysis of versican. *Arteriosclerosis, Thrombosis, and Vascular Biology*, **25** 180-185.
- Jung, Y., Isaacs, J.S., Lee, S., Trepel, J. & Neckers, L. (2003). IL-1 β -mediated up-regulation of HIF-1 α via an NF κ B/COX-2 pathway identifies HIF-1 as a critical link between inflammation and oncogenesis. *The Federation of American Societies for Experimental Biology Journal*, **17** 2115-2117.

- Karan, D., Lin, F.C., Bryan, M., Ringel, J., Moniaux, N., Lin, M.F. & Batra, S.K. (2003). Expression of ADAMs (a disintegrin and metalloproteases) and TIMP-3 (tissue inhibitor of metalloproteinase-3) in human prostatic adenocarcinomas. *International Journal of Oncology*, **23** 1365-1371.
- Kashiwagi, M., Enghild, J.J., Gendron, C., Hughes, C., Caterson, B., Itoh, Y. & Nagase, H. (2004). Altered proteolytic activities of ADAMTS-4 expressed by C-terminal processing. *The Journal of Biological Chemistry*, **279** 10109-10119.
- Kashiwagi, M., Tortorella, M.D., Nagase, H. & Brew, K. (2001). TIMP-3 is a potent inhibitor of aggrecanase 1 (ADAM-TS4) and aggrecanase 2 (ADAM-TS5). *The Journal of Biological Chemistry*, **276** 12501-12504.
- Kasper, H.U., Drebber, U., Dries, V. & Dienes, H.P. (2005). Liver metastases: Incidence and histogenesis. *Zeitschrift für Gastroenterologie*, **43** 1149-1157.
- Kaushal, G.P. & Shah, S.V. (2000). The new kids on the block: ADAMTSs, potentially multifunctional metalloproteinases of the ADAM family. *The Journal of Clinical Investigation*, **105** 1335-1337.
- Ki, D.H., Jeung, H., Park, C.H., Kang, S.H., Lee, G.Y., Lee, W.S., Kim, N.K., Chung, H.C. & Rha, S.Y. (2007). Whole genome analysis for liver metastasis gene signatures in colorectal cancer. *International Journal of Cancer*, **121** 2005-2012.
- Kieseier, B.C., Pischel, H., Neuen-Jacob, E., Tourtellotte, W.W. & Hartung, H.P. (2003). ADAM-10 and ADAM-17 in the inflamed human CNS. *Glia*, **42** 398-405.
- Kishimoto, T., Akira, S., Narazaki, M. & Taga, T. (1995). Interleukin-6 family of cytokines and gp130. *Blood*, **86** 1243-1254.
- Ko, S.Y., Lin, S.C., Wong, Y.K., Liu, C.J., Chang, K.W. & Liu, T.Y. (2007). Increase of disintegrin metalloprotease 10 (ADAM10) expression in oral squamous cell carcinoma. *Cancer Letters*, **245** 33-43.
- Kodama, T., Ikeda, E., Okada, A., Ohtsuka, T., Shimoda, M., Shiomi, T., Yoshida, K., Nakada, M., Ohuchi, E. & Okada, Y. (2004). ADAM12 is selectively overexpressed in human glioblastomas and is associated with glioblastoma cell proliferation and shedding of heparin-binding epidermal growth factor. *American Journal of Pathology*, **165** 1743-1753.
- Kuefer, R., Day, K.C., Kleer, C.G., Sabel, M.S., Hofer, M.D., Varambally, S., Zorn, C.S., Chinnaiyan, A.M., Rubin, M.A. & Day, M.L. (2006). ADAM15 disintegrin is associated with aggressive prostate and breast cancer disease. *Neoplasia*, **8** 319-329.
- Kuninaka, S., Yano, T., Yokoyama, H., Fukuyama, Y., Terazaki, Y., Uehara, T., Kanematsu, T., Asoh, H. & Ichinose, Y. (2000). Direct influences of pro-inflammatory cytokines (IL-1 β , TNF- α , IL-6) on the proliferation and cell-surface antigen expression of cancer cells. *Cytokine*, **12** 8-11.

- Kuno, K., Bannai, K., Hakozaiki, M., Matsushima, K. & Hirose, K. (2004). The carboxyl-terminal half region of ADAMTS-1 suppresses both tumorigenicity and experimental tumor metastatic potential. *Biochemical and Biophysical Research Communications*, **319** 1327-1333.
- Kuno, K., Okada, Y., Kawashima, H., Nakamura, H., Miyasaka, M., Ohno, H. & Matsushima, K. (2000). ADAMTS-1 cleaves a cartilage proteoglycan, aggrecan. *Federation of European Biochemical Societies Letters*, **478** 241-245.
- Kuntz, E. & Kuntz, H-D. (2005). *Hepatology, Principles and Practice: History, Morphology, Biochemistry, Diagnostics, Clinic, Therapy*. Second ed., Germany, Springer.
- Laemmli, U.K. (1970). Cleavage of structural proteins during the assembly of the head of bacteriophage T4. *Nature*, **227** 680-685.
- Lai, L.C., Kadory, S., Cornell, C. & Lennard, T.W.J. (1993). Possible regulation of soluble ICAM-1 levels by interleukin-1 in a sub-set of breast cysts. *International Journal of Cancer*, **55** 586-589.
- Lambert, E., Dassé, E., Haye, B. & Petitfrère, E. (2004). TIMPs as multifacial proteins. *Critical Reviews in Oncology/Hematology*, **49** 187-198.
- Lammich, S., Kojro, E., Postina, R., Gilbert, S., Pfeiffer, R., Jasionowski, M., Haass, C. & Fahrenholz, F. (1999). Constitutive and regulated α -secretase cleavage of Alzheimer's amyloid precursor protein by a disintegrin metalloprotease. *The Proceedings of the National Academy of Science, USA*, **96** 3922-3927.
- Le Pabic, H., Bonnier, D., Wewer, U.M., Coutand, A., Musso, O., Baffet, G., Clement, B. & Theret, N. (2003). ADAM12 in human liver cancers: TGF- β -regulated expression in stellate cells is associated with matrix remodeling. *Hepatology*, **37** 1056-1066.
- Lee, D.C., Sunnarborg, S.W., Hinkle, C.L., Myers, T.J., Stevenson, M.Y., Russell, W.E., Castner, B.J., Gerhart, M.J., Paxton, R.J., Black, R.A., Chang, A. & Jackson, L.F. (2003). TACE/ADAM17 processing of EGFR ligands indicates a role as a physiological convertase. *Annals of the New York Academy of Sciences*, **995** 22-38.
- Lee, S-J., Namkoong, S., Kim, Y., Kim, C., Lee, H., Ha, K., Chung, H., Kwon, Y. & Kim, Y. (2006). Fractalkine stimulates angiogenesis by activating the raf-1/MEK/ERK- and PI3K/Akt/eNos-dependent signal pathways. *American Journal of Physiology - Heart and Circulation Physiology*, **291** H2836-H2846.
- Lefort, K., Mandinova, A., Ostano, P., Kolev, V., Calpini, V., Kolfschoten, I., Devgan, V., Lieb, J., Raffoul, W., Hohl, D., Neel, V., Garlick, J., Chiorino, G. & Dotto, G.P. (2007). Notch1 is a p53 target gene involved in human keratinocyte tumor suppression through negative regulation of ROCK1/2 and MRCK- α kinases. *Genes and Development*, **21** 562-577.

- Li, L.N., Zhang, H.D., Yuan, S.J., Tian, Z.Y. & Sun, Z.X. (2007). Establishment and characterization of a novel human colorectal cancer cell line (CLY) metastasizing spontaneously to the liver in nude mice. *Oncology Reports*, **17** 835-840.
- Lipman, N.S., Jackson, L.R., Trudel, L.J. & Weis-Garcia, F. (2005). Monoclonal versus polyclonal antibodies: Distinguishing characteristics, applications, and information resources. *Institute for Laboratory Animal Research*, **46** 258-268.
- Liu, K.Z., Man, A., Shaw, R.A., Liang, B., Xu, Z. & Gong, Y. (2006a). Molecular determination of liver fibrosis by synchrotron infrared microspectroscopy. *Biochimica et Biophysica Acta - Biomembranes*, **1758** 960-967.
- Liu, Y.J. Xu, Y. & Yu, Q. (2006b). Full-length ADAMTS-1 and ADAMTS-1 fragments display pro- and antimetastatic activity, respectively. *Oncogene*, **25** 2452-2467.
- Livak, K.J. & Schmittgen, T.D. (2001). Analysis of relative gene expression data using real-time quantitative PCR and the 2^{(-delta delta C(T))} method. *Methods*, **25** 402-408.
- Llamazares, M., Obaya, A.J., Moncada-Pazos, A., Heljasvaara, R., Espada, J., Lopez-Otin, C. & Cal, S. (2007). The ADAMTS12 metalloproteinase exhibits anti-tumorigenic properties through modulation of the ras-dependent ERK signalling pathway. *Journal of Cell Science*, **120** 3544-3552.
- Lodish, H., Berk, A., Zipursky, S.L., Matsudaira, P., Baltimore, D. & Darnell, J. (2000). Cancer. In: Tenney, S. (ed.). *Molecular Cell Biology*. Fourth ed., USA, W.H. Freeman and Company, 1054-1084.
- Loechel, F., Overgaard, M.T., Oxvig, C. & Albrechtsen, R. (1999). Regulation of human ADAM12 protease by the prodomain. *The Journal of Biological Chemistry*, **274** 13427-13433.
- Lu, X., Lu, D., Scully, M.F. & Kakkar, V.V. (2007). Structure-activity relationship studies on ADAM protein-integrin interactions. *Cardiovascular & Hematological Agents in Medicinal Chemistry*, **5** 29-42.
- Luo, D.Z., Vermijlen, D., Ahishali, B., Triantis, V., Plakoutsi, G., Braet, F., Vanderkerken, K. & Wisse, E. (2000). On the biology of pit cells, the liver-specific NK cells. *World Journal of Gastroenterology*, **6** 1-11.
- Luque, A., Carpizo, D.R. & Iruela-Arispe, M.L. (2003). ADAMTS1/METH1 inhibits endothelial cell proliferation by direct binding and sequestration of VEGF165. *The Journal of Biological Chemistry*, **278** 23656-23665.
- Majerus, E.M., Zheng, X., Tuley, E.A. & Sadler, J.E. (2003). Cleavage of the ADAMTS13 propeptide is not required for protease activity. *The Journal of Biological Chemistry*, **278** 46643-46648.
- Martinez-Hernandez, A. (1984). The hepatic extracellular matrix. Electron immunohistochemical studies in normal rat liver. *Laboratory Investigation*, **51** 57-74.

- Masui, T., Hosotani, R., Tsuji, S., Miyamoto, Y., Yasuda, S., Ida, J., Nakajima, S., Kawaguchi, M., Kobayashi, H., Koizumi, M., Toyoda, E., Tulachan, S., Arii, S., Doi, R. & Imamura, M. (2001). Expression of METH-1 and METH-2 in pancreatic cancer. *Clinical Cancer Research*, **7** 3437-3443.
- Mazzocca, A., Coppari, R., de Franco, R., Cho, J.Y., Libermann, T.A., Pinzani, M. & Toker, A. (2005). A secreted form of ADAM9 promotes carcinoma invasion through tumor-stromal interactions. *Cancer Research*, **65** 4728-4738.
- McColloch, D.R., Akl, P., Samarasinghe, H., Herington, A.C. & Odorico, D.M. (2004). Expression of the disintegrin metalloprotease, ADAM-10, in prostate cancer and its regulation by dihydrotestosterone, insulin-like growth factor I, and epidermal growth factor in the prostate cancer cell model LNCaP. *Clinical Cancer Research*, **10** 314-323.
- McLane, M.A., Marcinkiewicz, C., Vijay-Kumar, S., Wierzbicka-Patynowski, I. & Niewiarowski, S. (1998). Viper venom disintegrins and related molecules. *Proceedings of the Society for Experimental Biology and Medicine*, **219** 109-119.
- McMillan, D.C. & McArdle, C.S. (2007). Epidemiology of colorectal metastases. *Surgical Oncology*, **16** 3-5.
- Meng, J.Y., Kataoka, H., Itoh, H. & Kono, M. (2001). Amyloid β protein precursor is involved in the growth of human colon carcinoma cell *in vitro* and *in vivo*. *International Journal of Cancer*, **92** 31-39.
- Merchant, N.B., Voskresensky, I., Rogers, C.M., LaFleur, B., Dempsey, P.J., Graves-Deal, R., Revetta, F., Foutch, A.C., Rothenberg, M.L., Washington, M.K. & Coffey, R.J. (2008). TACE/ADAM-17: A component of the epidermal growth factor receptor axis and a promising therapeutic target in colorectal cancer. *Clinical Cancer Research*, **14** 1182-1191.
- Mężyk, R., Bzowska, M. & Bereta, J. (2003). Structure and functions of tumor necrosis factor- α converting enzyme. *Acta Biochimica Polonica*, **50** 625-645.
- Milani, S., Pinzani, M. & Casini, A. (1992). Interstitial collagenase gene is differentially expressed in human liver and cultured fat-storing cells. *Hepatology*, **16** 186.
- Milla, M.E., Leesnitzer, M.A., Moss, M.L., Moss, M.L., Clay, W.C., Carter, H.L., Miller, A.B., Su, J.L., Lambert, M.H., Willard, D.H., Sheeley, D.M., Kost, T.A., Burkhart, W., Moyer, M., Blackburn, R.K., Pahel, G.L., Mitchell, J.L., Hoffman, C.R. & Becherer, J.D. (1999). Specific sequence elements are required for expression of functional tumor necrosis factor- α -converting enzyme (TACE). *The Journal of Biological Chemistry*, **274** 30563-30570.

- Mitsui, Y., Mochizuki, S., Kodama, T., Shimoda, M., Ohtsuka, T., Shiomi, T., Chijiwa, M., Ikeda, T., Kitajima, M. & Okada, Y. (2006). ADAM28 is overexpressed in human breast carcinomas: Implications for carcinoma cell proliferation through cleavage of insulin-like growth factor binding protein-3. *Cancer Research*, **66** 9913-9920.
- Miyazaki, T., Kato, H., Nakajima, M., Faried, A., Takita, J., Sohda, M., Fukai, Y., Yamaguchi, S., Masuda, N., Manda, R., Fukuchi, M., Ojima, H., Tsukada, K. & Kuwano, H. (2004). An immunohistochemical study of TIMP-3 expression in oesophageal squamous cell carcinoma. *British Journal of Cancer*, **91** 1556-1560.
- Mohammed, F.F., Smookler, D.S., Taylor, S.E., Fingleton, B., Kassiri, Z., Sanchez, O.H., English, J.L., Matrisian, L.M., Au, B., Yeh, W.C. & Khokha, R. (2004). Abnormal TNF activity in Timp3^{-/-} mice leads to chronic hepatic inflammation and failure of liver regeneration. *Nature Genetics*, **36** 969-977.
- Morini, S., Carotti, S., Carpino, G., Franchitto, A., Corradini, S.G., Merli, M. & Gaudio, E. (2005). GFAP expression in the liver as an early marker of stellate cells activation. *Italian Journal of Anatomy and Embryology*, **110** 193-207.
- Muehlhoefer, A., Saubermann, L.J., Luedtke-Heckenkamp, K., Xavier, R., Blumberg, R.S., Podolsky, R.S., Podolsky, D.K., MacDermott, R.P. & Rreinecker, H.C. (2000). Fractalkine is an epithelial and endothelial cell-derived chemoattractant for intraepithelial lymphocytes in the small intestinal mucosa. *Journal of Immunology*, **164** 3368-3376.
- Murillo, M.M., del Castillo, G., Sanchez, A., Fernandez, M. & Fabregat, I. (2005). Involvement of EGF receptor and c-Src in the survival signals induced by TGF- β 1 in hepatocytes. *Oncogene*, **24** 4580-4587.
- Nagase, H., Visse, R. & Murphy, G. (2006). Structure and function of matrix metalloproteinases and TIMPs. *Cardiovascular Research*, **69** 562-573.
- Nakabayashi, H., Takata, K., Miyano, K., Yamane, T. & Sato, J. (1982). Growth of human hepatoma cells lines with differentiated functions in chemically defined medium. *Cancer Research*, **42** 3858-3863.
- Nakagawa, T., Kabuto, M., Kubota, T., Koderu, T. & Sato, K. (1999). Production of amyloid β protein precursor as a proteinase inhibitor by human astrocytic tumors. *Anticancer Research*, **19** 2963-2968.
- Nakashima, T., Okuda, K., Kojiro, M., Jimi, A., Yamaguchi, R., Sakamoto, K. & Ikari, T. (1983). Pathology of hepatocellular carcinoma in Japan. *Cancer*, **51** 863-877.
- Nath, D., Williamson, N.J., Jarvis, R. & Murphy, G. (2001). Shedding of c-Met is regulated by crosstalk between a G-protein coupled receptor and the EGF receptor and is mediated by a TIMP-3 sensitive metalloproteinase. *Journal of Cell Science*, **114** 1213-1220.

- Naylor, M.S., Stamp, G.W.H. & Balkwill, F.R. (1990). Investigation of cytokine gene expression in human colorectal cancer. *Cancer Research*, **50** 4436-4440.
- Nutt, C.L., Matthews, R.T. & Hockfield, S. (2001). Glial tumor invasion: A role for the upregulation and cleavage of BEHAB/brevican. *The Neuroscientist*, **7** 113-122.
- Nyberg, P., Ylipalosaari, M., Sorsa, T. & Salo, T. (2006). Trypsins and their role in carcinoma growth. *Experimental Cell Research*, **312** 1219-1228.
- Oda, K., Matsuoka, Y., Funahashi, A. & Kitano, H. (2005). A comprehensive pathway map of epidermal growth factor receptor signaling. *Molecular Systems Biology*, doi: **10.1038/msb4100014**.
- Ohta, M., Tanaka, F., Yamaguchi, H., Sadanaga, N., Inoue, H. & Mori, M. (2005). The high expression of fractalkine results in a better prognosis for colorectal cancer patients. *International Journal of Oncology*, **26** 41-47.
- Ohtsuka, T., Shiomi, T., Shimoda, M., Kodama, T., Amour, A., Murphy, G., Ohuchi, E., Kobayashi, K. & Okada, Y. (2006). ADAM28 is overexpressed in human non-small cell lung carcinomas and correlates with cell proliferation and lymph node metastasis. *International Journal of Cancer*, **118** 263-273.
- Ohuchi, E., Imai, K. & Fujii, Y. (1997). Membrane type 1 matrix metalloproteinase digests interstitial collagens and other extracellular matrix macromolecules. *The Journal of Biological Chemistry*, **272** 53-58.
- Okano, K., Yamamoto, J., Kosuge, T., Yamamoto, S., Sakamoto, M., Nakanishi, Y. & Hirohashi, S. (2000). Fibrous pseudocapsule of metastatic liver tumors from colorectal carcinoma. clinicopathologic study of 152 first resection cases. *Cancer*, **89** 267-275.
- Oleksowicz, L., Bhagwati, N. & DeLeon-Fernandez, M. (1999). Deficient activity of von Willebrand's factor-cleaving protease in patients with disseminated malignancies. *Cancer Research*, **23** 2244-2250.
- O'Shea, C., McKie, N., Buggy, Y., Duggan, C., Hill, A.D.K., McDermott, E., O'Higgins, N. & Duffy, M.J. (2003). Expression of ADAM-9 mRNA and protein in human breast cancer. *International Journal of Cancer*, **105** 754-761.
- Parkin, D.M., Bray, F., Ferlay, J. & Pisani, P. (2005). Global cancer statistics, 2002. *CA: A Cancer Journal for Clinicians*, **55** 74-108.
- Paschos, K.A., Canovas, D. & Bird, N.C. (2009). The role of cell adhesion molecules in the progression of colorectal cancer and the development of liver metastasis. *Cellular Signalling*, **21** 665-674.
- Pfaffl, M.W. (2001). A new mathematical model for relative quantification in real-time RT-PCR. Online: *Nucleic Acids Research*, **29** e45.

- Pietrzik, C.U., Hoffmann, J., Stober, K., Chen, C.Y., Bauer, C., Otero, D.A.C., Roch, J.M. & Herzog, V. (1998). From differentiation to proliferation: The secretory amyloid precursor protein as a local mediator of growth in thyroid epithelial cells. *The Proceedings of the National Academy of Science, USA*, **95** 1770-1775.
- Plumb, J., McQuaid, S., Cross, A.K., Surr, J., Haddock, G., Bunning, R.A.D. & Woodroffe, M.N. (2006). Upregulation of ADAM-17 expression in active lesions in multiple sclerosis. *Multiple Sclerosis*, **12** 375-385.
- Porter, S., Clark, I.M., Kevorkian, L. & Edwards, D.R. (2005). Review article: The ADAMTS metalloproteinases. *Biochemical Journal*, **386** 15-27.
- Porter, S., Scott, S.D., Sassoon, E.M., Williams, M.R., Jones, J.L., Girling, A.C., Ball, R.Y. & Edwards, D.R. (2004). Dysregulated expression of adamalysin-thrombospondin genes in human breast carcinoma. *Clinical Cancer Research*, **10** 2429-2440.
- Porter, S., Span, P.N., Sweep, F.C.G.J., Tjan-Heijnen, V.C.G., Pennington, C.J., Pedersen, T.X., Johnsen, M., Lund, L.R., Romer, J. & Edwards, D.R. (2006). *ADAMTS8* and *ADAMTS15* expression predicts survival in human breast carcinoma. *International Journal of Cancer*, **118** 1241-1247.
- Powe, D.G., Brough, J.L., Carter, G.I., Bailey, E.M., Stetler-Stevenson, W.G., Turner, D.R. & Hewitt, R.E. (1997). TIMP-3 mRNA expression is regionally increased in moderately and poorly differentiated colorectal adenocarcinomas. *British Journal of Cancer*, **75** 1678-1683.
- Primakoff, P. & Myles, D.G. (2000). The ADAM gene family: Surface proteins with adhesion and protease activity. *Trends in Genetics*, **16** 83-87.
- Radinsky, R. (1995). Molecular mechanisms for organ-specific colon carcinoma metastasis. *European Journal of Cancer*, **31A** 1091-1095.
- Rahman, M., Lane, A., Swindell, A. & Bartman, S. (2005). *Introduction to flow cytometry*. UK, AbD seroTec.
- Rajaganeshan, R., Prasad, R., Guillou, P.J., Chalmers, C.R., Scott, N., Sarkar, R., Poston, G. & Jayne, D.G. (2007). The influence of invasive growth pattern and microvessel density on prognosis in colorectal cancer and colorectal liver metastases. *British Journal of Cancer*, **96** 1112-1117.
- Ray, J.M. & Stetler-Stevenson, W.G. (1994). The role of matrix metalloproteinases and their inhibitors in tumour invasion, metastasis and angiogenesis. *European Respiratory Journal*, **7** 2062-2072.
- Reed, J.R., Leon, R.P., Hall, M.K. & Schwertfeger, K.L. (2009). Interleukin-1 β and fibroblast growth factor receptor 1 cooperate to induce cyclooxygenase-2 during early mammary tumorigenesis. Online: *Breast Cancer Research*, **11** R21.

- Ringel, J., Jesnowski, R., Moniaux, N., Luttgies, J., Ringel, J., Choudhury, A., Batra, S.K., Kloppel, G. & Lohr, M. (2006). Aberrant expression of a disintegrin and metalloproteinase 17/tumor necrosis factor- α converting enzyme increase the malignant potential in human pancreatic ductal adenocarcinoma. *Cancer Research*, **66** 9045-9053.
- Robertson, M.J. & Ritz, J. (1990). Biology and clinical relevance of human NK cells. *Blood*, **76** 2421-2438.
- Rocks, N., Paulissen, G., El Hour, M., Quesada, F., Crahay, C., Gueders, M., Foidart, J.M., Noel, A. & Cataldo, D. (2008). Emerging roles of ADAM and ADAMTS metalloproteinases in cancer. *Biochimie*, **90** 369-379.
- Rocks, N., Paulissen, G., Quesada Calvo, F., Polette, M., Gueders, M., Munaut, C., Foidart, J.M., Noel, A., Birembaut, P. & Cataldo, D. (2006). Expression of a disintegrin and metalloprotease (ADAM and ADAMTS) enzymes in human non-small-cell lung carcinomas (NSCLC). *British Journal of Cancer*, **94** 724-730.
- Rodríguez-Manzaneque, J.C., Milchanowski, A.B., Dufour, E.K., Leduc, R. & Iruela-Arispe, M.L. (2000). Characterization of METH-1/ADAMTS1 processing reveals two distinct active forms. *The Journal of Biological Chemistry*, **275** 33471-33479.
- Rodríguez-Manzaneque, J.C., Westling, J., Thai, S.N., Luque, A., Knauper, V., Murphy, G., Sandy, J.D. & Iruela-Arispe, M.L. (2002). ADAMTS1 cleaves aggrecan at multiple sites and is differentially inhibited by metalloproteinase inhibitors. *Biochemical and Biophysical Research Communications*, **293** 501-508.
- Roemer, A., Schwettmann, L., Jung, M., Kristiansen, G., Schnorr, D., Loening, S.A., Jung, K. & Lichtinghagen, R. (2004). Increased mRNA expression of ADAMs in renal cell carcinoma and their association with clinical outcome. *Oncology Reports*, **11** 529-536.
- Roy, D., Sarkar, S. & Felty, Q. (2006). Levels of IL-1 β control stimulatory/inhibitory growth of cancer cells. *Frontiers in Bioscience*, **11** 889-898.
- Roy, R., Zhang, B. & Moses, M.A. (2006). Making the cut: Protease-mediated regulation of angiogenesis. *Experimental Cell Research*, **312** 608-622.
- Rundhaug, J.E. (2003). Matrix metalloproteinases, angiogenesis, and cancer. *Clinical Cancer Research*, **9** 551-554.
- Russell, D.L., Doyle, K.M.H., Ochsner, S.A., Sandy, J.D. & Richards, J.S. (2003). Processing and localisation of ADAMTS-1 and proteolytic cleavage of versican during cumulus matrix expansion and ovulation. *The Journal of Biological Chemistry*, **278** 42330-42339.
- Ryder, S.D. (2003). Guidelines for the diagnosis and treatment of hepatocellular carcinoma (HCC) in adults. *Gut*, **52** 1-8.

- Sahin, U., Weskamp, G., Kelly, K., Zhou, H.M., Higashiyama, S., Peschon, J., Hartmann, D., Saftig, P. & Blobel, C.P. (2004). Distinct roles for ADAM10 and ADAM17 in ectodomain shedding of six EGFR ligands. *The Journal of Cell Biology*, **164** 769-779.
- Sakakibara, K., Igarashi, S. & Hatahara, T. (1985). Localization of type III procollagen aminopeptide antigenicity in hepatocytes from cirrhotic human liver. *Virchows Archiv*, **408** 219-228.
- Sander, L.E., Trautwein, C. & Liedtke, C. (2007). Is interleukin-6 a gender-specific risk factor for liver cancer? *Hepatology*, **46** 1304-1305.
- Schäfer, A., Schulz, C., Eigenthaler, M., Fraccarollo, D., Kobsar, A., Gawaz, M., Ertl, G., Walter, U. & Bauersach, J. (2004). Novel role of the membrane-bound chemokine fractalkine in platelet activation and adhesion. *Blood*, **103** 407-412.
- Schlomann, U., Wildeboer, D., Webster, A., Antropova, O., Zeuschner, D., Knight, C.G., Docherty, A.J.P., Lambert, M., Skelton, L., Jockusch, H. & Bartsch, J.W. (2002). The metalloprotease disintegrin ADAM28. *The Journal of Biological Chemistry*, **277** 48210-48219.
- Schlöndorff, J., Becherer, J.D. & Blobel, C.P. (2000). Intracellular maturation and localization of the tumour necrosis factor α convertase (TACE). *Biochemical Journal*, **347** 131-138.
- Schütz, A., Hartig, W., Wobus, M., Grosche, J., Wittekind, C. & Aust, G. (2005). Expression of ADAM15 in lung carcinomas. *Virchows Archiv*, **446** 421-429.
- Seals, D.F. & Courtneidge, S.A. (2003). The ADAMs family of metalloprotease: Multidomain proteins with multiple functions. *Genes and Development*, **17** 7-30.
- Selden, C., Khalil, M. & Hodgson, H.J.F. (1999). What keeps hepatocytes on the straight and narrow? Maintaining differentiated function in the liver. *Gut*, **44** 443-446.
- Sharghi-Namini, S., Fan, H.P., Sulochana, K.N., Potturi, P., Xiang, W., Chong, Y.S., Wang, Z.Y., Yang, H. & Ge, R.W. (2008). The first but not the second thrombospondin type 1 repeat of ADAMTS5 functions as an angiogenesis inhibitor. *Biochemical and Biophysical Research Communications*, **371** 215-219.
- Sheikh, M.S. & Fornace, A.J. (2000). Death and decoy receptors and p53-mediated apoptosis. *Leukemia*, **14** 1509-1513.
- Shimada, H., Tanaka, K., Matsuo, K. & Togo, S. (2006). Treatment for multiple bilobar liver metastases of colorectal cancer. *Langenbeck's Archives of Surgery*, **391** 130-142.
- Shintani, Y., Higashiyama, S., Ohta, M., Hirabayashi, H., Yamamoto, S., Yoshimasu, T., Matsuda, H. & Matsuura, N. (2004). Overexpression of ADAM9 in non-small cell lung cancer correlates with brain metastasis. *Cancer Research*, **64** 4190-4196.

- Simpson, K.J., Lukacs, N.W., Colletti, L., Strieter, R.M. & Kunkel, S.L. (1997). Cytokines and the liver. *Journal of Hepatology*, **27** 1120-1132.
- Somerville, R.P., Longpre, J.M., Apel, E.D., Lewis, R.M., Wang, L.W., Sanes, J.S., Leduc, R. & Apte, S.S. (2004). ADAMTS7B, the full-length product of the *ADAMTS7* gene, is a chondroitin sulfate proteoglycan containing a mucin domain. *The Journal of Biological Chemistry*, **279** 35159-35175.
- Somerville, R.P., Longpre, J.M., Jungers, K.A., Engle, J.M., Ross, M., Evanko, S., Wight, T.N., Leduc, R. & Apte, S.S. (2003). Characterization of ADAMTS-9 and ADAMTS-20 as a distinct ADAMTS subfamily related to *Caenorhabditis elegans* GON-1. *The Journal of Biological Chemistry*, **278** 9503-9513.
- Somerville, R.P.T., Jungers, K.A. & Apte, S.S. (2004). Discovery and characterization of a novel, widely expressed metalloprotease, ADAMTS10, and its proteolytic activation. *The Journal of Biological Chemistry*, **279** 51208-51217.
- Stern, R. (2004). Hyaluronan catabolism: A new metabolic pathway. *European Journal of Cell Biology*, **83** 317-325.
- Stessels, F., Van den Eynden, G., Van der Auwera, I., Salgado, R., Van den Heuvel, E., Harris, A.L., Jackson, D.G., Colpaert, C.G., Van Marck, E.A., Dirix, L.Y. & Vermeulen, P.B. (2004). Breast adenocarcinoma liver metastases, in contrast to colorectal liver metastases, display a non-angiogenic growth pattern that preserves the stroma and lacks hypoxia. *British Journal of Cancer*, **90** 1429-1436.
- Stöcker, W., Grams, F., Baumann, U., Reinemer, P., Gomis-Ruth, F.X., McKay, D.B. & Bode, W. (1995). The metzincins - topological and sequential relations between the astacins, adamalysins, serralyins, and matrixins (collagenases) define a superfamily of zinc-peptidases. *Protein Science*, **4** 823-840.
- Sturm, J.W., Magdeburg, R., Berger, K., Petruch, B., Samel, S., Bönninghoff, R., Keese, M., Hafner, M. & Post, S. (2003). Influence of TNF α on the formation of liver metastases in a synergic mouse model. *International Journal of Cancer*, **107** 11-21.
- Stylianou, S., Clarke, R.B. & Brennan, K. (2006). Aberrant activation of Notch signaling in human breast cancer. *Cancer Research*, **66** 1517-1525.
- Sunnarborg, S.W., Hinkle, C.L., Stevenson, M., Russell, W.E., Raska, C.S., Peschon, J.J., Castner, B.J., Gerhart, M.J., Paxton, R.J., Black, R.A. & Lee, D.C. (2002). Tumor necrosis factor- α converting enzyme (TACE) regulates epidermal growth factor receptor ligand availability. *The Journal of Biological Chemistry*, **277** 12838-12845.
- Szymanska, R. & Schmidt-Pospula, M. (1979). Studies of liver's reticuloendothelial cells by Tadeusz Browicz and Karl Kupffer. A historical outline. *History of Medicine*, **42** 331-336.

- Takeda, S., Igarashi, T., Mori, H. & Araki, S. (2006). Crystal structures of VAP1 reveal ADAMs' MDC domain architecture and its unique C-shaped scaffold. *The European Molecular Biology Organisation Journal*, **25** 2388-2396.
- Tanabe, C., Hotoda, N., Sasagawa, N., Sehara-Fujisawa, A., Maruyama, K. & Ishiura, S. (2007). ADAM19 is tightly associated with constitutive Alzheimer's disease APP α -secretase in A172 cells. *Biochemical and Biophysical Research Communications*, **352** 111-117.
- Tanaka, Y., Miyamoto, S., Suzuki, S.O., Ok, E., Yagi, H., Sonoda, K., Yamazaki, A., Mizushima, H., Maehara, E. & Nakano, H. (2005). Clinical significance of heparin-binding epidermal growth factor-like growth factor and a disintegrin and metalloprotease 17 expression in human ovarian cancer. *Clinical Cancer Research*, **11** 4783-4792.
- Tannapfel, A., Anhalt, K., Hausermann, P., Sommerer, F., Benicke, M., Uhlmann, D., Witzigmann, H., Hauss, J. & Wittekind, C. (2003). Identification of novel proteins associated with hepatocellular carcinomas using protein microarrays. *Journal of Pathology*, **201** 238-249.
- Thompson, E.W. & Price, J.T. (2002). Mechanisms of tumour invasions and metastasis: Emerging targets for therapy. *Expert Opinions on Therapeutic Targets*, **6** 217-233.
- Tian, B.L., Wen, J.M., Zhang, M., Xu, R.B. & Luo, C.J. (2002). The expression of ADAM12 (meltrin- α) in human giant cell tumours of bone. *Journal of Clinical Pathology incorporating Molecular Pathology*, **55** 394-397.
- Tisdale, M.J. (2002). Cachexia in cancer patients. *Nature Reviews Cancer*, **2** 862-871.
- Tortorella, M.D., Arner, E.C., Hills, R., Easton, A., Korte-Sarfaty, J., Fok, K., Wittwer, A.J., Liu, R. & Malfait, A. (2004). α_2 -macroglobulin is a novel substrate for ADAMTS-4 and ADAMTS-5 and represents an endogenous inhibitor of these enzymes. *The Journal of Biological Chemistry*, **279** 17554-17561.
- Tortorella, M.D., Pratta, M., Lui, R., Austin, J., Ross, O.H., Abbaszade, I., Burn, T. & Arner, E. (2000). Sites of aggrecan cleavage by recombinant human aggrecanase-1 (ADAMTS-4). *The Journal of Biological Chemistry*, **275** 18566-18573.
- Toussey, T., Jorissen, E., Reiss, K. & Hartmann, D. (2006). (Make) stick and cut loose - Disintegrin metalloproteases in development and disease. *Birth Defects Research*, **78** 24-46.
- Towbin, H., Staehelin, T. & Gordon, J. (1979). Electrophoretic transfer of proteins from polyacrylamide gels to nitrocellulose sheets: Procedure and some applications. *Proceedings of the National Academy of Science, USA*, **76** 4350-4354.
- Trochon, V., Li, H., Vasse, M., Frankenne, F., Thomaidis, A., Soria, J., Lu, H., Gardner, C. & Soria, C. (1998). Endothelial metalloprotease-disintegrin protein (ADAM) is implicated in angiogenesis *in vitro*. *Angiogenesis*, **2** 277-285.

- Trochon-Joseph, V., Martel-Renoir, D., Mir, L.M., Thomaidis, A., Opolon, P., Connault, E., Li, H., Grenet, C., Fauvel-Lafeve, F., Soria, J., Legrand, C., Soria, C., Perricaudet, M. & Lu, H. (2004). Evidence of antiangiogenic and antimetastatic activities of the recombinant disintegrin domain of metargidin. *Cancer Research*, **64** 2062-2069.
- Tucker, R.P. (2004). The thrombospondin type 1 repeat superfamily. *The International Journal of Biochemistry & Cell Biology*, **36** 969-974.
- Turner, S.L., Blair-Zajdel, M.E. & Bunning, R.A.D. (2009). ADAMs and ADAMTSs in cancer. *British Journal of Biomedical Science*, **66** 117-128.
- Umehara, H., Bloom, E.T., Okazaki, T., Nagano, Y., Yoshie, O. & Imai, T. (2004). Fractalkine in vascular biology: From basic research to clinical disease. *Arteriosclerosis, Thrombosis and Vascular Biology*, **24** 34-40.
- Ushiki, T. (2002). Collagen fibers, reticular fibers and elastic fibers. A comprehensive understanding from a morphological viewpoint. *Archives of Histology and Cytology*, **65** 109-126.
- Valkovskaya, N., Kayed, H., Felix, K., Hartmann, D., Giese, N.A., Osinsky, S.P., Friess, H. & Kleeff, J. (2007). ADAM8 expression is associated with increased invasiveness and reduced patient survival in pancreatic cancer. *Journal of Cellular and Molecular Medicine*, **11** 1162-1174.
- Van Wart, H.E. & Birkedal-Hansen, H. (1990). The cysteine switch: A principle of regulation of metalloproteinase activity with potential applicability to the entire matrix metalloproteinase gene family. *The Proceedings of the National Academy of Science, USA*, **87** 5578-5582.
- Vandesompele, J., De Preter, K., Pattyn, F., Poppe, B., Van Roy, N., De Paepe, A. & Speleman, F. (2002). Accurate normalization of real-time quantitative RT-PCR data by geometric averaging of multiple internal genes. Online: *Genome Biology*, **3** 0034.1-0034.11.
- Vázquez, F., Hastings, G., Ortega, M.A., Lane, T.F., Oikemus, S., Lombardo, M. & Iruela-Arispe, M.L. (1999). METH-1, a human ortholog of ADAMTS-1, and METH-2 are members of a new family of proteins with angio-inhibitory activity. *The Journal of Biological Chemistry*, **274** 23349-23357.
- Vermeulen, P.B., Colpaert, C., Salgado, R., Royers, R., Hellemans, H., Van den Heuvel, E., Goovaerts, G., Dirix, L.Y. & Van Marck, E. (2001). Liver metastases from colorectal adenocarcinomas grow in three patterns with different angiogenesis and desmoplasia. *Journal of Pathology*, **195** 336-342.
- Viapiano, M.S., Bi, W.L., Piepmeier, J., Hockfield, S. & Matthews, R.T. (2005). Novel tumor-specific isoforms of BEHAB/brevican identified in human malignant gliomas. *Cancer Research*, **65** 6726-6733.

- Viapiano, M.S., Hockfield, S. & Matthews, R.T. (2008). BEHAB/brevican requires ADAMTS-mediated proteolytic cleavage to promote glioma invasion. *Journal of Neuro-Oncology*, **88** 261-272.
- Viapiano, M.S. & Matthews, R.T. (2006). From barriers to bridges: Chondroitin sulfate proteoglycans in neuropathology. *Trends in Molecular Medicine*, **12** 488-496.
- Volin, M.V., Woods, J.M., Amin, M.A., Connors, M.A. & Koch, A.E. (2001). Fractalkine: A novel angiogenic chemokine in rheumatoid arthritis. *American Journal of Pathology*, **159** 1521-1530.
- Wajant, H., Pfizenmaier, K. & Scheurich, P. (2003). Tumour necrosis factor signaling. *Cell Death and Differentiation*, **10** 45-65.
- Wang, P., Tortorella, M.D., England, K., Malfait, A.M., Thomas, G., Arner, E.C. & Pei, D. (2004). Proprotein convertase furin interacts with and cleaves pro-ADAMTS4 (aggrecanase-1) in the *trans*-Golgi network. *The Journal of Biological Chemistry*, **279** 15434-15440.
- Wasmuth, H.E., Zaldivar, M.M., Berres, M., Werth, A., Scholten, D., Hillebrandt, S., Tacke, F., Schmitz, P., Dahl, E., Wiederholt, T., Hellerbrand, C., Berg, T., Weiskirchen, R., Trautwein, C. & Lammert, F. (2008). The fractalkine receptor CX3CR1 is involved in liver fibrosis due to chronic hepatitis C infection. *Journal of Hepatology*, **48** 208-215.
- Wheeler, M.D. (2003). Endotoxin and Kupffer cell activation in alcoholic liver disease. *National Institute on Alcohol Abuse and Alcoholism*, **27** 300-306.
- Whitworth, M.K., Sheen, A., Rosa, D.D., Duff, S.E., Ryder, D., Burumdayal, A., Wiener, K., Hawkins, R.E., Saunders, M., Valle, J.W., Sherlock, D. & Jayson, G.C. (2006). Impact of laparotomy and liver resection on the peritoneal concentrations of fibroblast growth factor 2, vascular endothelial growth factor and hepatocyte growth factor. *Journal of Cancer Research and Clinical Oncology*, **132** 41-44.
- Wight, T.N. & Merrilees, M.J. (2004). Proteoglycans in atherosclerosis and restenosis: Key roles for versican. *Circulation Research*, **94** 1158-1167.
- Wildeboer, D., Naus, S., Amy Sang, Q.X., Bartsch, J.W. & Pagenstecher, A. (2006). Metalloproteinase disintegrins ADAM8 and ADAM19 are highly regulated in human primary brain tumors and their expression levels and activities are associated with invasiveness. *Journal of Neuropathology and Experimental Neurology*, **5** 516-527.
- Wilhelm, S., Gröbler, B. & Heinz, H. (c2006). *Confocal laser scanning microscopy: Principles*. Online at:
<http://zeiss-campus.magnet.fsu.edu/referencelibrary/pdfs/ZeissConfocalPrinciples.pdf>.

- Winau, F., Hegasy, G., Weiskirchen, R., Weber, S., Cassan, C., Sieling, P.A., Modlin, R.L., Liblau, R.S., Gressner, A.M. & Kaufmann, S.H. (2007). Ito cells are liver-resident antigen-presenting cells for activating T cell responses. *Immunity*, **26** 117-129.
- Wiseman, B.S. & Werb, Z. (2002). Stromal effects on mammary gland development and breast cancer. *Science*, **296** 1046-1049.
- Xu, L., Hui, A.Y., Albanis, E., Arthur, M.J., O'Byrne, S.M., Blaner, W.S., Mukherjee, P., Friedman, S.L. & Eng, F.J. (2005). Human hepatic stellate cell lines, LX-1 and LX-2: New tools for analysis of hepatic fibrosis. *Gut*, **54** 142-151.
- Yamaguchi, Y. (2000). Lecticans: Organisers of the brain extracellular matrix. *Cellular and Molecular Life Sciences*, **57** 276-289.
- Yamamoto, S., Higuchi, Y., Yoshiyama, K., Shimizu, E., Kataoka, M., Hijiya, N. & Matsuura, K. (1999). ADAM family proteins in the immune system. *Immunology Today*, **20** 278-284.
- Yamasaki, M., Takemasa, I., Komori, T., Watanabe, S., Sekimoto, M., Doki, Y., Matsubara, K. & Monden, M. (2007). The gene expression profile represents the molecular nature of liver metastasis in colorectal cancer. *International Journal of Oncology*, **30** 129-138.
- Yoshimura, T., Tomita, T., Dixon, M.F., Axon, A.T.R., Robinson, P.A. & Crabtree, J.E. (2002). ADAMs (A disintegrin and metalloproteinase) messenger RNA expression in helicobacter pylori-infected, normal, and neoplastic gastric mucosa. *The Journal of Infectious Diseases*, **185** 332-340.
- Zar, J.H. (1999). *Biostatistical analysis*. Fourth ed., UK, Prentice Hall International, Inc.
- Zeng, Z., Sun, Y., Shu, W. & Guillem, J.G. (2001). Tissue inhibitor of metalloproteinase-3 is a basement membrane-associated protein that is significantly decreased in human colorectal cancer. *Diseases of the Colon and Rectum*, **44** 1290-1296.
- Zhang, H., Kelly, G., Zerillo, C., Jaworski, D.M. & Hockfield, S. (1998). Expression of a cleaved brain-specific extracellular matrix protein mediates glioma cell invasion *in vivo*. *The Journal of Neuroscience*, **18** 2370-2376.
- Zheng, X., Chung, D., Takayama, T.K., Majerus, E.M., Sadler, J.E. & Fujikawa, K. (2001). Structure of von Willebrand factor-cleaving protease (ADAMTS13), a metalloprotease involved in thrombotic thrombocytopenic purpura. *The Journal of Biological Chemistry*, **276** 41059-41063.
- Zheng, X., Jiang, F., Katakowski, M., Kalkanis, S.N., Hong, X., Zhang, X., Zhang, Z.G., Yang, H. & Chopp, M. (2007). Inhibition of ADAM17 reduces hypoxia-induced brain tumor cell invasiveness. *Cancer Science*, **98** 674-684.

- Zigrino, P., Mauch, C., Fox, J.W. & Nischt, R. (2005). ADAM-9 expression and regulation in human skin melanoma and melanoma cell lines. *International Journal of Cancer*, **116** 853-859.
- Zimmermann, D.R. & Dours-Zimmerman, M.T. (2008). Extracellular matrix of the central nervous system: From neglect to challenge. *Histochemistry and Cell Biology*, **130** 635-653.
- Zimmers, T.A., McKillop, I.H., Pierce, R.H., Yoo, J. & Koniaris, L.G. (2003). Massive liver growth in mice induced by systemic interleukin 6 administration. *Hepatology*, **38** 326-334.
- Zlokovic, B.V. (2006). Remodeling after stroke. *Nature Medicine*, **12** 390-391.
- Zvibel, I., Halay, E. & Reid, L.M. (1991). Heparin and hormonal regulation of mRNA synthesis and abundance of autocrine growth factors: Relevance to clonal growth of tumors. *Molecular and Cellular Biology*, **11** 108-116.

Journal Publication

Turner, S.L., Blair-Zajdel, M.E. & Bunning, R.A.D. (2009). ADAMs and ADAMTSs in cancer. *British Journal of Biomedical Science*, **66** 117-128.

Conference Presentations (Poster)

Turner, S.L., Bird, N.C., Mangnall, D., Blair-Zajdel, M.E. & Bunning, R.A.D. Study into the expression of ADAM17, ADAMTS-1, -4, -5 and TIMP3 by hepatoma cell line HepG2 and hepatic stellate cell line LX-2. Cancer Degradome Symposium, 8th – 9th October 2008, London, UK

Turner, S.L., Bird, N.C., Mangnall, D., Blair-Zajdel, M.E. & Bunning, R.A.D. Study into the expression of ADAM17, ADAMTS-1, -4, -5 and TIMP3 by hepatic stellate cell line LX-2 and hepatoma cell line HepG2. 14th International Symposium on Cells of the Hepatic Sinusoid, 31st August – 4th September 2008, Tromso, Norway

Turner, S.L., Bird, N.C., Mangnall, D., Blair-Zajdel, M.E. & Bunning, R.A.D. Study into the modulation of ADAM17, ADAMTS-1, -4, -5 and TIMP3 by cytokines in the hepatoma cell line HepG2 and hepatic stellate cell line LX-2. British Society for Immunology, 4th June 2007, Sheffield, UK

Departmental Presentations (Oral)

Turner, S.L., Bird, N.C., Mangnall, D., Blair-Zajdel, M.E. & Bunning, R.A.D. Investigation of ADAM17 and ADAMTS-1, -4 and -5 in primary and metastatic liver carcinoma. Bioscience Forum, 1st April 2009, Sheffield, UK

Turner, S.L., Bird, N.C., Mangnall, D., Blair-Zajdel, M.E. & Bunning, R.A.D. Investigating ADAM17 and ADAMTS-1, -4 and -5 in metastatic liver disease and liver regeneration. 1st Joint Faculty of Health and Wellbeing and Honorary Clinical Professors Meeting, 7th December 2008, Sheffield, UK

Turner, S.L., Bird, N.C., Mangnall, D., Blair-Zajdel, M.E. & Bunning, R.A.D. Investigating ADAM17 and ADAMTS-1, -4 and -5 in metastatic liver disease and liver regeneration. Bioscience Forum, 28th November 2007, Sheffield, UK

Turner, S.L., Bird, N.C., Mangnall, D., Blair-Zajdel, M.E. & Bunning, R.A.D. Studies on the role of ADAM17 and ADAMTS-1, -4 and -5 in metastatic liver disease and liver regeneration. Bioscience Forum, 25th October 2006, Sheffield, UK

Departmental Presentations (Poster)

Turner, S.L., Bird, N.C., Mangnall, D., Blair-Zajdel, M.E. & Bunning, R.A.D. Studies into ADAM17 and ADAMTS-1, -4 and -5 in metastatic liver disease. Research User Involvement Project, 25th September 2009, Sheffield, UK

Turner, S.L., Bird, N.C., Mangnall, D., Blair-Zajdel, M.E. & Bunning, R.A.D. Study into the expression of ADAM17, ADAMTS-1, -4, -5 and TIMP3 by hepatic stellate cell line LX-2 and hepatoma cell line HepG2. Faculty of Health and Wellbeing Poster Session, 17th December 2008, Sheffield, UK

Turner, S.L., Bird, N.C., Mangnall, D., Blair-Zajdel, M.E. & Bunning, R.A.D. Studies into ADAM17 and ADAMTS-1, -4 and -5 in metastatic liver disease and liver regeneration. Research User Involvement Project, 18th June 2008, Sheffield, UK

Turner, S.L., Bird, N.C., Mangnall, D., Blair-Zajdel, M.E. & Bunning, R.A.D. ADAM17 gene expression in the HepG2 human hepatocellular carcinoma cell line. Faculty of Health and Wellbeing Poster Session, 13th December 2006, Sheffield, UK